Measuring sap flow and stem water content in trees: a critical analysis and development of a new heat pulse method (Sapflow+)

Thesis

submitted in fulfillment of the requirements for the degree of

Doctor (PhD) in Applied Biological Sciences

by

ir. Maurits Vandegehuchte

May 2013

Promoter

Prof. dr. ir. Kathy STEPPE

Department of Applied Biology and Environmental Biology,
Laboratory of Plant Ecology, Universiteit Gent

Members of the examination board

Prof. dr. ir. Patrick VAN DAMME

Department of Plant Production,
Laboratory of Tropical and Subtropical Agriculture and Ethnobotany, Universiteit Gent

Prof. dr. ir. Wim CORNELIS

Department of Soil Management,
Soil Physics SOPHY, Universiteit Gent

Prof. dr. Nico KOEDAM

Department of Biology,
Laboratory of Plant Biology and Nature Management, Vrije Universiteit Brussel

Prof. dr. ir. Kris VERHEYEN

Department of Forest and Water Management,
Forest and Nature Lab, Universiteit Gent

Prof. dr. Caroline VINCKE

Earth and Life Institute,
Forest Science and Engineering, Université Catholique de Louvain

Dr. Melanie ZEPPEL

Department of Biological Sciences,
Climate and Forest Ecosystem Modelling group, Macquarie University

Dean

Prof. dr. ir. Guido VAN HUYLENBROECK

Rector

Prof. dr. Paul VAN CAUWENBERGE

The research reported in this thesis was conducted at the Department of Applied Ecology and Environmental Biology (Laboratory of Plant Ecology) of the Ghent University, Belgium. This research and the research stay on North Stradbroke Island were funded by the Research Foundation – Flanders (FWO, Flanders, Belgium). The author is a PhD fellow of the FWO-Flanders.

Dutch translation of the title:

Meten van sapstroom en stamwaterinhoud in bomen: een kritische analyse en ontwikkeling van een nieuwe warmtepuls methode (Sapflow+)

Citation of this thesis:

Vandegehuchte, M. W. (2013). Measuring sap flow and stem water content in trees: a critical analysis and development of a new heat pulse method (Sapflow+). PhD thesis, Ghent University, Belgium.

ISBN-number: 978-90-5989-610-9

Acknowledgement - Dankwoord

Beste lezer, u behoort ongetwijfeld tot één van twee grote lezersgroepen. De ene groep bestaat uit zij die dit werk volledig doorlezen of hier en daar de delen eruit pikken waarin ze, vanuit wetenschappelijk oogpunt, geïnteresseerd zijn. De tweede zijn zij die enkel deze eerste bladzijden lezen uit interesse voor het meer menselijke aspect van de wetenschap of wie weet, in de hoop er ergens hun naam in terug te vinden. Toch zijn beide groepen voor dit doctoraat even belangrijk geweest. Ik hoop dan ook dat deze eerste en alle daaropvolgende bladzijden niemand van deze beide groepen teleur zullen stellen.

Ten eerste wil ik mijn promotor, Kathy Steppe, bedanken. Niet omdat het zo hoort, wel omdat er niemand anders is die zoveel tot dit werk heeft bijgedragen als jij. Vier jaar geleden zorgde je enthousiasme als lesgever ervoor dat ik mijn thesis bij het Labo Plantecologie wou doen. Na een avontuur in Tunesië spoorde je me aan om te beginnen doctoreren en hielp je me mijn FWO beurs binnen te halen. Sindsdien heb ik altijd met veel plezier met je samen gewerkt. Je hielp me ideeën uitdenken en uitdagingen aan te gaan, waarbij je enthousiasme aanstekelijk werkte. Daarnaast verloor je nooit je geduld als ik weer eens een veel te gehaaste versie van een paper doorstuurde en jij er nauwgezet alle schrijf- en schoonheidsfoutjes uithaalde. Bovendien steunde je me steeds in mijn wilde plannen om een bestaande theorie op de korrel te nemen, in bomen te gaan slingeren of de gevaren van de mangroves te trotseren. En naast het wetenschappelijke aspect was er steeds tijd voor een leuke babbel of een toffe activiteit, of het nu in schaatsen in de buurt van Gent was of een kampvuur in de bergen van Obora. Bedankt om voor mij zoveel deuren te openen, mij te blijven vertrouwen in mijn werk en voor je creatieve inbreng in wat we tot

stand hebben gebracht. Ik hoop dan ook dat ik nog een tijdje deel kan uitmaken van de toffe bende die het Labo Plantecologie onder jouw leiding geworden is.

Dat brengt ons naadloos bij de rest van de bende, zonder wie het labo maar een stille en lege plaats zou zijn. Bedankt aan iedereen voor de gezellige koffiepauzes, middagpauzes, uitgelopen labo activiteiten en zoveel meer. De doc's (Tommeke, Hans, Veerle en Wouter) wil ik bedanken om mij drie jaar geleden als groentje op te nemen in de groep. Nachtelijke zwempartijen, in bomen klimmen en avondlijke pintjes waren een goede afwisseling tussen het wetenschappelijke werk door, ik hoop dan ook dat er nog veel dergelijke ondernemingen mogen volgen! Tom, hopelijk zien we je af en toe nog eens opduiken nu je bij ILVO werkt. Wouter, veel succes in Australië, als je iemand nodig hebt om de mangroves in te duiken, weet je me te vinden. Hans, hopelijk kan ik je binnenkort prof noemen en mag ik eens wat sapstroom gaan meten op je lianen. Veerle, nogmaals sorry voor het stelen van uw bureau. Jasper en Annelies, van studiegenoten zijn we geëvolueerd tot collega's. Bedankt voor die leuke eerste jaren op ons eiland. En dan is er natuurlijk ook de 'nieuwere' generatie. Naast Jochen en Marjolein, wil ik vooral Lidewei, Elizabeth, Ingvar en Bart bedanken voor de fijne momenten op 'onze' bureau. Muren intrappen, pseudowetenschappelijke discussies voeren en al typend met twee vingers 'hard werken' heeft al voor veel plezante momenten gezorgd.

En dan kom ik bij de eigenlijke helden van ons labo: Geert en Philip. Zonder jullie was dit boekje er niet geweest. De vele uren die jullie hebben besteed aan het mee ontwerpen en maken van sensoren, het omhakken van bomen (met gevaar voor eigen leven), het installeren van de gemaakte sensoren, heen en weer rijden naar Wageningen en Gontrode… ze zijn ontelbaar. Om nog maar te zwijgen van de laatste spurt voor ik naar Australië vertrok. Het samenwerken was altijd een genoegen, de frietjes tussendoor meer dan verdiend. En nu dit boekje er ligt, wordt het tijd om de belofte in te lossen: 'het stoveke' wacht op jullie… Natuurlijk wil ik hier ook de latere aanvulling van het technisch team bedanken. Erik en Thomas, zonder jullie was de Sapflow+ er niet geweest in zijn huidige vorm. Ann, Margot en Pui Yi, jullie counterden mijn slordigheid met administratieve punctualiteit en steeds met de glimlach. I <3 SAP maar jullie toch nog meer. Bedankt voor al jullie harde werk, ik apprecieer het enorm.

Los van de Labo collega's, zijn er nog vele andere collega's die hier verdienen vermeld te worden. First of all, I would like to thank Leonardo Reyes, partner in science crime. Both our collaboration in Ghent as our work afterwards have made me appreciate you as a person, yes, as a friend. I hope that your new life in London gives you al the (scientific) challenges you are looking for. I would also like to express my gratitude towards prof. Nadja Nadezhdina and prof. Jan Cermak for the great week at Obora and for introducing me to the world of sap flow. It is wonderful that, besides a sometimes different point of view on sap flow methodology, we have been able to work so well together. Ook prof. Frank Sterck, Paul Copini en Edo Gerkema van Wageningen UR wil ik bedanken voor de fijne samenwerking gedurende de MRI meetcampagne.

Dirk De Pauw wil ik enorm bedanken voor alle steun die hij gegeven heeft bij mijn modelleeravonturen, de software ontwikkeling en de vlotte respons op mijn suggesties en vragen. Je hebt me in totaal waarschijnlijk meer dan een half jaar tijd bespaard.

Finally, for the science part, I am most grateful to prof. David Lockington, dr. Adrien Guyot and the entire MBRS crew for giving me the opportunity to conduct experiments in the wonderful mangrove ecosystem of Straddie. Adrien and Nina, thanks for the warm welcome, the help with setting up the sensors and the nice moments in between it all. I hope you find your way in the future, whether in Grenoble or still in Brissie with or without the mime guy. Captain Matt, without you the Belgies would not have been able to work at one of the most beautiful sites in the world. You brought us there and back safely on your vessel, played Santa bringing us food and lightened the work with your fine sense of humour. Shark's alley will never be the same again, many thanks for all the great Ozzie moments. En natuurlijk mag ik de Belgies zelf niet vergeten, Michiel, Mieke, Stefanie en Niels, het was een waar genoegen om jullie 'meneer den tutor' te zijn gedurende die twee maanden.

Maar gelukkig was er naast de wetenschap afgelopen jaren ook nog voldoende tijd voor zoveel meer. Daarom bedankt aan iedereen die er de laatste jaren buiten het werk voor me was. Jantje en Sabine, Anneke en Vinnie, Stijntje en Valerie, Cilia en Charles en Karel en Caroline, tof om te zien dat we na onze gezamenlijke unieftijd nog steeds samen plezier maken. Ik hoop dat we dat zo kunnen houden en kijk al

uit naar wat de toekomst jullie allemaal brengt. Jan, extra bedankt voor de twee leuke jaren dat we samen op kot zaten en dat je me vorig jaar onder je dak hebt laten kamperen. Ik zal dan ook mijn uiterste best doen zo goed mogelijk te getuigen volgende week. Boys, bedankt voor de vele banquets. Binnenkort is het dringend weer eens mijn beurt. Klaas, ook bedankt voor de hulp met de kolommen in het prille begin van mijn doctoraat. JNM'ers, jullie zijn met teveel om allemaal persoonlijk op te noemen. Bedankt voor al die jaren natuur, kampen, activiteiten en plezier. VP, ik ben blij dat ik een jaar jullie voorzitter mocht zijn, jullie zijn een fantastische bende! JNM Gent, bedankt om me als West-Vlaming onderdak te bieden, de vele avonturen waren onvergetelijk. Toch zijn er een paar JNM'ers die ik wel wil vernoemen. Anton en Pieter (aangevuld door Hanne), jullie zijn de beste huisgenoten en vrienden die je je kan inbeelden. De cursussen, de activiteiten, de avonden, de feestjes, de reizen… stuk voor stuk geweldig. Moge er nog veel, veel meer van dat volgen. Pepijn en Maarten, Spanje en Noorwegen waren overweldigend. Laat het het begin van een traditie worden. Ik begin alvast een busje te zoeken en wat kano's op te blazen. Bart en Pieter, menig vrijdagmiddag hebben jullie me van vertier voorzien, ik hoop dat ik binnenkort jullie boekske kan lezen. Hetzelfde geldt voor Sam, mijn bijna-buur en regelmatige passant tussen de bureaus en respectievelijke koffielokalen. Liezert, bedankt voor de onvergetelijke jaren en voor alles wat je me geleerd hebt waar een universiteit nooit in zou kunnen slagen. Een vriendschap om te koesteren.

Ten slotte bedankt aan mijn familie. Broers, eens te meer treed ik in jullie voetsporen. Ik ken jullie letterlijk mijn hele leven en zou me geen leven zonder jullie kunnen voorstellen. Na onze jeugd delen we nu ook de rest van het verhaal en daar ben ik jullie ontzettend dankbaar voor. Jullie hebben me, als grote broers, mee opgevoed en zo mee mijn leven bepaald. De vele momenten van lol trappen, samen op stap gaan en elkaar steunen zijn onbeschrijfelijk. Michiel en Eva, bedankt dat ik altijd jullie deur mag platlopen als ik daar zin in heb, jullie zijn als een tweede thuis. Kleine Lukas, ik kijk er naar uit om je verder te zien opgroeien en samen hansje-pansje te verwelkomen. Martijn en Bieke, altijd tof om jullie avonturen uit de US en nu Zwitserland te lezen. Ondanks de afstand voelt het meteen weer aan als vroeger als ik jullie in levende lijve zie. Hopelijk kunnen we binnenkort eens samen de bergen daar trotseren. Pa en ma, de kleinen is nu weer wat groter. Bedankt voor de gelukzalige, zorgeloze jeugd, de vele kansen, de hulp bij het verbouwen, de nooit

aflatende steun en het vertrouwen in mijn, soms wat haastige, ondernemingen. Betere ouders kan je niet dromen. Opa en oma, bedankt voor de mooie momenten samen, het prachtige voorbeeld dat jullie ons geven en de oprechte interesse in waar we mee bezig zijn. En dan zijn er natuurlijk nog Rit (toch een beetje een tweede mama geworden), Simon, Jolijn en Daan. Jullie hebben me meteen laten thuis voelen daar in de Kempen. Een warm nest waar ik met plezier langskom.

En als laatste is er natuurlijk Celien. Van een wetenschapper wordt verwacht dat hij wat hij rondom zich ervaart, tracht te begrijpen en verklaren. Maar ik weet dat wat ik bij jou ervaar, nooit ga kunnen of willen begrijpen, laat staan verklaren. Bedankt voor de fantastische jaren die we samen al gehad hebben en voor de jaren die nog komen!

Gent, Mei 2013

Contents

List of abbreviations and symbols

Abbreviations

CAG	Calibrated Average Gradient
CO_2	Carbon dioxide
CHP	Compensation Heat Pulse
DOY	Day Of the Year
FEM	Finite Element Model(ling)
HD	Heat Dissipation
HFD	Heat Field Deformation
HR	Heat Ratio
LVDT	Linear Variable Displacement Transducer
MC	Water content
MC_{FSP}	Water content at Fibre Saturation Point
MRI	Magnetic Resonance Imaging
NaCl	Sodium Chloride
NTG	Natural Temperature Gradient
RH	Relative Humidity
SHB	Stem Heat Balance
SPAC	Soil Plant Atmosphere Continuum
SF	Sap Flow
SFD	Sap Flux Density

SFD_{err}	Relative error in Sap Flux Density
TD	Thermal Dissipation
TDP	Thermal Dissipation Probe
THB	Trunk Heat Balance
VPD	Vapour Pressure Deficit
WBD	Wet Bulb Depression
WSSE	Weighted Sum of Squared Errors
2D	Two-dimensional
3D	Three-dimensional

Latin symbols

A	Cross-sectional area
AC	Actual soil water conductivity
A_{stem}	Stem cross-sectional area
C	Solute concentration
c_d	Specific heat capacity dry wood
c_{dw}	Specific heat capacity of the woody matrix
c_s	Specific heat capacity of xylem sap
c_w	Specific heat capacity of water
D	Thermal diffusivity
D_{in}	Inner diameter of the stem segment (without bark)
D_{out}	Outer diameter of the stem segment (with bark)
d	Distance/thickness
e^0	Saturated water vapour pressure
e	Actual water vapour pressure
F_v	Void fraction of the wood
F_{v_FSP}	Void fraction of the wood at fibre saturation point
g	Gravitational acceleration
h	Height
k	Sensitivity instance
k_{soil}	Proportionality factor between the soil water potential and the xylem root water potential
K	Thermal conductivity
K_{ax}	Axial thermal conductivity

K_d	Thermal conductivity of dry wood
K_{d_FSP}	Thermal conductivity of wood at fibre saturation point
K_{rad}	Radial thermal conductivity
K_{tg}	Tangential thermal conductivity
K_w	Thermal conductivity of water
$\vec{K}$	Thermal conductivity vector
l	Length of the stem segment
L	Radial hydraulic conductivity of the virtual membrane separating the stem storage compartment from the xylem compartment
L_{sw}	Sapwood depth
M	Mass
m_w	Molar mass of water
N	Number
N_{eq}	Osmotic equivalent
P	Hydrostatic pressure
P_h	Heat input heater needle
q	Heat input per unit length of the heater
Q	Thermal energy
Q_T	Temperature to which the amount of heat liberated per unit length of the line would raise a unit volume of the substance
R	Universal gas constant
R_s	Resistance
R_s'	Resistance per unit length
R^{st}	Flow resistance between stem xylem and storage compartment
R^x	Flow resistance in the stem xylem
r	Radius
s	Relative sensitivity
ΔS	Thickness of the storage compartment
t	Time
t_c	Time after application of the heat pulse at which the temperature at x_{up} is equal at the temperature at x_{down}
t_m	Time at which the temperature at a given distance after application of a heat pulse is maximal
T	Temperature

T_{air}	Air temperature
T_{as}	Temperature measured in the asymmetric HFD needle
T_{d}	Downstream temperature
T_{dew}	Dew point temperature
T_{ref}	Temperature measured in the axial reference HFD needle
T_{stem}	Stem temperature
T_{u}	Upstream temperature
ΔT	Temperature difference
ΔT_{a}	Average temperature gradient between the downstream and upstream temperature
ΔT_{0}	Temperature difference at zero flow
ΔT_{down}	Temperature increase downstream from the heater after application of a heat pulse
ΔT_{up}	Temperature increase upstream from the heater after application of a heat pulse
ΔT_{sym}	Temperature difference between the upper and lower axial HFD needles
ΔT_{as}	Temperature difference between the tangential and lower HFD needles
$\Delta T_{s\text{-}a}$	Temperature difference between axial downstream and tangential measurement needle
$\Delta T_{0(s\text{-}a)}$	Temperature difference between axial downstream and tangential measurement needle at zero flow
U	Voltage
V_{h}	Heat velocity
V_{h_corr}	Heat velocity corrected for wounding
V_{st}	Stem storage volume
V_{w}	Partial molal volume of pure water
w_{d}	Dry weight
w_{f}	Fresh weight
W_{st}	Water mass stored in the stem storage compartment
x	Axial distance
x_{up}	Upstream axial distance
x_{down}	Downstream axial distance
y	Tangential distance

Z_{ax}	Distance between the axial HFD needles
Z_{tg}	Distance between the tangential and lower axial HFD needles

Greek symbols

Γ	Critical value for the pressure component (Ψ_p^{st}) which must be exceeded to produce (positive) growth in the storage compartment
γ	Collinearity index
δ^{meas}	Sensitivity measure
ε	Bulk elastic modulus of living tissue in relation to reversible dimensional changes (water storage)
ε_0	Proportionality constant
θ	Source component value
μ_w	Chemical water potential
μ_w^0	Chemical reference water potential
π	Number Pi
Π	Osmotic pressure
ρc	Volumetric heat capacity
ρ	Density
ρ_d	Dry wood density
ρ_s	Sap density
ρ_w	Density of water
ρ_{wood}	Density of dry wood
σ	Surface tension at the air-liquid interface
τ	Matrix potential
ϕ	Extensibility of cell walls in relation to non-reversible dimensional changes (water storage)
Ψ	Water potential
Ψ_m	Matrix water potential
Ψ_l	Leaf water potential
Ψ_p	Pressure water potential
Ψ_Π	Osmotic water potential

Ψ_{soil}	Soil water potential
Ψ_{stem}	Stem water potential
Ψ^{r}	Xylem water potential in the roots
Ψ^{x}	Xylem water potential in the stem
Ψ_{p}^{s}	Sap water potential
Ψ^{st}	Storage water potential
Ψ_{p}^{st}	Storage pressure water potential
Ψ_{Π}^{st}	Storage osmotic water potential

Introduction and outline of the thesis

Besides humans, terrestrial plants are the main living organisms influencing the local and global water cycles. By transpiring, plants take up enormous amounts of water from the soil and transport these to their leaves, releasing the water as vapour to the atmosphere. As a mere indication, the total amount of this water transport in the world's dense, tropical forests can be up to ~32 x 10^{15} kg per year (Hetherington & Woodward, 2003).

The need of water for plant development and growth has led to several branches of science, many as old as humanity itself. People have known from the very beginning that in order to obtain vegetable food for human or animal consumption, whether by gathering or cultivation, water is of crucial importance. During the ages, strategies to deal with local water scarcity have shifted from a nomadic lifestyle (Kaniewski *et al.*, 2012), moving to those places where water was in abundance, over early irrigation channels derived from river beds to wind driven water pumps and, more recently, highly specialized irrigation techniques based on plant-driven models (Steppe *et al.*, 2008). Next to water as a resource for plant production, the importance of plant-water relations has found acceptance in other branches of science as well, amongst others to investigate colonization by fungi and insects, fertilization, stress monitoring, reforestation and ecosystem changes. More recently, the importance of plant water use has also been acknowledged in the global change concept (Huntington, 2006). Knowing that water vapour has a magnifying effect on

the global temperature change and that more intense drought events can cause widespread forest decline (Choat *et al.*, 2012), a correct estimation of ecosystem transpiration is crucial to accurately predict future climate changes and associated consequences such as civil conflicts (Hsiang *et al.*, 2011). To estimate these contributions of plant transpiration to global and local water cycles, typically vegetation models are used (Hanson *et al.*, 2004), whether on the single-plant or the ecosystem scale.

To understand the hydraulic functioning of plants in relation to the preset research objectives, measurements of plant water use are essential. Worldwide, sap flow methods are applied to monitor plant water status and validate vegetation models. These methods determine flow direction as well as relative and absolute flow, establishing the link between plant water uptake, release and storage. Hence, whether it is to assess the correct irrigation dose, to monitor forest vitality or to obtain trustworthy modelling results, reliable sap flow measurements are indispensable.

Since the beginning of the previous century when dyes were applied to trace sap flow in stems and roots (James & Baker, 1933; Dixon, 1936; Kramer, 1940), sap flow measurement methods have greatly evolved. The application of heat as a tracer has made sap flow measurements much less destructive and, even though modern techniques such as Magnetic Resonance Imaging or isotope analysis clearly have their value in sap flow research, heat-based sensors remain the most practical and cost-effective option for sap flow assessment. Since the pioneering work of Huber (1932), a wide range of heat-based sap flow methods have been developed. While all these methods have their merits and have led to interesting ecophysiological findings, many methods are limited in the range of sap flow rate or sap flux density they can measure and are dependent on thermal wood properties or empirical calibrations. Moreover, wounding and natural temperature gradients can highly influence the quantitative results. Therefore, the primary objective of this PhD study was to investigate these limitations and try to come up with possible solutions.

However, before the basic principles of sap flow measurements could be tackled, a thorough understanding of the mechanisms leading to sap flow had to be acquired. **Chapter 1** describes the driving forces behind plant water uptake and the pathways water follows on its journey through the plant. Hydraulic redistribution as a way of

water transport going against the expected flow direction is unveiled as a process following the same fundamentals as common sap flow from soil to atmosphere. Finally, the main measurable variables describing tree water use are discussed as, together with sap flow measurements, they form the basics of experimental plant-water research.

The information on how sap flow in plants can be measured is spread throughout the scientific literature with most manuscripts focusing on a single method. While **Chapter 1** describes the mechanisms underlying sap flow, **Chapter 2** assembles and critically comments on the current state of knowledge on sap flow measurement methodology. While *sap flow rate* methods are briefly mentioned as a means to determine the integrated flow through the entire plant or stem section in a given time span (m^3 s^{-1}), the chapter mainly zooms in on *sap flux density* methods, determining the flow of sap through a certain sapwood area in a given time span (m^3 m^{-2} s^{-1}). The latter leads to a more specific assessment of sap flow on a spatial scale, enabling more in-depth investigation of ecophysiological traits such as radial and circumferential variability of sap flow or specific aspects of hydraulic redistribution. Next to the theoretical background of the existing methods, this chapter also provides a discussion on the most important factors influencing sap flow methods.

As the only continuous heat based sap flow method encompassing radial sap flow profiles, high resolution monitoring for both regular and reverse flows as well as enabling sap flow calculations without the need to assume night-time zero flow conditions, the Heat Field Deformation method (HFD) (Nadezhdina *et al.*, 2012) has proven its use in many sap flow studies. However, the underlying methodology is based on an erroneous use of thermal diffusivity as a sapwood parameter. **Chapter 3** explains why thermal diffusivity should not be related to the empirical HFD temperature ratio and suggests an improved correlation between the latter and sap flux density, stressing that the HFD method should be considered empirical while acknowledging its many advantages.

Given the empirical nature of continuous heat based sap flux density methods such as the HFD, the interest of the scientific community has shifted towards heat pulse methods as they have a theoretical thermodynamic background. All existing heat pulse sap flux density methods are founded on the same isotropic heat conduction-convection equation as mentioned by Marshall (1958). Sapwood, however, is

anisotropic, necessitating an anisotropic theory. This shortcoming in sap flow method development is addressed in **Chapter 4** where the correct basic theory is derived and the consequences for existing sap flow research are unravelled.

Of the heat pulse methods, the most versatile is no doubt the Heat Ratio method (Burgess *et al.*, 2001a). Although limited for high flows, this method enables measurements of average, low as well as reverse flows, converting the measured temperature ratios to sap flux density based on the axial thermal diffusivity of the sapwood. The latter is determined during zero flow conditions, based on a method of mixtures applied to a sapwood sample cored from the tree. In this method of mixtures, however, the meaning of the water content is misinterpreted, leading to incorrect diffusivity calculations. **Chapter 5** proposes a correction to this method, including the proper incorporation of sapwood water content.

Given the limitations of existing sap flux density methods, the urge arose to search for alternatives. **Chapter 6** tries to tackle these limitations by presenting a new sap flux density method, the Sapflow+ method, enabling sap flux density measurements independent of thermal diffusivity determination across the entire naturally occurring range of sap flows. Moreover, this method holds the promise of simultaneously determining stem water content.

After the theoretical development of the Sapflow+ method and the confirmation of its applicability by lab tests, **Chapter 7** presents how the Sapflow+ method can be applied in harsh field conditions to study tree water use. An experiment was set up in on North Stradbroke Island, Australia to assess water use of *Avicennia* and *Rhizophora*, two dominant mangrove species. By measuring stem diameter variations, water potentials and sap flux density, the differences in water use of these co-occurring species coping with the challenging environmental conditions were revealed.

Finally, **Chapter 8** summarizes the main findings of this PhD study and formulates their implications and challenges for ongoing and future research. It is discussed which questions remain unanswered and where promising areas of future research lie.

In summary, this PhD thesis addresses the following main questions:

- Which current methods are available to determine sap flow in plants?
- On which basis are these methods found?
- What are the differences between these methods and their limitations?
- How can sap flow measurements still be improved?

1

Water transport in trees

Trees are sanctuaries. Whoever knows how to speak to them, whoever knows how to listen to them, can learn the truth. They do not preach learning and precepts, they preach, undeterred by particulars, the ancient law of life.

Hermann Hesse, Bäume. Betrachtungen und Gedichte

1.1 The driving forces of stem tree water transport and storage

The question of how large trees such as redwoods can transport water over distances more than 100 m has fascinated man since centuries. Thorough research has led to the general acceptance that water moves through plants in a passive way, driven by differences in water potential according to the cohesion-tension theory (Dixon & Joly, 1894; Slatyer, 1967; Tyree & Zimmerman, 2002).

1.1.1 Water potential as driving force

Water moves passively from a higher to a lower chemical water potential. This chemical water potential (μ_w in J mol^{-1}), corresponding to the free energy of water, can be expressed as:

$$\mu_w = \mu_w^0 - V_w\Pi + V_w P - V_w\tau + m_w\ g\ h \qquad (1.1)$$

with μ_w^0 the chemical potential of pure water for a specific reference state, V_w the partial molal volume of pure water (18.0×10^{-6} m^3 mol^{-1}), Π the osmotic pressure (Pa) caused by the attraction of water by dissolved solutes, P the hydrostatic pressure (Pa), τ the matrix potential caused by capillary forces (Pa) and $m_w\ g\ h$ the term describing the influence of gravity with m_w the molar mass of water (kg mol^{-1}), g the gravitational acceleration (9.81 m s^{-2}) and h the vertical height compared to the reference state (m).

The difference between μ_w and the reference state μ_w^0 represents the amount of work needed to move one mole of water from the reference to the actual level of chemical water potential with the reference defined as pure water at atmospheric pressure, at zero height level and at the same temperature as the considered system. When diverting from this reference state, the water is not in equilibrium and tends to passively flow towards a location where the difference with the reference state is lower.

Although explaining passive water flow, the concept of chemical water potential is not very practical as chemical potentials are difficult to measure in field conditions. Therefore, plant physiologists prefer to work with water potentials (Ψ), expressed in pressure units (Pa, or more commonly MPa) and obtained by dividing the chemical potential by V_w:

$$\Psi = \frac{\mu_w - \mu_w^0}{V_w} = P - \tau - \Pi + \rho_w\ g\ h \qquad (1.2)$$

with ρ_w the density of water (kg m^{-3}). As both V_w and μ_w^0 are constants, water will passively flow from a higher (less negative) to a lower (more negative) water potential Ψ. This water potential can be divided in different components:

The pressure potential Ψ_p (= P), indicating the physical pressure on the water, which can be either positive or negative.

The negative matrix potential Ψ_m (=-τ), representing the interactions between the water and air in numerous capillary interstices in plant tissues or soils due to the attraction between water and hydrophilic surfaces. Notice that Ψ_m and Ψ_p are mostly considered as one, describing the hydrostatic pressure which can be positive when water exerts pressure against the cell wall (turgor) or negative when water is under tension as in the xylem elements (see Section 0). Throughout this thesis, pressure potential Ψ_p will include the matrix potential.

The negative osmotic potential Ψ_Π (=-Π) due to the presence of dissolved solutes as water tends to be transferred from a lower to a higher concentration of solutes across a semipermeable membrane. Ψ_Π can be determined according to the Van 't Hoff's equation:

$$\Psi_\Pi = -\Pi = -RTC \qquad (1.3)$$

with R the universal gas constant (8.31 J mol^{-1} K^{-1}), C the solute concentration (mol m^{-3}) and T the solution temperature (K). Hence, the higher the solute concentration, the more negative Ψ_Π.

The positive gravitational potential Ψ_g (=$\rho_w\ g\ h$), related to the gravitational forces exerted on the water at a certain height h. This potential is only taken into account for tall trees.

This water potential concept is applicable for water in the liquid phase throughout the soil-plant-atmosphere continuum (SPAC). For water in the vapour phase, at the boundary of leaf and atmosphere level, Ψ is expressed by the Spanner equation (Spanner, 1951a):

$$\Psi = \frac{R \cdot T}{V_w} ln\left(\frac{e}{e^0}\right) \qquad (1.4)$$

where R is again the universal gas constant (8.31 J mol^{-1} K^{-1}), T the absolute temperature (K) and e^0 and e the saturated and actual water vapour pressure (Pa), respectively.

Even though the concept of water potentials explains the transport of water from a higher (less negative) to a lower (more negative) water potential, it does not indicate how these water potentials are created within the tree. To this end, the cohesion-tension theory was developed (Dixon & Joly, 1894; Tyree, 1997).

1.1.2 The cohesion-tension theory

The cohesion-tension theory states that water inside the apoplast of trees, the cell wall continuum of a plant containing the dead conductive xylem cells, forms a continuous string thanks to the cohesion forces between water molecules, caused by hydrogen bonds. If then at one end of this string the water is being attracted because of a lower water potential, the water molecules will resist to be pulled apart and a tension will be propagated within the water string. This cohesiveness of water molecules, together with the adhesive forces between water molecules and the walls of xylem elements, allows water to be transported within the stem.

But what induces these lower water potentials, creating the attractive forces on these water strings, causing them to be under tension? As the gravitational potential is always positive, it can be ruled out. Hence, these forces must be caused by changes in pressure and/or osmotic potential. The most influential cause of a decreasing pressure potential leading to upward sap flow is transpiration. This process comprises the water loss from leaves to the atmosphere, pulling up the water strings through all components of the SPAC (see section 1.2). Within the leaves, a meshwork of small interstices exists, created by the cellulose microfibrils in the cell walls. These interstices act as a fine capillary network where water is in contact with the air. Because of the strong adhesion between water and these cell walls, many curvatures (menisci) are formed, inducing a negative pressure potential in the sap directly behind the menisci (Nobel, 1999):

$$\Psi_p^s = -\frac{2\sigma}{r} \qquad (1.5)$$

where σ is the surface tension at the air-liquid interface (0.0728 N m^{-1} at 20°C) and r is the radius (m) of the meniscus, which is by convention positive for a concave

surface. As during transpiration water evaporates into the inter-cellular spaces of the leaf, this radius r decreases, causing the pressure potential to become more negative and, hence, creating a tension in the water string.

Next to transpiration, other processes can induce tension in the water column, causing water to move downwards within the SPAC or even in opposite directions within the tree. This phenomenon is termed hydraulic redistribution and is the subject of Section 1.3.

As according to the cohesion-tension theory strong negative pressures are induced, the water column will be in a highly metastable state. For over a century, this has led the cohesion-tension theory to be subject to criticism (Zimmermann *et al.*, 1994; Canny, 1995; Zimmermann *et al.*, 2004), leading to alternative theories explaining sap flow in plants. Canny (1995) developed the compensating pressure theory, stating that the tension in the water column due to transpiration is compensated by the pressure exerted by the surrounding tissues, protecting the water from going into the metastable state. This theory, however, has been widely disputed in a series of meticulous studies and has never been proved by experimental data (Stiller & Sperry, 1999; Tyree & Zimmerman, 2002). More recently, Zimmerman *et al.* (2004) roused the debate again, stating that 'negative xylem pressure values of several megapascals exist only in the realm of science fiction'. These authors argue that water in tall trees moves in analogy to the lifting of ships by consecutive watergates thanks to occasional axial barriers or adherence to gel matrices. Their main argument against strong negative xylem pressures seems to be the possible errors induced by pressure bomb measurements (Scholander *et al.*, 1965). Similar negative pressures have, however, been measured independently by applying centrifugal forces or stem psychrometers (Dixon & Tyree, 1984; Holbrook *et al.*, 1995). Moreover, the statements of Zimmerman *et al.* (2004) were immediately countered in a commentary of Angeles *et al.* (2004), subscribed by over forty international experts in tree water relations, stating that the work of Zimmerman *et al.* (2004) is misleading in its discussion on the fundamentals of the cohesion-tension theory and that the latter is widely supported as the only theory consistent with the enormous amount of data on water transport in plants. Therefore, this theory will also be accepted as correct throughout this study.

1.2 Flowing through the tree: the pathways of water

From all the water taken up by the roots, 95% or more leaves the tree again through transpiration (Ridge, 2002). This water loss can be seen as a side effect of photosynthesis, the process converting the energy of the sun into sugars, the basic building components of plants. Nevertheless, this water flow is of crucial importance as it transports mineral nutrients from the soil to the leaves and cools down these leaves as protection against high solar radiation. Moreover, without the positive pressure that water exerts on cell walls (referred to as turgor pressure), plants would not be able to grow. The following sections describe the different cell types and tissues water encounters on its way through the plant.

1.2.1 Transpiration from the leaves

While water transport in trees is often described as starting at the roots, it is the water loss from the leaves that induces flow. Imagine a healthy tree before sunrise, its different flow paths filled with water. When the sun rises, the leaves' stomata open, allowing the diffusion of CO_2 in the substomatal cavities to enable photosynthesis (Figure 1.1). However, as the water potential of the atmosphere is highly negative according to the Spanner equation (Eq. 1.4), water vapour from the substomatal cavities and intercellular air spaces will be drawn away through the stomata. This induces evaporation of water from the surface of the mesophyll cells, reducing the menisci of water-air interfaces and, hence, lowering the water potential (Section 1.1.2). Because of this lowered water potential, water is transported from the xylem in the vascular bundles to the mesophyll cells, further propagating tension throughout the water conducting system in the stem and roots.

Next to stomatal transpiration, water may also diffuse across the cuticle (cuticular transpiration) (Jones, 1992). The resistance to evaporation through the cuticle, which is not adjustable by the plant on the short-term and predominantly dependent on the thickness of the cuticle, is, however, much larger than the stomatal resistance. Moreover, the latter can be actively regulated by the plant as a response to internal factors, such as the internal CO_2, or external conditions, such as light, temperature, relative air humidity and soil water availability. Hence, unless stomata are (nearly) closed, cuticular transpiration only accounts for a small percentage in leaf water loss (Nobel, 1999; Phillips *et al.*, 2010; Zeppel *et al.*, 2010).

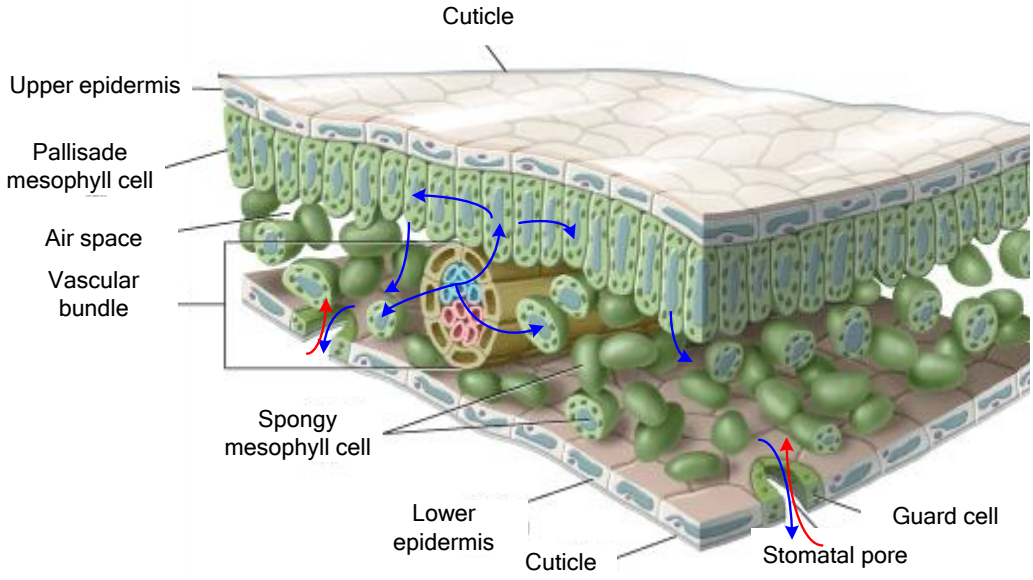

Figure 1.1 *Schematic transverse leaf section, indicating the various cell types. The blue arrows indicate the diffusion of water to the atmosphere via the stomata, inducing water flow from the vascular bundle, while the red arrows represent the uptake of* CO_2 *(adapted from http://glencoe.MCgraw-hill.com/sites/0078759864/student_view0/unit6/chapter22/standardized_test_practice.html)*

1.2.1 Water flow in stems

The water drawn from the leaves induces tension which propagates throughout the water conducting elements in the stem, called xylem (Figure 1.2). Together with the photosynthate-conducting tissue, indicated as phloem, the xylem makes up the vascular system which can be found in the entire tree, from root to leaves. Both of these transport tissues are produced by the vascular cambium, differentiating secondary phloem outwards to the bark and secondary xylem inwards. While the phloem mainly consists of living tissue, transporting photosynthesis products from sources to sinks throughout the plant, xylem mainly comprises dead cells. These cells do not only serve as water conducting pathways, they also provide structural support for non-woody plants and young trees. For older trees, this support function is taken over by the non-conducting heartwood, generated from the inner part of the xylem which has lost its conducting function over time (Raven *et al.*, 1992).

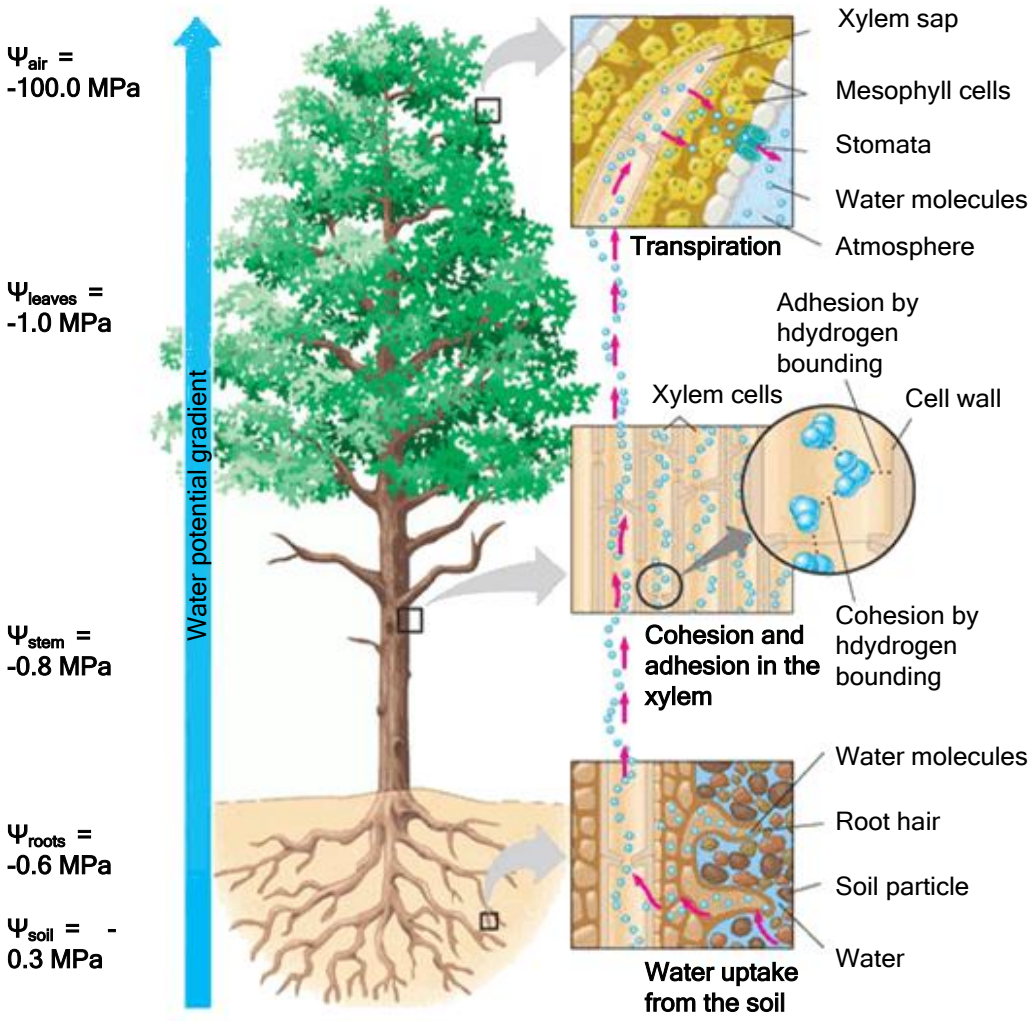

Figure 1.2 *A schematic representation of water movement through the SPAC. Removed from the leaves by transpiration, water is sucked up from the roots, following the gradient in water potential, created according to the cohesion-tension theory (adapted from Campell & Reece, 2008).*

Xylem flow

Within the xylem, a distinction can be made between vessel elements (only found in angiosperms) or the more primitive tracheids (found in angiosperms, gymnosperms and the lower vascular plants) (Figure 1.3a). For both types, conducting elements are axially arranged end-to-end. However, whereas tracheids typically have tapered ends, the generally shorter and broader vessel elements are adjoined by blunt ends. The cell wall of these ends are distinctively perforated (hence the name perforation plates), reducing the axial resistance within the vessel network, providing a suited pathway for water transport. Tracheids, on the other hand, do not contain

perforation plates, forcing the water to flow through much smaller holes in their touching boundaries, creating a higher axial resistance towards water flow (Pittermann, 2010).

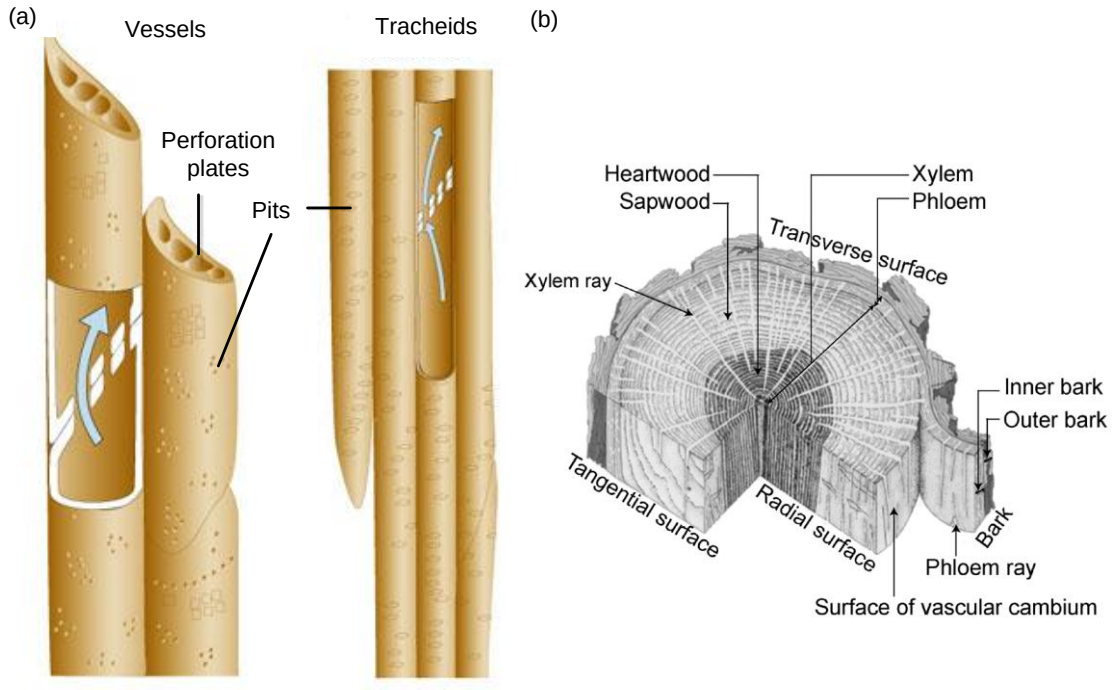

Figure 1.3 *(a) The different water conducting cell types in the secondary xylem of trees: vessels and tracheids (adapted from Campbell et al., 2004); and (b) structure and composition of a woody angiosperm stem section (adapted from Raven et al. (1992))*

Next to axial transport, water can also flow laterally between xylem cells. The thick lateral secondary walls of these cells, which makes xylem very inelastic, are punctured with small pits (Figure 1.3a). These pits, only existing of a very thin and porous primary cell wall, allow the free passage of water and nutrients while limiting the passage of air, pathogens and particles (Choat *et al.*, 2003). Via the pits, xylem elements are integrated into a complex network, giving the water the necessary flexibility of altering its flow path in case water conductance through certain cells fails. As water under tension in the xylem is in a metastable state, little stress is needed to induce air bubble formation in the conducting cells (cavitation). If then the tension of the xylem sap decreases below a certain threshold value, air from cavitated vessels will penetrate the largest pit membranes, filling the adjacent vessels, a process known as 'air seeding'. As these vessels cease to function, the water has to find another way upwards. As for other pits the cavitation threshold will be higher (a more negative water potential), the water can relocate through

these pits to those cells that still hold their conductive capacities. If, however, the tension further increases due to extended stress, too many xylem elements may become cavitated, blocking upwards sap flow and finally resulting in plant wilting.

Next to vessel elements and tracheids, the xylem system also comprises fibres and parenchyma cells. The latter are, in contrast with the conductive elements, living cells which form xylem rays (Figure 1.3b) facilitating lateral movement of water and solutes into and out of the conducting cells. Moreover, these cells form storage compartments for carbohydrates. Xylem fibres, on the other hand, are slender, lignified cells offering structural support to the xylem.

Secondary xylem is generally not uniformly produced throughout the year (Gricar, 2010). The cyclic pattern of seasonal cambial activity leads to a distinction in early wood, with typically less dense and wider vessels, produced at the beginning of the growing season, and late wood, which is produced at the end of the growing season and typically contains denser and narrower vessels. While for some species, there is hardly any structural difference between early wood and late wood (the so called diffuse porous species), for others the distinction is clear, enhancing the visibility of the growth rings (the so called ring porous species) (Butterfield & Meylan, 1980). It should, however, be noticed that the distinction between early and late wood is not only species, but also environmentally dependent as it has been shown that different trees from the same species may or may not show large differences between early and late wood based on seasonal intensity (Robert *et al.*, 2011b). Diffuse and ring porous species are often grouped together, forming the hardwoods of angiosperms, while the wood of gymnosperms is frequently referred to as softwood or coniferous wood. The latter also may or may not show clear distinctions between early and late wood depending on species and environmental conditions.

Phloem flow

While the transport of water and nutrients takes place in the xylem, water-dissolved photoassimilates are conducted via the phloem. This plant tissue consists of two cell types: sieve elements and companion cells (Figure 1.4a) (Taiz & Zeiger, 2006). In gymnosperms and lower vascular plants, the sieve elements (sieve cells) are generally longer, less wide and more tapered than the sieve tube elements found in angiosperms. Both sieve elements lose their nucleus, tonoplast (and thus their

vacuole), Golgi bodies and ribosomes as they mature. Nevertheless, the cytoplasm, cell membrane, endoplasmatic reticulum, few mitochondria and phloem-specific proteins and plastids remain. Therefore, these elements are still considered as living cells (Knoblauch & Peters, 2010). To metabolically sustain these sieve elements, they are neighboured by specialized cells, called albuminous cells in gymnosperms and companion cells in angiosperms. These cells do have nuclei and generally hold many mitochondria, providing energy to the sieve elements. Besides, these neighbouring cells are connected to the sieve elements by plasmodesmata, allowing transport of solutes to and from the sieve elements.

Transport of phloem sap is facilitated by the sieve plate, the end-to-end connection between sieve-tube elements, grouping them in sieve tubes. This sieve plate consists of clusters of pores through which the protoplasts of adjacent sieve-tube elements are connected. Therefore, phloem sap moving through the sieve tube does not need to cross cell membranes.

Next to sieve elements and their accompanying cells, phloem also comprises parenchyma cells, with storage as their primary goal, and fibres (sometimes sclereids), giving strength to the tissue. In contrast to xylem cells, phloem cells are never lignified, making the phloem tissue much more elastic.

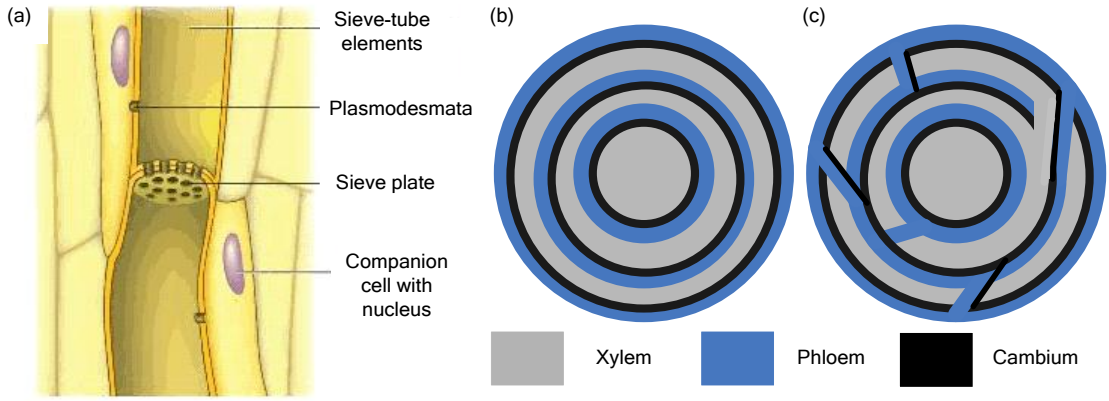

Figure 1.4 *(a) Longitudinal view of phloem tissue, including sieve tube elements and companion cells (Campbell et al., 2004); (b) successive cambia organised in concentric cylinders; and (c) successive cambia organised in a reticulate network (adapted from Robert et al. (2011a))*

In angiosperm trees, the phloem is mostly situated in the bark, separated from the xylem by the vascular cambium (Figure 1.3b). Besides the phloem, the bark also consists of the periderm and cortex, forming the outermost tissues of the stem. Not

all species show this clear boundary between phloem at the outer part and xylem more centrally in the stem. While girth expansion in vascular plants is generally the result of the meristematic activity of one cylindrical vascular cambium, some species produce several successive cambia (Figure 1.4b) (Carlquist, 2007). These cambia can literally develop successively although also simultaneous development is possible (Schmitz *et al.*, 2008). Next to this concentric organisation of successive cambia, some species such as *Avicennia* have shown an intricate three-dimensional network of cambia, resulting in a patchy growth pattern where active growth displaces around the stem circumference with time (Schmitz *et al.*, 2008; Robert *et al.*, 2011a).

While the transport of water and nutrients in the xylem is tension driven, the flow of phloem sap is determined by sink-source interactions according to the pressure-flow hypothesis (Münch, 1930). This hypothesis states that the flow in the phloem tissue is driven by an osmotically generated pressure gradient between sources and sinks. As at the source level photoassimilates are actively or passively transported in the phloem, the osmotic potential is lowered, attracting water from the surrounding tissues such as the xylem cells. This added water increases the hydrostatic potential of the phloem cells (turgor). At the sink level, these photoassimilates are unloaded from the phloem, decreasing its osmotic potential in the phloem and forcing water towards the sinks. The pressure difference which is thus created, sustains the flow from sources to sinks throughout the tree. This flow is further aided by apoplastic loading steps between the sieve tubes, acting as relays throughout the flow pathway (Lang, 1979; Knoblauch & Peters, 2010). As source unloading in the phloem leads to water attraction from the xylem, an additional tension in the xylem sap is created, causing the so called 'Münch's counterflow'. This upwards xylem flow occurs even in the absence of transpiration to sustain the water recycling in the phloem tissue (Windt *et al.*, 2006; De Schepper & Steppe, 2010).

1.2.2 Water flow in roots

From the stem, xylem elements continue in the roots. If water is drawn upwards during transpiration, the tension in the root xylem will rise, attracting water from the soil through the root system.

Root hairs, which are fine extensions of the epidermal cells, ensure a large contact surface with the surrounding soil, facilitating water uptake. After an easy passage through the single-cell layer of the root epidermis, waters moves through the root cortex via two dominant pathways: the apoplast and the symplast (Figure 1.5). During the apoplastic pathway, water moves within the continuum of cell walls and extra-cellular spaces outside living cells while for the symplastic pathway it moves within the protoplasm of the cells, connected by narrow plasmodesmata. A third, less common, pathway consists of the non-plasmodesmic water transport between cells, requiring the water to cross the cell membranes when entering and leaving the cells (Taiz & Zeiger, 2006).

To travel from the cortex to the apoplastic xylem in the stele, water is forced to cross the endodermis. This tissue consists of a single layer of cells of which the anticlinal walls are impregnated with waxy materials such as suberin and lignin and form the Casparian strip. Because of its composition, this waterproof Casparian strip does not allow apoplastic transport, forcing the water to take the symplastic pathway, a unique feature in the tree water transport system. This forced symplastic transport has several implications (Tyerman *et al.*, 2002). It does not only prevent water loss through the roots in case of extreme drought events, it also enables the roots to actively regulate their hydraulic conductivity by adapting the abundance and permeability of aquaporins (water transporting proteins). Besides, the Casparian strip allows accumulation of solutes in the xylem during conditions of high soil water availability and low transpiration rates. As this increased solute concentration will lower the osmotic potential, water will be attracted towards the root xylem across the symplastic membranes, causing a positive hydrostatic pressure. This 'root pressure' has been attributed to rehydrate embolized xylem conduits and allow the relocation of nutrients (Pickard, 2003; Clearwater *et al.*, 2007). A typical example of root pressure is the leakage of sugary xylem sap from damaged stems at the beginning of spring, when root reserves are remobilized before budburst.

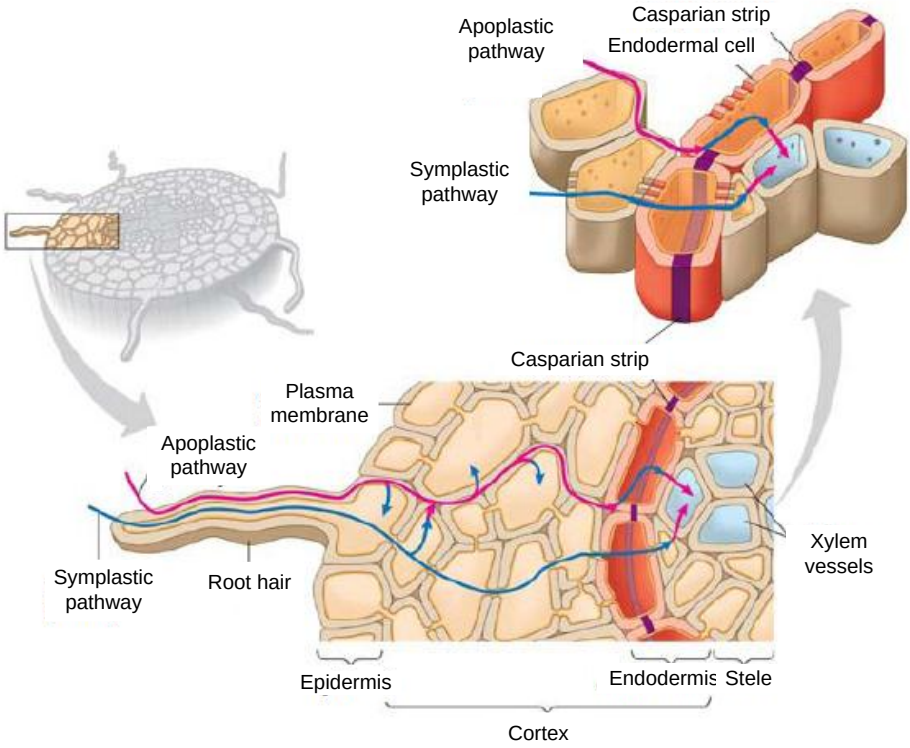

Figure 1.5 *A schematic representation of the water pathways inside the roots, focussing on the role of the Casparian strips (source: http://www.nicerweb.com/bio1152/Locked/media/ch36/root_transport.html).*

1.3 Taking the other route: hydraulic redistribution

In the previous sections, the upwards xylem flow, induced by transpiration at the leaves, was used as an example to understand the cohesion-tension theory and to present the different water conducting plant tissues. Water, however, is not solely transported from roots to leaves as water uptake and release are dynamic processes, including storage and redistribution phenomena.

1.3.1 Water storage

Generally, a time lag can be noticed between the transpiration at leaf level and the water uptake by the root system. As water is transpired from the leaves, tension is created throughout the xylem sap, pulling the water upwards. Because of the hydraulic resistance between leaves and roots, the amount of water taken up by the root system cannot immediately fulfil the demand of water at the leaves. To meet this shortage, water is released from the different storage compartment located

throughout the tree (Sevanto *et al.*, 2002; Steppe *et al.*, 2006; De Schepper & Steppe, 2010). On the other hand, when transpiration decreases, the water potential in the xylem increases, inducing water flow from the xylem back to the surrounding storage compartments. According to Tyree & Zimmerman (2002), three different mechanisms of water storage can be distinguished.

Living cells form the first storage compartment, consisting of elastic cells which are in the stem mainly located in the bark (phloem, cambium and parenchyma) and the wood rays (Zweifel *et al.*, 2000). Changes in water content of these elastic tissues are accompanied by volume changes, visible as shrinking and swelling of the stem. As long as the cells are not damaged, this storage process is reversible.

The second storage compartment is formed by the capillaries in the lumens of inactive xylem elements and intercellular spaces of the active xylem tissues. This capillary water is almost entirely released if the water potential lowers beneath -0.5 MPa (Tyree & Ewers, 1991). This process is also reversible.

A final storage mechanism is the release of water due to cavitation. This threshold at which this water release occurs is dependent on the diameter of the intervessel pits, ranging from -0.5 MPa for some species to -5 MPa or more for others (Tyree & Ewers, 1991).

1.3.2 Hydraulic redistribution

Next to transport to and from the storage tissues, xylem sap can also be relocated within the xylem. This phenomenon is generally referred to as 'hydraulic redistribution' (Nadezhdina *et al.*, 2010) and is a passive movement of water, controlled by competing soil and plant water potential gradients and corresponding pathway resistances (Nadezhdina *et al.*, 2009).

Many studies have shown that water can transfer passively from moist to drier portions of the soil profile via roots (Burgess *et al.*, 1998; Meinzer *et al.*, 2004; Oliveira *et al.*, 2005; Brooks *et al.*, 2006; Howard *et al.*, 2009; Domec *et al.*, 2010; Prieto *et al.*, 2011). Depending on the flow direction of the water in the soil, three types of hydraulic redistribution are distinguished (Figure 1.6). The term 'hydraulic lift' describes the upward movement of water from deep wet to shallow dry soil layers (Figure 1.6a), while the reverse movement from shallow to deeper soil is

sometimes referred to as 'downward hydraulic redistribution' (Figure 1.6c). Next to these vertical flows, water may also be transported laterally (lateral redistribution, Figure 1.6b) from moist to drier soil patches. This redistribution of water in the soil helps to maintain the soil water content in a range that prevents the soil water potential from dropping to the critical threshold that would cause root hydraulic failure due to cavitation (Domec *et al.*, 2004; Warren *et al.*, 2007; Siqueira *et al.*, 2009). As hydraulic redistribution in the soil accounts for more than 20% of the water taken up during transpiration, it even affects land-surface climatology (Brooks *et al.*, 2002; Lee *et al.*, 2005).

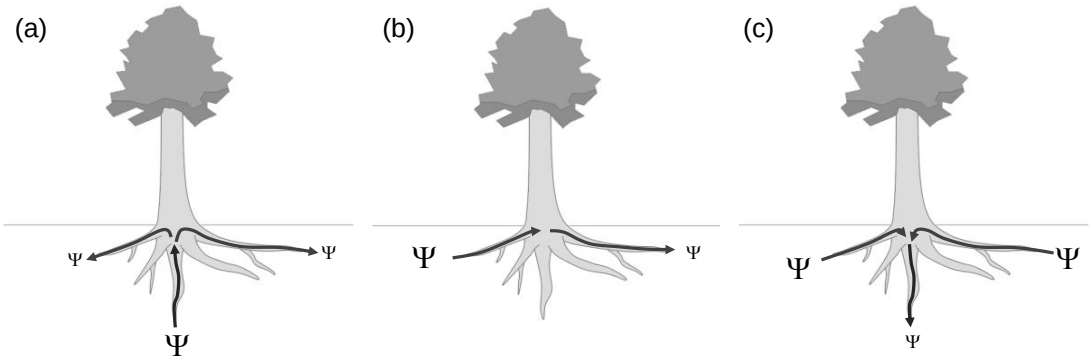

Figure 1.6 *Scheme of the different types of hydraulic redistribution in the soil compartment. (a) Hydraulic lift; (b) Lateral redistribution; and (c) Downward hydraulic redistribution. Different Ψ sizes indicate different water potentials: the bigger the symbol, the higher (less negative) the water potential. Arrows indicate the flow direction. Adapted from Nadezhdina et al. (2010).*

Hydraulic redistribution, however, does not only take place in the roots. Stephen Hales (1727) conducted an experiment almost 300 years ago, providing evidence of the possibility of reverse flow in tree stems (Figure 1.7).

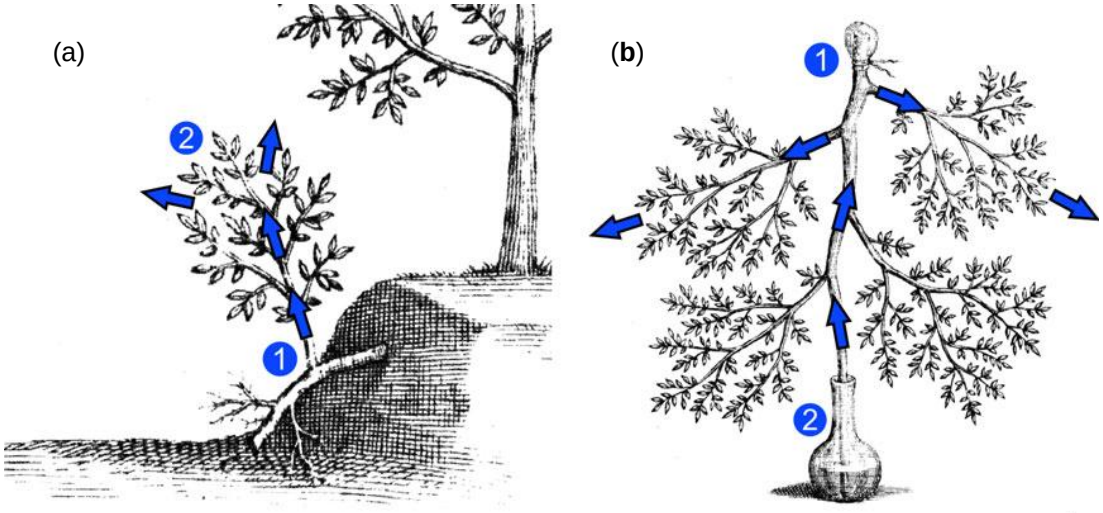

Figure 1.7 *Illustration of the experiment conducted by Hales (1727) showing the water flow in a large branch of an apple tree. The flow changed from roots (1)-leaves (2) direction during transpiration (a) to the leaves (2)-roots (1) direction after branch severing when its cut upper tip was put into water (b) (Nadezhdina et al., 2009).*

This reverse flow can be the result of several different processes, again passively driven by water potential gradients (Figure 1.8). Canopy water uptake occurs when water absorbed by leaves during rain, fog or dew events is transported from the wet foliage to the dryer stem, root or soil compartments (Figure 1.8a). This foliar absorption of water has shown to play a significant role in the water balance of many ecosystems during drought events (Yates & Hutley, 1995; Burgess & Dawson, 2004; Breshears *et al.*, 2008; Limm *et al.*, 2009; Simonin *et al.*, 2009). Next to water uptake, water can also be redistributed within the tree. During moments of low transpiration because of stomatal closure, whether at night or during conditions of very high vapour pressure deficits (VPD) at daytime, water can move from the different storage tissues to those compartments where water potential is highly negative (Figure 1.8b). This 'tissue dehydration' occurs mainly under extreme and prolonged drought conditions, when soil water potential drops below leaf water potential (Nadezhdina *et al.*, 2010).

While soil moisture measurements, water potential determination and isotope analysis can indicate general flow directions and, hence, point to hydraulic

redistribution, it was not until the use of sap flow methods allowing bi-directional flux measurements that the true complexity of this phenomenon could be assessed. Nadezhdina *et al.* (2009) conducted a field experiment in which part of the roots were located in drier soil while the opposite roots were adequately wetted. By applying HFD sap flow sensors, it could be seen that water was taken up from the wetted roots and then transported upwards in the stem before reversing to meet the dry soil of the opposite roots during night (Figure 1.8c). Moreover, while the inner xylem of the dry roots was conducting water to the soil, the outer xylem conducted water back upwards. This simultaneous occurrence of both regular and reverse flow points to radial sectoring, a feature which also has been noticed without hydraulic redistribution events (Orians *et al.*, 2004; David *et al.*, 2012).

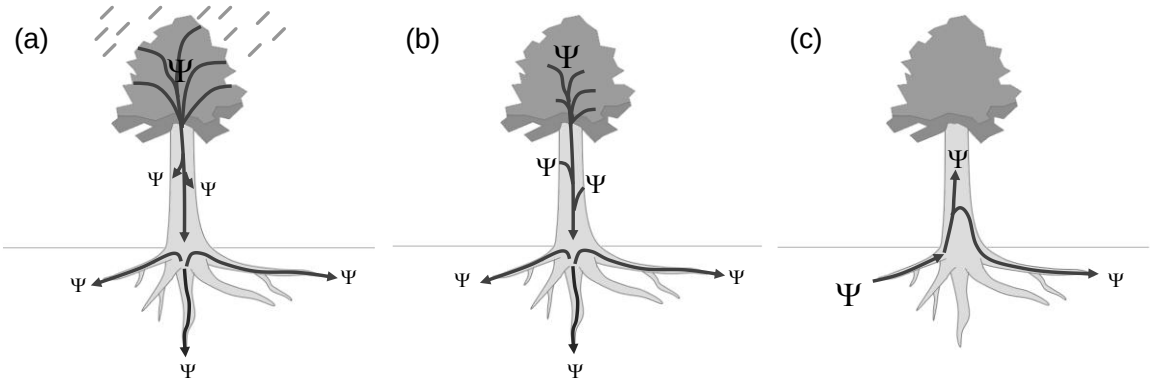

Figure 1.8 *Scheme of the different types of hydraulic redistribution in the below-ground tree compartments: (a) canopy wetting by rain, fog or dew increases the water potential to nearly zero, stimulating reverse flow to the stem and roots; (b) in cases of severe drought, water from internal storage can flow downwards if transpiration is low; and (c) water being redistributed in the stem following water potential gradients via the path of lowest resistance, allowing both upward and downward flow in the same transversal stem section (adapted from Nadezhdina et al. (2009)).*

Even though hydraulic redistribution is becoming an increasingly important feature in hydrodynamic plant research, many questions remain unresolved. To further improve our understanding of this phenomenon and allow its integration in plant water use models, reliable measurements of tree water use variables are essential. The next and final section of this introductory chapter will discuss the most important methods to determine plant water use variables before focussing on the main subject of this study: sap flow measurements.

1.4 Measuring tree water use variables

'The numbers tell the tale' is a commonly heard expression in science, indicating that hypotheses and theories need to be sustained by factual measurements. It is obvious that fundamental concepts such as the cohesion-tension theory or hydraulic redistribution could only have been developed thanks to measurement methods allowing the assessment of a wide range of tree water use variables. This section briefly describes the most common methods to determine water potentials throughout the SPAC and to assess stem diameter changes, together with sap flow the most important variables in plant water use research.

1.4.1 Water potential measurements

Soil water potential

Soil matrix water potential is measured either by measuring properties of the soil which change with the water potential such as water content, electromagnetic radiation, infrared reflectance, thermal or electrical conductivity or by equilibrating the liquid or gas phase of the water in some reference medium with the liquid phase of the soil (Campbell, 1988). The most commonly applied method to determine soil matrix potential in-situ is probably tensiometry. Tensiometers exist of a porous cup, connected to a tube filled with de-ionised water (Sormail & Vachaud, 1969). At the top of this tube, a pressure transducer registers pressure changes above the water-air meniscus in the tube. As the cup is placed firmly in contact with the soil, the water inside the tensiometer will equilibrate with the soil water over the porous ceramic cup. When properly calibrated by means of a pressure calibrator, this simple method directly and continuously allows the determination of soil water matrix potentials. If, however, the surrounding soil becomes to dry, air will be able to enter the ceramic cup, distorting the tensiometer readings. Moreover, at low water potentials, water will start to evaporate inside the tube, causing cavitation inside the instrument. Therefore, tensiometers are limited to water potentials within the approximate range of 0 to -0.1 MPa, although equitensiometers are able to measure more negative water potentials.

A method to assess soil water potential as combination of matrix and osmotic potential is soil psychrometry. Based on the work of Hill (1930) and Spanner (1951b), Monteith & Owen (1958) employed the Peltier effect in their thermocouple

psychrometer design to measure the total suction of soil water. To this end, a fresh soil sample is placed in a small chamber with a high thermal mass. Within this chamber, the sample is left to equilibrate to ensure that the water potential of the air in the chamber is in equilibrium with the water potential of the soil sample. After equilibration, a small current is sent through the copper-constantan thermocouple located in the chamber above the soil sample. This Peltier current will cause the thermocouple to cool down below the dew point, inducing a water droplet to form on its surface. Then, the Peltier current is switched off and the thermocouple temperature rises again, causing a measurable voltage different because of the Seebeck effect. During the evaporation of the droplet, the temperature of the thermocouple stays constant, forming a plateau in the voltage readout. When the droplet is completely evaporated, the temperature further increases until it is again at its original value. This process results in a typical psychrometer output (Figure 1.9) in which the wet bulb depression (WBD) indicates the voltage difference between the output during evaporation of the droplet and the reference output. This WBD can be linearly related to the water potential based on a calibration of the psychrometer with NaCl solutions of which the water potentials are known.

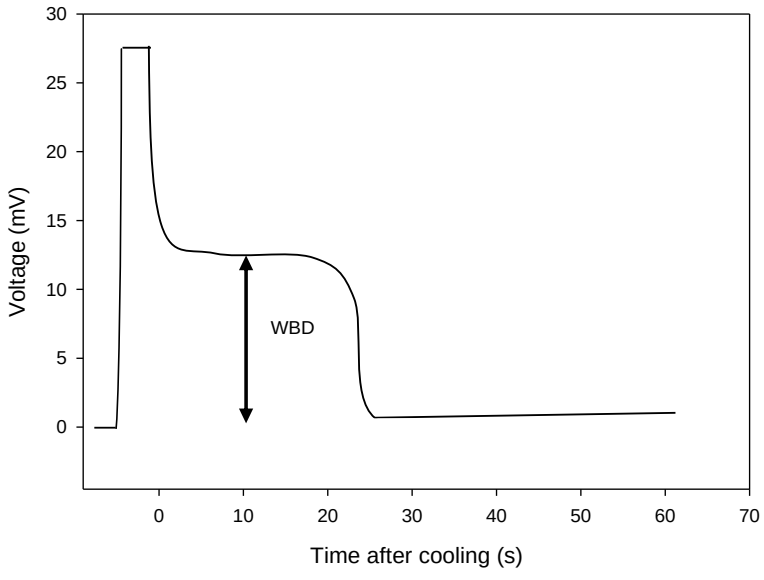

Figure 1.9 *Typical psychrometer output showing the voltage signal over time after the cooling of the thermocouple. The voltage difference between the evaporation output and the reference signal is indicated as the wet bulb depression (WBD) and is proportional to the water potential of the soil sample.*

The soil psychrometer as described above has a major practical limitation. Because of the need for stable temperature conditions and the insertions of soil sample in the psychrometer chamber, the method is limited to laboratory research (Monteith & Owen, 1958). Recently, however, soil psychrometers have been developed that allow on-site measurements. These have the minor disadvantage that they cannot be used in completely saturated soils and can only measure at sufficiently large depths in order to reach thermal equilibrium of the small psychrometer chambers.

Stem water potential

Similarly as for soil water potential measurements, the psychrometer principle can be applied to determine stem water potential. It was, however, not until the work of Dixon & Tyree (1984) that a practically applicable stem psychrometer was developed. These authors attached a small chamber holding two thermocouples to the sapwood after cutting away the bark. One of the thermocouples touches the sapwood while the other measures the temperature in the chamber, allowing measurement of and correction for the temperature gradient between the sample and the dew point measuring junction.

Leaf water potential

While leaf water potential can be measured with leaf psychrometers as well, this technique is less practical as a psychrometer chamber is much more difficult to properly attach on a leaf surface compared to a stem surface. Moreover, leaves are more prone to temperature changes which may influence the measurements. The more traditional device for measuring leaf or twig water potentials is the Scholander pressure bomb (Scholander *et al.*, 1965). This method is based on the fact that, when a leaf petiole or twig is cut, the xylem sap, which was under tension before cutting, will recede into the xylem below the cut surface. If then the leaf or twig is placed upside down in the chamber of the pressure bomb, a positive pressure can be raised which forces the sap back to the surface of the cut end. This positive pressure equals in absolute terms the tension that existed in the sap before the plant material was severed. If the osmotic potential of the sap can be ignored, this tension approximately equals the total water potential.

Measurements of water potentials of these three compartments have substantiated the cohesion-tension theory as under well watered conditions, water potentials

decline from soil to leaves during transpiration, forming a clear gradient to induce xylem sap flow.

1.4.2 Stem diameter fluctuations

The exchange of water between the internal storage pools and the transpiration stream causes small but detectable changes in the stem diameter of the tree, causing a typical day-night pattern (see Section 1.3.1). Moreover, irreversible growth causes a more linear expansion of the stem diameter over time during well watered conditions (Figure 1.11).

Stem growth rate of trees has been measured since the beginning of the eighteenth century. To this end, several different devices where developed, of which the manual band dendrometer was the most commonly applied (Studhalter *et al.*, 1963). While these manual 'dendrobands' only allow to determine average growth rates, modern automatic dendrobands or point dendrometers enable continuous measurements at high time resolutions.

Point dendrometers or Linear Variable Displacement Transducers (LVDTs) are based on the displacement of a cylindrical ferromagnetic core in a hollow metallic cylinder in which several coils are assembled (Figure 1.10 a). Shrinking or swelling of the stem moves the core inside the coil assembly which induces a voltage output. This output can then be related to the displacement by calibrating the point dendrometer in a fixed set-up during which a stepwise displacement is enforced on the sensor. Point dendrometers have the advantage that they can measure azimuthal differences in growth rate, allowing to study the phenomenon of 'patchy growth', known to occur in some species (Schmitz *et al.*, 2008). Automated band dendrometers, on the other hand, are assumed to provide more accurate estimations of average radial increments as the measurements represent a mean of all azimuthal radii (Pesonen *et al.*, 2004). These dendrobands consist of a stainless-steel band encircling the tree which is attached with a fastening mechanism to a rotating potentiometer (Figure 1.10 b). A constant force in the fastening mechanism ensures that the band rotates the axis of the potentiometer without sliding. Hence, movements in the steel band, because of shrinking or swelling, are transmitted to the potentiometer, creating a voltage signal. Based on a similar calibration as for the point dendrometer, the diameter variation can then be determined.

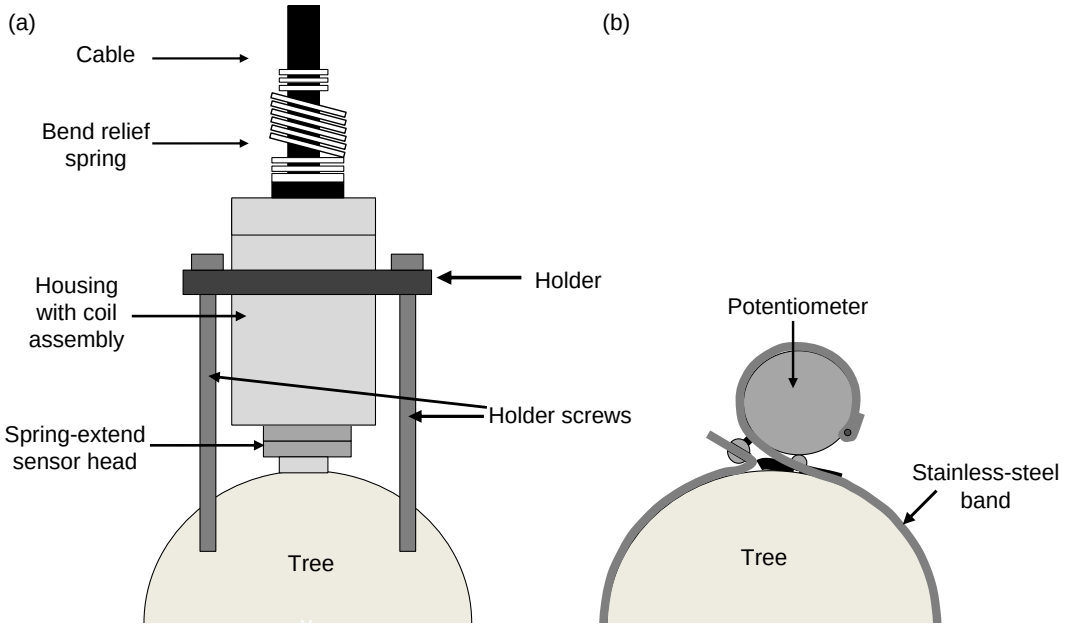

Figure 1.10 *(a) Point dendrometer, consisting of a movable rod fixed to a spring-extend sensor head. Shrinking and swelling of the tree causes the rod to be displaced in the housing, creating a voltage output linearly proportional to the displacement; and (b) band dendrometer, consisting of a stainless-steel metallic band tightened to the tree and fixed onto a potentiometer. Stem diameter variations cause the potentiometer to turn, inducing a voltage output again linearly proportional to the displacement.*

Next to the above mentioned contact methods, also optical methods have been developed to obtain measurements remotely. These are, however, much more expensive and their use has mainly been restricted to experimental studies in laboratory conditions (Pesonen *et al.*, 2004). Therefore, these will not be discussed in this work.

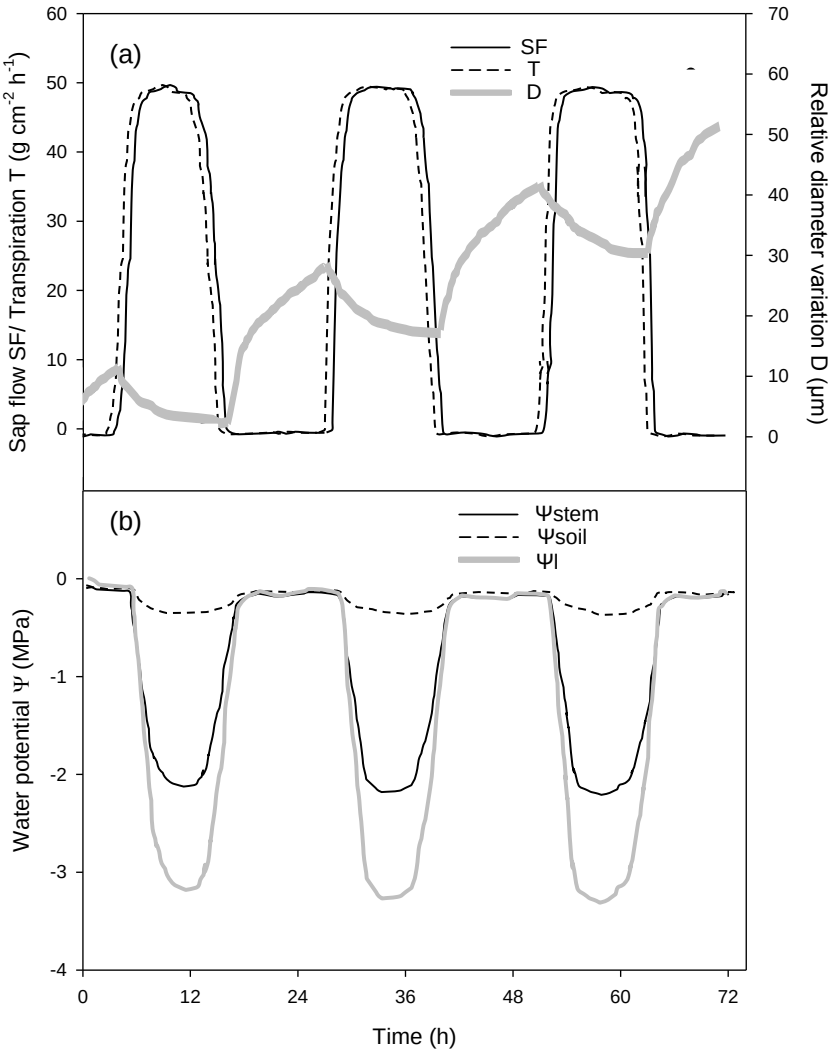

Figure 1.11 *A theoretical example of measured water use variables for a well watered tree: (a) a time lag exists between the transpiration T and the measured sap flow SF. During the morning, the water demand at leaf level exceeds the xylem supply, causing the stem to shrink. In the afternoon, the stomata start to close, reducing transpiration while sap is still being transported upwards, causing the stem to swell. Overall, a net growth occurs as new cells are formed; and (b) the stem (Ψstem), leaf (Ψl) and soil (Ψsoil) water potential, showing a clear gradient in which the water potential becomes more negative along the upwards flow path in the tree.*

Stem diameter variations and water potentials give a qualitative measure of water storage and flow direction and are an indication for drought stress in plants. Sap flow measurements, however, allow a quantitative assessment of water use in trees, besides a more profound investigation of flow directions and spatial flow variability. While for the estimation of stem diameter variations and water potentials the

measurement methods seem adequately developed, sap flow methods, although proven indispensable in plant-water research, still hold some limitations. The remainder of this PhD study will focus on these limitations and how to overcome them. However, to this end, a basic notion of existing sap flow methods is necessary. The following chapter therefore describes the most widely applied sap flow methods, their applicability and the factors most influencing their accuracy.

2

Commonly applied sap flow measurement methods and their limitations

After: Vandegehuchte, M.W. & Steppe, K. (2012). Sap flux density measurement methods: working principles and applicability. Functional Plant Biology, 40: 213-223.

Abstract

Sap flow measurements have become increasingly important in plant science. Since the early experiments with dyes, many methods have been developed. Most of these are based on the application of heat in the sapwood which is then transported by the moving sap. By measuring changes in the temperature field around the heater, sap flow can be derived. Although these methods have the same basis, their working principles largely vary. A first distinction can be made between those measuring the sap flow rate (m^3 s^{-1}) such as the Stem Heat Balance and Trunk sector Heat Balance

method and those measuring sap flux density (m^3 m^{-2} s^{-1}). Within the latter, the Thermal Dissipation and Heat Field Deformation methods are based on continuous heating, while the Heat Pulse Velocity, Tmax, Heat Ratio and Calibrated Average Gradient methods are based on the application of heat pulses. Each of these methods has its advantages and limitations. This chapter reviews the existing methods to understand the basics of sap flow methodology and as a stepping stone to allow further improvement in sap flux density measurement techniques.

2.1 Introduction

As mentioned in the general introduction of this PhD study, the scientific interest in measuring sap flow to study plant water relations is not new. Application of dyes to trace sap flow in stems and roots has been practiced since the beginning of the previous century (Dixon, 1914; James & Baker, 1933; Kramer, 1940). However, as this method necessitates plant cutting to determine the ascent of the dye, alternatives were sought. Huber (1932) was one of the first to report the use of heat as a tracer to determine sap flow. By measuring the time it took for a heat pulse to reach a certain distance downstream from the heater, a measure for sap flux density was obtained. This method was further developed by Dixon (1936) and Huber and Schmidt (1937), adding a correction to account for conduction velocity. It was, however, Marshall (1958) who described the analytical background of heat conduction-convection which led to the theoretical basis for further development of the heat pulse based sap flux density methods.

Besides these heat pulse methods, others which apply continuous heating were developed. The work of Vieweg and Ziegler (1960) underlay the development of the Heat Balance methods to determine sap flow rate (Daum, 1967; Cermak *et al.*, 1973; Kucera *et al.*, 1977; Sakuratani, 1981, 1984; Baker & Van Bavel, 1987; Steinberg *et al.*, 1989) and the continuous heat sap flux density methods (Ittner, 1968; Balek & Pavlik, 1977; Granier, 1985; Nadezhdina *et al.*, 1998; Nadezhdina *et al.*, 2012).

Within the existing sap flow methods, a distinction must be made between those measuring sap flow rate (m^3 s^{-1} or g h^{-1}), determining the total sap flow in a plant stem or stem section, and those measuring sap flux density (m^3 m^{-2} s^{-1} or cm^3 cm^{-2} h^{-1}), assessing the amount of sap flowing through a certain surface per time. While the former are very useful for estimating whole plant water use, they are less suited to

investigation of variation in sap flow within the plant, e.g. radial sap flow profiles or hydraulic redistribution. As sap flux density methods can discern spatial differences in sap flux density within the plant, whether circumferentially, radially or vertically, they allow more detailed investigation of hydraulic plant traits. Assessment of radial variation can be obtained by applying multiple sensors or incorporating measurement points at different depths within a single sensor.

Sap flow rate can be measured by either the Stem Heat Balance (SHB) or Trunk Heat Balance (THB) method. Both methods solve the heat balance over a stem section of the plant during continuous application of heat to the tissue, applying a constant or variable power. As these methods have been clearly described by Smith and Allen (1996) and the operational principles of the methods remain unaltered, readers are referred to this work for more in-depth information on sap flow rate methodology. The purpose of this chapter is to present an updated review on recent developments in sap flux density measurement methods as these will be the further focus of this PhD study. By describing the underlying theory of each method and discussing some of their most common practical and theoretical issues, we hope to encourage further improvements. This chapter does not provide a complete description of all sap flux density methods, readers are instead referred to the original methodology papers for each method in the corresponding section. Neither does it provide a description of the benefits that sap flow methods have provided in plant science nor of sampling or scaling problems. Table 2.1 provides a comparison of the main features of all the sap flux density methods included in this chapter.

Table 2.1 *An overview of most common sap flux density methods, indicating the measurement frequency, in which range they are applicable, if they are influenced by Natural Temperature Gradients (NTG) or wounding, whether wound corrections are available and if so, which type and some important comments.*

Method	Measures	Frequency	Range	Zero flow needed	NTG	Wounding	Wound correction	Comments
Empirical continuous methods								
Thermal Dissipation	sap flux density ($m^3\ m^{-2}\ s^{-1}$)	continuous	low, moderate and high flows	yes	yes	yes	not developed	needs empirical calibration
Heat Field Deformation	sap flux density ($m^3\ m^{-2}\ s^{-1}$)	continuous	reverse to high flows	no	?	yes	not developed	needs empirical calibration
Theoretical heat pulse methods								
Compensation Heat Pulse	sap flux density ($m^3\ m^{-2}\ s^{-1}$)	pulsed	moderate and high flows	no	no	yes	$V_{h\_corr}=a+bV_h+cV_h^2$	
Tmax	sap flux density ($m^3\ m^{-2}\ s^{-1}$)	pulsed	moderate and high flows	depending on diffusivitydetermination	no	yes	$V_{h\_corr}=a+bV_h+cV_h^2$	needs diffusivity determination

Heat Ratio	sap flux density ($m^3\ m^{-2}\ s^{-1}$)	pulsed	reverse, to moderate flows	depending on diffusivity determination	no	yes	$V_{h\_corr}=dV_h$	needs diffusivity determination
Calibrated Average Gradient	sap flux density ($m^3\ m^{-2}\ s^{-1}$)	pulsed	zero to high flows	no	yes	yes	not developed	needs empirical calibration

2.2 Continuous heat sap flux density methods

2.2.1 Thermal dissipation (TD) method

The Thermal Dissipation method (TD), often referred to as TDP (thermal dissipation probe) or HD (heat dissipation) method, as developed by Granier (1985, 1987) based on the work of Vieweg and Ziegler (1960), is the most widely applied sap flux density method because of its simplicity and low costs. It enables low, average and high sap flux density estimations but needs zero flow conditions for its calculations. The method relates sap flux density *SFD* (m^3 m^{-2} s^{-1}) to a temperature difference ΔT (K), measured between a constant heated probe and an unheated probe located 10 cm lower in the xylem, based on an experimental regression for three species (*Pseutotsuga menziessii* (Mirb.) Franco, *Pinus nigra* Arnold and *Quercus pedunculata* Ahrh.) and artificial columns filled with synthetic fibre and sawdust:

$$SFD = 0.000119\left(\frac{\Delta T_0 - \Delta T}{\Delta T}\right)^{1.231} \qquad (2.1)$$

where ΔT_0 is the temperature difference ΔT assessed during a period of zero flow. The method is not capable of distinguishing flow direction as reverse flow will also decrease ΔT. Moreover, the original assumption of Granier (1985) that the experimental regression coefficients as shown in Eq. 2.1 are species independent, which was confirmed for *Prunus malus* and *Castanea sativa* (Köstner *et al.*, 1998), has been contested by many studies. Underestimations, ranging between 6 and 90 %, have been reported for a wide variety of species when comparing the TD to other methods (Lundblad *et al.*, 2001; Bovard *et al.*, 2005; Silva *et al.*, 2008; Iida & Tanaka, 2010) or during new calibration experiments on excised stem or branch segments (de Oliveira Reis *et al.*, 2006; Taneda & Sperry, 2008; Bush *et al.*, 2010; Hultine *et al.*, 2010; Steppe *et al.*, 2010), cut trees (Lu & Chacko, 1998; Uddling *et al.*, 2009) or potted plants (Braun & Schmid, 1999; McCulloh *et al.*, 2007). Several possible reasons have been indicated for these underestimations (Lu *et al.*, 2004), including deviations from the original sensor design, gradients in the radial *SFD* profile (Clearwater *et al.*, 1999; Wullschleger *et al.*, 2011) and wound effects (Wullschleger *et al.*, 2011). Moreover, Clearwater *et al.* (1999) have shown that if the probe is partly installed in non-conductive tissue, large underestimations occur. Therefore, they suggested the following correction:

$$\Delta T_{sw} = \frac{\Delta T - b\Delta T_m}{a} \qquad (2.2)$$

with ΔT_{sw} being the corrected temperature difference for the portion of the heated probe within conductive sapwood, ΔT_m the temperature difference for the portion of the probe in inactive xylem (assumed equal to ΔT_0) and *a* and *b* the proportion of the length of the heated probe in contact with the sapwood and inactive xylem, respectively. This correction, however, necessitates an accurate estimation of the position of boundaries between active and inactive xylem that are spanned by the probe, which is often difficult to obtain in practice without destructive measurements.

Hence, while the original goal of the TD method was to formulate a generally applicable, species independent empirical relation between the measured temperature ratio and sap flux density, it is now clear that species or even tree specific calibrations are necessary to obtain accurate results. Given these specific calibrations, the TD method enables measurements of low, average and high *SFD* if zero flow occurs to determine ΔT_0. In practice, however, zero flow is often not reached because of night-time water uptake for vegetative or reproductive growth, replenishment of internal storage (Zweifel *et al.*, 2001; Steppe *et al.*, 2006), Münch counterflow (De Schepper & Steppe, 2010) and water loss due to a high vapour pressure deficit in combination with a high wind speed (Snyder *et al.*, 2003). In these cases, ΔT_0 values will be underestimated, leading to underestimations of *SFD*. Therefore, it has been suggested to use the maximum ΔT_0 value reached during a measurement campaign if destructive determination of ΔT_0 by cutting the sapwood above and below the sensor is not possible (Lu *et al.*, 2004). If, however, reverse flow occurs, this procedure would lead to overestimations of *SFD*. Hence, while the TD method allows many repetitions given its low costs and is easy to apply, which explains its popularity in ecophysiological research, it is mainly suited to determine relative flow changes as accurate sap flux density measurements require specific calibrations and a correct estimation of zero flow.

2.2.2 Heat field deformation (HFD) method

Like the TD method, the HFD method is based on temperature changes measured in a changing heat field around a continuously heated needle. However, while the TD method only measures axial temperature differences, the HFD method also consists

of a tangential needle, making it sensitive towards a wide range of sap flux densities (Nadezhdina *et al.*, 1998; Nadezhdina *et al.*, 2012). Moreover, thanks to the symmetrical axial needle configuration, also zero and reverse flows can be determined (Figure 2.1). The first needle is installed above the heater (axial direction), the second needle next to the heater (tangential direction) and the third needle below the heater (axial direction). Temperature differences measured between the upper and lower (axial) needles (ΔT_{sym}) allow for both bi-directional and very low flow measurements. The temperature differences measured between the tangential and the lower axial needle (ΔT_{as}) are important to distinguish high from low sap flux densities. Additionally, the HFD sensor needles are equipped with thermocouples at several depths, enabling radial sap flux density profile assessment. This feature can, however, also be incorporated in the other sap flux density methods.

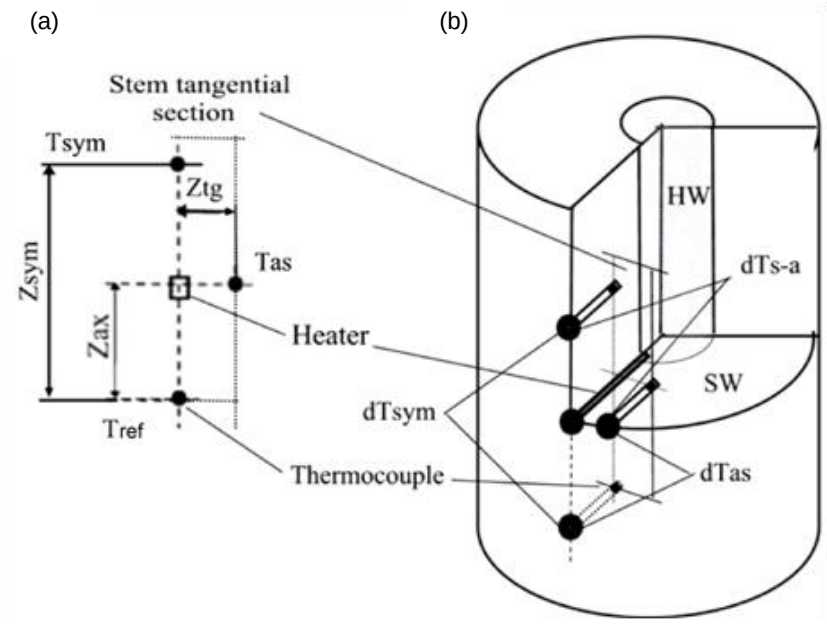

Figure 2.1 *(a) Schematic of a tangential section of the stem xylem with arrangements of the thermocouples around the heater of the HFD sensor; and (b) Schematic of the HFD sensor installed in the sapwood (SW) of a stem. Two temperature differences are measured: the symmetrical temperature difference (dT_{sym}) and the asymmetrical temperature difference (dT_{as}). The third temperature difference ($dT_{s\text{-}a}$) can be calculated as the difference between dT_{sym} and dT_{as}. After Nadezhdina et al. (2012).*

Basically, the HFD method is founded on an empirical temperature ratio which has shown to be related to sap flux density (Nadezhdina, 1988; Nadezhdina *et al.*, 1998; Nadezhdina, 1999; Nadezhdina *et al.*, 2012)

$$SFD = D\frac{\Delta T_{s-a} + \Delta T_{0(s-a)}}{\Delta T_{as}}\frac{Z_{ax}}{Z_{tg}}\frac{1}{L_{sw}} \qquad (2.3)$$

with $\Delta T_{s\text{-}a}$ the temperature difference between the axial downstream and tangential measurement needle, $\Delta T_{0(s\text{-}a)}$ this difference at zero flow (originally referred to as the *K* value (Nadezhdina *et al.*, 1998)) and ΔT_{as} the temperature difference between the tangential and axial upstream needle, respectively. This temperature ratio is linked to *SFD* by multiplication with thermal diffusivity *D* (m^2 s^{-1}), a spatial correction factor Z_{ax} Z_{tg}^{-1} and a correction for sapwood depth L_{sw} (m). For *D*, a nominal value of 2.5×10^{-3} cm^2 s^{-1} is typically used as suggested by Marshall (1958). The addition of these terms to the original HFD temperature ratio are, however, somewhat random as they are empirically derived and therefore do not seem based on found thermodynamics (Nadezhdina *et al.*, 2012).

Unlike the TD method or heat balance sensors, zero flow is not necessary to determine $\Delta T_{0(s\text{-}a)}$ as it can be derived by linear extrapolation of ΔT_{as} or $\Delta T_{s\text{-}a}$ vs $\Delta T_{sym}/\Delta T_{as}$ with ΔT_{sym} the temperature difference between the axial downstream and upstream needle (Figure 2.2). Because of its sensitivity towards a wide range of sap flux densities and the integration of measurements at multiple depths, the HFD method has played a crucial role in the research on hydraulic redistribution and radial sap flux density profiles (Nadezhdina *et al.*, 2002; Nadezhdina *et al.*, 2009; Nadezhdina, 2010; Nadezhdina *et al.*, 2010; Leonardo Reyes-Acosta & Lubczynski, 2012).

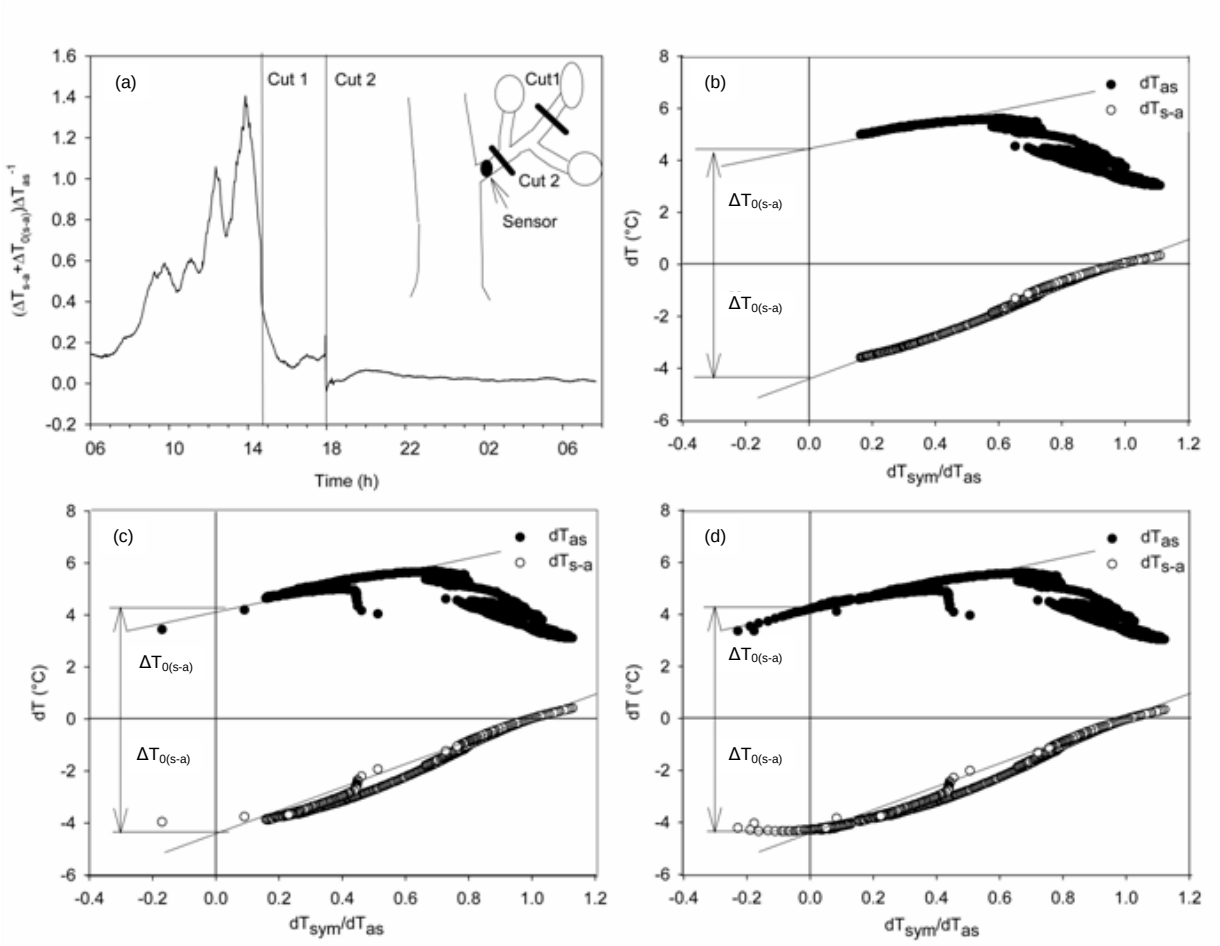

Figure 2.2 *(a) HFD temperature ratio with a schematic diagram of the gradually cutting of shoots of a branch to provide conditions of zero flow; (b) dT_{as} and dT_{s-a} for measurements when the branch is still intact (no cutting); (c) dT_{as} and dT_{s-a} for measurements when the branch is cut at position 1; and (d): dT_{as} and dT_{s-a} for measurements when the branch is cut at position 2. After Nadezhdina et al. (2012).*

2.2.3 Natural temperature gradients

Natural temperature gradients (NTG) are temperature gradients occurring in the sapwood of plants that are not caused by the intentional heating from the sap flow measuring methods. These gradients have, amongst others, been attributed to differences in thermal heat storage in the soil, stem and root tissues resulting in temperature differences between the sap and the plant tissues (Cermak & Kucera, 1981; Köstner *et al.*, 1998; Do & Rocheteau, 2002a) and to the influence of direct solar radiation (Lu *et al.*, 2004). While these influences can be minimized by

shielding the gauge from radiation and locating it sufficiently high above the ground, the effect of natural gradients can never be excluded completely.

The influence of NTG on the TD method has been extensively studied and has shown to lead to errors of over 100% if not corrected for (Goulden & Field, 1994; Do & Rocheteau, 2002a, 2002b; Lu *et al.*, 2004; Reyes-Acosta *et al.*, 2012). The first attempts to correct for NTG were focussed on measuring NTG on neighbouring trees or on different positions in the tree that are being monitored (Köstner *et al.*, 1998). These methods, however, require NTG to be uniform within or between trees. Therefore, more recent corrections are based on NTG measurements by periodically switching the heater off. Do & Rocheteau (2002b) developed a cyclic TD system for which a specific calibration was developed to account for non-steady state temperatures regimes, significantly reducing the influence of NTG. This method was updated by Ayutthaya *et al.* (2010) who improved the calibration coefficients. Recently, Reyes-Acosta *et al.* (2012) further improved this method by extrapolating the TD signal to thermal equilibrium, allowing the use of the original Granier calibration. Moreover, their method enabled shorter measuring intervals, leading to a higher measurement resolution. A further improvement of this method would be the use of a single heated probe as was applied by Do *et al.* (2011) for their original cycling method as this would reduce costs and complexity.

The influence of NTG on HFD measurements has not been reported yet. Because of the shorter distances between the needles and their closer proximity to the heater, the influence of NTG is expected to be smaller for the HFD than for the TD method.

2.3 Heat pulse sap flux density methods

Unlike the continuous heat methods mentioned above, heat pulse methods are based on the fundamental heat conduction-convection equation as presented by Marshall (1958), derived from Carslaw and Jaeger (1947), for an instantaneous ideal heater. All heat pulse methods derive heat pulse velocity V_h from measured temperature differences at specific locations around the heater after application of a heat pulse. As the measurement procedures are based on the dissipation of the heat after application of the pulse, heat pulse methods cannot measure continuously, with the measurement frequency depending on the time span needed

to reach thermal equilibrium again after having applied the heat pulse. These heat velocities then need to be converted to sap flux densities:

$$SFD = \frac{\rho_d}{\rho_s}(MC + \frac{c_{dw}}{c_s})V_h \qquad (2.4)$$

where *SFD* is the sap flux density (m^3 m^{-2} s^{-1}), V_h the heat velocity (m s^{-1}), *MC* the sapwood water content (weight of water over dry weight of wood), c_{dw} the specific heat capacity of the woody matrix (1200 J kg^{-1} K^{-1}, Edwards and Warwick (1984)), ρ_d the dry density of the sapwood (kg m^{-3}), ρ_s the density of the sap (assumed to be the density of water, 1000 kg m^{-3}) and c_s the specific heat capacity of the sap (assumed to be that of water, 4186 J kg^{-1} K^{-1}, Edwards and Warwick (1984)). Dry wood density and water content are usually derived from wood-core measurements, implying that variations in *MC* are often not taken into account, unless other techniques are applied such as Time Domain Reflectometry (Wullschleger *et al.*, 1996a; Nadler *et al.*, 2003; Nadler *et al.*, 2006), Frequency Domain Reflectometry (Hao *et al.*, 2013), Magnetic Resonance Imaging (Van As *et al.*, 2009) or vibration methods (Iki *et al.*, 2009). However, these methods require additional equipment and analysis and the gravimetric method remains the reference method to determine *MC* in trees.

As heat pulse methods are based on temporal temperature differences at the same measurement position, unlike continuous methods which apply spatial temperature differences between different positions, they are hardly susceptible to NTG (with the exception of the Calibrated Average Gradient method) (Table 2.1).

2.3.1 Compensation Heat Pulse velocity (CHP) method

The CHP method, often also referred to as heat pulse velocity (HPV) method, is based on the time t_c after application of the heat pulse at which the temperature at a distance x_{up} upstream of the heater needle is equal to the temperature at a distance x_{down} downstream of the heater (Swanson, 1972; Swanson & Whitfield, 1981):

$$V_h = \frac{x_{down} - x_{up}}{2t_c} \qquad (2.5)$$

This method has the advantage that it is independent of thermal diffusivity, a sapwood characteristic that has to be determined for the Tmax and HR method. However, Eq. 2.5 is developed for an ideal heat pulse with an infinitesimally small

length and is not theoretically correct for a step heat pulse, leading to underestimations that increase with pulse length.

Moreover, CHP fails to measure reverse, low or very high flows (<5 cm h^{-1} and >100 cm h^{-1}) as then no intersection between the upstream and downstream temperatures occur. Besides, Green *et al.* (2009) have shown that for low wood water contents (from 28 to 55%), V_h decreases for increasing water contents. Despite these shortcomings, the CHP method is widely applied for irrigation purposes (e.g. Edwards & Warwick, 1984; Green & Clothier, 1988; Tognetti *et al.*, 2004; Pereira *et al.*, 2007; Madurapperuma *et al.*, 2009a; Madurapperuma *et al.*, 2009b) and to assess water use of trees in ecophysiological research (e.g. Morris & Collopy, 1999; Hirose *et al.*, 2005; Liu *et al.*, 2012; Ma *et al.*, 2012).

2.3.2 Tmax method

The Tmax method (Cohen *et al.*, 1981), determines V_h based on the time t_m at which the temperature measured at a distance d from the heater becomes maximal:

$$V_h = \frac{\sqrt{d^2 - 4D\,t_m}}{t_m} \qquad (2.6)$$

with D the thermal diffusivity of the sapwood ($m^2\ s^{-1}$), determined during zero flow conditions:

$$D = \frac{d^2}{4t_m} \qquad (2.7)$$

Eq. 2.6 and 2.7 were later updated by Kluitenberg & Ham (2004) for step heat pulses instead of instantaneous heat pulses:

$$V_h = \sqrt{\frac{4D}{t_0}\ln\left(1-\frac{t_0}{t_m}\right)+\frac{d^2}{t_m(t_m-t_0)}} \qquad (2.8)$$

$$D = \frac{d^2}{4t_m}\frac{t_0}{(t_m-t_0)}\left[\ln\left(\frac{t_m}{t_m-t_0}\right)\right]^{-1} \qquad (2.9)$$

where t_0 is the heat pulse duration.

Green *et al.* (2003) have shown that a curve smoothing procedure led to better results as t_m is difficult to accurately determine from the raw temperature data

during low flows because of noise. However, even with curve smoothing procedures, the Tmax method cannot distinguish between zero and low flux densities (<20 $cm^3\ cm^{-2}\ h^{-1}$) as the relationship between t_m and *SFD* is non-unique at these low flux densities (Figure 2.3) (Becker, 1998). Besides, as for the heat balance and the TD method, zero flow conditions are difficult to ensure, making non-destructive *D* estimations impractical. Both Cohen *et al.* (1981) and Green *et al.* (2003) have, however, confirmed that a 10% error in *D* only leads to errors of up to 3% in V_h and hence *SFD*. Because its the higher complexity in comparison to the CHP method, the Tmax method has been less frequently applied. Nevertheless, the field of plant-water research has undoubtedly benefited from its use (e.g. Cohen, 1991; Schiller & Cohen, 1998; Cohen *et al.*, 2008).

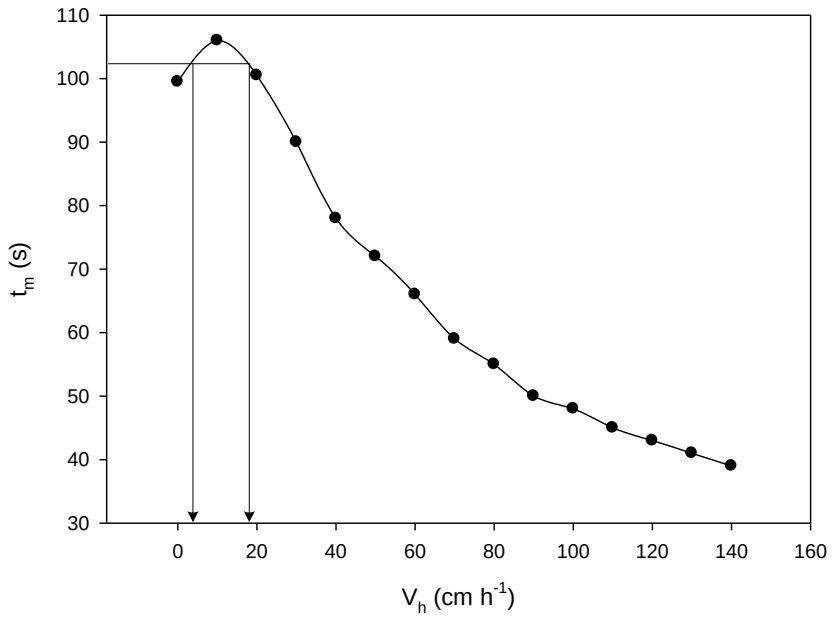

Figure 2.3 *Time to maximum (t_m) versus heat velocity V_h based on the FEM output for a measurement probe at 1 cm downstream from the heater, a water content of 0.75, a dry wood density of 550 kg m^{-3} and an axial and tangential thermal conductivity of 0.63 and 0.42 W m^{-1} K^{-1}, respectively. Wound effects were included in the model.*

2.3.3 Heat Ratio (HR) method

In an answer to the difficulties in measuring low flows with the CHP and Tmax method, Burgess *et al.* (2001a) developed the HR method, based on a suggestion presented in Marshall (1958):

$$V_h = \frac{D}{x} \ln\left(\frac{\Delta T_{down}}{\Delta T_{up}}\right) \qquad (2.10)$$

with ΔT_{down} and ΔT_{up} the increases in temperature at equal distances x (m) downstream and upstream from the heater needle, respectively. In practice the temperature ratio $\Delta T_{down}/\Delta T_{up}$ does not remain constant with time because of non-ideality due to wound effects. However, the rate of change in this temperature ratio becomes negligible after about 60 s. Therefore, the average temperature ratio of measurements between 60 and 100 s after application of the heat pulse are used to determine V_h.

As for the Tmax method, D needs to be determined. Burgess *et al.* (2001a) based this determination on previous work of Swanson (1983) who applied an empirical equation deducted by Siau (1971), only necessitating a wood core sample to determine MC and ρ_d. Another option is to determine D according to Eq. 2.7. For the HR method, however, a 10% error in D will lead to an equal error in V_h, making this option less favorable as zero flow can be difficult to ensure.

Given a good estimation of D, the HR method has proven its value for measuring low and reverse flows. It is, however, limited for high flows (>55 $cm^3\ cm^{-2}\ h^{-1}$) (Bleby *et al.*, 2008) as for these flows, the ΔT_{up} signal decreases, reducing the sensitivity of Eq. 2.10. Nevertheless, since its description by Burgess *et al.* (2001a), the HR method has rapidly gained popularity and has been applied throughout the entire spectrum of plant-water research, ranging from irrigation (Madurapperuma *et al.*, 2009a) and the impact of tree and stand structure on tree water use (Ambrose *et al.*, 2009; Pfautsch *et al.*, 2010) to those phenomena requiring accurate measurements of low and reverse flow such as nocturnal sap flow (e.g. Dawson *et al.*, 2007; Fisher *et al.*, 2007) and hydraulic redistribution (e.g. Hultine *et al.*, 2003b; Burgess & Dawson, 2004; Oliveira *et al.*, 2005a; Oliveira *et al.*, 2005b; Scott *et al.*, 2008).

Recently, Clearwater *et al.* (2009) developed an external HR method enabling sap flux density measurements for small diameter stem (< 5 mm). D was derived based on Eq. 2.7 and was found to be dependent on both the stem and the cork material applied to fix the sensor. Promising results were obtained for low and reverse flows ($-7.5\ cm\ h^{-1} < V_h < 7.5\ cm\ h^{-1}$).

2.3.4 Calibrated Average Gradient (CAG) method

Another promising heat pulse method, the CAG method, has been proposed by Testi & Villalobos (2009). These authors extended the CHP method to enable low and even zero flow measurements. Both results from Finite Element Models (FEM) and field experiments confirmed that for low flows (V_h<30 cm h^{-1}), V_h was linearly correlated to ΔT_a, the average temperature difference between the downstream and upstream temperature sensors during the 180 seconds after application of the heat pulse (Figure 2.4). By extrapolating this linear relationship, which is only dependent on sensor characteristics and thermal properties of the sapwood, low and zero flows can be measured based on ΔT_a, while for high flows, the original CHP method is applied. The use of the average temperature gradient, however, implies that the CAG method is likely to be influenced by NTG. While for the other methods, only the temperatures before and after application of the heat pulse are of importance, here the temperature difference between downstream and upstream positions is needed during the entire 180 s. By extrapolating this linear relationship, which is only dependent on sensor characteristics and thermal properties of the sapwood, low and zero flows can be measured based on ΔT_a, while for high flows, the original CHP method is applied.

The use of the average temperature gradient, however, implies that the CAG method is likely to be influences by NTG. While for the other methods, only the temperatures before and after application of the heat pulse are of importance, here the temperature difference between downstream and upstream positions is needed during the entire 180 s. Hence, while for the other methods the relative temperature changes are not influenced by a shift in absolute temperature, this will likely affect the CAG method, reducing the ΔT_a signal for positive gradients from roots to crown and vice versa and, hence, influencing the linear relationship between V_h and ΔT_a. Therefore, the effects of NTG on the CAG method should be further investigated. Moreover, if the thermal properties of the sapwood change significantly during the measurement period, a new linear relationship should be established.

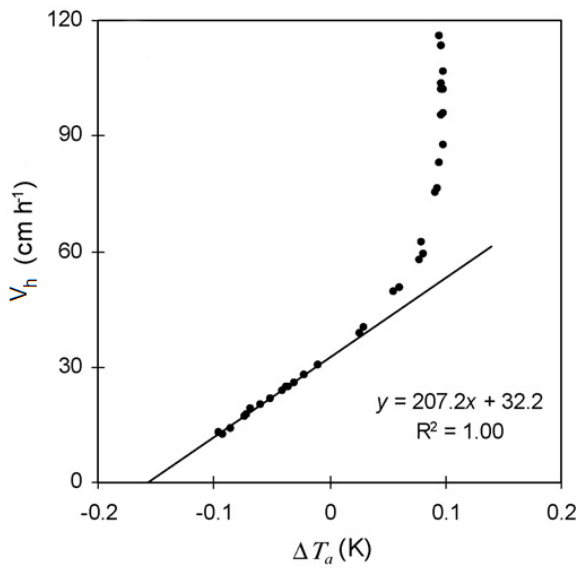

Figure 2.4 *V_h versus ΔT_a for Olea europaea. The line is the regression of V_h on ΔT_a obtained with the data pairs where ΔT_a<0 K, taken during 24 h (adapted from Testi and Villalobos (2009)).*

2.4 Sensor spacing

All sap flux density methods are based on the insertion of measurement and heater needles into the sapwood. With exception of the TD method, all methods have probe spacing directly incorporated in their sap flux density equations. Hence, while for the TD method exact spacing is less important as long as the reference probe is not influenced by the heated probe, for the other methods correct spacing is crucial (Cohen *et al.*, 1981; Swanson, 1983; Burgess *et al.*, 2001a). Probe misplacement can be assessed by placing over-length probes in the drill holes, enabling measurement of the spacing and angle between the probes (Hatton *et al.*, 1995). Moreover, for the HR method, Burgess *et al.* (2001a) measured probe placement in situ, based on zero flow conditions. However, parallel placement of the needles remains crucial for accurate results and is often difficult to ensure, especially at large sapwood depths. If probes are installed parallel, but needles are tangentially displaced, this cannot be taken into account. Generally, applying a specific drill-bit template for each heat pulse method can improve probe positioning during sensor installation.

2.5 Wounding

When inserting probes in the sapwood, flow is locally obstructed with the obstructed zone dependent on sensor geometry and probe size and, to a lesser extent, probe material (Swanson & Whitfield, 1981; Barrett *et al.*, 1995; Green *et al.*, 2003). Barrett *et al.* (1995) have shown that wounding also affects wood density and fibre direction, especially in the axial direction. Besides these direct wound effects, probe insertion also induces the formation of wound tissue which alters wood properties and, hence, heat dissipation in this wood in the longer term (Moore *et al.*, 2009). This long-term effect can be avoided by regularly reinstalling sensors during long-term experiments, although little research has been done on the required frequency of reinstallation (Moore *et al.*, 2009).

Short-term wounding, on the other hand, has been assessed to be an important error-inducing factor for the TD method (Wullschleger *et al.*, 2011). These authors developed a numerical heat flow model to assess TD performance, allowing investigation of error inducing factors both separately and combined. They determined that physical disruption of the xylem due to wounding was a significant cause of error, besides gradients in the radial sap flux density profile.

Moreover, Wullschleger *et al.* (2011) have shown that the TD method is sensitive to changes in thermal conductivity and, hence, is dependent on sapwood characteristics. This implies that for a specific tree species, the calibration could change due to varying dry wood density of the sapwood and, even for a single tree, could change due to variations in sapwood water content as wounding progresses. According to their modelling results, a combination of these error inducing factors can lead to both under- and overestimations of sap flux density when using the original calibration coefficients. These authors justly warn users of the TD method to interpret their results with caution and plead for an approach where numerical modelling is combined with updated calibration coefficients to improve TD method accuracy. Unlike for the TD method, wounding has not been thoroughly assessed for the HFD method, although it is expected to have a similar influence on the results.

Next to the continuous heat methods, flow path obstruction due to wounding also greatly influences the sap flux density results for heat pulse methods. Based on Finite Element Modelling (FEM), it has been shown that wounding partially interrupts

sap flow, leading to underestimations of V_h and hence *SFD* of up to 50% and more (Swanson, 1983; Burgess *et al.*, 2001a; Green *et al.*, 2003). Therefore, wound correction equations were developed for the existing heat pulse systems based on FEM. Wound width has been shown to have a much larger effect than probe material, calibration factors based only on wound width therefore seem sufficient for a given sensor configuration (Swanson, 1983; Green *et al.*, 2003). For the CHP method, Swanson & Whitfield (1981) developed readily applicable wound correction coefficients a, b and c for the correction equation $V_{h\_corr}=a+bV_h+cV_h^2$, where V_{h_corr} is the heat velocity corrected for wound effects (Table 2.1). While Cohen *et al.* (1981) derived correction factors for the Tmax method empirically, Green *et al.* (2003) presented similar wound corrections for the Tmax method as those developed by Swanson and Whitfield (1981) for the CHP method. For the HR method, Burgess *et al.* (2001a) have shown that a linear correction equation is sufficient.

For hardwood species with a markedly non-uniform distribution of sap-conducting vessels, however, an additional correction factor besides the wound correction may be necessary. This type of wood diverges more from the assumption of thermal homogeneity, on which the heat conduction-convection equations are based, than for softwoods or hardwoods with closely-spaced and more uniform xylem elements (Swanson, 1983; Green & Clothier, 1988). This correction factor can be empirically determined or derived from enhanced FEM including vessel anatomy.

In the various models used to assess wounding, flow obstruction is implemented as a region of zero flow starting from the most upstream sensor needle and stretching on downstream with a width slightly larger than the sensor needles. While the effect of different wound widths and sapwood water contents have been simulated, the axial length of the zero flow region has never been mentioned (Swanson & Whitfield, 1981; Burgess *et al.*, 2001a; Green *et al.*, 2003). Nevertheless, it is likely that this length will differ depending on wood anatomy. In addition, apart from flow obstruction, wood properties also can be locally altered due to installation. It would be interesting to investigate wound effects for different sapwood types and assess possible differences in wound correction factors. Also, FEM could be improved by including differences in vessel anatomy. In this way, the accuracy of heat pulse based sap flux density estimates might be enhanced.

2.6 General conclusions

Throughout the years, many sap flow methods have been developed, each with their advantages and disadvantages. Heat balance methods integrate flow in the entire stem or in a large stem section of the plant, giving a good indication of total plant water use. Sap flux density methods, on the other hand, give more precise information on flow directions and spatial flow distribution. For many methods, wounding influences sap flow results. Despite the existing wound corrections for the heat pulse methods, a more thorough insight in wound effects, including long-term experiments combining sap flow methods with FEM and more advanced techniques such as Magnetic Resonance Imaging, will likely further improve sap flow methodology.

So far, the HFD is the only method enabling measurements across the entire naturally occurring sap flow range. However, the link between *SFD* and the HFD temperature ratio is somewhat obscure, raising questions on the accuracy of HFD measurements. Therefore, the next chapter discusses the original HFD equation (Eq. 2.3) more thoroughly.

3

Erroneous use of thermal diffusivity in the Heat Field Deformation method

After: Vandegehuchte, M.W. & Steppe, K. (2012). Interpreting the Heat Field Deformation method: Erroneous use of thermal diffusivity and improved correlation between temperature ratio and sap flux density. Agricultural and Forest Meteorology, 162-163: 91-97.

Abstract

The Heat Field Deformation (HFD) method is a modern technique to assess sap flux density in trees by applying an equation which relates an empirical temperature ratio to the thermal diffusivity of the sapwood. However, this relation is based on a misinterpretation of thermal diffusivity, leading to physically incorrect units of sap

flux density. Moreover, the HFD method has recently been shown to occasionally underestimate actual sap flux densities, raising the question whether species specific calibration is necessary. This chapter calls attention to a correct interpretation of thermal diffusivity and investigates the correlation between sap flux density and the HFD temperature ratio based on a 3D Finite Element Model. It is shown that the original terms linking the HFD temperature ratio to sap flux density do not follow fundamental thermodynamics and, therefore, the HFD method should be considered merely empirical. Besides, the method is not only dependent on sapwood characteristics but also on sap flux density itself, necessitating a specific calibration equation.

3.1 Introduction

The main goals of the development of the Heat Field Deformation (HFD) method were (i) establishing a good linear correlation between measured temperature signals and sap flow for both low and high sap flow rates, (ii) the possibility to measure reverse flows and (iii) the ability to perform sap flow calculations without the need to assume night-time zero flow conditions. Moreover, it was also an objective to be able to determine sap flux densities at different depths within the sapwood (Nadezhdina *et al.*, 1998; Nadezhdina *et al.*, 2012).

As explained in section 2.2.2, the HFD method is principally based on the dynamics of a temperature ratio including a symmetrical (axial) and an asymmetrical (tangential) temperature difference to characterize the changing heat field around a continuous heater for different sap flux densities (Figure 2.1). To relate this temperature ratio to sap flux density, it was multiplied by thermal diffusivity based on the approaches of Marshall (1958) and Saddler & Pitman (1970) to determine sap flow by heat based sensors. To obtain units of $m^3\ m^{-2}\ s^{-1}$, the thermal diffusivity was then multiplied by $Z_{ax}\ Z_{tg}^{-1}\ L_{sw}^{-1}$ (Eq. 2.3), with Z_{ax} the distance between the heater and axial measurement needles, Z_{tg} the distance between the heater and tangential measurement needle and L_{sw} the sapwood depth. Here, $L_{sw}\ Z_{tg}$ was considered to be a measure for the sapwood cross-sectional area where deformation of the heat field occurs and hence sap is flowing while the implementation of $Z_{ax}\ Z_{tg}^{-1}$ partially corrects for needle spacing (Nadezhdina *et al.*, 1998; Nadezhdina *et al.*, 2012). Hence, Eq. 2.3 is supposed to determine actual sap flux density ($m^3\ m^{-2}\ s^{-1}$).

Without doubt, Eq. 2.3 has its merits in sap flow research, having revealed several tree physiological phenomena, never measured before. It has been used to investigate hydraulic redistribution (Nadezhdina *et al.*, 2006; 2008; 2009; 2010), xylem structure and functionality (Nadezhdina, 2010), radial sap flow (Nadezhdina *et al.*, 1998; Jimenez *et al.*, 2000; Saveyn *et al.*, 2008; Steppe *et al.*, 2009) and modelling of water use and transpiration (Chiesi *et al.*, 2002; Oltchev *et al.*, 2002; Verbeeck *et al.*, 2007; Van der Zande *et al.*, 2009). The method appeals because of its sensitivity across a wide range of sap flow rates and this for several sapwood depths, even though recently deviations between actual sap flux densities determined gravimetrically and HFD measured sap flux densities have been reported (Steppe *et al.*, 2010).

This chapter investigates the thermodynamic background of the HFD method and its parameters and points out some misunderstandings concerning its units. Moreover, by applying a FEM, the accuracy of the HFD method is questioned and a mathematical relation between sap flux density and the HFD temperature ratio is developed to correct its original flaws.

3.2 Thermodynamic background HFD method

When looking at the measured temperature differences (Eq. 2.3), it is clear that the heat transport on which the HFD method is based, consists of two dimensions: the axial and tangential dimension. This can be thermodynamically explained by the assumption of a perfect linear heater in a homogeneous medium: by equally heating the stem in its radial direction, the temperature field will be radially constant. This is one of the fundamental assumptions of heat-based sap flow methods applying a linear heater (Marshall, 1958; Burgess *et al.*, 2001b; Tatarinov *et al.*, 2005). Therefore, these methods can be considered two dimensional. The radial profile which can be obtained by the HFD method is thus the combination of several two dimensional measurements at different depths. Therefore, the application of L_{sw} as a radial parameter in this two dimensional method is incorrect.

The main reason to include L_{sw} was to obtain units of $m^3\ m^{-2}\ s^{-1}$ (Nadezhdina *et al.*, 2012). However, even though multiplication of thermal diffusivity with $Z_{ax}\ Z_{tg}^{-1}\ L_{sw}^{-1}$ leads to these units, they are not units of sap flux density. Thermal diffusivity D ($m^2\ s^{-1}$), as a measure of the rate by which the sapwood can absorb heat from its

surroundings (Bouguerra, 2001), is the ratio of the thermal conductivity K (W m^{-1} K^{-1}) of the sapwood on the one hand and the product of the fresh density ρ (kg m^{-3}) and the heat capacity c (J kg^{-1} K^{-1}) of the sapwood on the other hand:

$$D = \frac{K}{\rho c} \qquad (3.1)$$

In this formula, thermal conductivity K (W m^{-1} K^{-1}) is defined as the amount of heat flowing per time unit through a body of 1 m thickness with a surface of 1 m^2 and a temperature difference of 1 K between both surfaces:

$$K = {Q\ d}\big/{A\ t\ \Delta T} \qquad (3.2)$$

with Q the amount of thermal energy (J), d the thickness of the material (m), A the cross-sectional area of the material (m^2), ΔT the temperature difference between both surfaces (K) and t the time (s). This parameter thus describes the ability of the sapwood to transmit heat when subjected to a temperature gradient. For axial sap flow, A thus represents the cross-sectional area of the sapwood, while d represents the axial dimension corresponding to the flow direction. The density of the sapwood ρ (kg m^{-3}) is the mass M of the volume with cross-sectional area A and thickness d. The heat capacity c (J kg^{-1} K^{-1}) is the amount of thermal energy Q' stored in this mass M for a temperature change ΔT of 1 K (Marshall, 1958).

To gain insight in the dimensional unit (m²) of the thermal diffusivity D, the following equation is defined:

$$D = \frac{K}{\rho c} = \frac{{Q\ d}\big/{A\ t\ \Delta T}}{\left({M}\big/{A\ d}\right)\left({Q'}\big/{M\ \Delta T}\right)} = \frac{d\ (A\ d)}{A\ t} \qquad (3.3)$$

The m² thus actually represents a volume of sapwood ($A\ d$) per sapwood cross-sectional area (A) multiplied by an axial direction d, as this is the direction of heat flow because of sap flow (Figure 3.1). Therefore, as in Eq. 2.3 the thermal diffusivity is multiplied by an axial and divided by a radial and tangential dimension, the units of the original HFD equation do not represent a flux density and have no physical meaning. To obtain the correct dimensions, it is necessary to divide by an axial distance. Moreover, the thermal diffusivity represents the entire sapwood (both

wood matrix and water), leading to heat flux velocities V_h and not sap flux densities. Hence, an additional conversion according to Eq. 2.4 would be needed to obtain *SFD*.

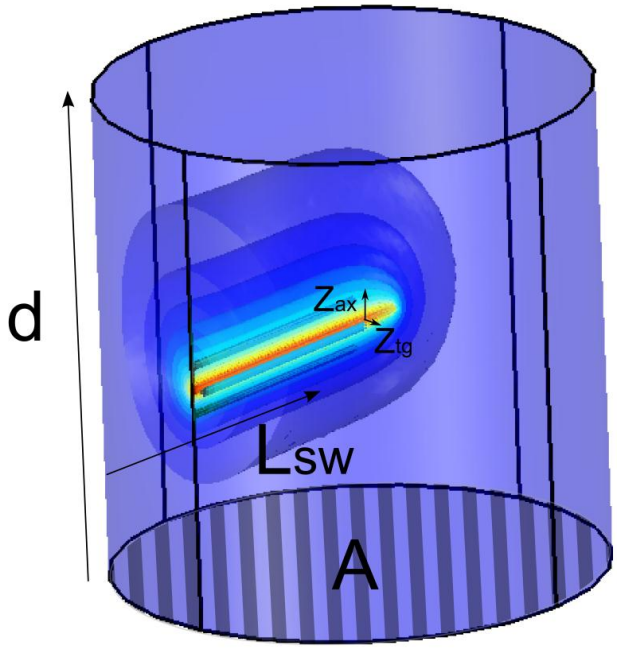

Figure 3.1 *Schematic representation of the HFD sensor with the dimensional units for diffusivity and sensor spacing, with L_{sw} the sapwood depth, A the sapwood cross-sectional area, d the axial dimension corresponding to the flow direction, Zax and Ztg the axial an tangential distance between the heater and the axial and tangential measurement needles, respectively. Note that in this representation, no hardwood is taken into account.*

By which axial distance should the thermal diffusivity then be divided to obtain physically correct sap flux densities? A logic choice would seem to divide by the distance from the axial sensor needle to the heater (=Z_{ax}) as done for other heat-based systems (Marshall, 1958; Saddler & Pitman, 1970; Cohen *et al.*, 1981; Burgess *et al.*, 2001b). However, both for the systems based on Marshall (1958) and Saddler & Pitman (1970), the sap flow equations are directly derived from the fundamental heat conduction-convection equation. This is not the case for the HFD ratio, making the multiplication with any parameter, even the thermal diffusivity *D* itself, an arbitrary choice. Therefore, as the combination of parameters in Eq. 2.3 in relation to the HFD ratio do not add any interpretational value to the HFD method, it should be considered an empirical method for which any parameter linking the HFD ratio to sap flux density, could be used, supposing a linear relation between the HFD ratio and sap flux density. This prevents false interpretation of supposedly thermodynamic features such as the thermal diffusivity.

3.3 Materials and method

To thoroughly investigate the HFD method, a 3D FEM was developed. A moist wood segment of 20 cm height and 10 cm width with a varying sapwood depth was modelled, holding a heater needle and three measurement needles. The boundary temperature was constant at 20 °C.

This FEM solves the partial differential equation governing heat transport in each defined node of the 3D structure:

$$\rho c \frac{\partial T}{\partial t} = \vec{K}\left(\frac{\partial^2 T}{\partial x^2} + \frac{\partial^2 T}{\partial y^2} + \frac{\partial^2 T}{\partial z^2}\right) + \rho c V_h \left(\frac{\partial T}{\partial x} + \frac{\partial T}{\partial y} + \frac{\partial T}{\partial z}\right) + P_h \qquad (3.4)$$

with T temperature (K), t time (s), V_h convective heat velocity (m s^{-1}), ρ density (kg m^{-3}), c specific heat capacity (J kg^{-1} K^{-1}) and $\vec{K}$ the vector of thermal conductivity (W m^{-1} K^{-1}) of the medium (comprising of axial (K_{ax}), tangential (K_{tg}) and radial (K_{rad}) conductivity, respectively) in which the temperature changes take place. As moist wood is anisotropic, containing directionally different thermal properties, K_{ax} was always set higher as or equal to K_{tg}. As the heater was inserted radially, K_{rad} had no influence on the results. P_h (W m^{-3}) is the amount of heat released in a unit of volume at the point (x,y) per unit of time. For the measurement and heater needles, the properties of steel were chosen for implementation in the model (ρ=7850 kg m^{-3}, c=475 J kg^{-1} K^{-1}, K= 44.5 W m^{-1} K^{-1}). Heat velocity was related to sap flux density according to Eq. 2.4.

Simulations for a range of sap flux densities were conducted for which the ratio ($\Delta T_{0(s\text{-}a)}$ +$\Delta T_{s\text{-}a}$) ΔT_{as}^{-1} was calculated and compared with the sap flux density for differences in wood properties (thermal conductivity, dry wood density and water content) covering the natural range for woody species. To test the influence of heat input on the HFD method, it was set between 9 and 18 W cm^{-1}. As in the HFD method continuous heating is applied, measurements were supposed to be stable at 120 s after the heater was switched on. The influence of the needle spacing was tested to investigate the importance of the original correction factor Z_{ax} Z_{tg}^{-1}. For the rest of the simulations, the same distances as mentioned by Nadezhdina *et al.* (1998; 2012) were applied (Z_{ax}=15 mm, Z_{tg}=5 mm) as these distances were mentioned to lead to the highest sensitivity for the HFD ratio to changes in sap flux density.

3.4 Results and discussion

3.4.1 Characteristics of the HFD temperature ratio

Influence of heat input

Figure 3.2a and b show the relation between the HFD ratio modelled for increasing heat velocities (V_h) with different heat inputs. Even though for varying heat inputs the absolute temperatures clearly differ (Figure 3.2a), the HFD ratio does not change (Figure 3.2b). Similar results were obtained if the time to stabilization was set larger than 120 s, confirming that the system was in thermal equilibrium after this period of time. Therefore, for the remainder of the results, a fixed heat input q (heat input per unit length of the heater) of 9.4 W m^{-1} will be used and temperature values are always those at 120 s after its application.

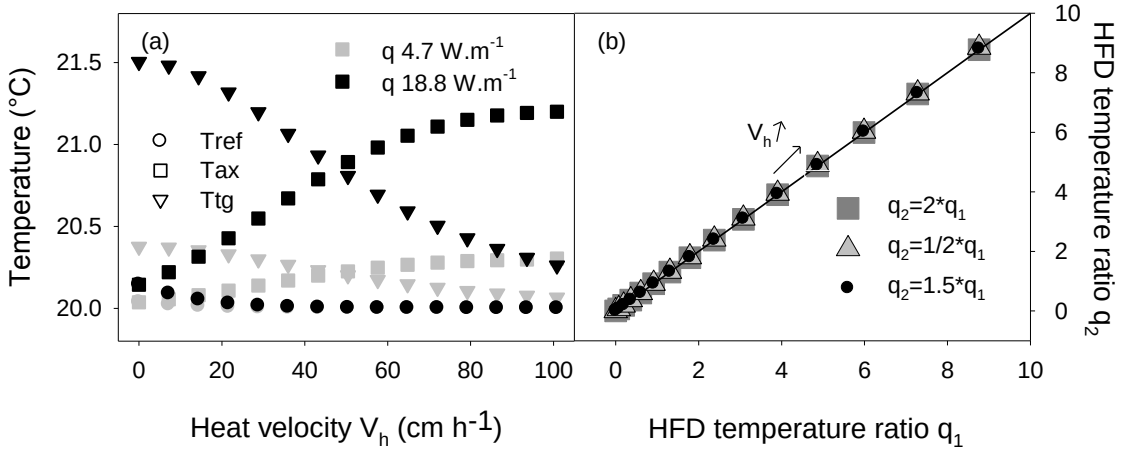

Figure 3.2 *(a) T_{ref}, T_{ax} and T_{tg} at 120s after switching on the heater for different heat velocities (and hence sap flux densities), both for a heat input of 18.8 W m^{-1} and 4.7 W m^{-1}; (b) HFD temperature ratios for increasing heat velocities (V_h) calculated with different heat inputs and q_1=9.4 W m^{-1}.*

Two dimensionality of the HFD ratio

Varying the sapwood depth of the 3D model while maintaining the same convective flux did not affect the measured temperatures, confirming the theory that the HFD method is basically two dimensional.

Linearity of the HFD ratio

The HFD method has been said to be highly sensitive towards a wide range of sap flux densities (Nadezhdina *et al.*, 1998; Nadezhdina *et al.*, 2012). Figure 3.3a confirms that the HFD ratio increases with increasing sap flux density, but not linearly. The relative error, calculated as the difference between the sap flux density and the HFD ratio divided by the sap flux density, decreases for increasing sap flux densities (Figure 3.3b), even though the absolute error increases (Figure 3.3a). Multiplication of the HFD ratio with constant parameters as is done in Eq. 2.3 can, hence, reduce the absolute errors, but can not resolve the relative sap flux density dependency of the ratio. As a result of these findings,the measurements at different sapwood depths will only give an approximation of the radial profile as the relative error will be different for each depth, given the radial variation in sap flux density.

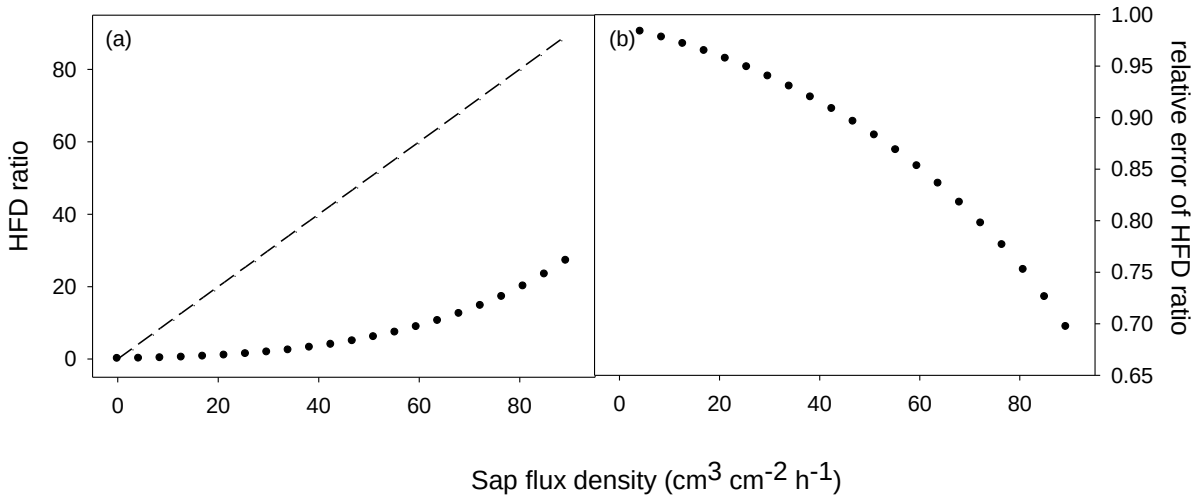

Figure 3.3 *(a) Relationship between the HFD ratio and the sap flux density. The dashed line represents the 1:1 line; and (b) relative error of the HFD ratio, calculated as the difference between the sap flux density and the HFD ratio divided by the sap flux density,*

Moreover, this relative discrepancy is not only influenced by the sap flux density but is also depending on the axial and tangential conductivity (Figure 3.4a) and dry wood density (Figure 3.4b), even though the effect of the latter on the HFD ratio is rather small (a 40% difference in dry wood density only led to a maximal difference of 12% difference in HFD ratio). The water content does not influence the ratio significantly if all other parameters remain unchanged (Figure 3.4c). In reality, however, changes in water content are coupled with changes in thermal

conductivity. Hence, variation in wood properties between tree species can lead to large relative differences in HFD ratio for the same sap flux density (Figure 3.4d). Besides, even variation within species, both spatially and temporally, could induce changes in the HFD ratio, although it is expected that these differences are rather small as the variation in thermal parameters and dry wood density within species is much smaller than between species (Skaar, 1988).

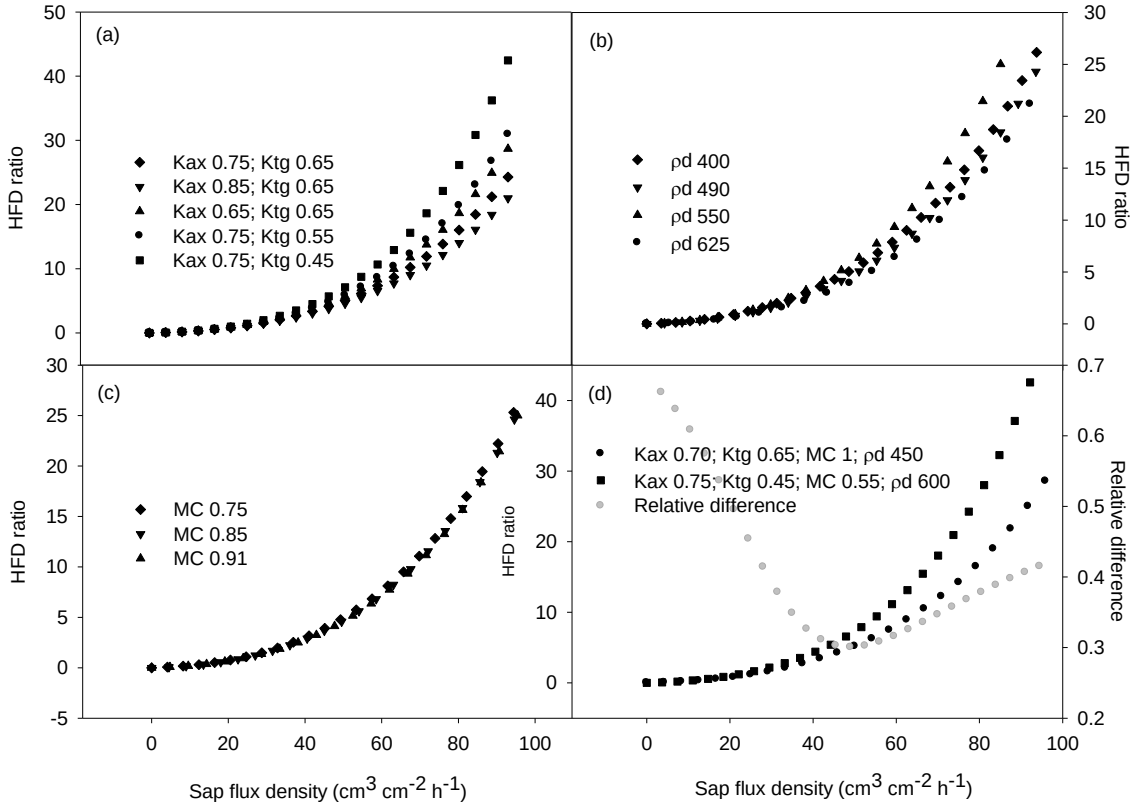

Figure 3.4 *Sap flux density dependency of (a) the HFD ratio for different axial (K_{ax}) and tangential (K_{tg}) thermal conductivities (W m^{-1} K^{-1}), a dry wood density (ρ_d) of 490 kg m^{-3} and a water content of 0.91; (b) the HFD ratio for different dry wood densities(ρ_d) for K_{ax}=0.75 W m^{-1} K^{-1}, K_{tg}=0.65 W m^{-1} K^{-1} and MC=0.91; (c) the HFD ratio for different water contents (MC) with K_{ax}=0.75 W m^{-1} K^{-1}, K_{tg}=0.65 W m^{-1} K^{-1} and ρ_d =550 kg m^{-3}; and (d) HFD ratios for varying wood properties and the relative difference between them.*

Influence of needle spacing on the HFD ratio

Figure 3.5a shows that changes in Z_{ax} hardly influence the HFD ratio if Z_{tg} remains unaltered, while changes in Z_{tg} lead to large differences for moderate and high flows (>20 cm^3 cm^{-2} h^{-1}). Apparently, the $\Delta T_{0(s\text{-}a)}$ value largely compensates for changes in Z_{ax}. Moreover, if Z_{ax} is changed, this will only have a small effect on the T_{as} signal for

high flows as then the T_{ref} needle is less influenced by the heater. Hence, displacing this needle will only lead to small differences in T_{ref}. If, however, Z_{tg} is altered, then for high flows the T_{as} signal will be much more affected as the T_{as} needle should be in close proximity of the heater to ensure sufficient sensitivity towards high flows.

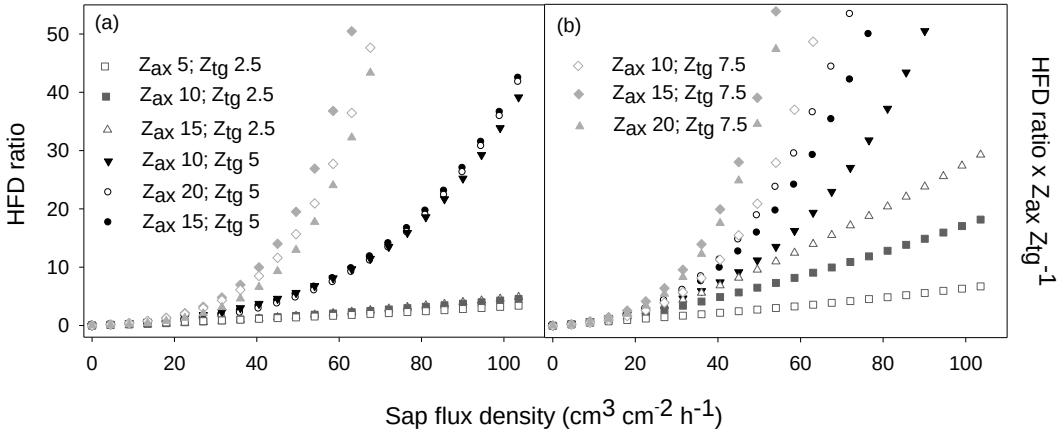

Figure 3.5 *(a) HFD ratio for different combinations of Z_{ax} and Z_{tg} distances (mm); and (b) these same HFD ratios multiplied by the term Z_{ax} Z_{tg}^{-1}*

In Figure 3.5b, it can be seen that there is a more even spread of HFD ratios if these are multiplied with the Z_{ax} Z_{tg}^{-1} term. When comparing, for instance, the spacing Z_{ax}15 Z_{tg}2.5 with Z_{ax}10 Z_{tg}5, the Z_{ax} Z_{tg}^{-1} term indeed led to a smaller deviation in HFD ratios as the difference in Figure 3.5b is smaller in comparison to the difference in Figure 3.5a even though for sap flux densities >60 cm^3 cm^{-2} h^{-1} they still greatly differ. Moreover, for other combinations (for instance Z_{ax}15 Z_{tg}5 and Z_{ax}20 Z_{tg}5), the divergence even increases when the Z_{ax} Z_{tg}^{-1} term is applied. The absolute changes in HFD ratio with or without the term Z_{ax} Z_{tg}^{-1} due to changes in needle spacing will be dependent on the thermal properties of the wood (data not shown), although the same conclusions hold. Hence, even though the term Z_{ax} Z_{tg}^{-1} clearly influences Eq. 2.3, it cannot be considered an absolute spacing correction.

3.4.2 From temperature ratio to sap flux density

As the temperature ratio is dependent on wood properties and needle spacing, this dependency needs to be included in the link with sap flux density. This is in agreement with the lab and field experiments of Steppe *et al.* (2010), who stated that recalibration of the HFD method might be necessary for each new tree species.

While Steppe *et al.* (2010) determined a single calibration factor for their species, the model results show that this will only be sufficient in a certain range of sap flux densities as no linear relation exists between the ratio and sap flux density. Therefore, a mathematical relationship should be fitted to the data:

SFD=f(HFD) *(3.5)*

with HFD the value of the HFD ratio (-), taking into account the influence of needle spacing, K_{ax}, K_{tg}, ρ_b and MC as well as the sap flux density dependency of HFD. Although several relationships can be fitted to the data, a trade off between goodness of fit and model simplicity (number of parameters to estimate) should be taken into account. While high order polynomial regressions lead to an acceptable low sum of squared error, these regressions require a large number of parameters to be estimated. By running a curve analysis, fitting more than 40 both linear and non-linear regression functions to the data, the following relationships were obtained that led to a good fit for all combinations of input thermal properties and needle distances and had maximum four empirical parameters to estimate:

$$SFD = \frac{a + bHFD}{1 + cHFD + dHFD^2} \quad (3.6)$$

$$SFD = \frac{ab + cHFD^d}{b + HFD^d} \quad (3.7)$$

$$SFD = \frac{-a + \sqrt{a^2 + 4bHFD}}{2b} \quad (3.8)$$

with a, b, c and d empirical parameters for each equation (Figure 3.6 as an example). As the HFD ratio is empirical, these parameters will have no strict physical meaning. Hence, similar as for the TD method (Granier, 1985), the dimensions of these parameters are not of importance although they can easily be derived from Eq. 3.6, 3.7 and 3.8 as the HFD ratio itself is dimensionless. While for Eq. 3.8 only two parameters need to be estimated, this fit underestimates lower flows and overestimates higher flows and should, hence, be avoided. As the standard error for Eq. 3.6 (1.840) is systematically higher than for Eq. 3.7 (0.280), the latter is preferred.

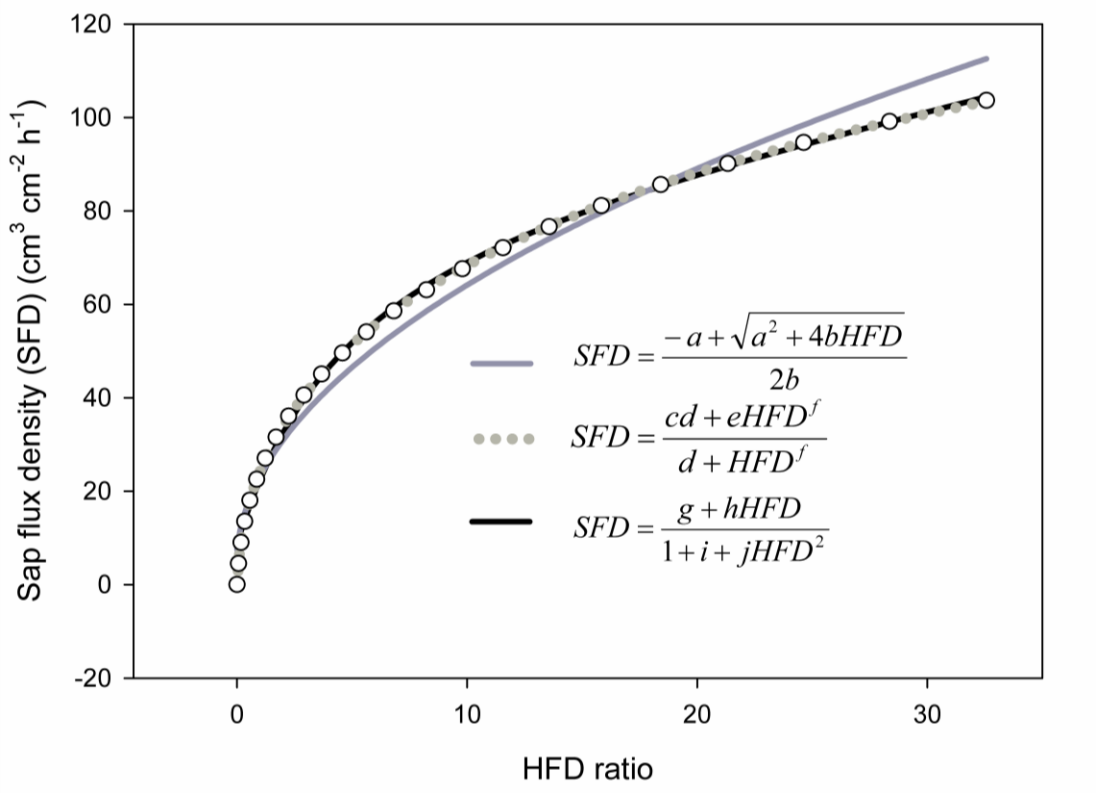

Figure 3.6 *Mathematical relation between sap flux density and modelled HFD ratio with a=0.0207, b=0.0028, c=-0.603, d=8.650, e=239, f=0.543, g=4.562, h=24.01, i=0.282, j=-0.00258 (K_{ax}=0.75 W m^{-1} K^{-1}, K_{tg}=0.65 W m^{-1} K^{-1}, ρ_d=550 kg m-3, MC=0.85).*

To determine this correction equation, a validation experiment similar as done by Steppe *et al.* (2010) could be set up. This way, both the non-linearity of the HFD ratio and its dependency on wood properties are taken into account while the advantages of the original HFD ratio, namely its sensitivity in a wide range of sap flux densities and the possibility to establish a radial profile, remain.

These findings raise the question as to what extent results mentioned in previously conducted studies applying the HFD method are correct. As has been shown by Steppe *et al.* (2010), Eq. 2.3 can lead to large underestimations of sap flux density. These underestimations will, however, be largely dependent on the applied L_{sw} value and, to a smaller extent, on the thermal properties of the sapwood, making error estimations difficult as these values are often unknown. In general, underestimations of up to 50% can be expected (Steppe *et al.*, 2010), which is of importance if absolute water use of trees was investigated. Fortunately, most research has been focussing on relative flow patterns within the low to moderate flow range to study phenomena such as radial flow, xylem structure and

functionality and hydraulic redistribution. Even though relative deviations must have occurred, due to the non-linearity of the HFD ratio, the presented patterns are clear and distinct and, hence, the conclusions correct.

3.5 Conclusions

Although the HFD method has proven its use in many studies because of its sensitivity towards low, high and reverse flows and the possibility to measure flow at different depths, the thermal diffusivity in its original equation is often wrongly interpreted. Therefore, the method should be considered entirely empirical rather than semi-empirical as the link between the empirical temperature ratio and sap flux density is not based on fundamental thermodynamics. To enable accurate sap flux density estimations from the HFD ratio, mathematical relations were derived which necessitate species-specific calibration. This can be done by forcing a range of sap flux densities on a cut stem segment and comparing the HFD results with the gravimetric reference data. This calibration procedure is, however, impractical for large scale field measurements. Therefore, heat pulse methods seem preferential as they do not require specific calibrations and, as indicated in Chapter 2, are not susceptible to NTG.

4

The anisotropic heat conduction-convection equation as basis for heat pulse sap flow methods

After: Vandegehuchte, M.W. & Steppe, K. (2012). Use of the correct heat conduction-convection equation as basis or heat pulse sap flow methods in anisotropic wood. Journal of Experimental Botany, 63: 2833-2839.

Abstract

Heat pulse methods to determine sap flux density in trees are based on the theory of heat conduction and convection in an isotropic medium, with thermal properties of the medium not directionally differing. However, sapwood is clearly anisotropic, implying a difference in thermal conductivity along and across the grain, and hence necessitates the theory for an anisotropic medium. This difference in thermal conductivities, which can be up to 50 %, is however not taken into account in the key

equation leading to the currently available heat pulse methods. Despite this flaw, these methods remain theoretically correct as they are based on derivations of the key equation, ruling out any anisotropic aspects. Nevertheless, it remains important to specify the thermal characteristics of the sapwood according to axial, tangential or radial direction and to refer to and use the proper anisotropic theory. This will avoid confusion and misinterpretation of thermal properties when dealing with sap flux density measurements or erroneous results when modelling heat transport in sapwood.

4.1 Introduction

If heat pulse based sap flow methods are based on a theory only applicable for isotropic materials, not differentiating between directionally different thermal properties, can they then be accurate for an anisotropic material such as sapwood in which axial thermal conductivity differs from tangential thermal conductivity? This chapter will answer this pertinent question by summarizing and comparing the heat pulse theory for both isotropic and anisotropic media.

Heat pulse methods are based on the theoretical background for heat flow in sapwood as developed by Marshall (1958) based on the work of Carslaw & Jaeger (1947). This theory is based on the analytical solution of the partial differential equation for combined conduction and convection of heat in a specified medium. If this equation can be solved for the convection term, the velocity by which heat transfers through the medium, such as sapwood, can be determined and from this, sap flux density can be calculated.

For the application of an instantaneous line source of heat along the z-axis in an isotropic medium, the following analytical solution is obtained:

$$\Delta T = \frac{Q_T}{4\pi Dt} \exp\left[-\frac{(x - V_h t)^2 + y^2}{4Dt} \right] \qquad (4.1)$$

with ΔT (K) the difference between the temperature at position (x,y) before application of the heat pulse and a time t (s) after application of the heat pulse, Q_T (K m²) defined as the temperature to which the amount of heat liberated per unit length of the line would raise a unit volume of the substance, D the thermal

diffusivity ($m^2\ s^{-1}$) and V_h the heat pulse velocity ($m\ s^{-1}$). This heat pulse velocity is directly proportional to sap flux density according to Eq. 2.4.

It is this equation that was used by Marshall (1958) and many others (Cohen *et al.*, 1981; Swanson & Whitfield, 1981; Swanson, 1983; Green & Clothier, 1988; Burgess *et al.*, 2001a) as the basis for the development of heat pulse based sap flow measurement methods.

4.2 Assumption of isotropic medium versus actual anisotropic sapwood

Sapwood, however, is composed of conductive elements which main goal is axial transport. Hence, the structure and thermal properties of sapwood differ according to the directional orientation, whether axial or tangential. Marshall (1958) already stated that dry wood is not isotropic, but has a greater thermal conductivity along the grain (K_{ax}) than across the grain (K_{tg}). He also acknowledged that wet wood might also be anisotropic, although probably to a lesser extent. For fresh wood segments with a water content higher than the fibre saturation point, the axial thermal conductivity (K_{ax}) can be up to two times larger than the radial (K_{rad}) or tangential (K_{tg}) conductivity, depending on wood species (Maku, 1954; Steinhagen, 1977). Moreover, when applying the equations as mentioned in Swanson (1983) based on the work of Turrell *et al.* (1967) and Siau (1971) for the calculation of K_{ax} and K_{tg}, it is clear that K_{tg} (and hence thermal diffusivity, D_{tg}) is remarkably smaller across all dry wood densities and water contents with K_{tg} on average (54±7.5) % of K_{ax} (Figure 4.1). This approach was also applied by Burgess *et al.* (2001a) to determine axial thermal diffusivity (D_{ax}) for the Heat Ratio method (see Chapter 5).

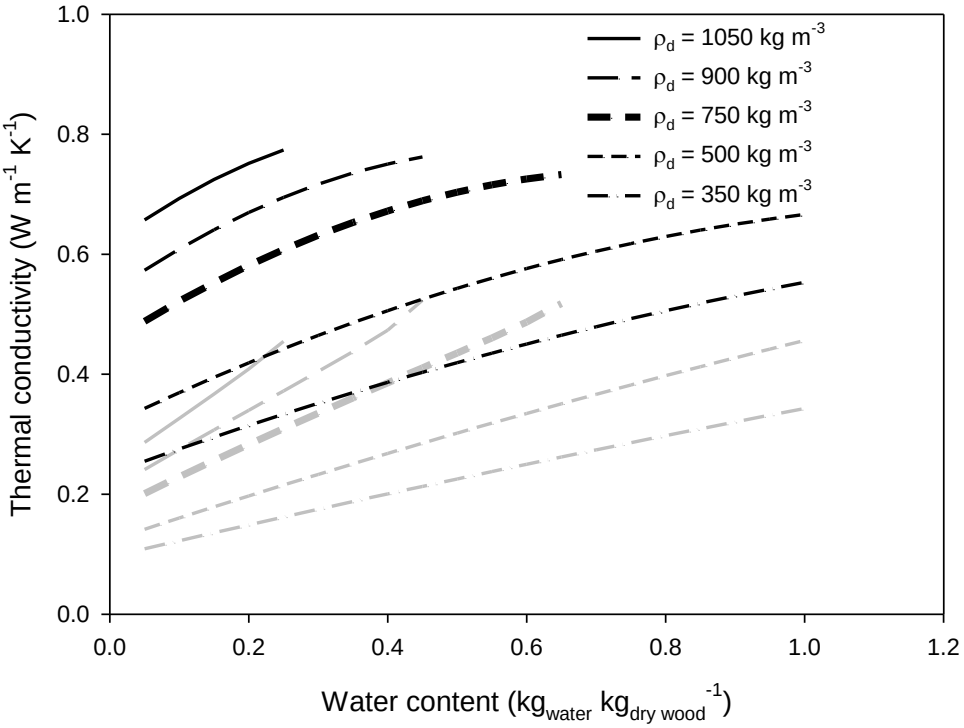

Figure 4.1 *Axial (black lines) and tangential (grey lines) thermal conductivities for different water contents and dry wood densities (ρ_b) as calculated according to Turrell et al. (1967)) based on Siau (1971).*

When considering anisotropy, the analytical solution of the partial differential equation for combined conduction and convection of heat, from which Eq. 4.1 was derived for isotropic media, becomes:

$$\Delta T = \frac{Q_T \rho c}{4\pi\sqrt{K_{ax}K_{tg}}\,t} \exp\left[-\frac{\rho c}{4t}\left(\frac{(x-V_h t)^2}{K_{ax}} + \frac{y^2}{K_{tg}}\right)\right] \qquad (4.2)$$

And it is, hence, this equation (Eq. 4.2) that should be the key equation for sap flow measurements based on pulsed heating by an ideal line heater instead of Eq. 4.1 which has, so far, been used as reference equation.

4.3 Implications of anisotropy for current sap flow methods

Applying Eq. 4.1 and 4.2 for heat transport in sapwood with a given dry wood density and water content and the same heat input, clearly leads to different

temperature patterns in the wood (Figure 4.2). These different patterns are caused bydifferences in thermal diffusivity, with the isotropic diffusivity taken as the geometric mean of the axial and tangential diffusivity (Figure 4.3). This also affects the parameters used in the methods based on Eq. 4.1 to determine sap flux density, such as the Tmax method and the Heat Ratio method. For the Tmax method, the difference in temperature field results in a difference in t_m (Figure 4.4a), while for the Heat Ratio method, the ratio ($\Delta T_{down}/\Delta T_{up}$) is clearly influenced (Figure 4.4b).

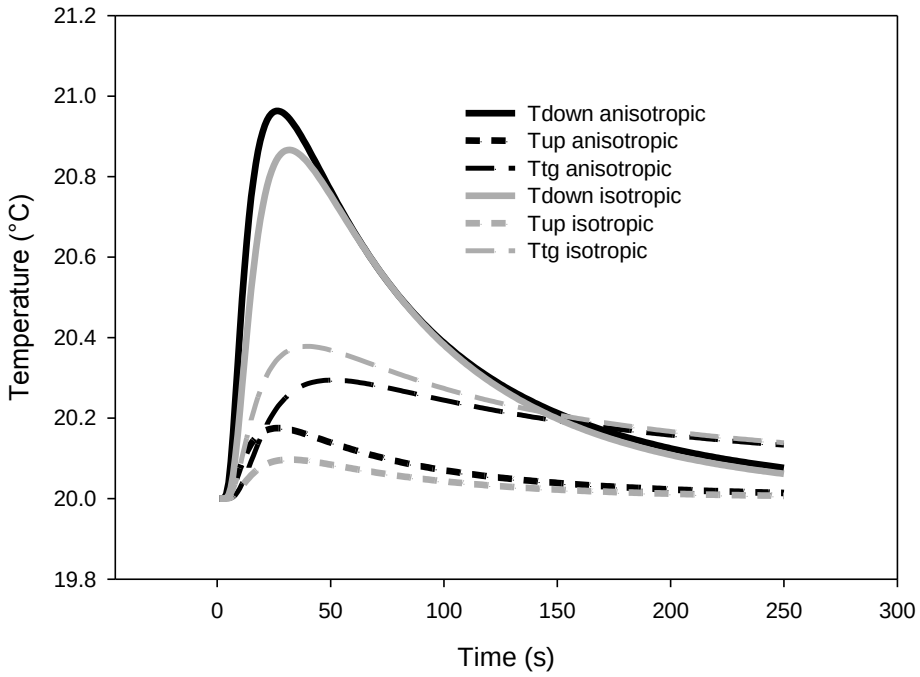

Figure 4.2 *Temperatures at 6 mm axially downstream, upstream and tangentially from the heater for a water content of 70% and dry wood density of 550 kg m^{-3}. For the isotropic case, the thermal diffusivity D was taken as the geometric mean of D_{ax} and D_{tg} of the anisotropic case.*

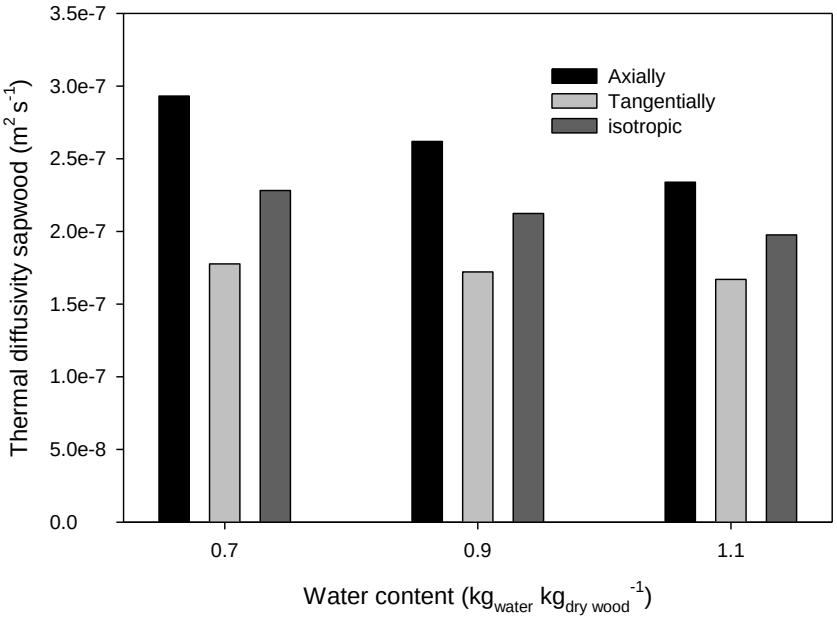

Figure 4.3 *Thermal diffusivities for both the isotropic and anisotropic case for different water contents. The dry wood density was taken as 550 kg m^{-3}. The isotropic thermal diffusivity was taken as the geometric mean of D_{ax} and D_{tg} of the anisotropic case.*

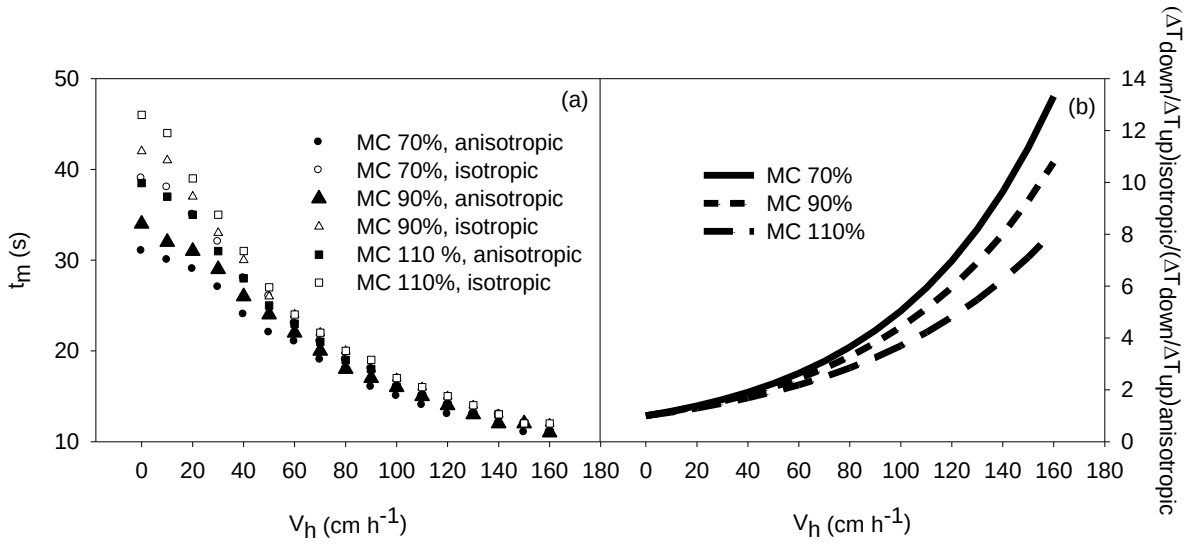

Figure 4.4 *(a) Time to maximum (t_m) values and (b) ratio of the HR method temperature ratio ($\Delta T_{down}/\Delta T_{up}$) for isotropic and anisotropic sapwood with different water contents. The isotropic thermal diffusivity D was taken as the geometric mean of D_{ax} and D_{tg} of the anisotropic case.*

If Eq. 4.1 is not valid for sapwood with anisotropic thermal conductivity, does this imply that the methods based on this equation are not applicable? Not necessarily, because most methods are based on derivations from Eq. 4.1. Marshall (1958) based

his measurements of V_h and D on the substitution of two points on the temperature-time curve (t_1,T_1) and (t_2,T_2):

$$\ln\left(\frac{\Delta T_1 t_1}{\Delta T_2 t_2}\right) = -\frac{\rho c (x - V_h t_1)^2}{4K_{ax} t_1} - \frac{\rho c y^2}{4K_{tg} t_1} + \frac{\rho c (x - V_h t_2)^2}{4K_{ax} t_2} + \frac{\rho c y^2}{4K_{tg} t_2} \qquad (4.3)$$

If the measurement point is now chosen at an axial distance x (with y=0), this becomes:

$$\ln\left(\frac{\Delta T_1 t_1}{\Delta T_2 t_2}\right) = -\frac{\rho c (t_1 - t_2)^2}{4K_{ax} t_1 t_2}(x^2 - V_h{}^2 t_1 t_2) \qquad (4.4)$$

or

$$\ln\left(\frac{\Delta T_1 t_1}{\Delta T_2 t_2}\right) = -\frac{(t_1 - t_2)^2}{4D_{ax} t_1 t_2}(x^2 - V_h{}^2 t_1 t_2) \qquad (4.5)$$

When applying this equation to two other points t_3 and t_4 so that t_1+t_4=t_2+t_3=2t_2, a similar equation is obtained, leading to two equations with two unknown variables: D_{ax} and V_h. These equations can then easily be solved to obtain expressions for both D_{ax} and V_h. If the same mathematics are applied on Eq. 4.1, the same result is obtained which makes clear that the thermal diffusivity as calculated by Marshall (1958) really is the axial thermal diffusivity (Figure 4.5). Hence, by locating the measurement needles only in the axial direction and choosing specific data points on the temperature-time curve, the difference introduced by anisotropy between Eq. 4.1 and 4.2 is ruled out. This is also the case for the Heat Ratio method (Burgess *et al.*, 2001a). Here, the same distances of the axial measurement points upstream and downstream from the heater needle were applied which also negates the difference between axial and tangential conductivity (Figure 4.6).

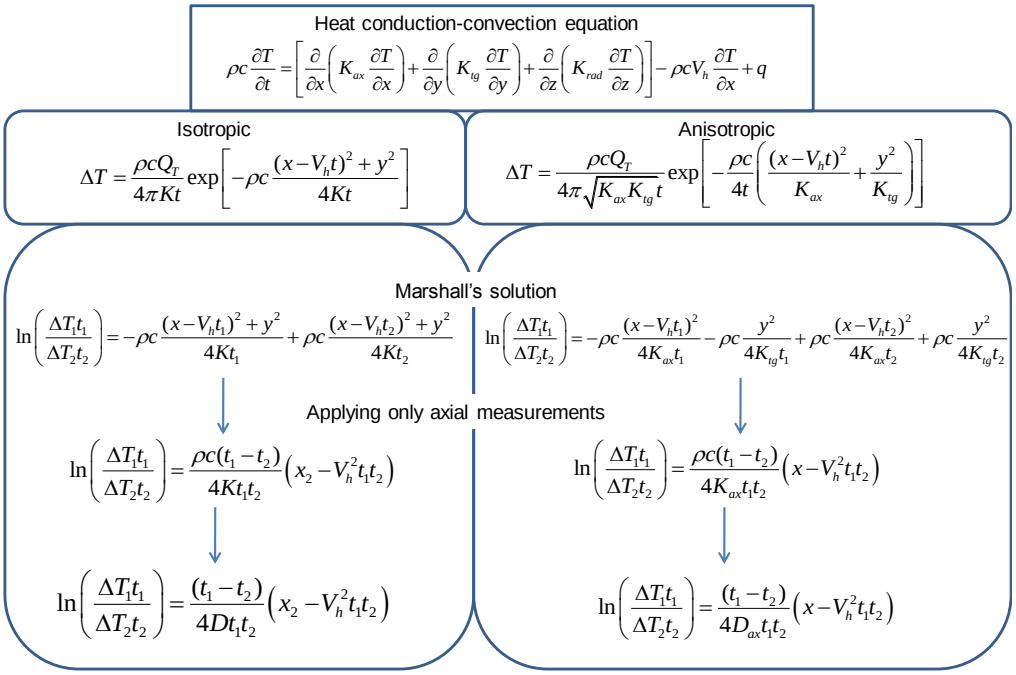

Figure 4.5 *Marshall's solution of Eq. 4.1 to determine V_h and D_{ax} (Marshall, 1958). By using only axial measurements and substituting specific points of the temperature-time curve, the influence of anisotropy is ruled out. Similar equations can be developed for t_3 and t_4 to obtain two equations including V_h and D_{ax} which can then be determined.*

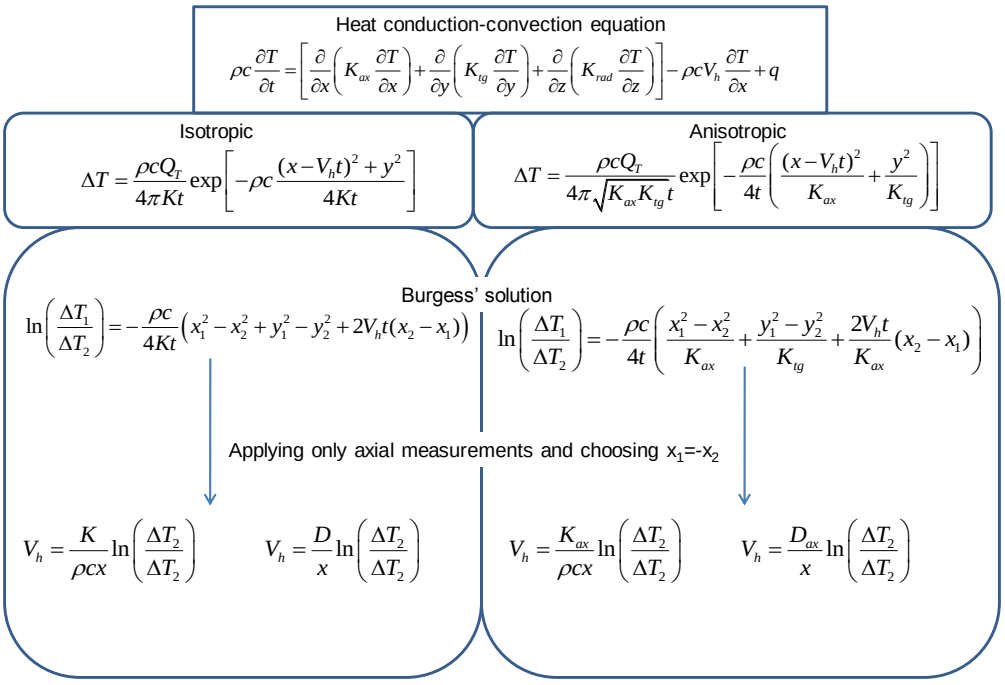

Figure 4.6 *Burgess' solution of Eq.4.1, based on Marshall (1958), to determine V_h. By measuring on specific distances upstream and downstream of the heater ($x_1=-x_2$), the actual axial conductivity is applied, even when starting from the isotropic theory.*

This also holds for the Tmax method of Cohen *et al.* (1981) (Figure 4.7). Even though thermal diffusivity is mentioned in this work as D in Eq. 4.1, in practice D_{ax} is being measured. By using the derivative of Eq. 4.1 for a measurement needle located axially from the heater, correct equations for both D_{ax} during conditions of zero flow and V_h are obtained:

$$D_{ax} = \frac{x^2}{4t_m} \tag{4.6}$$

$$V_h = \frac{\sqrt{x^2 - 4D_{ax}t_m}}{t_m} \tag{4.7}$$

with t_m the time at which ΔT is maximal. D_{tg} can be determined when measuring the temperature curve at a tangential distance (0,y) from the heater needle (Figure 4.7):

$$D_{tg} = \frac{y^2}{4t_m} \tag{4.8}$$

Note that it is incorrect to apply any distance d as mentioned in Cohen *et al.* (1981) (Eq. 2.6, 2.7) as a distinction between axial and tangential distances needs to be made to obtain the corresponding diffusivities.

Also for the Compensation Heat Pulse method, the isotropic and anisotropic theory lead to the same heat velocity results as the intersection point between upstream and downstream temperature profiles remains constant. Hence, it can be concluded that currently existing heat-pulse sap flux density measurement methods remain valid, even though they are based on an inaccurate theory, as by mathematical manipulations the same results are obtained as if the correct anisotropic theory would have been applied. It is now also clear that these methods determine the actual axial thermal diffusivity and not a mean of axial and tangential or overall thermal diffusivity as is sometimes mistakenly thought.

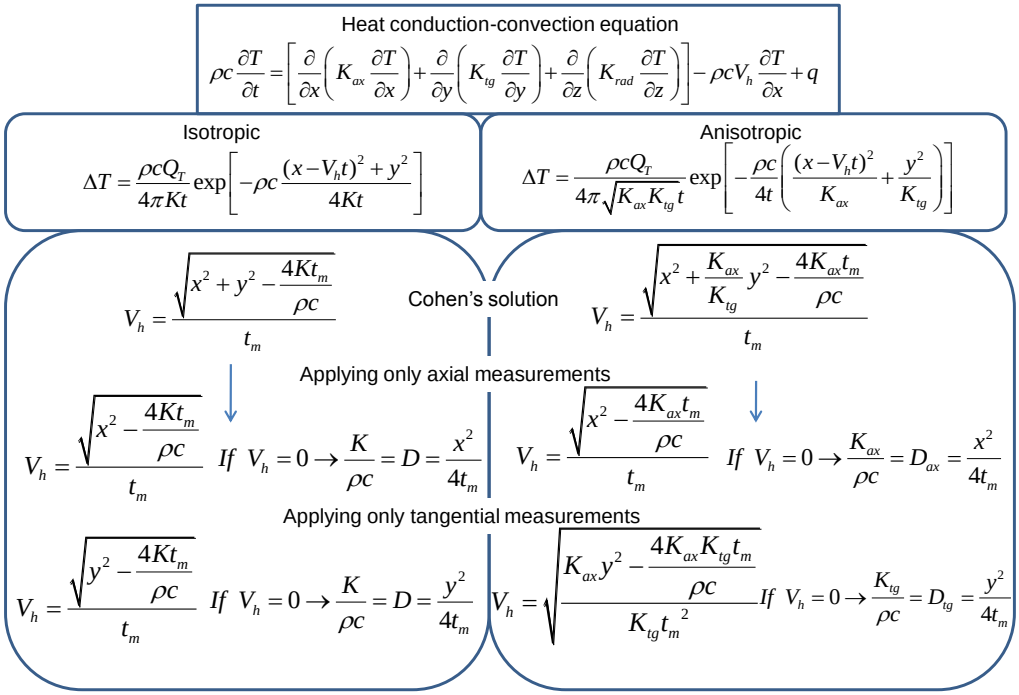

Figure 4.7 *By differentiating Eq. 4.1 to determine the time at which the maximal ΔT occurs, a solution for V_h is obtained. When applying only axial measurements, the actual axial thermal conductivity is used for these calculations*

The difference in D_{ax} and D_{tg} (or K_{ax} and K_{tg}) must also be made when numerical models are used to assess heat pulse measurement systems based on Eq. 4.1. This difference was taken into account by using the method of mixtures of Turrell *et al.* (1967) in combination with the determination of dry wood thermal conductivity by Siau (1971) in both the work of Swanson (1983) and Green, Clothier & Jardine (2003) for their FEM to assess the errors of several heat pulse methods. In earlier work of Swanson & Whitfield (1981), the axial conductivity was taken as twice the tangential conductivity, independent of wood water content and, hence, only partially accounting for the differences between K_{ax} and K_{tg}.

However, in Jones, Hamer & Higgs (1988) this difference was overlooked. These authors correctly stated that all heat pulse methods could benefit from the use of curve-fitting procedures, but directly implemented Eq. 4.1, thereby neglecting the anisotropy of the sapwood. This error was also made by Becker (1998) for a theoretical example and, more recently, by Chen *et al.* (2012) in their statistical method to determine probe spacing and wood thermal diffusivity. As these authors did not differentiate between axial and tangential thermal diffusivity, their numerical analyses need to be reconsidered. Next to these known examples, perhaps

others have made the same mistake, erroneously implementing Eq. 4.1 instead of 4.2.

4.4 Towards more accurate equations

Eq. 4.1, for an isotropic, and Eq. 4.2, for an anisotropic medium, are valid for instantaneous pulses only, which is however never the case in practice. Both Swanson (1983) and later Kluitenberg & Ham (2004) noted that for pulses longer than 2 seconds, application of the instantaneous pulse theory can lead to important errors (up to 10%) in determination of thermal diffusivity and sap flux density. Therefore, it was suggested to implement the theory applicable for a step pulse. For an anisotropic medium, this results in following equations:

$$\Delta T = \frac{q}{4\pi\sqrt{K_{ax}K_{tg}}}\int_0^t t^{-1}\exp\left[-\frac{\rho c}{4t}\left(\frac{(x-V_h t)^2}{K_{ax}}+\frac{y^2}{K_{tg}}\right)\right]dt \quad \text{for } 0<t<=t_0 \qquad (4.9)$$

$$\Delta T = \frac{q}{4\pi\sqrt{K_{ax}K_{tg}}}\int_{t-t_0}^t t^{-1}\exp\left[-\frac{\rho c}{4t}\left(\frac{(x-V_h t)^2}{K_{ax}}+\frac{y^2}{K_{tg}}\right)\right]dt \quad \text{for } t_0<t \qquad (4.10)$$

where q (W m^{-1}) is the amount of heat liberated per unit length of the heater per time. Eq. 4.9 and 4.10 can be numerically solved. When differentiating Eq. 4.10 to time, similarly as was done by Cohen *et al.* (1981) for an instantaneous pulse, both D_{ax} and D_{tg} can be determined. We tested this method on a cut segment of European beech (*Fagus sylvatica* L.) for several gravimetrically determined water contents by positioning two sensor needles at 7.5 mm from the heater, respectively axially and tangentially (Figure 4.8). The results confirm an important difference between D_{ax} and D_{tg}. Not only is D_{ax} 1.8 to 2.3 larger than D_{tg}, it is also more influenced by the water content of the sapwood.

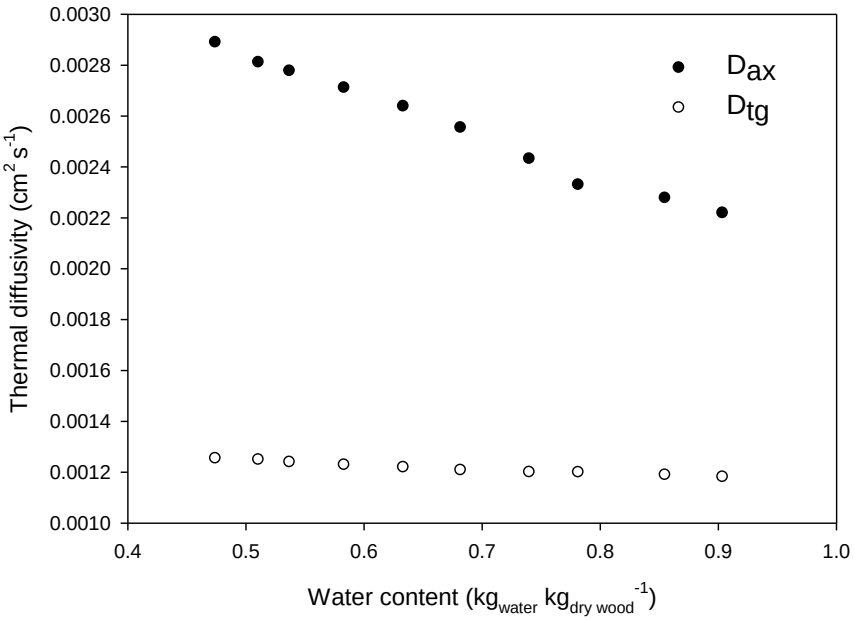

Figure 4.8 *Axial and tangential thermal diffusivity for European beech at different water contents calculated in analogue with the Tmax method (Cohen et al., 1981) but applied for a step heat pulse (Eq. 4.9 and 4.10)*

4.5 Conclusion

Throughout literature on heat pulse based sap flow measurement methods, there seems to be an inconsistency when referring to thermal diffusivity of sapwood. Despite clear evidence that sapwood is an anisotropic material for which axial diffusivity D_{ax} and tangential diffusivity D_{tg} will be markedly different, thermal diffusivity is often addressed as an overall diffusivity for the whole material, based on Eq. 4.1 (Marshall, 1958; Cohen *et al.*, 1981; Jones *et al.*, 1988; Cohen *et al.*, 1993; Becker, 1998; Nadezhdina *et al.*, 1998; Burgess *et al.*, 2001a; Green *et al.*, 2003; Bleby *et al.*, 2004; Kluitenberg & Ham, 2004; Green *et al.*, 2009). Nevertheless, the existing heat pulse based sap flow methods are still theoretically correct and yield actual D_{ax} values due to their reliance on derivations of Eq. 4.1 and the use of only axial needle positioning. However, when applying Eq. 4.1 for numerical modelling or for other purposes for which the mathematical derivations do not cancel out the isotropic effect, this will lead to errors in both diffusivity and sap flux density calculations. To avoid further confusion and prevent mistakes in future research, we suggest to mention Eq. 4.2 when referring to the development of heat pulse sensors and to consequently discriminate between axial or tangential thermal diffusivity and/or

conductivity. Furthermore, we encourage the use of Eq. 4.9 and 4.10, because they will be more accurate than those based on the instantaneous pulse theory.

Besides derivations from the heat conduction-convection equation, another way to determine D_{ax} is to apply the method of mixtures mentioned in Turrell *et al.* (1967) in combination with the dry wood thermal conductivity determinations of Siau (1971) which was specifically derived for the axial and tangential direction. The next chapter, however, shows that in this method, sapwood water content was wrongly interpreted, making it incorrect as the fibre saturation point is not taken into account.

5

Differentiating between bound and unbound water in the method of mixtures for diffusivity calculation

After: Vandegehuchte, M.W & Steppe, K. (2012). Improving sap flux density measurements by correctly determining thermal diffusivity, differentiating between bound and unbound water. Tree Physiology, 32: 930-942

Abstract

Several heat-based sap flow methods, such as the Tmax and the Heat Ratio method, include the axial thermal diffusivity D_{ax} of the sapwood as a crucial parameter. Despite its importance, little attention has been paid to determine D_{ax} in a plant physiological context. Therefore, D_{ax} is mostly set as a constant, calculated during

zero flow conditions or from a method of mixtures, taking into account wood density and water content. In this latter method, however, the meaning of the water content is misinterpreted, making it theoretically incorrect for D_{ax} calculations in sapwood. A correction to this method, which includes the correct application of the water content, is proposed. This correction was tested for European and American beech and *Eucalyptus caliginosa* Blakely & McKie. Depending on the dry wood density and water content, the original approach over- or underestimates D_{ax} and, hence, sap flux density by 10 % and more.

5.1 Introduction

While the Compensation Heat Pulse method (Swanson & Whitfield, 1981; Green & Clothier, 1988) operates independent of the axial thermal diffusivity D_{ax} of the sapwood, for the Heat Ratio and the Tmax method, (Marshall, 1958; Cohen *et al.*, 1981; Burgess *et al.*, 2001a; Clearwater *et al.*, 2009), D_{ax} is a crucial parameter to determine sap flux density. As in the HR equation D_{ax} is directly linearly proportional to sap flux density, an error of x % will lead to an equal error in sap flux density and, hence, calculated sap flow. This high linear sensitivity of sap flow measurements towards D_{ax} has been reported in the sensitivity analysis of Steppe *et al.* (2010). For the Tmax method, the influence of D_{ax} on sap flux density is less straightforward. The sensitivity analysis of Cohen *et al.* (1981) indicates that a 10 % error in D_{ax} only leads to a maximal error of 3 % in sap flux density for a probe spacing of 5 mm and even smaller for larger probe spacings.

Despite its importance as parameter in sap flow calculations, little attention has thus far been paid to characterize D_{ax} in a plant physiological context. Most research has been done on wood that is used as construction material and the results are therefore only applicable for dry wood samples. These dry samples have a water content *MC*, calculated as the ratio of the weight of water divided by the dry weight of the sapwood, below the point where only bound water is present (fibre saturation point, *FSP*) (Harada *et al.*, 1998; Suleiman *et al.*, 1999; Adl-Zarrabi *et al.*, 2006). Simpson & TenWolde (1999) state that D_{ax} measurements for water content values above 25 % are few in number and generally lack accuracy. As the water content in sapwood of living trees ranges between 98% to 249 % for conifers and between 44 %

and 162 % for hardwoods, dependent on species and seasonality (Skaar, 1988), there clearly is a lack in D_{ax} knowledge for sap flow applications.

As explained in section 4.3, Marshall (1958) determined D_{ax} by applying Eq. 4.2 for specific times after application of the heat pulse, mentioning a range of 0.0014 to 0.0040 $cm^2\ s^{-1}$. These values are based on the equations for an ideal heat pulse. In addition, this method seems impractical as the four used time points need to be specifically chosen to reach the requisite of $t_1+t_4=t_2+t_3=2t_2$. For the Tmax method, the weaknesses are that zero flow conditions are required and that it is based on one time point which is difficult to determine as the measured temperatures during zero flow have a broad peak, impeding the determination of t_m (Green *et al.*, 2003). The method as mentioned in Burgess *et al.* (2001a) based on the work of Swanson (1983), Turrell *et al.* (1967) and Siau (1971) is not dependent on point measurements of temperatures after application of a heat pulse nor on zero flow conditions as a sample is taken from the sapwood, but determines D_{ax} based on an empirical relationship for which only a fresh wood sample needs to be taken. Given the growing popularity of the HR method, this approach to determine D_{ax} has been frequently applied. Table 5.1 gives an overview of recent papers in which thermal diffusivity was calculated accordingly. From the 43 papers investigated, 29 mentioned the application of the method as described in Burgess *et al.* (2001a), while 11 did not mention it specifically, but did apply HR measurements to quantify sap flow. Hence, it is assumed that in these studies, the method was also applied. In only 3 papers, the HR method was used relatively, pre-empting the use of thermal diffusivity.

Table 5.1 *An overview of literature in which the Heat Ratio method is applied. For 40 papers, thermal diffusivity is calculated according to the approach mentioned in Burgess et al. (2001).*

Year published	Publications in which D_{ax} is determined according to Burgess *et al.* (2001a)
2011	Hernandez-Santana *et al.* (2011); Staudt *et al.* (2011)
2010	Ambrose *et al.* (2010); Bleby *et al.* (2010); Er-Raki *et al.* (2010): Macfarlane *et al.* (2010); MCElrone *et al.* (2010); Miller *et al.* (2010); Pfautsch *et al.* (2010); Zeppel *et al.* (2010)
2009	Hao *et al.* (2009); Hu *et al.* (2009); Madurapperuma *et al.* (2009a; 2009b); Mitchell *et al.* (2009); O'Grady *et al.* (2009); Pfautsch *et al.* (2009); Turnipseed *et al.* (2009); Winters *et al.* (2009)
2008	Moore *et al.* (2008); Scott *et al.* (2008); Zeppel *et al.* (2009)
2007	Fisher *et al.* (2007); MCElrone *et al.* (2007); Scholz *et al.* (2007); Warren *et al.* (2007); West *et al.* (2007)
2006	Burgess & Bleby (2006); Langensiepen *et al.* (2006)
2005	Oliveira *et al.* (2005)
2004	Bleby *et al.* (2004); Bucci *et al.* (2004); Burgess & Dawson (2004); Hultine *et al.* (2004); Williams *et al.* (2004)
2003	Hultine *et al.* (2003a; 2003b); Kurpius & Goldstein (2003); Kurpius *et al.* (2003); Yepez *et al.* (2003)
2002	Scholz *et al.* (2002)

5.1.1 But are we missing the point when applying the thermal diffusivity theory?

Although the recalculation based on fresh/dry sapwood density and water content determined from a sapwood sample is currently considered as the way to determine D_{ax} in sap flow research (Burgess *et al.*, 2001a), the underlying theory is incorrect for sapwood with water contents above the fibre saturation point which is the case for most, if not all, transpiring trees during sap flow measurements. The approach proposed by Burgess *et al.* (2001a) applies the method of mixtures as mentioned in Skaar (1988) to determine c (J kg^{-1} K^{-1}) of wet wood:

$$c = \frac{w_d c_d + c_w (w_f - w_d)}{w_f} \qquad (5.1)$$

where w_f is the fresh and w_d the oven-dried weight of a wood sample (kg) and c_w and c_d the specific heat capacity of water (4186 J kg^{-1} K^{-1}) and dry wood (1200 J kg^{-1} K^{-1}) at 20°C, respectively (Edwards & Warwick, 1984). This method is known to underestimate c of wet wood because the energy in the wood-water bonds is not taken into account (Kelsey & Clarke, 1956). These authors state that this could lead to differences up to 10 %. Morton & Hearle (1975) highlighted that c of sorbed water itself is lower than that of free liquid water. This was however not taken into account in the calculations of Kelsey & Clarke (1956) nor in the calculation of Hearmon & Burcham (1955) as they used the same c for both free and bound water. Nevertheless, bound water, when the water content exceeds the fibre saturation point (MC_{FSP}), generally accounts for about 30 % of the total water expressed as water mass per dry wood mass (Siau, 1984), although this value can be higher for low dry wood densities and lower for high dry wood densities (Skaar, 1988). It is thus difficult to conclude if this manner of determining c will lead to over- or underestimations for sapwood, which generally contains high percentages of free water. However, the method of mixtures is generally considered as a reliable calculation procedure (Stamm & Loughborough, 1935; Steinhagen, 1977).

Similarly as for c, a method of mixtures, modified from Turrel *et al.* (1967) and also mentioned in Swanson (1983), is used to determine axial thermal conductivity K_{ax} (W m^{-1} K^{-1}):

$$K_{ax} = K_w MC \frac{\rho_d}{\rho_w} + K_d \left(1 - MC \frac{\rho_d}{\rho_w}\right) \qquad (5.2)$$

with K_w and K_d the thermal conductivity of water (0.5984 W m^{-1} K^{-1}) and dry wood at 20˚C, *MC* the water content of the sample (ratio of water weight to dry wood weight) and ρ_w and ρ_d the densities of water and dry wood (kg m^{-3}). To determine K_{ax} of dry wood (K_d), an equation based on a theoretical model developed by Siau (1971) is used:

$$K_d = 0.04186\ (21.0 - 20.0 F_v) \qquad (5.3)$$

with F_v the void fraction of the wood. This equation was obtained by a single-cell model with cell dimensions of unity length, width and height and an internal lumen with a length and width of dimension a ($=\sqrt{F_v}$) (Figure 5.1). For a flux in the direction of the fibre axis, K_d becomes:

$$K_d = K_{mx}(1 - F_v) + K_{air} F_v \qquad (5.4)$$

with K_{mx} the (axial) thermal conductivity of the (wet) wood matrix and K_{air} the thermal conductivity of air. To obtain Eq. 5.3, Eq. 5.4 was fitted to K_d data found in literature and a good agreement was obtained when using 0.0001 cal cm^{-1} s^{-1} K^{-1} (0.04186 W m^{-1} K^{-1}) for K_{air} and 0.0021 cal cm^{-1} s^{-1} K^{-1} (0.8791 W m^{-1} K^{-1}) for K_{mx} (Siau, 1971). Thus far, the method seems theoretically sound, neglecting similar implications of using a mixed-model as for the determination of *c*. However, the conductivity single-cell model of Siau (1971) is based on a combination of *K* of cell wall material (with a certain water content) and an air filled lumen without unbound water. Hence, the model was developed for non-saturated wood.

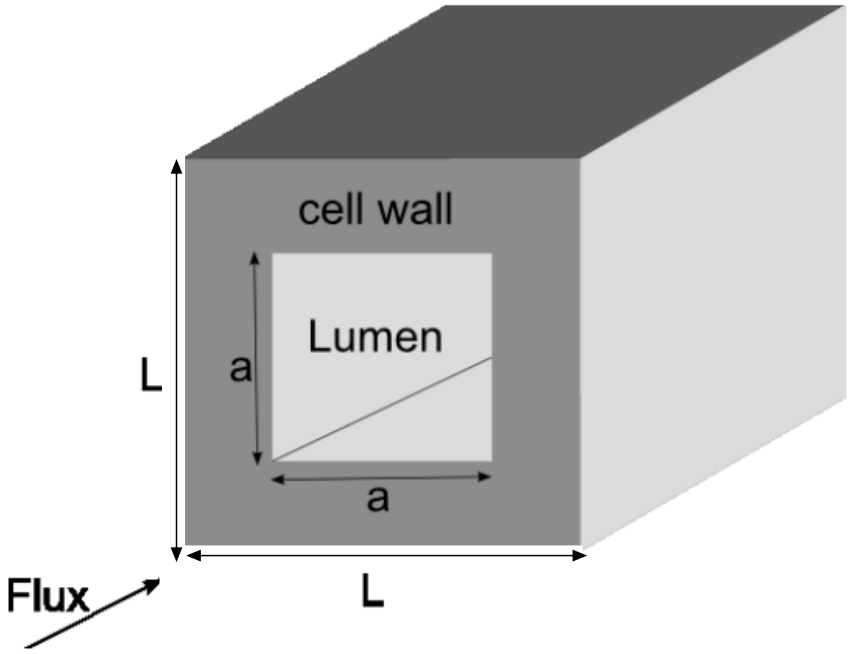

Figure 5.1 *Geometrical model for a single wood cell on which the theory of Siau (1971) is based, with L the length and width of the wood cell and a the length and width of the internal lumen.*

In this model, the void fraction is defined as:

$$F_v = 1 - G((\rho_w / \rho_{cw}) + MC) \qquad (5.5)$$

with G the specific gravity of wood (dry mass per fresh volume divided by the density of water) at water content MC (moisture per dry weight), ρ_{cw} the cell wall density (1530 kg m^{-3}, Kollmann and Côté (1968)) and ρ_w the sap (=water) density (1000 kg m^{-3}). This void fraction thus indicates the volume fraction of air in the wood. Interestingly, this expression is valid for water contents below the fibre saturation point. When deducing Eq. 5.4 from the conductivity single-cell model, Siau (1971) highlighted that K_d is not independent of MC. He reasoned that an increase in water content decreases the porosity F_v of the wood resulting in an increase in K_d. This reasoning is however an oversimplification of reality, as the rise in K_d will not only be due to a decrease in porosity but also due to the fact that the thermal conductivity of (bound) water is higher than that of completely dry wood components without water or air (0.10512 $W.m^{-1}.K^{-1}$ according to Stamm (1964)). Nevertheless, for practical purposes of wood that is used as a construction material, Siau (1971) concluded that K_{mx} can be considered independent of MC. The fit of experimental data to Eq. 5.4 led to small deviations for MC ranging from 0 to 25 %,

justifying his assumption. This fit led to the value of 0.0021 cal cm^{-1} s^{-1} K^{-1} for K_{mx} and Eq. 5.3.

However, the main implication of the use of this model in sap flow research lays in the interpretation of *MC*. In the first part of Eq. 5.2, describing the contribution of water to the total thermal conductivity, *MC* is used as a measure for the amount of free water. In the second part of Eq. 5.2, describing the contribution of dry wood, the same *MC* is used. The conductivity K_d, however, already takes into account the water bound in the wood matrix. This implies that *MC* ascribed to free water will be smaller than total *MC* calculated as the difference between fresh weight and oven-dry weight divided by the fresh weight of a sample. Moreover, the void fraction F_v represents the void fraction at fibre saturation point which will be larger than the void fraction at higher water contents.

5.1.2 Corrected equation to determine thermal conductivity K_{ax}

For a correct application of the concept, Eq. 5.4 should be used to calculate the total thermal conductivity for *MC* below the fibre saturation point as was intended by Siau (1971). For higher *MC*, the following equation should be used:

$$K_{ax} = K_w(MC - MC_{FSP})\frac{\rho_d}{\rho_w} + K_{mx}(1 - F_{v\_FSP}) + K_{air}F_v \qquad (5.6)$$

with MC_{FSP} the water content at fibre saturation point and F_{v_FSP} equal to $1\text{-}G((\rho_w/\rho_{cw})+ MC_{FSP})$, the volume fraction at fibre saturation point. However, here K_{mx} and K_{air} will not hold the same value as in Eq. 5.4 as the applied volume fractions differ. Hence, the empirical derived coefficients as determined by Siau (1971) are no longer applicable. Therefore, it will be assumed that F_v in Eq. 5.6 is equal to F_{v_FSP}. This will only induce an overestimation in K_{ax} of a few percent given the small thermal conductivity of air compared to total wood thermal conductivity. Hence, the equation becomes:

$$K_{ax} = K_w(MC - MC_{FSP})\frac{\rho_d}{\rho_w} + K_{mx}(1 - F_{v\_FSP}) + K_{air}F_{v\_FSP}$$

or

$$K_{ax} = K_w(MC - MC_{FSP})\frac{\rho_d}{\rho_w} + 0.04186(21.0 - 20.0F_{v\_FSP}) \quad (5.7)$$

Eq. 5.7 is more correct in determining thermal diffusivity in sapwood compared to Eq. 5.2 which has thus far been used. The objectives of this chapter are to estimate the errors in thermal diffusivity and sap flux density across varying wood properties due to application of the erroneous Eq. 5.2 which does not distinguish between bound and unbound water in sapwood.

5.2 Materials and Methods

5.2.1 Sensitivity analysis

To assess the difference in water use according to current practice for HR measurements and the results generated using Eq. 5.7, the relative error (SFD_{err}) in sap flux density (SFD) was determined, calculated as the difference between SFD obtained based on Eq. 5.2 and based on Eq. 5.7, respectively, divided by SFD based on Eq. 5.7. To gain insight into the influence of the different parameters in Eq. 5.2 and 5.7 on this relative error, the centralized relative sensitivity function of this relative error SFD_{err} towards each parameter θ was calculated as:

$$S(SFD_{err}) = \frac{\theta}{SFD_{err}} \frac{SFD_{err}(\theta + \Delta\theta) - SFD_{err}(\theta - \Delta\theta)}{2\Delta\theta} \quad (5.8)$$

with $\Delta\theta$ taken as 1 % of the source component value θ. This way, the relative sensitivities of SFD_{err} to MC, MC_{FSP} and ρ_d were calculated. Besides, a sensitivity measure δ^{meas} similar to that of Brun *et al.* (2002), Steppe *et al.* (2006) and De Pauw *et al.* (2008) was calculated:

$$\delta^{meas} = \frac{1}{N}\sum_{k=1}^{N} s_{i,k}{}^2 \quad (5.9)$$

where k is the sensitivity MC instance, N the number of MC instances for the sensitivity function and $s_{i,k}$ the relative sensitivity of SFD_{err} to the parameter i of interest (MC, MC_{FSP} or ρ_d). As MC_{FSP} generally ranges between 15 and 35 %, depending on wood species (Skaar, 1972), these values were implemented in the simulation. For dry wood density, Skaar (1972) mentions a range from 310 kg m^{-3} for Western Red

Cedar up to 1100 kg m^{-3} for Ceylon Satinwood. Note that ρ_d also varies within species, depending on age, height and environmental conditions.

5.2.2 Plant material

To assess the implications of the misinterpretation of the method of Siau (1971) in the field, experiments were conducted in which wood sections were taken from European (*Fagus sylvatica* L.) and American (*Fagus grandifolia* Ehrh.) beech, both diffuse-porous hardwoods. Sapwood sections of three 10- to 20-years old European beech trees were taken at the experimental forest 'Aelmoeseneie' of Ghent University (Gontrode, Belgium) and sections from two 60- to 70-years old American beech trees were taken from Whitehall forest, the experimental forest of the University of Georgia (Athens, Georgia, USA). The trees had a stem diameter at breast height ranging from 14 to 21 cm.

For each cut tree, a sapwood section was taken at breast height. For two of the European and American beech trees, wood sections were also taken at 50 cm above breast height. After measuring the fresh weight of these sections, the volume was determined by immersing the fresh wood sample, tightly wrapped in parafilm (Parafilm M, SPI supplies/Structure Probe Inc., West Chester, PA 19380, USA) to avoid water adsorption, in water and applying Archimedes' principle. Afterwards, the sections were dried to determine their dry weight. From these measurements, *MC*, ρ_d and F_v and F_{v_FPS} were determined. Fibre saturation point values were estimated according to Roderick & Berry (2001):

$$MC_{FSP}=0.2\ (\rho_d\ \rho_w^{-1})^{-1/2} \qquad (5.10)$$

with ρ_d (kg m^{-3}) the dry wood density and ρ_w the density of water (1000 kg m^{-3}).

5.2.3 Thermal conductivity versus water content: original versus corrected method

For one European beech tree, a stem segment of approximately 1 m was cut in the forest. The ends of this segment were sealed with parafilm (Parafilm M, SPI supplies/Structure Probe Inc., West Chester, PA, 19380, USA) and enclosed in a plastic bag to minimize evaporation. After transportation to the Laboratory of Plant Ecology, Ghent University, a small section of sapwood of approximately 250 cm^3 was cut from the centre of this larger segment. This section was weighed, left to dry and

then wrapped in parafilm (Parafilm M, SPI supplies/Structure Probe Inc., West Chester, PA 19380, USA) for one hour to ensure a homogenous water content. Then the weight of the section was measured. This was repeated to obtain a range of water contents from approximately 0.45 to 0.8. Afterwards, the volume of the section was determined according to the Archimedes' principle. These measurements allowed us to establish a relation between thermal conductivity and water content both for the original and the corrected method.

5.2.4 Implications of the correction for actual sap flow measurements

To assess the implications of an inaccurate estimation of thermal diffusivity due to a misinterpretation of water content, sap flow in an *Eucalyptus caliginosa* was measured using the HR method (Burgess *et al.*, 2001a). From this *Eucalyptus caliginosa*, a segment with diameter 9.1 cm was freshly cut, prepared and hung in a gravimetric validation system similarly as done by Steppe *et al.* (2010). This way, HR measured sap flow with the diffusivity calculated according to both Eq. 5.2 and 5.7 could be compared with gravimetric data of sap flow. For this experiment, a commercially available HR sensor was used, consisting of a heater needle and two measurement needles located 5 mm upwards and downwards of the heater needle, respectively (ICT International PTY LTD, Armidale, Australia). For this sensor, the diameter of the needles is 1.5 mm and their length 35 mm and a wound width of 1.71 mm was determined. In each measurement needle, two thermocouples are located at respectively 7.5 and 22.5 mm from the needle tip, located respectively 3 and 18 mm below the bark. For these measurements, D_{ax} was calculated according to both Eq. 5.2 and 5.7. To partially correct for the radial sap flux density profile, also an HFD sensor (ICT International PTY LTD, Armidale, Australia) was installed (Steppe *et al.*, 2010). This sensor was installed 10 cm axially upstream and 90° tangentially from the HR sensor and has the ability to estimate sap flux densities at eight different depths, with 10 mm between each measurement depth and the first depth at 3 mm below the bark. Hence, for both sensors, a measurement point is located at 3 mm below the bark for which the ratio of the HR to the HFD sap flux density was determined. By multiplying this ratio to the sap flux densities obtained by the HFD sensor at the other seven depths, a radial profile was calculated based on the accuracy of the HR measurements (Steppe *et al.*, 2010). Hence, it was possible to determine the sap flow through the segment more accurately, combining the

relative HFD radial profile with the absolute values of the HR method. As the measured flows were rather low (<25 cm^3 cm^{-2} h^{-1}), the relative radial sap flux density pattern of the HFD was assumed to be correct (see Chapter 3).

The fibre saturation point was determined according to Eq. 5.10. A wood section of 19.6 cm^3 was taken at the position of the HR sensor from which fresh weight, dry weight and volume were determined, necessary to calculate thermal diffusivity.

5.3 Results

Figure 5.2 shows the results of applying Eq. 5.2 and 5.7 for different dry wood densities (ρ_d) and fibre saturation points (MC_{FSP}) over a wide range of water contents.

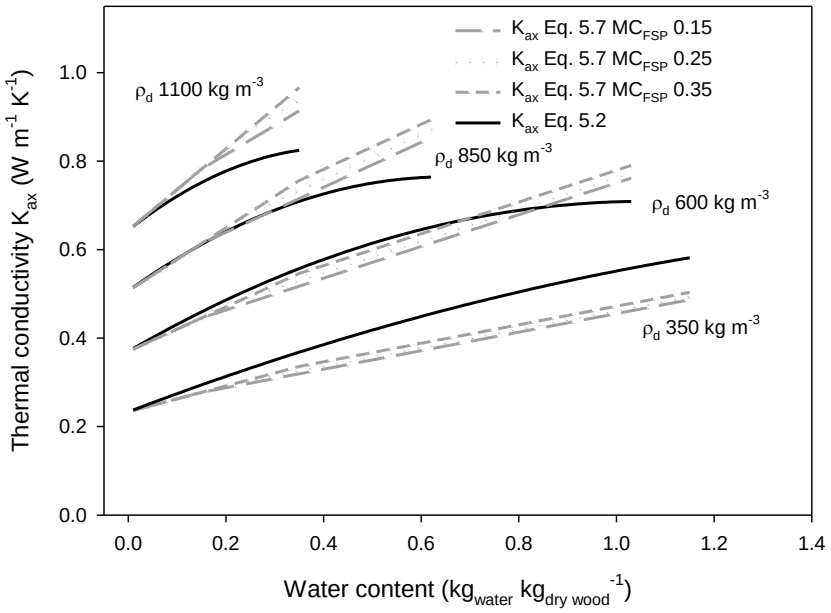

Figure 5.2 *Application of Eq. 5.2 and 5.7 for different dry wood densities (ρ_d). For Eq. 5.7, fibre saturation points ranging between 15 and 35% were implemented (striped gray lines). For each ρ_d, thermal conductivity K_{ax} increases for rising fibre saturation points.*

In Figure 5.3, the relative error in sap flux density (SFD_{err}) due to the application of Eq. 5.2 instead of Eq. 5.7 is given for these same sapwood parameters. The corresponding relative sensitivities of SFD_{err} to MC, MC_{FSP} and ρ_d are presented in Figure 5.4 while Figure 5.5 represents the sensitivity measures δ^{meas}.

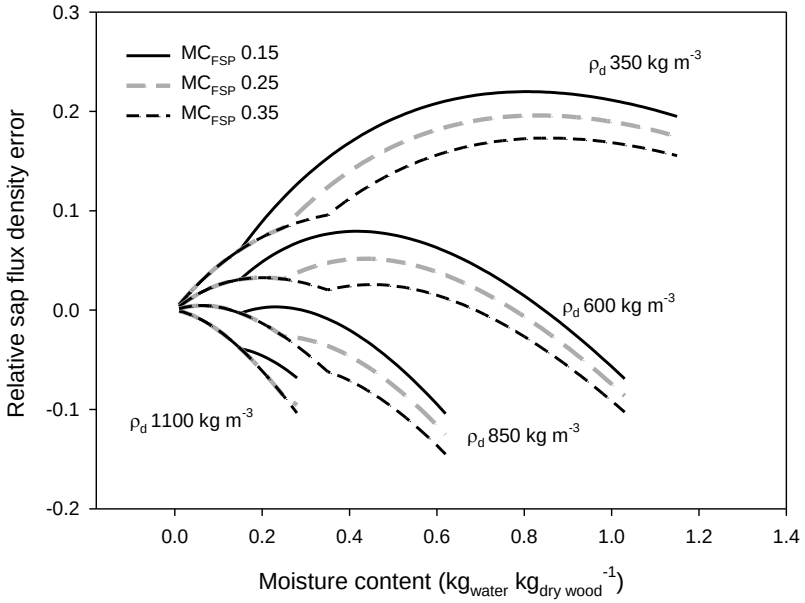

Figure 5.3 *The relative error in sap flux density, calculated as the ratio of the difference between sap flux density applying D_{ax} based on Eq. 5.2 and based on Eq. 5.7, respectively, to the sap flux density applying D_{ax} based on Eq. 5.7, for different water*

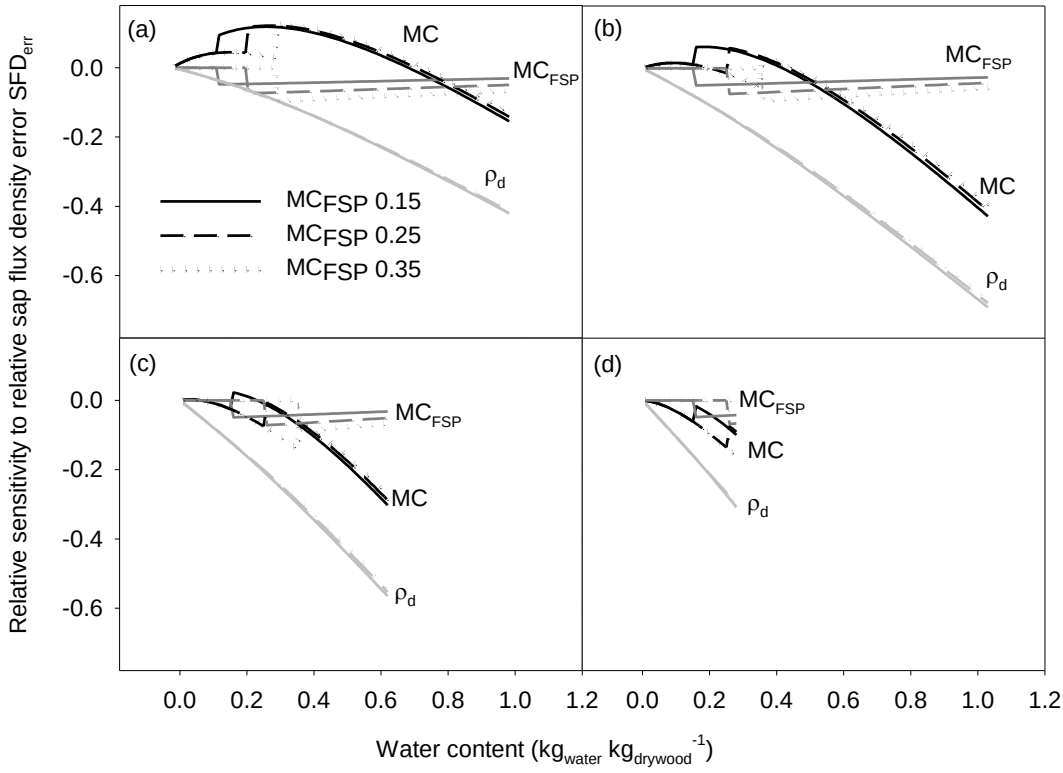

Figure 5.4 *Relative sensitivities of the relative error in sap flux density (SFD_{err}) to water content (MC), fibre saturation point (MC_{FSP}) and dry wood density (ρ_d) for ρ_d 350 kg m^{-3} (a), 600 kg m^{-3} (b), 850 kg m^{-3} (c) and 1100 kg m^{-3} (d).*

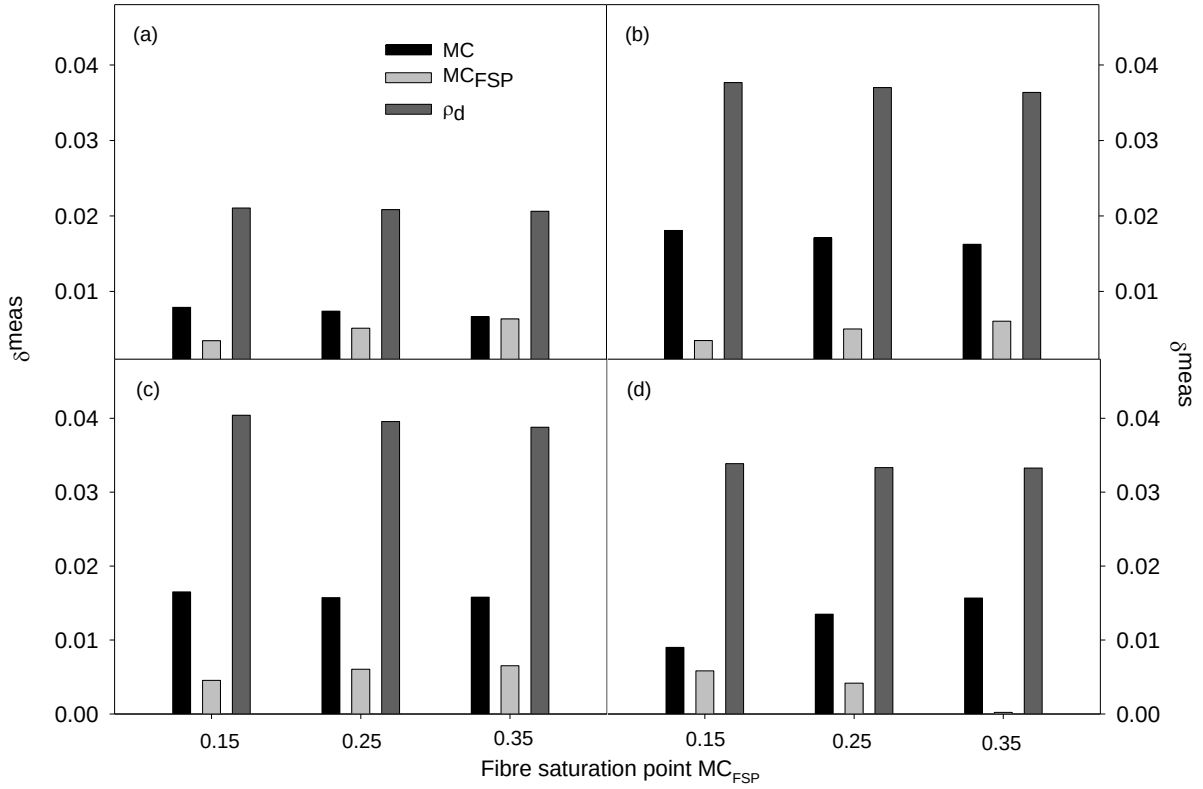

Figure 5.5 *Sensitivity measure δ^{meas} for water content (MC), fibre saturation point (MC_{FSP}) and dry wood density (ρ_d) for different MC_{FSP} and ρ_d 350 kg m^{-3} (a), 600 kg m^{-3} (b), 850 kg m^{-3} (c) and 1100 kg m^{-3} (d).*

Table 5.2 shows the water content, dry wood density and corresponding thermal conductivity according to Eq. 5.2 and Eq. 5.7 for both the European and the American beech sections. The percentage over- or underestimation due to the application of Eq. 5.2 in comparison to Eq. 5.7 is given in Figure 5.6. For the dry wood densities available, the use of Eq. 5.2 leads to underestimations of axial thermal diffusivity (and hence sap flux density) of up to 10 %. Overall, based on a modified Levene test to test for homogeneity of variance, the variability between tree species is not more significant than the variability between trees of the same species or even variability within the same tree according to height. Samples taken at different heights can lead to large differences in calculated thermal diffusivity. Figure 5.7 shows the thermal conductivities according to Eq. 5.2 and 5.7 for different water contents of the European beech sample. Apparently, errors were larger for lower and practically zero for higher water contents for this specific dry wood density, which corresponds to the data presented in Figure 5.2. Overall, the error for this specific sapwood sample was maximally 4.5 %.

Table 5.2 *Characteristics and calculated thermal conductivity K_{ax} according to both Eq. 5.2 and 5.7 for the experimental trees. EU indicates European beech while US refers to American beech. BH stands for Breast Height. For each sample, the corresponding stem diameter at sample height, sample volume, water content (MC) and dry wood density (ρ_d) are given.*

Tree	Sampling height	Sample volume (cm^3)	*MC*(-)	ρ_d ($kg.m^{-3}$)	K_{ax} (Eq. 5.2) ($W.m^{-1}.K^{-1}$)	K_{ax} (Eq. 5.7) ($W.m^{-1}.K^{-1}$)
EU1	BH	76	0.77	585	0.68	0.67
	BH+50	53	0.79	567	0.67	0.66
EU2	BH	62	0.86	674	0.72	0.80
	BH+50	68	0.91	653	0.72	0.79
EU3	BH	87	0.84	685	0.72	0.81
US1	BH	20	0.99	620	0.71	0.79
	BH+50	90	0.99	586	0.70	0.74
US2	BH	122	0.66	723	0.72	0.76
	BH+50	160	0.80	606	0.69	0.70

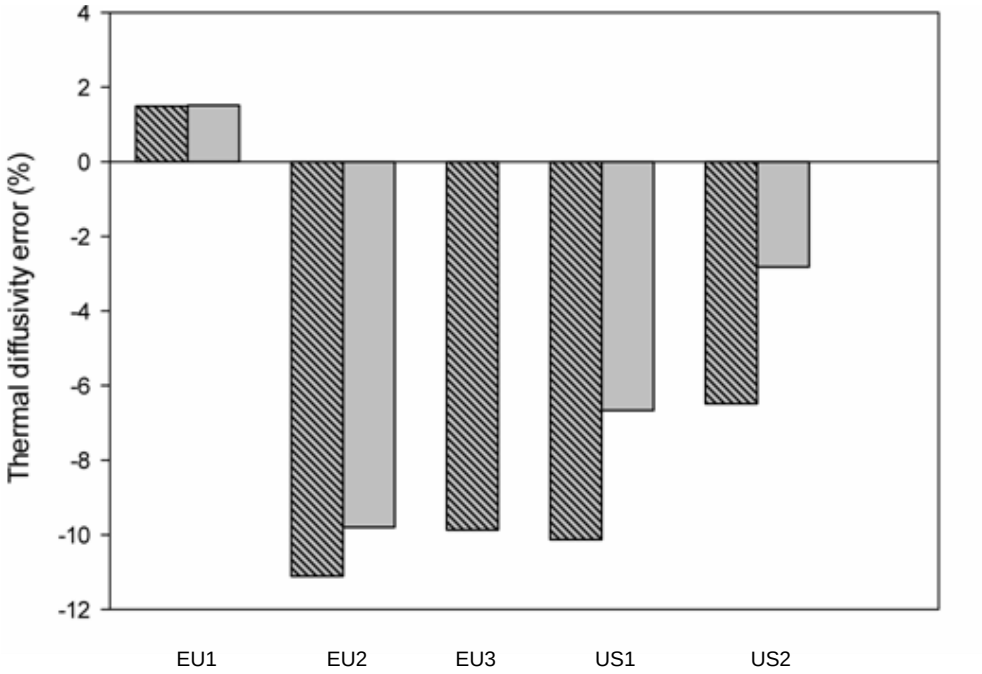

Figure 5.6 *Relative error in thermal diffusivity calculated as (D_{ax}(Eq. 5.2)-D_{ax}(Eq.5.7))/D_{ax}(Eq. 5.7) for European and American beech. The striped bars indicate the lower sections (BH), while the full bars are located 50 cm higher (BH+50).*

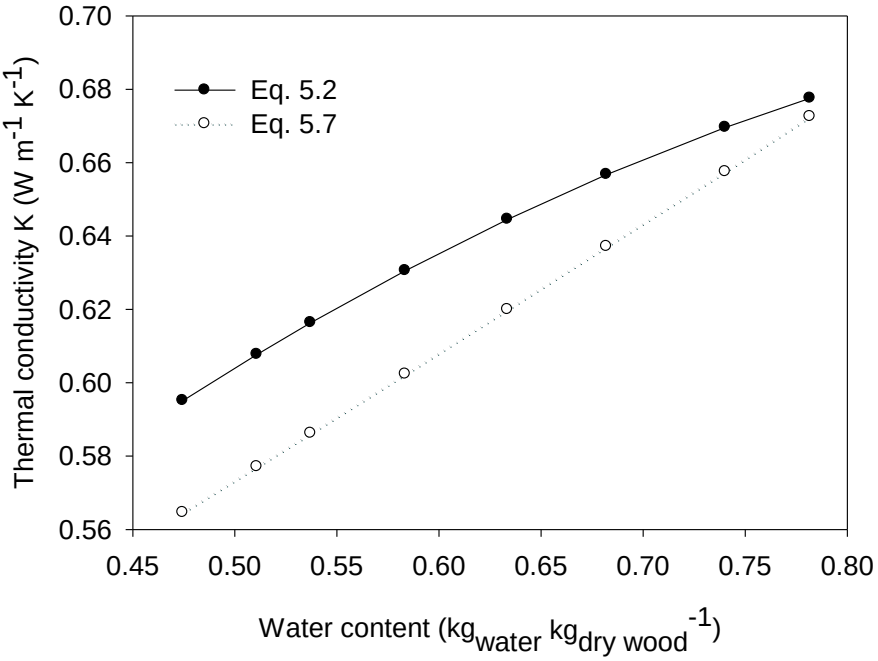

Figure 5.7 *Thermal conductivity (W m^{-1} K^{-1}) calculated according to Eq. 5.2 and 5.7 for different water contents for European beech with dry wood density 585 kg m^{-3}.*

When comparing the obtained sap flow using both Eq. 5.2 and Eq. 5.7 with the gravimetric reference data for *Eucalyptus caliginosa*, it is clear that Eq. 5.7 leads to a better fit (Figure 5.8) when applying the HR method, corrected for the relative radial profile obtained with HFD. Linearly regressing the difference in results based on Eq. 5.2 and those based on Eq. 5.7 versus the gravimetric sap flux densities led to a significant slope of 0.11. Hence, for this experiment, an underestimation of about 11 % for D_{ax} was obtained when applying Eq. 5.2 instead of Eq. 5.7.

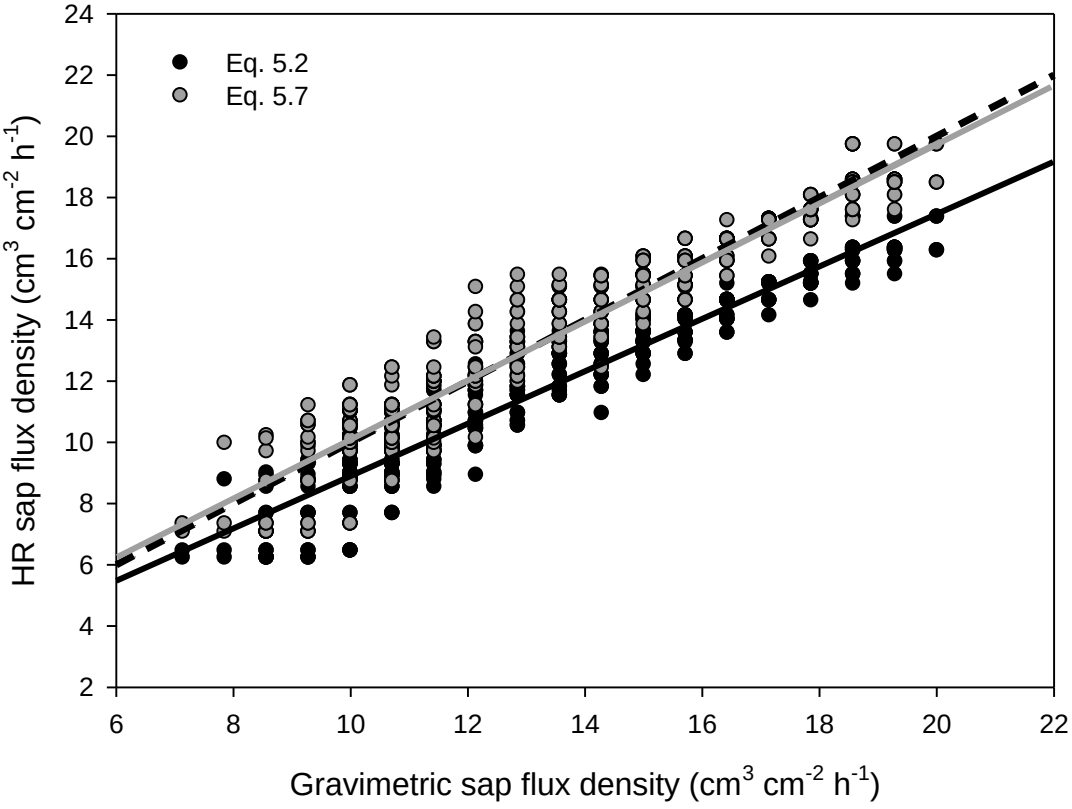

Figure 5.8 *Sap flux density based on the Heat Ratio method with the diffusivity according to Eq. 5.2 (black line) and Eq. 5.7 (grey line) for an Eucalyptus caliginosa tree (dry wood density 565 kg m^{-3} and water content 1.17) compared to the gravimetric reference. The dashed line is the 1:1 line.*

5.4 Discussion

As is clear from Figure 5.2, variations in water content, fibre saturation point as well as dry wood densities amongst and within species, can lead to large over- or underestimations of K_{ax}. This results in a relative sap flux density error varying between –15 and +22 %, dependent on ρ_d, MC and MC_{FSP} (Figure 5.3). For the lower

dry wood densities (~350 kg m^{-3}), application of Eq. 5.2 leads to overestimation of *SFD*, while for the upper values (~1000 kg m^{-3}) it leads to underestimation. For average ρ_d (~600 kg m^{-3}) and *MC* of approximately 0.8, the error is negligible. Clearly, the relative error is highly influenced by differences in ρ_d, which is confirmed in the sensitivity analysis (Figure 5.4 and Figure 5.5). Notice that δ^{meas} for *MC* is always higher than for MC_{FSP}, even though for low dry wood densities the relative sensitivity to *MC* approximates the relative sensitivity to MC_{FSP} for water contents between 0.7 and 1. Moreover, MC_{FSP} can be estimated according to Eq. 5.10, even though this is only an empirical relationship and prone to slight over- or underestimations. As ρ_d is known to be dependent not only on species but also on age, height and environmental conditions, this parameter should be measured in close proximity of the installed sap flow sensor. Likewise, differences in *MC* of 60 % and more have been reported for different species (Peck, 1953). Moreover, *MC* poses a greater challenge than ρ_d as it has been shown to also vary seasonally up to 25 % (Peck, 1953; Gibbs, 1958; Henderson & Choong, 1968) and even 40 % (Gibbs, 1958). More recently, Borghetti *et al.* (1998) have shown a clear relationship between water content in the xylem of twigs and twig water potential. As they have shown diurnal patterns for twig water potential, these same patterns will occur for twig water content, implying not only seasonally but also diurnal *MC* changes. Moreover, Scholz *et al.* (2007) have detected daily changes of up to 18 % in relative water content, calculated as the ratio of the differences between fresh and dry wood and saturated and dry wood, for savanna species in Brazil. This implies that thoroughly accurate measurements can only be made when the water content is known at the time of measuring.

The results of the field experiment confirm the findings of the sensitivity analysis. Clearly the difference between Eq. 5.2 and 5.7 is determined by both water content and dry wood density (Figure 5.6). From Figure 5.7, one would expect that Eq. 5.2 overestimates for low water contents, but is quite accurate for higher water contents of about 80 %. From Figure 5.6 and Table 5.2 however, it is clear that water content alone is not sufficient to explain the over- or underestimations as for water contents of about 80 %, large underestimations are obtained. These results also indicate that within the same tree, differences in both water content and/or dry wood density can occur, again stressing the importance of measuring both these parameters in proximity of the sensor.

Figure 5.8 shows the possible impact of using Eq. 5 during field measurements of sap flux density. Here, the relative difference in sap flux density due to this single misinterpretation was about 11 %. When absolute measurements of sap flow are needed, such differences can undoubtedly lead to erroneous results and interpretations.

Up to now, Eq. 5.2 was considered applicable for sapwood without considering the correct meaning of *MC*, hence missing the point of the original theory as developed by Siau (1971). Unfortunately, in the papers mentioned in Table 5.1, no indications are given of the dry wood density or water content used to calculate the thermal diffusivity according to Eq. 5.2, making an estimation of the errors in sap flux density for these studies impossible. However, for the model mentioned in Wullschleger *et al.* (2011) where K_{ax} is calculated according to Eq. 5.2 with a K_d value for dry wood based on Jones *et al.* (2004), an error of about 15 % is made for an assumed fibre saturation point of 0.3. Other heat transport models have probably based the implementation of K_{ax} on Eq. 5.2 as well.

Eq. 5.7 has the advantage of a correct underlying theory, although a slight overestimation can be expected because of the simplification needed to apply the empirical coefficients of Siau (1971) and the additional parameter MC_{FSP} needs to be estimated. This parameter, however, can easily be estimated based on ρ_d (Eq. 5.10). Moreover, Eq. 5.7 is not very sensitive towards MC_{FSP}, especially for high water contents as is mostly the case for transpiring trees (Figure 5.4). Therefore, a wrong estimation of this particular parameter will only lead to small errors in D_{ax} calculations according to Eq. 5.7. A much larger challenge lays in the determination of the water content. While this parameter is measured at the moment of sampling, the seasonal and daily variations are not taken into account. Taking multiple samples during the season will improve accuracy, but is often practically difficult due to enhanced tree damage. However, as the Tmax method has the prerequisite of zero flow conditions and limitations of a single point measurement, Eq. 5.7 seems to be the more favorable method for D_{ax} determinations in the field as to our knowledge, no other methods exist for determining thermal diffusivity during non-zero flow conditions. Nevertheless, a combination of methods is desirable. For instance, combining Time Domain Reflectometry (Wullschleger *et al.*, 1996a; Nadler *et al.*, 2006) or tomography (Brazee *et al.*, 2011; Bieker & Rust, 2012) estimates of relative changes in water content with absolute measurements of D_{ax} based on Eq.

5.7 will likely result in improved sap flux density measurements but is of course more labour and cost intensive. Another option is to apply the Compensation Heat Pulse method as its operating principle is independent of D_{ax}. Unfortunately, this method is unable to resolve low or reverse flows.

5.5 Conclusions

Thermal diffusivity is a crucial parameter in modern sap flow calculation methods such as the Heat Ratio method. However, due to a misinterpretation of *MC* in the analytical equations, the current applied methodology to determine D_{ax} can lead to over- or underestimations of up to 10 % and more, depending on dry wood density, water content and fibre saturation point when compared with the more accurate approach which is presented in this chapter.

6

Development of the Sapflow+ method to measure sap flux density and water content

After: *Vandegehuchte, M.W. & Steppe, K. (2012). A triple-probe heat pulse method for measurement of thermal diffusivity in trees. Agricultural and Forest Meteorology, 160: 90-99.*

Vandegehuchte, M.W. & Steppe, K. (2012). Sapflow+: a four needle heat pulse sap flow sensor enabling non-empirical sap flux density and water content measurements. New Phytologist, 196: 306-317.

BE2012/0030: Een methode voor het meten van sapstroom, waterinhoud en thermische eigenschappen in planten

Abstract

So far, no non-empirical method exists to measure reverse, low as well as high sap flux densities independently of thermal diffusivity. Besides, existing sap flow methods require multiple destructive wood core measurements to determine temporal changes in sapwood water content, necessary to convert heat velocity to sap flux density. In this chapter, a non-empirical heat pulse based method and coupled sensor are presented which measure temperature changes around a linear heater in both axial and tangential directions after application of a heat pulse. By fitting the correct heat conduction-convection equation to the measured temperature profiles, heat velocity and water content of the sapwood can be determined. An identifiability analysis and validation tests on artificial and real stem segments of European beech (*Fagus sylvatica* L.) confirm the applicability of the method, leading to accurate determinations of heat velocity, water content and, hence, sap flux density. The proposed method enables sap flux density measurements across the entire natural occurring sap flux density range of woody plants. Moreover, the water content during low flows can be determined, enabling a correct conversion from heat velocity to sap flux density without multiple destructive core measurements.

6.1 Introduction

As mentioned in previous Chapters, existing heat-based sap flow methods all have their merits, but also suffer from specific limitations. The HFD method enables sap flux density measurements at different depths in the sapwood and has the strength of distinguishing high, low and reverse flows, but it remains empirical and can lead to over- or underestimations depending on sap flux density, water content and thermal characteristics of the wood (Chapter 3) (Vandegehuchte & Steppe, 2012b). The TD method has suffered from these same limitations and is known to largely underestimate sap flux density (Steppe *et al.*, 2010).

For the heat pulse methods, the CHP method has the advantage that thermal diffusivity does not need to be determined. However, it is incapable of determining low and reverse flows (Becker, 1998; Green *et al.*, 2009; Steppe *et al.*, 2010). This was partly resolved by Testi & Villalobos (2009) who used the CAG method, extending measurement possibilities towards the lower sap flow range. This method, however,

necessitates an empirical calibration which is dependent on the thermal characteristics of the sapwood. The HR method (Burgess *et al.*, 2001a) can measure both low and reverse flows but performs poorly at high flow rates (Burgess & Dawson, 2008) and applies an inaccurate protocol to determine thermal diffusivity, necessary as input parameter for the sap flux density calculations (Chapter 5). The Tmax method (Cohen *et al.*, 1981) determines thermal diffusivity correctly, but is based on a zero flows and a single point analysis, making it susceptible to scatter. Moreover, like the CHP method, it is unable to correctly estimate low and reverse flows (Green *et al.*, 2009). Besides, all heat pulse methods measure heat velocity which needs to be converted to sap flux density based on water content of the sapwood. To this end, wood cores are taken to estimate water contents. As taking multiple wood cores increases wood damaging, temporal variations in water content are usually not taken into account which may induce large errors in calculated sap flux densities. While relative changes in stem water content can be estimated by applications of methods such as Time or Frequency Domain Reflectometry, resistivity tomography, gamma-ray attenuation and electrical resistance, these methods require additional equipment, are difficult to interpret and struggle to take the spatial variability of the sapwood into account (Wullschleger *et al.*, 1996b; Nadler & Tyree, 2008; Bieker & Rust, 2012). At present, sap flux density and stem water content can be measured simultaneously by Magnetic Resonance Imaging (Van As *et al.*, 2009) but this laboratory technique is expensive, necessitates specific tuning for different flow ranges and remains difficult to apply in the field despite recent progress (Jones *et al.*, 2012). While many methods have been developed to determine sap flux density or stem water content separately, to our knowledge no practically applicable method exists which combines both.

This Chapter describes how a new method and coupled sensor were developed, further referred to as Sapflow+, building on the available knowledge within the sap flow research community and combining the strengths of existing sap flow methods. The Sapflow+ method is capable of non-destructively measuring high, low and reverse sap flows, thermal wood properties and water content of the sapwood based on thermodynamics. A theory based on earlier work of Kluitenberg & Ham (2004) and the knowledge gained in Chapter 4 is presented to determine these parameters based on conduction and convection of a short-duration heat pulse away from an infinite line source in the sapwood. It is shown that by using this

theory, sap flow, thermal wood properties and water content can be determined by a four-needle probe. Results of both Finite Element Modelling and lab experiments are presented which demonstrate the applicability of the theory for measuring sap flux density and water content of fresh sapwood.

6.2 Materials and methods

6.2.1 Theory

The theory applied is developed for an infinitely long linear heater of zero radius in an infinitely large medium. Based on the work of Kluitenberg & Ham (2004) and Vandegehuchte & Steppe (2012c), the temperature distribution in an anisotropic media is expressed as (see also Chapter 4):

$$\Delta T = \frac{q}{4\pi\sqrt{K_{ax}K_{tg}}}\int_0^t t^{-1}\exp\left(-\frac{\rho c}{4t}\left(\frac{(x-V_h t)^2}{K_{ax}}+\frac{y^2}{K_{tg}}\right)\right)dt \qquad \text{for } 0<t<=t_0 \qquad (6.1)$$

$$\Delta T = \frac{q}{4\pi\sqrt{K_{ax}K_{tg}}}\int_{t-t_0}^t t^{-1}\exp\left(-\frac{\rho c}{4t}\left(\frac{(x-V_h t)^2}{K_{ax}}+\frac{y^2}{K_{tg}}\right)\right)dt \qquad \text{for } t_0<t \qquad (6.2)$$

with ΔT the temperature difference (K) between the measured temperature at time t (s) after application of the pulse and the measured temperature before the heat pulse, measured at a distance x (m) axial and y (m) tangential from the heater, respectively. K_{ax} is the axial and K_{tg} the tangential thermal conductivity (W m^{-1} K^{-1}), ρ the density (kg m^{-3}) of the sapwood, c the specific heat capacity of the sapwood (J kg^{-1} K^{-1}) and q the energy input per unit length of the heater per unit time (W m^{-1}). By measuring the temperature change ΔT at three different positions around the heater needle, a multi-parameter model which solves Eq. 6.1 and 6.2 for each position can be fitted to retrieve the parameters of interest, namely K_{ax}, K_{tg}, ρc (the volumetric heat capacity, J m^{-3} K^{-1}) and V_h. In this model, a temperature correction for changing sapwood temperatures independent of the heat pulses is applied. By determining the temperatures before and after the heat pulse, the slope of temperature change is calculated which is then subtracted from the modelled temperature changes.

This multi-parameter model was implemented, simulated and calibrated using the plant modelling software PhytoSim (Phyto-IT BVBA, Mariakerke, Belgium). For model

calibration the simplex method, originally developed by Nelder & Mead (1965), was used to minimize the weighted sum of squared errors between measured and simulated values of the temperatures. The weighted sum of squared errors objective value for each fit to the axial and tangential temperature data indicates the goodness of fit:

$$WSSE = \frac{1}{n}\sum_{i=1}^{k}\frac{1}{\sigma^2}\sum_{j=1}^{n}(m_{ij} - y_{ij})^2 \qquad (6.3)$$

where *WSSE* is the weighted sum of squared errors objective, *k* the number of objective variables (3, for each position at which the temperature is measured), σ^2 the measurement error variance for objective variable *i* (for the three temperature measurements a value of 0.02 for σ was applied, based on the calibration of the thermocouples in a warm water bath), *n* the number of measurement points for objective variable *i*, m_{ij} the j^{th} measurement value of objective variable *i* and y_{ij} the corresponding simulation value.

6.2.2 Water content

If the volumetric heat capacity (ρc, J m^{-3} K^{-1}) of the sapwood is known, its water content (*MC*, kg water per kg dry weight) can directly be determined (Swanson, 1983):

$$MC = \frac{1}{c_w}\left(\frac{\rho c}{\rho_d} - c_{dw}\right) \qquad (6.4)$$

with c_w and c_{dw} the heat capacity of water (4186 J kg^{-1} K^{-1}, Martin & Lang (1933)) and dry wood (1200 J kg^{-1} K^{-1}, Edwards & Warwick (1984)), respectively and ρ_d the dry wood density (kg m^{-3}), which can be measured once by sampling a wood core.

6.2.3 Sensor design

To apply the theory, a needle probe was designed consisting of a linear heater and three measurement needles located at specific distances, respectively, axially upstream, downstream and tangentially from the heater (Figure 6.1). The three stainless steel measurement needles have a length of 35 mm and a diameter of 1.1 mm. In each measurement needle a copper-constantan thermocouple is located at 20 mm from the needle basis. Notice that, similar as for the HR method, thermocouples could be installed at different depths to assess radial differences in

sap flux density. This, however, requires additional logging capacity. Due to practical limitations, it was in this set-up not possible to install more than one thermocouple in each measurement needle.

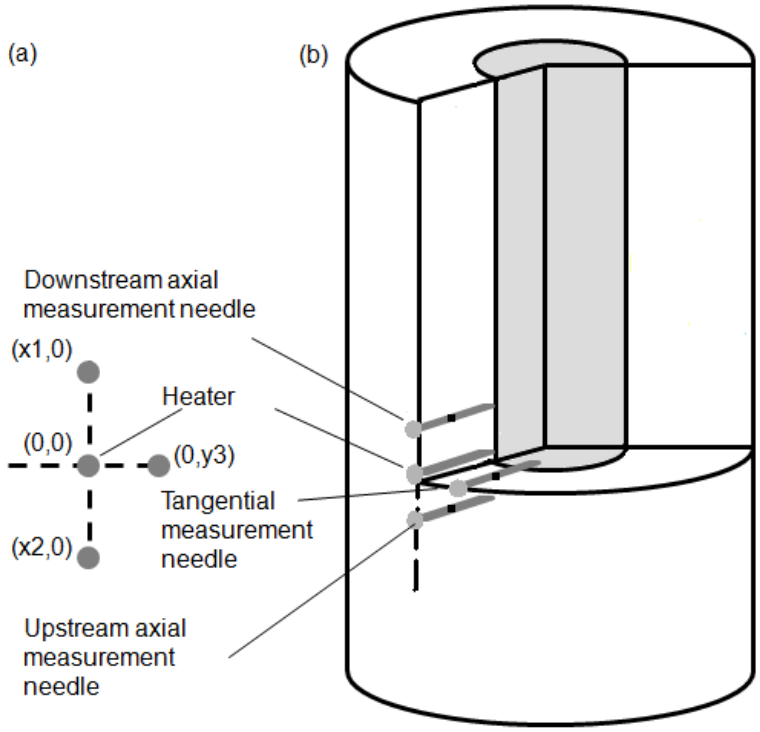

Figure 6.1 *(a) Schematic of a tangential section of the stem xylem with arrangements of the thermocouples around the heater of the Sapflow+ sensor; and (b) Schematic of the Sapflow sensor installed in the sapwood (SW) of a stem.*

The heater needle has a length of 38 mm and a diameter of 1.1 mm. The heater is slightly longer than the measurement needles to avoid side effects at the end of the sensor, similarly as for the HFD method. An enameled resistance wire with a known resistance (0.02341 Ω mm^{-1}) is coiled around this heater. Heat pulses of 6 seconds were generated by applying 5 V to the heater. The theoretical amount of heat released by this heater, q (W m^{-1}), was calculated similarly as done by Campbell *et al.* (1991):

$$q = \left(\frac{U}{R_s} \right)^2 R_s' \qquad (6.5)$$

with U (V) the applied voltage, R_s (Ω) the resistance of the heater and R_s' (Ω m^{-1}) the resistance of the heater per unit length.

A CR1000 datalogger (Campbell Scientific, Loughborough, UK) was used to control the heat pulse, monitor the applied voltage and measure the temperatures as a function of time.

6.2.4 Identifiability analysis

Application of the Sapflow+ model will only be successful when the parameters on which the model is calibrated, are identifiable. Therefore, an identifiability analysis, consisting of a sensitivity and a correlation analysis, was conducted for the model parameters ρc, K_{ax}, K_{tg} and V_h. Indeed, a model parameter is said to be identifiable if it has sufficient influence on the model outputs, in this case the changes in temperature before and after the pulse at three positions around the heater, ΔT_1, ΔT_2 and ΔT_3 (high sensitivity) and at the same time is not correlated with other model parameters (no linear dependencies with other model parameters) (De Pauw *et al.*, 2008).

To examine the first condition of parametrical identifiability, a sensitivity measure δ^{meas} similar to that of Brun *et al.* (2002), Steppe *et al.* (2006) and De Pauw *et al.* (2008) was used. This measure is an indication of the relative importance of the different parameters for the model output. The centralized relative sensitivity function of model variable y_i towards parameter θ was calculated as (see also Section 5.2.1):

$$S(y_i) = \frac{y_i(\theta + \Delta\theta) - y_i(\theta - \Delta\theta)}{2\Delta\theta} \frac{\theta}{y_i(\theta)} \qquad (6.6)$$

with $\Delta\theta$ taken as 1 % of the source component value θ.

The sensitivity measure δ^{meas} was then calculated as:

$$\delta^{meas} = \frac{\|S_c\|}{\sqrt{n}} \qquad (6.7)$$

with S_c the vector constructed by concatenating the sensitivity function vectors of T_1, T_2 and T_3, and n the total number of measurement instances (summed overall measured variables) which allows accounting for measurement quantities. $\|S_c\|$ corresponds to the norm of S_c which is the square root of the sum of squared values of each of the vector elements.

To assess correlations between the model parameters, a collinearity analysis was performed (Brun *et al.*, 2002; Steppe *et al.*, 2006) which allows detection of dependencies between the model parameters. To this end, the collinearity index γ was calculated based on the minimum eigenvalue of $\mathbf{S}^T\mathbf{S}$ with $\mathbf{S}$ the normalized sensitivity matrix composed of columns:

$$\gamma = \frac{1}{\sqrt{\lambda_{\min}\left[\mathbf{S}^T\mathbf{S}\right]}}, \mathbf{S} = \frac{S_c}{\|S_c\|} \qquad (6.8)$$

This collinearity index ranges between unity, if the sensitivity functions are orthogonal, and infinity for an exact linear dependency between the sensitivity functions. The threshold was put at 15 following Brun *et al.* (2002). Indices below 15 point to weak dependencies, whereas indices above 15 are associated with moderate to strong relations. These indices can be calculated for all model parameters or on a subset of specifically selected parameters.

The quality of the estimated parameters was further checked based on the parameter estimation error covariance matrix. From this matrix, the standard errors of the parameters can be calculated as $\sigma(\theta_i)=\sqrt{V_{ii}}$ with V_{ii} an element of the diagonal of the covariance matrix. Sensor verification

A 3D Finite Element Model (FEM) was implemented to compare the theoretical Eq. 6.1 and 6.2, developed for a perfect heater (infinite length and zero radius) in an infinitely large environment, with a more realistic situation. To this end, a cube of immobilized water with length 10 cm was modelled. In this cube, the three sensor needles and heater were located with their according dimensions, similarly as in Section 3.3. While for the HDF model a continuous heat input was applied, here a heat pulse of 160 W m^{-1} was implemented.

These modelling results were then compared with actual measurements in water immobilized with 2 g agar l^{-1} (Campbell *et al.*, 1991; Ren *et al.*, 2003). The small amount of agar was added to prevent natural convection in the water and is assumed to have a negligible effect on the thermal characteristics. This immobilized water has the advantage that it is in direct contact with the heater and needles. From the known thermal properties of this medium, the heat input q as calculated according to Campell *et al.* (1991) can then be checked for each sensor and a correction factor calculated if necessary.

6.2.5 Comparison of heat pulse methods

Next to immobilized water, moist wood was modelled according to the same principles and with the same dimensions as for the immobilized water. The wood was considered as an anisotropic medium in which unidirectional convection occurred. For this wood, a dry wood density of 550 kg m^{-3} was applied, with varying water contents and accordingly varying specific heat capacity and thermal conductivity (Vandegehuchte & Steppe, 2012a). In this wood, sap flux densities ranging from -15 (reverse flow) to 100 cm^3 cm^{-2} h^{-1} (high flow) were modelled. For this model the CHP, HR, Tmax and Sapflow+ method were compared for 6 s heat pulses of 160 W m^{-1}. For the Tmax method, formulas for a non-ideal heat pulse as mentioned in Kluitenberg & Ham (2004) adapted for anisotropic wood were applied (Eq. 2.8, 2.9) (Vandegehuchte & Steppe, 2012c), while for the CHP (Eq. 2.5) and the HR (Eq. 2.10) the original equations valid for an ideal heat pulse were applied (Swanson & Whitfield, 1981; Burgess *et al.*, 2001a). Notice that in these equations as mentioned in Section 2.3, D really is the axial diffusivity D_{ax}, as explained in Chapter 4.

Both for the HR and the CHP method, the original equations are theoretically not applicable for non-ideal pulses. For the HR method, however, it is mentioned in Burgess *et al.* (2001a) that there was no significant difference when applying heat pulses of 6 seconds compared to shorter pulses. This was also confirmed by comparing the theoretical results of applying the original HR equation to the temperatures as modelled by Eq. 6.1 and 6.2 for heat pulses ranging between 1 and 10 seconds. As no significant difference between these results was obtained, the original HR equation was deemed valid for pulses of 6 seconds. For the CHP method, on the other hand, an underestimation of 15 % was noticed when theoretically applying the ideal heat pulse equation for non-ideal heat pulses of 6 s. This underestimation needs to be taken into account when interpreting the results.

As all methods are based on the insertion of needles in the wood, distinction was made between wood without and with wound effects, the latter modelled as regions surrounding the sensor needles in which zero flow occurs with a width of 1.5 mm and a length stretching from 0.2 mm below the lower to 0.2 mm above the upper needle. This wound effect simulates the interruption of flow due to the invasiveness of the needles and will lead to a diversion from the ideal condition on which all

mentioned methods are based, namely a uniform flow distribution in the wood. This leads to underestimations in the calculated heat velocities. Based on the modelling results, however, a correction can be developed to take these wound effects into account (Swanson & Whitfield, 1981).

6.2.6 Measurements of sap flux density in artificial sapwood

The Sapflow+ method was tested on an artificial stem segment, consisting of a plastic cylinder filled with fine sawdust of European beech (*Fagus sylvatica* L.). This artificial segment has the advantage of a radial homogenous sap flux density profile and, given the high porosity, allowed a wide range of sap flux densities to be applied. The segment was installed in a verification system as proposed by Steppe *et al.* (2010) (Figure 6.2). Flow rates of water were held constant by maintaining a constant head of water pressure on the segment using the Mariotte's bottle principle (McCarthy, 1934). A closed water-filled 5-L Erlenmeyer flask was equipped with two glass tubes located at the same depth in the flask: one tube functioned as an air inlet, while the other, connected to a third glass tube via flexible tubing, functioned as a siphon. By adjusting the height of the flask (and thus the bottom of the air inlet), the water-filled siphon delivered the flow of water required to maintain a constant head (h = distance between the bottom of the air inlet and the surface of the segment) on the segment, regardless of the changing water level within the flask. Water passing through the segments was continuously measured using an electronic balance (PS 4500/C1, Henk Maas weegschalen BV, 4264 AW Veen, the Netherlands).

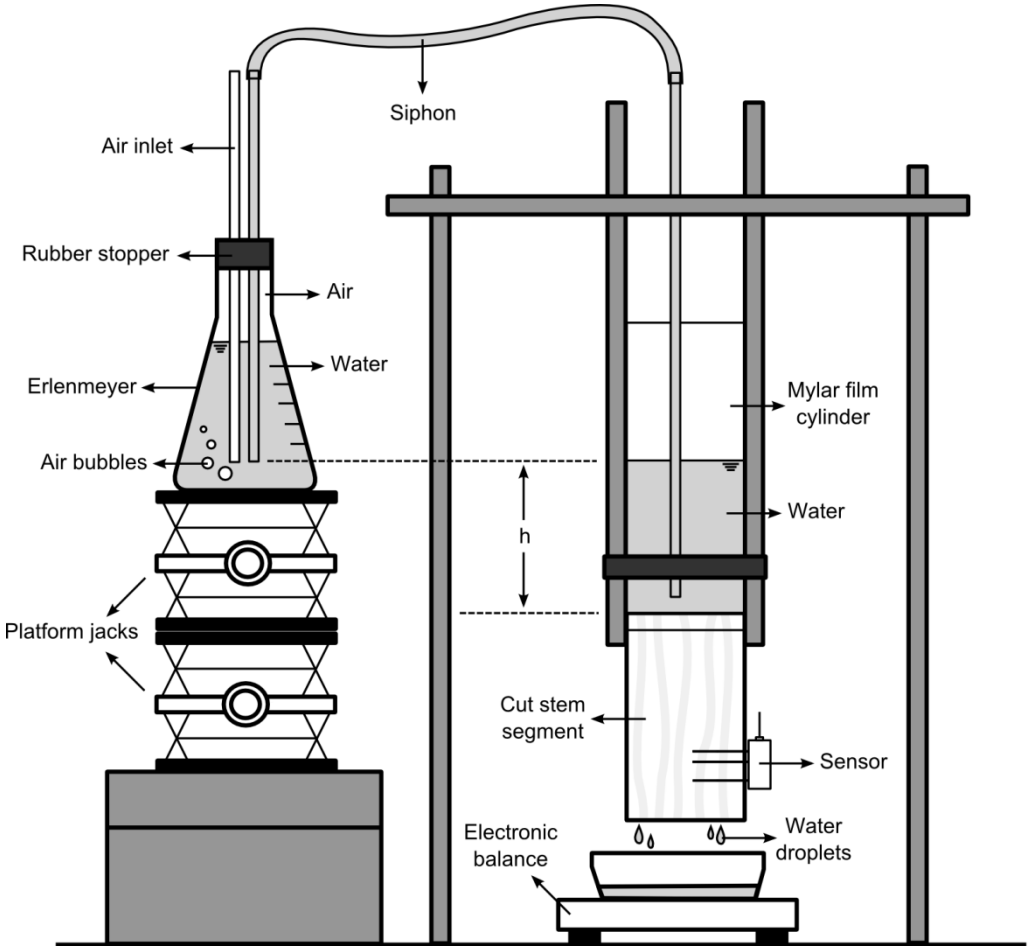

Figure 6.2 *Schematic diagram of the Mariotte-based verification system (from Steppe et al. (2010)) used for testing the accuracy of the Sapflow+ method.*

At the end of the measurements, the volume of the sawdust column was determined and the sawdust was dried and weighed to determine the dry wood density. As high flows for this artificial column were expected, a needle configuration of (10,0); (-5,0) and (0,5) mm was applied for the axial downstream, axial upstream and tangential needle, respectively, enabling comparison with the CHP method.

6.2.7 Measurements of sap flux density in sapwood

Next to the artificial segment, the method was also tested in sapwood of European beech (*Fagus sylvatica* L.). To this end, two trees of approximately 15-years old with a diameter at breast height of about 12 cm were cut at the experimental forest 'Aelmoeseneie' of Ghent University (Gontrode, Belgium). The cut ends were sealed with parafilm (Parafilm M, SPI supplies/Structure Probe Inc., West Chester, PA 19380, USA) and enclosed in plastic bags to minimize evaporation. The stems were

then transported to the Laboratory of Plant Ecology, Ghent University, and cut into segments of approximately 20 cm length.

Before installing the cut stem segments in the experimental set up, cut surfaces were wetted and trimmed using a razor blade to re-open possibly closed vessels (this was visually confirmed using a stereomicroscope). A 2-cm strip of bark at the top end of the segment was removed to ensure that water only passed through the stem xylem. On these segments, a 30-cm high plastic cylinder was fixed directly to the xylem using silicone and double-sticking adhesive tape. After a drying phase of ~18 hours for the silicone to harden, the Sapflow+ sensor was installed. Accurate vertical spacing and parallel drilling was achieved by using a drill-bit template. Notice that before installing the sensors, the bark was removed to ensure that the heater was completely located in the sapwood.

At the end of the experiment, a small disc of the segment was cut from which volume, moist weight and dry weight after drying 24 h in a 50°C oven were determined. From these values, water content and dry wood density were calculated. Besides, the segment was cut through at the needle position to accurately determine the exact spacing between the measurement needles and to measure the wound width. As lower flows were expected in comparison with the artificial column, it was preferred to compare the Sapflow+ results with the HR method. As it was noticed that for distances of 10 mm, the axial downstream signal was rather low which reduces the sensitivity of the HR method, a smaller distance of 7.5 mm was chosen, resulting in a needle configuration of approximately (7.5,0); (-7.5,0) and (0,7.5) mm for the axial downstream, axial upstream and tangential needle, respectively. Following equation for the HR method was applied (Burgess *et al.*, 2001a):

$$V_h = \frac{4D_{ax}t\ln(\Delta T_{down}/\Delta T_{up}) - x_{down}^2 + x_{up}^2}{2t(x_{up} - x_{down})} \qquad (6.9)$$

with D_{ax} the thermal diffusivity ($m^2\ s^{-1}$), ΔT_{down} and ΔT_{up} the downstream and upstream temperature differences, respectively, at time t after application of the pulse and x_{down} and x_{up} the exact axial downstream and upstream distances of the measurement needles to the heater, respectively. Unlike the original HR equation (Eq. 2.10), Eq. 6.9 takes into account differences in the upflow and downflow needle distance. Thermal diffusivity was determined according to Cohen *et al.* (1981) as it has been shown that the original method to determine D_{ax} presented in Burgess *et*

al. (2001a) was incorrect (Vandegehuchte & Steppe, 2012a). Table 6.1 summarizes the applied materials, methods and objectives of this Chapter.

Table 6.1 *Summary of the applied materials, methods and objectives.*

Material	Method	Objective
Immobilized water	Finite Element Modelling	Investigation of influence of theoretical assumptions leading to Eq. 6.1 & 6.2
	Immobilized water (2 g agar L^{-1})	Confirmation of modelling results
Wood	Finite Element Modelling	Estimation of wound effects
		Comparison of heat pulse methods
	Artificial column with sawdust	Gravitational validation of Sapflow+
		Comparison with CHP method
	Fagus sylvatica segments	Gravitational validation of Sapflow+
		Comparison with HR method

6.3 Results

6.3.1 Identifiability analysis

Figure 6.3a, b and c show the relative sensitivity functions for the ΔT signals, respectively at position (10 mm, 0 mm), (-5 mm, 0 mm) and (0 mm, 5 mm) from the heater needle. The sensitivity functions of the parameters are clearly different for the different measurement positions. For instance, a positive V_h will have a negative relative sensitivity for positions upstream and tangentially from the heater, while the relative sensitivity will be (partly) positive for downstream positions. K_{ax}, however, will have a positive relative sensitivity for axial positions, but negative for

the tangential position and vice versa for K_{tg}. Figure 6.3d gives an indication of the overall sensitivity of the parameters for different heat velocities. It should be noted that, for zero flow, the sensitivity measure for V_h is much lower than for the other parameters (not visible in Figure 6.3d). A 1 % change in V_h will hardly influence the ΔT signals if V_h is much lower than for the other parameters (not visible in Figure 6.3d). A 1 % change in V_h will hardly influence the ΔT signals if V_h is approximately zero. Nevertheless, the model remains practically applicable as an error of 1 % in the V_h determination for such a low value is negligible and, for higher absolute V_h values, the sensitivity increases rapidly. Moreover, as the collinearity index remained below 8.5 across the complete natural range of water contents and sap flux densities (from -15 to 110 cm^3 cm^2 h^{-1} (Vertessy *et al.*, 1997; Burgess & Bleby, 2006; Cohen *et al.*, 2008)), the model can be considered to be identifiable if the heat input and measurement positions are known.

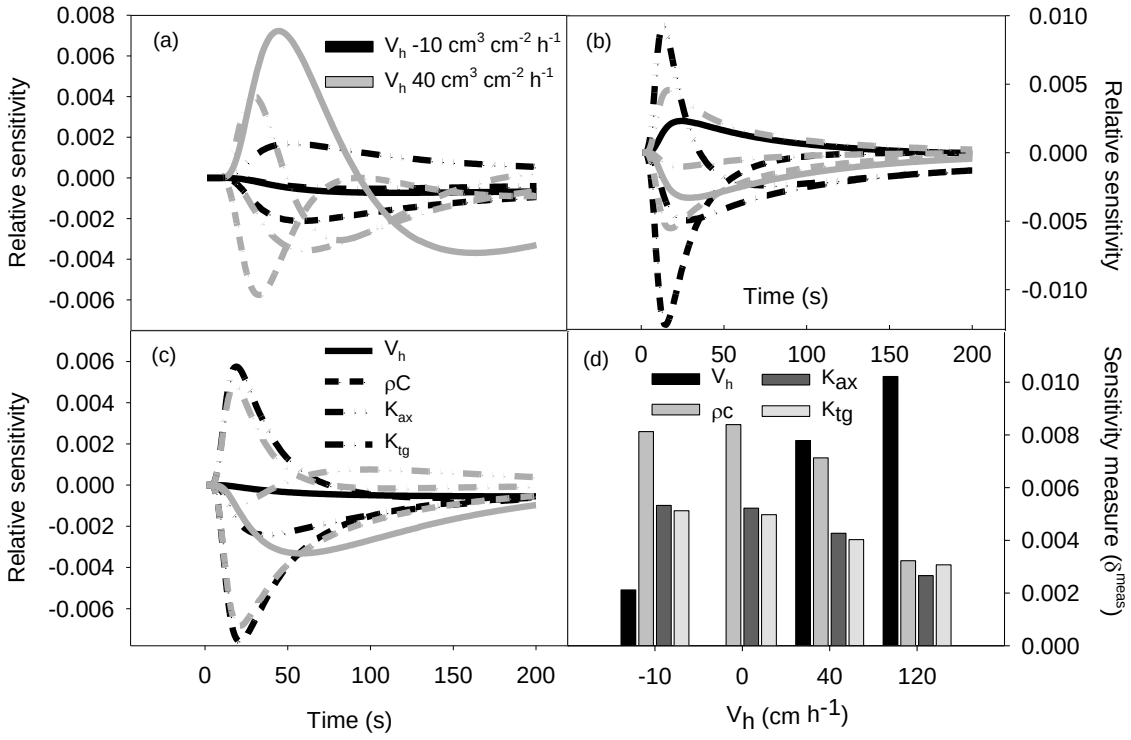

Figure 6.3 *Relative sensitivity functions for V_h (-10 cm^3 cm^{-2} h^{-1}: black, 40 cm^3 cm^{-2} h^{-1}: grey), ρc (2.4×106 J m^{-3} K^{-1}), K_{ax} (0.62 W m^{-1} K^{-1}) and K_{tg} (0.42 W m^{-1} K^{-1}) for position (10 mm, 0 mm) (a), (-5 mm, 0 mm) (b) and (0 mm, 5 mm) (c) with reference to the heater. The sensitivity measures for all parameters are given in (d) for different heat velocities.*

6.3.2 Sensor verification and calibration

Figure 6.4a shows the temperatures as obtained with FEM for a distance of 7.5 mm from the heater in immobilized water. As this medium is isotropic, exactly the same results are obtained whether the measurement needle is located axially or tangentially from the heater. Compared to the theoretical Eq. 6.1 and 6.2, there is only a small difference in temperatures obtained by FEM (Figure 6.4a). The small differences are probably a result of the fact that in the latter, actual needles are implemented with finite boundaries of a specific material, i.e. stainless steel. When applying Sapflow+ to the FEM data, following values are obtained (relative difference with the actual values is indicated between brackets): ρc: 4.108×10^{6} J m^{-3} K^{-1} (-1.8 %), K_{ax}, K_{tg}: 0.6176 W m^{-1} K^{-1} (+1.2 %) and V_h: 0 m^3 m^{-2} s^{-1}.

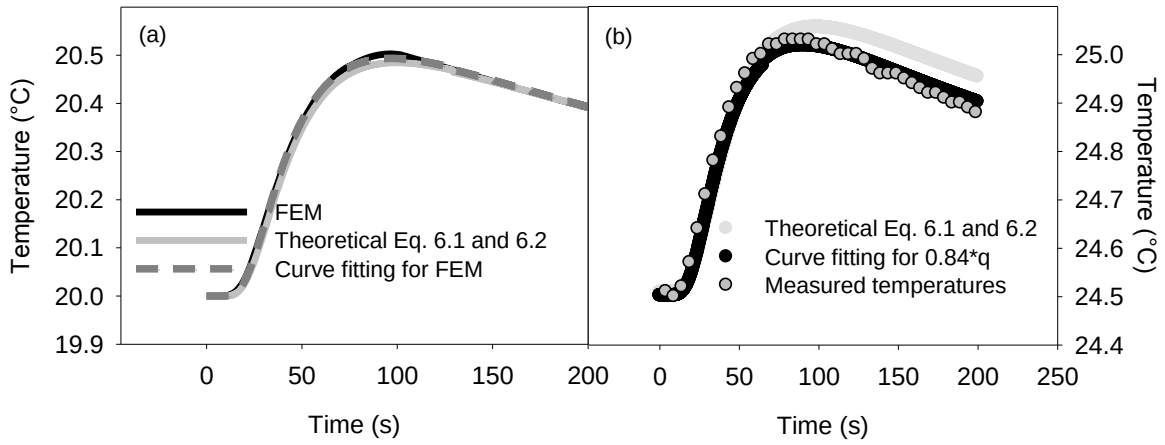

Figure 6.4 *(a) Temperature data at 7.5 mm from the heater for the Finite Element Model (FEM) of immobilized water compared with the theoretical Eq. 6.1 and 6.2 for the thermal properties of water ($\rho c=4.186\times10^{6}$ J m^{-3} K^{-1}, $K_{ax}=K_{tg}=0.61$ W m^{-1} K^{-1}, $V_h=0$ m^3 m^{-2} s^{-1}) and the application of Sapflow+ to the FEM data; (b) Measured temperatures with the Sapflow+ sensor in immobilized water compared to the fitted temperatures for the q calculated according to Campbell et al. (1991) and after calibration for q, leading to an optimal value of 0.84×q. For both the FEM as the actual measurements, a heat pulse of 6 s and 160 W m^{-1} was applied.*

In Figure 6.4b, actual measurements with the Sapflow+ sensor in immobilized water are given. As, for the three measurement needles at (0,7.5), (7.5,0) and (-7.5,0) mm from the heater, similar temperatures were obtained, the data are only plotted for one needle. When comparing these measurements with Eq. 6.1 and 6.2, the theory seems to overestimate the temperature. If, however, the heat input q, as calculated

according to Campell *et al.* (1991) is reduced, a good fit is obtained (objective value of 13.17 compared to 12 for an ideal fit).

Figure 6.5 stresses the importance of temperature correction. During the measurement, the ambient conditions generally change during the day, influencing the measured temperature peaks (Figure 6.5a). Without temperature correction, application of the presented method would lead to erroneous results. Figure 6.5b shows the curve fitting without calibration for the known thermal parameters of stabilized water when no temperature correction is applied. When calibrating the parameters of Eq. 6.1 and 6.2 to obtain a good fit, erroneous results are obtained (ρc=4.344×10^6 J m^{-3} K^{-1} (+4 %), K_{ax}=K_{tg}=0.824 W m^{-1} K^{-1} (+34 %)) and the fit only has an objective value of 694 compared to a 2.54 for an ideal fit. If, however, a temperature correction is applied, the method is again able to correctly determine the desired variables from the curve fitting procedure. The data further shown, have been corrected for temperature effects.

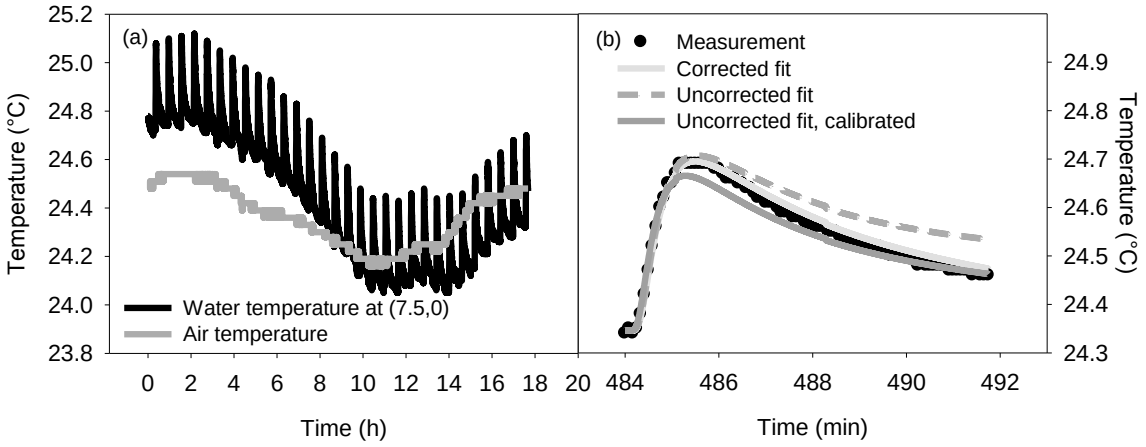

Figure 6.5 *(a) Measured air temperature and temperature in immobilized water at location (7.5,0) mm from the heater for heat pulses of 6 s and 105 W m^{-1}, applied every 45 min; and (b) Measured water temperature for one heat pulse compared to the curve fit for ρc=4. 186×10^6 J m^{-3} K^{-1} and K_{ax}=K_{tg}=0.61 W m^{-1} K^{-1} with and without temperature correction. When calibrating the fitted curve without temperature correction, values of 4.344×10^6 J m^{-3} s^{-1} (+4 %) for ρc, 0.824 W m^{-1} K^{-1} (+34 %) for K_{ax} and for K_{tg} and 0 m^3 m^{-2} s^{-1} for V_h are obtained.*

6.3.3 Comparison of heat pulse methods by FEM

In Figure 6.6a the calculated heat velocities according to the Sapflow+, Tmax, CHP and HR method are given for FEM of sapwood without wound effects. Similar results were obtained for other water contents and dry wood densities. Figure 6.7 shows that, for HR measurements at high heat velocities, the upstream ΔT signal is nearly zero while the downstream ΔT signal is lower than for lower heat velocities between 60 and 100 s, the time period for calculating the average $\Delta T_{down}/\Delta T_{up}$ signal.

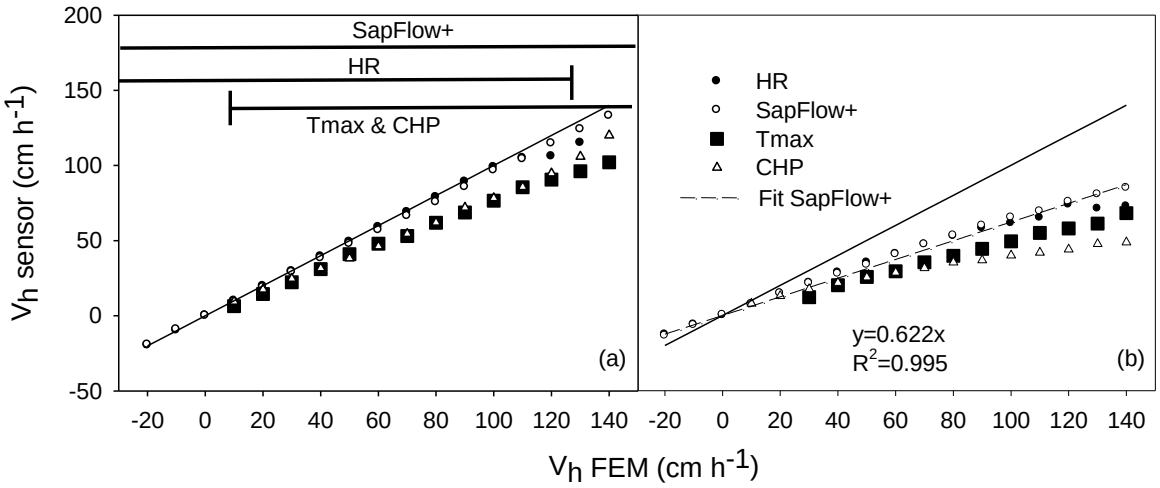

Figure 6.6 *Heat velocity calculated according to the Heat Ratio (HR), Tmax, Compensation Heat Pulse (CHP) and Sapflow+ method based on the temperature data obtained by FEM for sapwood with a dry wood density of 550 kg m^{-3} and a water content of 0.75 without (a) and with (b) wound effect. The heat velocity range for which each method is applicable is indicated. The full line indicates the 1:1 line.*

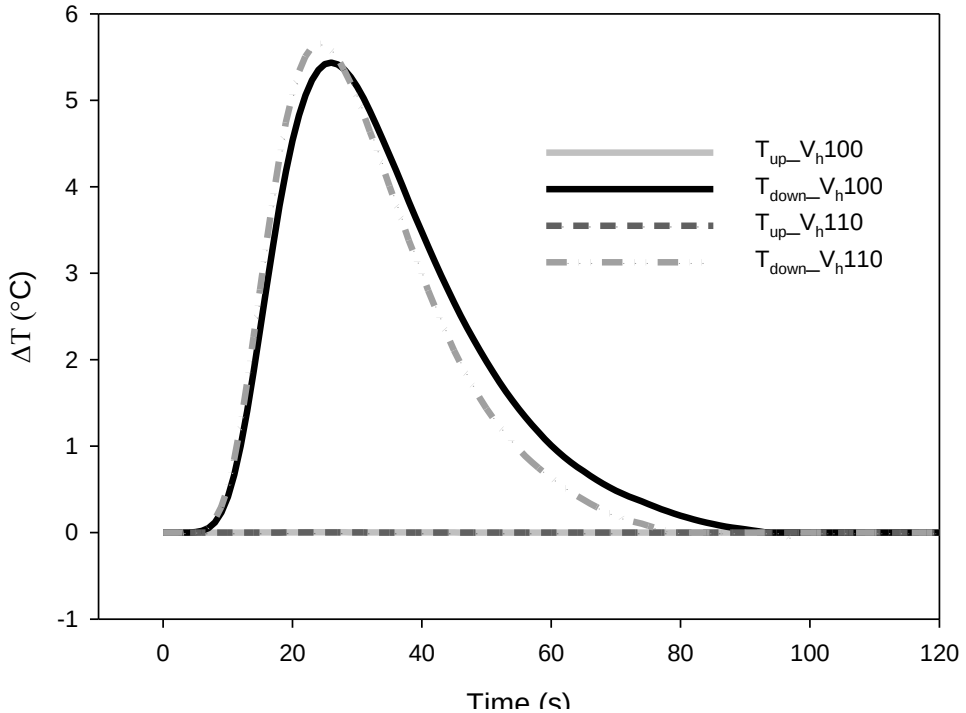

Figure 6.7 *The ΔT_{up} and ΔT_{down} HR signal for a heat velocity of 100 and 110 cm h^{-1}. While for the ΔT_{up} signal the difference for both flows is hardly noticeable, the ΔT_{down} signal between 60 and 100 s is clearly higher for V_h 100 cm h^{-1}.*

In addition to accurately determining heat velocity, Table 6.2 indicates that the Sapflow+ method is also capable of estimating the water content of the sapwood, a crucial parameter for the conversion of heat velocity to sap flux density. Moreover, the thermal conductivities of the sapwood are estimated as well, although less accurately as the method is less sensitive towards these parameters.

Table 6.2 *Water content (MC), axial and tangential conductivity (K_{ax}, K_{tg}) implemented in the Finite Element sapwood model (FEM) and the corresponding average values for heat velocities from -20 to 140 cm^3 cm^{-2} h^{-1} calculated with the Sapflow+ method (SF+). Standard deviations are given between brackets.*

MC FEM	*MC* SF+	K_{ax} FEM	K_{ax} SF+	K_{tg} FEM	K_{tg} SF+
0.748	0.748 (±0.013)	0.6275	0.607 (±0.014)	0.42	0.46 (±0.0230)
0.855	0.861 (±0.007)	0.6634	0.637 (±0.030)	0.44	0.467 (±0.022)
0.955	0.921 (±0.016)	0.6964	0.663 (±0.028)	0.46	0.467 (±0.018)
1.045	1.04 (±0.007)	0.7263	0.687 (±0.048)	0.48	0.511 (±0.027)

In practice, however, sap flux density measurements are influenced by wound effects. Figure 6.6b shows the modelling results when wound effects are introduced, which more closely correspond to reality in comparison with Figure 6.6a. Clearly all methods are affected. When fitting a linear regression, the Sapflow+ method led to the best fit and highest slope, although the R^2 value did not differ much compared to the other methods (Table 6.3). When regressing the difference between the Sapflow+ results and the results of the other methods, slopes were all significantly different from zero indicating a significant difference between the Sapflow+ and the other methods. For both the CHP and Tmax method, the intercept is also significantly different from zero. Moreover, the R^2 value for the regressed difference between Sapflow+ and HR method is only 0.566 because of the inaccurate HR results at high heat velocities (Table 6.3). The main difference, however, lays in the applicability of the methods across the sap flow range. Based on these modeling results, the Sapflow+ method is the only method leading to good results for negative, low a well as high heat velocities. Hence, by applying a simple linear wound correction (as can be seen in Figure 6.6b), accurate heat velocities across the entire range of sap flux densities can be determined by this method. The wound effect, however, also influences the calculated thermal parameters and hence water content (Figure 6.8). For low heat velocities ranging between -15 and 45 cm h^{-1}, the thermal parameters and water content are determined quite accurately (relative error <5 %). For larger absolute heat velocities, however, the relative errors increase and become more dependent on the water content. Based on the modelling results, however, a non-linear correction can be applied based on the pooled data for all water contents which will reduce the error to a maximum of 7 %.

Table 6.3 *Linear regression results of the different heat pulse methods resulting from the Finite Element sapwood model (FEM) with wound effects. Results were regressed against the implemented heat velocity V_h. Significant results are indicated by *.*

	SF+	HR	Tmax	CHP	SF+-HR	SF+-Tmax	SF+-CHP
Slope	0.62*	0.56*	0.48*	0.31*	0.057*	0.100*	0.294*
Intercept	1.56	3.18	0.40	8.47*	-1.62	4.857*	-4.847*
R^2	0.997	0.979	0.994	0.981	0.567	0.871	0.995

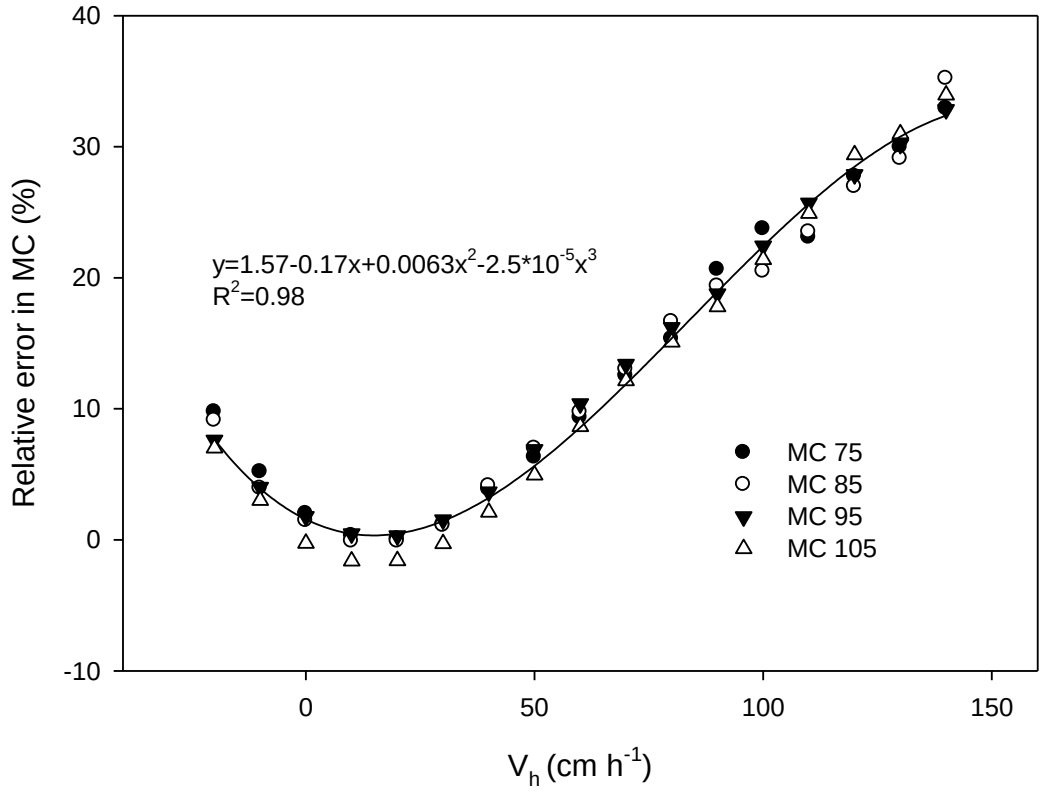

Figure 6.8 *Relative error (%) of water content calculated as the difference in water content determined by the Sapflow+ method and the model input water content divided by the model input water content, for different water contents and heat velocities.*

6.3.4 Measurements on artificial sapwood

Figure 6.9a shows the heat velocity calculated according to the Sapflow+ and the CHP method in comparison with the gravimetric heat velocity for the artificial column. As no direct measurement of *MC* was possible on the artificial column, the value determined by the Sapflow+ method for zero flow was applied for all measurements, given the negligible error for *MC* determination during zero flow in the modelling results. This value was also applied to calculate gravimetric heat velocity from the measured gravimetric sap flux density. In Figure 6.9b, the relative error in *MC* determined by Sapflow+, with the *MC* at zero flow determined by Sapflow+ taken as reference, is given. Again, the error increases with increasing heat velocity because of the interruption of flow around the needles (wound effect).

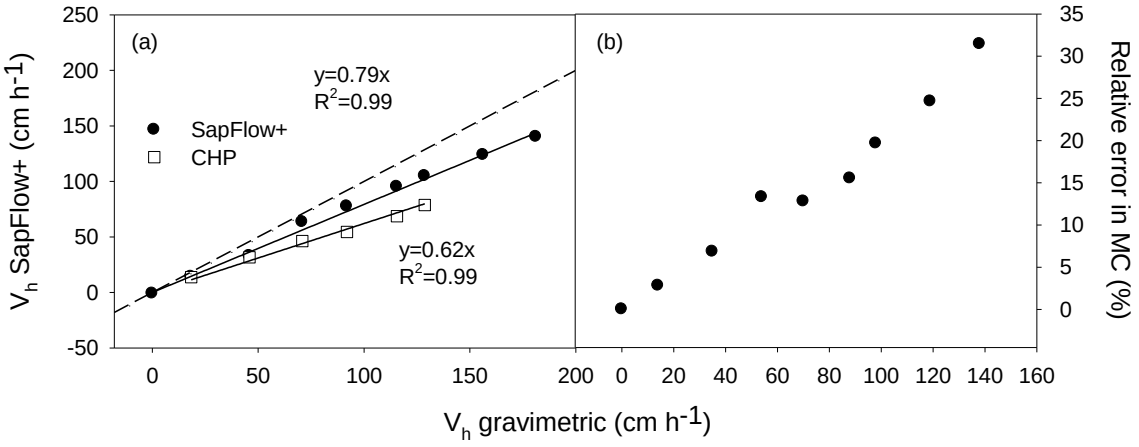

Figure 6.9 *(a) Heat velocity (V_h) in the artificial column calculated by Sapflow+ and the Compensation Heat pulse method (CHP) in comparison to the gravimetric heat velocity (determined from gravimetric sap flux density based on the water content calculated by Sapflow+ for zero flow). The broken line indicates the 1:1 line; and (b) Relative error in water content (MC) determination by Sapflow+ with the zero flow measurement as reference value.*

6.3.5 Measurements on sapwood

For real sapwood segments of European beech (*Fagus sylvatica* L.), a maximal heat velocity (derived from the sap flux density, dry wood density and water content of the sapwood according to Eq. 2.4) of 45 cm h^{-1} was obtained (Figure 6.10a). Regressing the Sapflow+ and HR results to the heat velocity led to a slope of 0.61 and R^2 of 0.982 for the HR method, and 0.61 and 0.978, respectively, for Sapflow+. Given an average wound width of 1.51 mm, the obtained slopes are in agreement with the modeling results. Clearly, for heat velocities up to 45 cm h^{-1}, the HR and Sapflow+ method perform equally. This was confirmed by linearly regressing the difference in the Sapflow+ and HR method results to the gravimetric heat velocity, which did not lead to a significant slope (p=0.824) or intercept (p=0.697) (Figure 6.11). Nevertheless, differences between stem segments can be noted (Table 6.4). It should be noted that, for both methods, measurements were only performed at a single sapwood depth. While the relative error in calculated water content was on average 0.8±1.4 % for zero flow conditions, it increased to 10 % for higher heat velocities (Figure 6.10b).

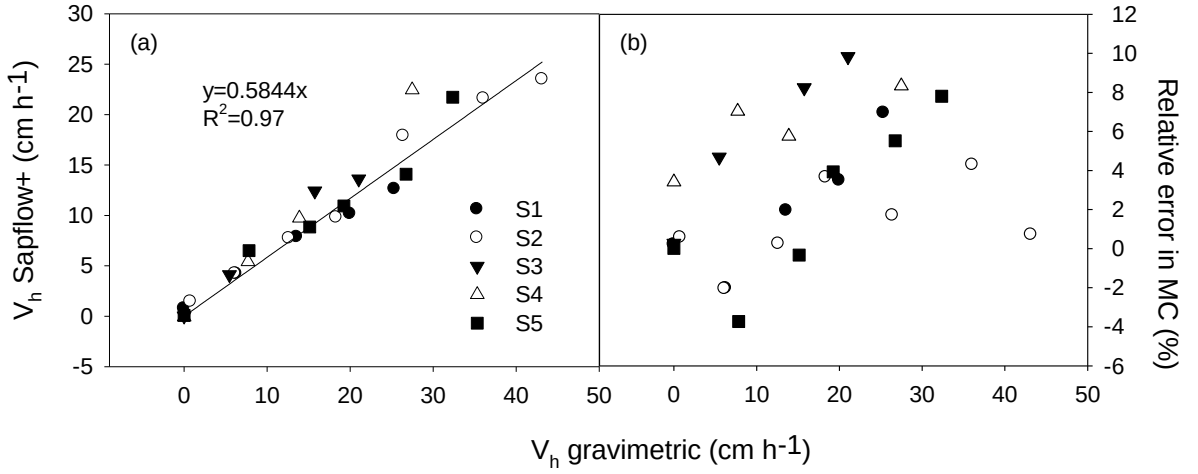

Figure 6.10 *(a) Heat velocity (V_h) in the stem segments calculated by Sapflow+ in comparison to the gravimetric heat velocity; and (b) Relative error in water content determination by the Sapflow+ method with the gravimetrically determined water content as reference value. For the 5 segments, an average wound width of 1.51 mm was measured.*

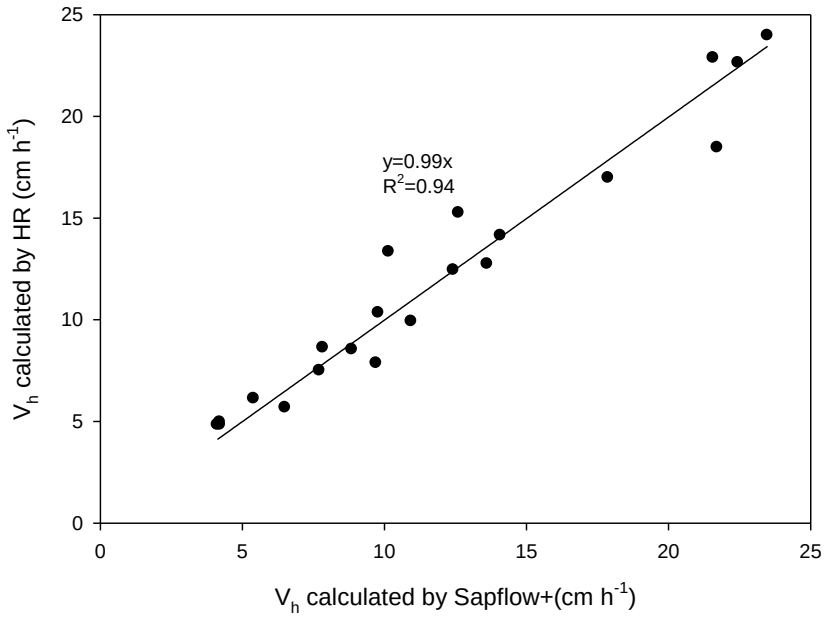

Figure 6.11 *Heat velocity (V_h) calculated by the Heat Ratio method (HR) versus heat velocity calculated by the Sapflow+ method for all sapwood segments. The full line indicates the 1:1 line.*

Table 6.4 *Linear regression results for the Sapflow+ method applied for the different stem segments as shown in Figure 6.10. Significant results are indicated by *.*

	S1	S2	S3	S4	S5
Slope	0.46*	0.55*	0.68*	0.82*	0.60*
Intercept	1.1*	0.97	0.40	-0.73	0.29
R^2	0.995	0.980	0.976	0.994	0.953

6.4 Discussion

6.4.1 Applicability of the Sapflow+ method

From the identifiability analysis, the model is theoretically able to correctly determine V_h, ρc, K_{ax} and K_{tg} across the entire natural range of sapwood water contents and sap flux densities. This was also confirmed by the results of FEM (Figure 6.4a). For the measurements in stabilized water, the fit was not as accurate as for FEM, unless the heat input was reduced in the Sapflow+ model (Figure 6.4b). As the heater needles are manufactured manually, the heater wire is not entirely inserted in the wood to facilitate coupling to the voltage source. Moreover, it is likely that some of the generated heat is taken up by the heater material itself and hence not given off to the surrounding wood. Therefore, a calibration procedure is necessary to correct the parameter q for every sensor. As q is only dependent on the heater needle itself and not on the thermal characteristics of the sapwood, this sensor-specific correction should be applicable for all further measurements.

To determine q correctly, it can be incorporated in the model calibration. If the quotient of the volumetric heat capacity ρc and the heat input q is again considered as a single parameter $q/\rho c$, this parameter can be estimated along with V_h, D_{ax} and D_{tg} by applying a curve fitting procedure on following equations:

$$\Delta T = \frac{q}{4\pi\rho c\sqrt{D_{ax}D_{tg}}}\int_0^t t^{-1}\exp\left(-\frac{1}{4t}\left(\frac{(x-V_h t)^2}{D_{ax}}+\frac{y^2}{D_{tg}}\right)\right)dt \quad \text{for } 0 < t <= t_0 \qquad (6.10)$$

$$\Delta T = \frac{q}{4\pi\rho c\sqrt{D_{ax}D_{tg}}} \int_{t-t_0}^{t} t^{-1} \exp\left(-\frac{1}{4t}\left(\frac{(x-V_h t)^2}{D_{ax}} + \frac{y^2}{D_{tg}}\right)\right) dt \quad \text{for } t_0 < t \qquad (6.11)$$

Identifiability analysis shows that this curve fitting leads to accurate estimations of $q/\rho c$ for low and average heat velocities (up to 50 cm h^{-1}) but the procedure is no longer identifiable for higher heat velocities. As a single wood core needs to be taken anyhow to determine the dry wood density, also the *MC* of this wood core can be determined by weighing its initial wet weight and its dry weight after drying. This way, ρc can be determined:

$$\rho c = \rho_d \left(c_w MC + c_{dw}\right) \qquad (6.12)$$

As ρc is now known at the moment of wood core sampling and $q/\rho c$ can simultaneously be determined from the model fitting, the correct q can be assessed and further applied in the measurements according to Eq. 6.1 and 6.2. This way, an in-situ calibration is obtained which is more practical than the calibration procedure based on measurements in stabilized water.

In addition to a correct heat input, precise positioning of the sensor needles needs to be known to obtain good results, which was also mentioned by Swanson (1983), Jones *et al.* (1988) and later by Kluitenberg *et al.* (1995) for other heat pulse based methods. A 5 % error in needle spacing can lead to up to 16 % error in calculated heat velocities and *MC*, with the error depending on the heat velocity and relatively larger for lower flows (Table 6.5).

Similar error percentages were obtained for other *MC* values. It is thus recommended to use a template to install the needles in the sapwood. In addition, a fixed sensor design can aid users to avoid spacing errors.

Table 6.5 *Error analysis for varying distances. The first three rows indicate the relative change in distance for the axial downstream, upstream and tangential position, respectively. The second column shows the absolute results obtained by Sapflow+ for a V_h of 50, 100 and 20 cm h^{-1} and an MC of 0.9 implemented in FEM with wounding. The lower rows show the relative change in V_h and MC due to the positioning errors for these values of V_h and MC.*

x_{down}	1	0.95	1.05	1	1	1	1	0.95	1.05	0.95	1.05	0.95	1.05	0.95	1	1.05	1.05	0.95	1	1	0.95	0.95	0.95	1.05	1.05	1.05
x_{up}	1	1	1	1.05	0.95	1	1	0.95	1.05	1.05	0.95	0.95	1.05	1	0.95	1	1	1	0.95	1.05	0.95	1.05	1.05	1.05	0.95	0.95
y_{tg}	1	1	1	1	1	0.95	1.05	1	1	1	1	0.95	1.05	0.95	0.95	1.05	0.95	1.05	1.05	0.95	1.05	1.05	0.95	0.95	0.95	1.05
V_h 50	35	0.95	1.05	1.00	1.00	1.00	1.00	1.00	1.05	0.95	1.05	0.95	1.05	1.05	1.00	1.05	1.05	0.95	1.00	1.00	0.95	0.95	0.95	1.05	1.05	1.05
MC 0.9	1.06	1.07	0.94	1.00	1.00	1.07	0.94	1.07	0.94	1.07	0.94	1.14	0.88	0.94	1.07	0.88	1.00	1.00	0.94	1.07	1.00	1.00	1.00	1.00	1.00	1.00
V_h 100	61	0.95	1.05	1.00	1.00	1.00	1.00	0.95	1.05	0.95	1.05	0.95	1.05	0.95	1.00	1.05	1.05	0.95	1.00	1.00	0.95	0.95	0.95	1.05	1.05	1.05
MC 0.9	1.27	1.06	0.94	1.00	1.00	1.06	0.94	1.06	0.94	1.06	0.94	1.10	0.89	1.10	1.06	0.89	1.00	1.00	0.94	1.06	1.00	1.00	1.10	1.00	1.00	0.89
V_h 20	13	0.90	1.11	0.95	1.06	1.00	1.00	0.95	1.05	0.84	1.16	0.95	1.05	0.90	1.06	1.11	1.11	0.90	1.06	0.95	0.95	0.84	0.84	1.05	1.16	1.16
MC 0.9	0.92	1.05	0.95	0.99	1.01	1.07	0.94	1.07	0.94	1.04	0.96	1.14	0.88	1.13	1.08	0.89	1.02	0.99	0.95	1.06	1.00	0.98	1.11	1.00	1.03	0.90

6.4.2 Comparison of Sapflow+ with other heat pulse methods

Similar to previous studies (Swanson, 1983; Green *et al.*, 2003), the FEM results (Figure 6.4) show that the Tmax and CHP method are limited in determining negative or low heat velocities (<5 cm h^{-1}), which was also confirmed for the CHP method in the artificial stem segment data (Figure 6.9a). Moreover, both Tmax and CHP underestimate V_h even without modelled wound effects. For the CHP method, this was expected, as the applied equation is not strictly valid for non-ideal pulses, which can be seen as a general shortcoming of the method because, in practice, pulses will never be ideal. Apparently, the Tmax method is more sensitive to the probe material than the Sapflow+ or HR method, for which the results agree closely with the 1:1 line without wounding. The HR method, furthermore, can resolve reverse and low heat velocities (Figure 6.6, Figure 6.10a) and agrees well with Sapflow+ for the stem segment measurements (Figure 6.11), but shows deviations for high heat velocities (>110 cm h^{-1}) in the modelling results (Figure 6.6). For these high heat velocities, the HR heat velocity levels off or even decreases as ΔT_{up} remains approximately the same, whereas ΔT_{down} slightly decreases between 60 and 100 s (Figure 6.7). Shifting the time period for which the average HR signal was calculated led to only slightly better results for the higher heat velocities; this was also indicated by Green *et al.* (2009), who stated that shorting the averaging window or altering the probe spacing will not largely improve the measurement range of the HR method. Moreover, for very high heat velocities, the ΔT_{up} signal becomes so small that the $\Delta T_{down}/\Delta T_{up}$ signal reaches extremely high values, leading to unrealistic high heat velocity results. In practice, these flaws will worsen the applicability of the HR method as ΔT signals below 0.02 °C are smaller than the detection limit of most thermometric systems. Generally, a maximum heat velocity of approximately 55 cm h^{-1} is presumed measurable with the HR method (Swanson, 1983; Burgess *et al.*, 2001a). A similar experiment for segments which allow higher sap flux densities would be beneficial to assess the difference between HR and Sapflow+ for higher flows. For these flows, the Sapflow+ method could make a difference, as it does not suffer from these sensitivity problems because, similar to the HFD method, three measurement needles are applied. This way, heat velocity can be accurately determined across the entire range of sap flux densities when applying a correct wound correction (Figure 6.5, Figure 6.9a). Given the symmetric positioning of the

axial temperature sensors, it can be assumed that good results will also be obtained for reverse flow in stem segments as the only difference will be that the upstream sensor needle will become the downstream needle and vice versa. The smaller underestimation for the artificial stem segment in comparison with the stem segments (Figure 6.9a, Figure 6.10a) is probably a result of the larger pores, allowing water to continue its flow path more easily around the sensor needles which results in a smaller wound effect.

In addition to its applicability across the entire range of sap flux density, the Sapflow+ method has the advantage that, unlike the Tmax or HR method, thermal diffusivity does not need to be determined separately as it is included in the model calibrations. Hence, thermal diffusivity will be a model output instead of an input, which is known to be prone to errors (Green *et al.*, 2003; Vandegehuchte & Steppe, 2012a). Another advantage is that the water content is simultaneously estimated with heat velocity with Sapflow+, at least for low flows ranging between -15 and 45 cm h^{-1}. Hence, unlike other methods which determine the sap flux density from the heat velocity by measuring the sapwood water content only once (taking a destructive wood core), Sapflow+ should enable regular updates of water content values which will lead to more accurate sap flux densities. At higher heat velocities, less heat is transported tangentially and radially, resulting in a narrower and axially longer heat field in comparison with lower heat velocities. As the area in which flow is interrupted by wounding lays within this narrow zone, the influence of this area will become more important, in comparison with a more broad heat field for lower heat velocities. When applying the non-linear correction (Figure 6.8), even estimations of water content changes at higher heat velocities can be made, although these will probably be less accurate as wound effects may vary depending on wood characteristics.

6.4.3 Challenges for the Sapflow+ method

The regression results for the separate stem segments show clear differences (Table 6.4). This is probably a result of radial and azimuthal variation in flow within the segments. As not only variation between trees but also within the sapwood of a single tree can occur as a result of stress factors, measurements at different depths seem indispensable. The application of multiple thermocouples at different depths could easily solve this, as has been shown for the HR method, for which the

commercial sensors enable measurements at two radial depths. Hence, given a more complicated fabrication of the sensors, Sapflow+ should be able to allow measurements at multiple depths. However, for ring-porous species with a marked distinction in early and late wood, additional correction factors might be necessary, similar as for other heat pulse methods (Chapter 2). In general, further validation of the method on different species and at a wider range of flows is necessary.

Another challenge lays in the accurate determination of *MC*. While at low flows the deviation from the gravimetric results seems acceptable (Figure 6.10), at higher flows the error is much larger. Even though a wound correction equation can reduce these errors, such an equation depends on the obstructed zone caused by needle installation which is dependent on sapwood properties. As the size and shape of this wound zone is not known in practical applications, *MC* determination at higher flows will be subject to large uncertainties. Validation experiments in combination with for instance Frequency Domain Reflectometry measurements should be conducted to test the accuracy of *MC* determination during low and high flows.

A more practical issue is the design of the sensor. As applied in this study, the sensor's operational system is an adapted CR1000 logger. This system is, however, not applicable in field conditions as it requires constant line voltage, has impractical dimensions and necessitates laborious data analysis. Therefore, a stand-alone sensor and coupled software should be developed which allows field applications and rapid data-analysis.

6.5 Conclusions

Overall, the results indicate that Sapflow+, by combining a three needle design similar to the HFD method with the strengths of a heat pulse regime as applied by the HR, CHP and Tmax method, performs well in determining heat velocity across the entire naturally occurring sap flow range (approximately -15 to 110 $cm^3\ cm^{-2}\ h^{-1}$). Moreover, water content at low flows (V_h<45 $cm\ h^{-1}$) can be estimated, necessary for the conversion of heat velocity to sap flux density. Nevertheless, wound corrections are required to overcome underestimations of heat velocity and water content determinations at higher flows. Thus far, existing wound corrections for the current available sap flow measurement methods are based on models similar as the FEM used in this study (Swanson & Whitfield, 1981; Burgess *et al.*, 2001a). However, as

wound effects seem to play a significant role in the performance of heat pulse based sensors and the correction factors that need to be applied, further research on this topic seems essential to obtain even more accurate results. It seems likely that wound effects not only depend on needle diameters, but also on wood characteristics which vary between and within tree species and might be influenced by the heating process itself. Therefore, a combination of modelling, gravimetric validation experiments and more advanced methods, such as MRI should be applied to increase our knowledge on these wound phenomena and enable accurate wound corrections for different wood types.

7

Practical application of the Sapflow+ method in mangrove water research

After: Vandegehuchte, M.W., Guyot, A., Hayes, M., Welti, N. Lockington, D. & Steppe, K. (2012). Opposite daily stem diameter changes for co-occuring mangrove species raise questions on environmental and endogenous growth control. In preparation.

7.1 Introduction

Mangroves grow worldwide in tropical and subtropical regions at the intertidal zones between land and sea. While only occupying a global area of approximately 13 million ha, their north-south distribution, ranging from ca. 30°N to ca. 38°S, is large (Quisthoudt *et al.*, 2012) (Figure 7.1).

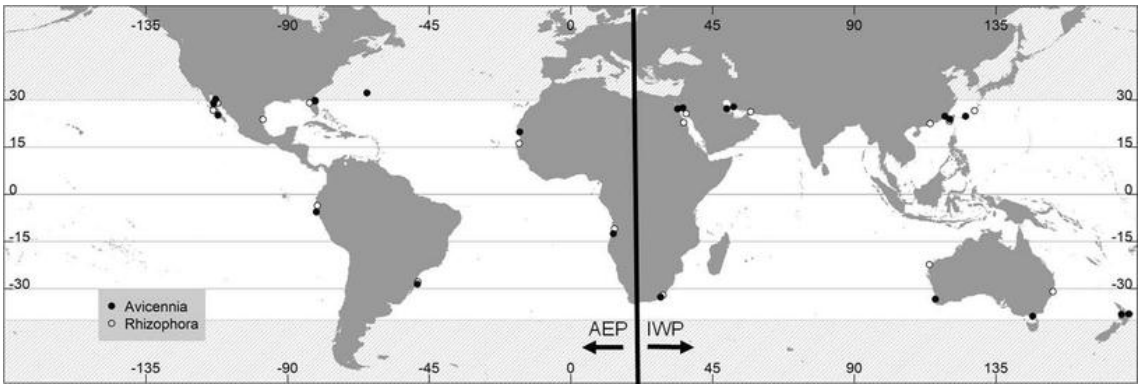

Figure 7.1 *World map of the mangrove latitudinal limits (indicated by dots) for the two most widespread mangrove genera Avicennia (full dots) and Rhizophora (open dots). AEP: Atlantic East Pacific biogeographic region; IWP: Indo-West Pacific biogeograpic region (Quisthoudt et al., 2012)).*

Their morphological and physiological flexibility allows mangroves to occupy areas with large gradients in salt concentration (from oligohaline, with a salinity ranging between 0.5 to 5 ppt to hyperhaline, with a salinity over 40 ppt), substrate type (from clayey to sandy sediments) and inundation regime (from twice a day to twice a month or less) (Quisthoudt *et al.*, 2012). Even though mangrove species show common characteristics such as an extensive, shallow root system and salt exclusion techniques, specific adaptations differ along mangrove species, often resulting in typical zonation patterns (Krauss *et al.*, 2008) with *Rhizophora* generally restricted to the seaward side of the mangrove forest where soil water salinity and inundation frequency are rather constant, while *Avicennia* can occur along the entire intertidal zone.

The harsh environment, in which mangrove trees thrive, hinders water uptake and plant growth in general. Mangrove soils are often high in organic matter, but frequent inundation leads to slow decomposition and a low release rate of inorganic nitrogen and phosphorus (Wanek *et al.*, 2007). Moreover, flooding causes the soil to become oxygen deficient and leads to accumulation of chemical compounds which

negatively affect plant growth (Barrett-Lennard, 2003; Colmer & Flowers, 2008). To enhance oxygen uptake, mangrove species are equipped with aerial roots which contain aerenchyma tissue, allowing rapid diffusion of oxygen from the lenticels to submerged or underground roots (Purnobasuki & Suzuki, 2005).

Next to oxygen depletion, flooding also leads to high salinity levels. Two major salt resistance mechanisms can be distinguished, allowing the regulation of cellular Na^+, Cl^- and K^+ concentrations (Drennan & Pammenter, 1982; Flowers & Colmer, 2008). *Rhizophora* primarily excludes salt at root level, based on ultrafiltration of salt from the water via tiny pores on the root system. *Avicennia*, on the other hand, allows the uptake of salt water at root level, filtering the salt locally through semi-permeable membranes and secreting the accumulated salt through excretion glands at leaf level. Other morphological adaptations limit water loss at canopy level, such as thick leaves with waxy cuticles (*Rhizophora*) and submerged stomata surrounded by trichomes (*Avicennia*).

Because of their specific adaptations, mangrove species have been able to colonize intertidal areas which remained inaccessible for most other species. In this intertidal zone, mangrove communities form nurseries and breeding grounds for a wide range of birds and marine organisms as they offer shelter and trap plant litter, leading to decomposition into nutrients and, hence, providing food (Hogarth, 2007). Moreover, mangrove forests have proven to be important for wood production, as a CO_2 sink as well as forming buffer regions against storms and tsunamis, protecting coastal ecosystems (Cahoon *et al.*, 2003; Stone, 2006; Duke *et al.*, 2007). To fulfil these essential functions, a dense structure in which healthy young trees are complemented by healthy, sufficiently large, older trees is necessary (Duke *et al.*, 2007). Mangrove forests, however, are known to decline worldwide by 1 to 2 % a year because of urbanization, aquaculture, coastal landfills or indirect effects of pollution and climate change (Valiela *et al.*, 2001; Duke *et al.*, 2007). Despite the need to protect mangroves, it is remarkable how little is known about the link between water use and growth characteristics of many mangrove species in field conditions, even though this key information seems indispensible to understand the unique life traits of mangrove and to assess future changes in mangrove forest density and dispersion. Becker *et al.* (1997) were the first to measure sap flux density in mangrove species, later followed by Krauss *et al.* (2007), Hao *et al.* (2009) and Muller *et al.* (2009). On the other hand, research has been conducted on

mangrove stem growth based on growth ring analysis and stem diameter changes (Downton, 1982; Schmitz *et al.*, 2008; Alongi, 2011; Robert *et al.*, 2011a; Robert *et al.*, 2011b). To our knowledge, however, no studies exist combining sap flow measurements with stem growth patterns.

This chapter has the intention to investigate water use and coupled dynamic growth of *Avicennia marina* (Forssk.) Vierh. and *Rhizophora stylosa* Griff. as examples of the two most dominant mangrove genera *Avicennia* and *Rhizophora*. Additionally, the experimental set-up allowed to test the Sapflow+ method in harsh field conditions.

7.2 Materials and methods

7.2.1 Field site

Measurements were conducted at the west coast of North Stradbroke Island, Queensland, Australia (S27˚27.061' E135˚25.806', Figure 7.2), a vegetated sand dune island. The island is characterized by sandy soils and acidic waterbodies intertwined by a complex mix of groundwater-fed lakes, swamps and creeks (Page *et al.*, 2012). These sandy soils and acidic waters lead to low nutrient availability in the mangrove ecosystem (Rogers & Westman, 1977). According to the Köppen classification (Kottek *et al.*, 2006), North Stradbroke Island is subjected to a dry humid subtropical climate, characterized by dry, cool winters and wet, humid summers. As measurements were conducted during August and September 2012, dry conditions were expected.

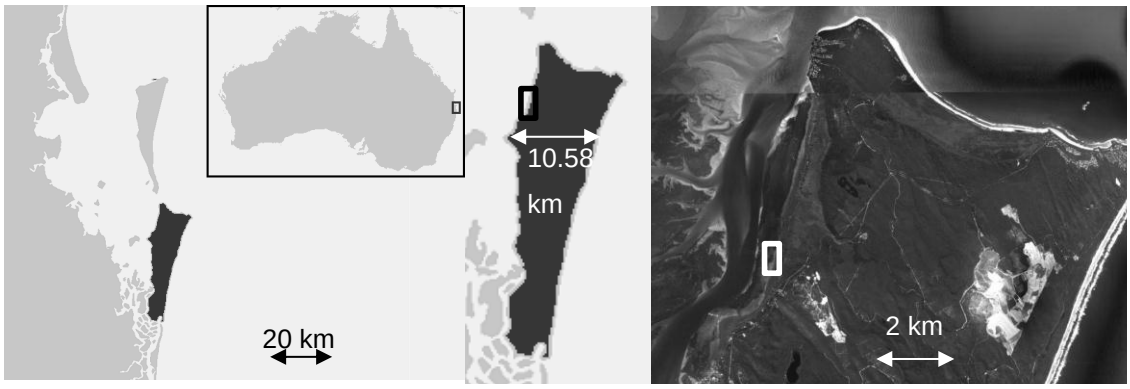

Figure 7.2 *Location of the field site at the west coast of North Stradbroke Island, Queensland, Australia.*

The field site was located in a long stretch of mangrove vegetation, dominated by *Avicennia marina* (Forssk.) Vierh. (or grey mangrove) and *Rhizophora stylosa* Griff. (or spotted red mangrove), intertwined by creeks, carrying fresh water from the upstream inland tropical forest. On this field site, three full grown trees of both *Avicennia marina* (Forssk.) Vierh. and *Rhizophora stylosa* Griff. were chosen, located in proximity of each other to avoid tidal effects and spatial salinity gradients (Figure 7.3, Table 7.1). The field site was subjected to tidal movement, flooding the site approximately twice every 24 hours.

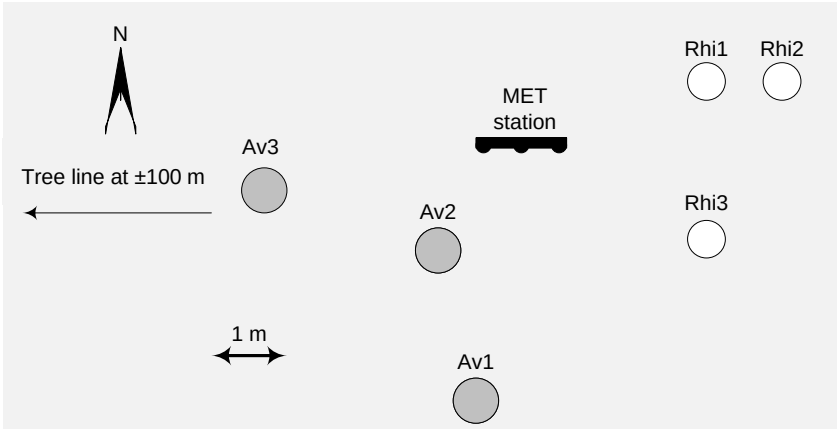

Figure 7.3 *Schematic of the measured trees at the mangrove site on the west coast of North Stradbroke Island, showing the measured Avicennia trees (grey circles), the measured Rhizophora trees (white circles) and the location of the weather station (MET station).*

Table 7.1 *Diameter at breast height (DBH) of the measured mangrove trees.*

Tree	Av1	Av2	Av3	Rhi1	Rhi2	Rhi3
DBH (cm)	19.4	30.6	18.1	18.8	11.7	17.2

7.2.2 Meteorological data

Air temperature, relative humidity, shortwave solar radiation, rainfall and windspeed were measured and recorded every ten minutes at 2 m above soil surface (HOBO weather station, Onset, Cape Cod, Massachusetts, USA). Vapour pressure deficit (*VPD*, kPa) was inferred from measured air temperature (T_{air}) and relative humidity (*RH*) according to Buck (1981):

$$VPD = e_0 - e \qquad (7.1)$$

with e the air vapour pressure and e_0 the saturated air vapour pressure, calculated as:

$$e_0 = 6.107\exp\left(\frac{17.27T_{air}}{T_{air} + 237.3}\right) \quad (7.2)$$

$$e = RH \times e^0 \quad (7.3)$$

Soil salinity and water table depth were determined with in situ pressure sensors (Aqua Troll 200, In-Situ Inc., Fort Collins, CO, USA) installed in piezometers, located close to the measured trees at depths of 25 and 180 cm. Actual measured soil water conductivity (AC in mS cm^{-1}) was converted to osmotic water potential Ψ_Π (MPa) based on McIntyre (1980):

$$\Psi_\Pi = 10^{1.091\log(AC)-1.46} \quad (7.4)$$

7.2.3 Ecophysiological measurements

All trees were equipped with a dendroband (DRL26 – Logging Band Dendrometer, ICT international, Armidale, NSW, Australia), continuously recording stem diameter variations. Stem water potentials were recorded with stem psychrometers (PSY-1 Stem Psychrometer, ICT International, Armidale, NSW, Australia). These psychrometers were cleaned and reinstalled as soon as the peltier curve indicated that the thermocouples were soiled.

To assess sap flux density and sapwood water content, each tree was equipped with a Sapflow+ sensor at the South side of the tree and a Heat Ratio sensor at the North side. Sapwood cores were taken once to assess sapwood water content and dry density gravimetrically and calculate the heat input of the Sapflow+ sensors as described in Chapter 6. As the Sapflow hardware applied in Chapter 6 was not practical to use in field conditions, a stand-alone logger was developed for each Sapflow+ sensor. During instalment of the sap flux density sensors, the bark was removed to ensure that the sensor needles were completely inserted in the sapwood. The HR sensors measured sap flux density at 0.75 cm and 2.25 cm below the cambium while the Sapflow+ sensors measured at depths of 1.5 cm and 2.5 cm below the cambium. The HR sensors measured sap flux density each 15 min while the Sapflow+ sensors had a frequency of one measurement each 40 minutes, the time necessary for the heat generated by the hand-made heaters to be fully

dissipated. As the main interest of the research concerned relative patterns, we chose not to convert measured heat velocity to sap flux density. This way, errors because of the conversion to sap flux density based on *MC* and wounding were avoided. Nevertheless, wound widths for both species were measured based on the cutting of three branch segments per species in which example holes were drilled. This resulted in average wound widths of 1.63±0.02 mm for *Avicennia* and 1.58±0.04 for *Rhizophora*.Besides these continuous measurements, stomatal conductance was measured hourly approximately from sunrise till two hours after sunset during four days (DOY 241, 247, 251 and 254) throughout the measurement period, applying a dynamic porometer (AP4 dynamic porometer, Delta-T Devices Ltd, Cambridge, UK) on Av1, Av3, Rhi2 and Rhi3. For every measurement, the average of three leaves located close to each other was taken. Measurements were always conducted on the same leaves throughout the day as well as for the different measurement days.

7.2.4 Dynamic stem growth model

By slightly modifying the mathematical flow and storage model of Steppe *et al.* (2006), a mechanistic model was obtained to assess dynamics in xylem and storage water potentials based on stem sap flux density and stem diameter variations (Figure 7.4). This model was applied as a tool to synthesise the conducted measurements and derive trends in osmotic potential of the stem storage tissue.

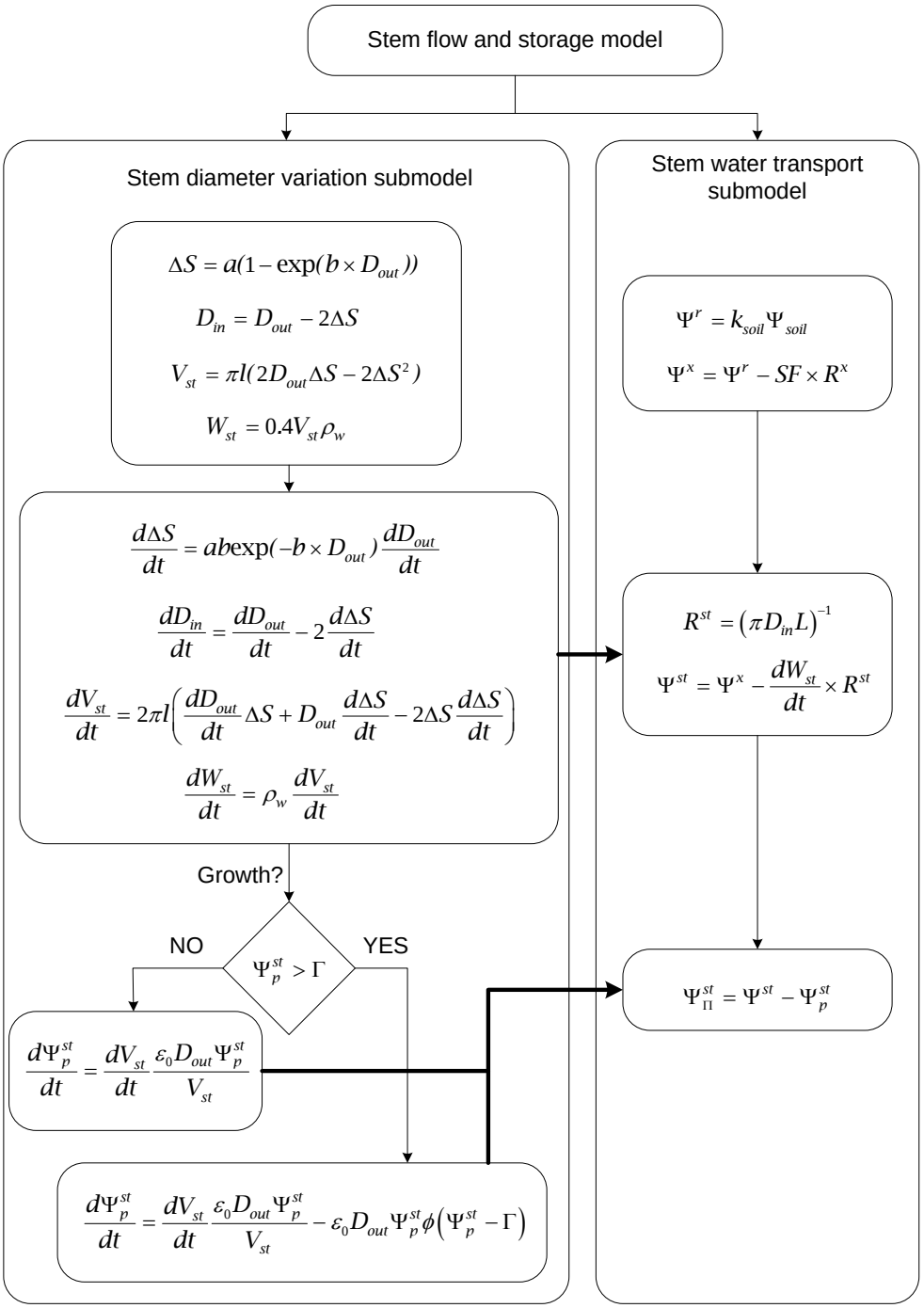

Figure 7.4 *Schematic overview of the model linking the dynamics of stem diameter variations to stem sap flow and storage. The links between the two submodels as mentioned in the text are indicated by arrows. Measurements of* D_{out} *form the input of the stem diameter submodel while the water transport submodel is run on SF measurements. Symbols are explained in the List of abbreviations and symbols and in the text.*

In this model, the thickness of the stem storage compartment ΔS (m) is linked to the outer stem diameter D_{out} (m) via an empirical relationship (Génard *et al.*, 2001; Steppe *et al.*, 2006):

$$\Delta S = a(1 - \exp(b \times D_{out})) \qquad (7.5)$$

with a and b empirical parameters. Based on measurements of bark thickness and stem diameter of the investigated *Avicennia* and *Rhizophora* trees, rough estimates of a and b were obtained, with a=0.0035 and b=18.47 m^{-1} for *Avicennia* and a=0.0153 and b=10.03 m^{-1} for *Rhizophora*, respectively. From ΔS and the measured D_{out}, the inner diameter of the stem D_{in} consisting of the outer diameter minus the storage tissue can be calculated, as well as the water flow (dV_{st}/dt in $m^3\ s^{-1}$) in and out of the stem storage tissue, with l (m) the length of the stem which was measured for both species. This V_{st} is directly linked to the storage tissue pressure water potential Ψ_p^{st}, distinguishing between elastic growth ($\Psi_p^{st} < \Gamma$) (Eq. 7.6) or both elastic and plastic growth ($\Psi_p^{st} > \Gamma$) (Eq. 7.7) (Lockhart, 1965):

$$\left(\frac{dV_{st}}{dt}\right)_{el} = \frac{V_{st}}{\varepsilon}\frac{d\Psi_p^{st}}{dt} \qquad (7.6)$$

$$\left(\frac{dV_{st}}{dt}\right)_{el+pl} = \frac{V_{st}}{\varepsilon}\frac{d\Psi_p^{st}}{dt} + V_{st}\phi\left(\Psi_p^{st} - \Gamma\right) \qquad (7.7)$$

with ϕ the extensibility of cell walls in relation to non-reversible dimensional changes ($MPa^{-1}s^{-1}$), ε the bulk elastic modulus of living tissue in relation to reversible dimensional changes (MPa) and Γ the critical value (in MPa) for the pressure component (Ψ_p^{st}) which must be exceeded to produce (positive) growth in the storage compartment. For this threshold pressure Γ, different values have been observed, ranging from 0.1 to 0.9 MPa (Green *et al.*, 1971; Green & Cummins, 1974; Hsiao & Xu, 2000). Based on the reasoning of Génard *et al.* (2001) that Γ has to be higher for stem tissues than for the young tissues or individual cells on which most of the measurements have been made, the upper value of 0.9 MPa was chosen for the simulations.

The bulk elastic modulus is considered proportional to D_{out} and Ψ_p^{st}:

$$\varepsilon = \varepsilon_0 D_{out} \Psi_p^{st} \qquad (7.8)$$

with ε_0 a proportionality constant (Génard *et al.*, 2001; Steppe *et al.*, 2006).

The obtained variables from this diameter driven growth submodel can then be applied in the water transport submodel. In this submodel xylem water potential Ψ^x (MPa) is derived from the root water potential Ψ^r (considered proportional to the soil water potential Ψ^{soil} applying a proportionality factor k_{soil}), the measured sap flow SF (mg s^{-1}) and the xylem resistance to flow R^x (MPa s mg^{-1}). R^x and k_{soil} can be calibrated based on stem water potential measurements. If Ψ^x is known, the water potential of the storage tissue can be determined based on the flow to and from this compartment and the exchange resistance R^s (MPa s mg^{-1}) between stem storage and stem xylem compartments. The latter is determined based on the assumption that the stem storage and xylem compartments are separated by a virtual membrane with a radial hydraulic conductivity L (m MPa^{-1} s^{-1}) (Steppe *et al.*, 2006). The mass flow of water to and from the storage compartment is determined from the volumetric flow assuming a constant water density of 1000 kg m^{-3} and taking into account that only 40 % of the total stem storage volume V_{st} consists of water (Steppe *et al.*, 2006). Knowing the pressure water potential of the storage tissue from the diameter submodel, the osmotic water potential of the storage tissue Ψ_{Π}^{st} can then be derived.

While k_{soil} and R^x can independently be assessed through calibration of the modelled xylem water potentials based on the psychrometric measurements, the parameters L, ϕ and ε_0 remain unknown. Also, an initial value of Ψ_p^{st} must be fed to the model. For L, values obtained from cells of higher plant tissues between 1.1×10^{-10} and 1.67×10^{-4} m $MPa^{-1}s^{-1}$ have been mentioned (Dainty & Preston, 1963; Dale & Sutcliffe, 1986). For cell wall extensibility ϕ, Hsiao *et al.* (1998) mention a range from 8.33×10^{-6} to 5.56×10^{-5} for young plants, although for older tissues this the extensibility is likely to be an order of magnitude lower (Génard *et al.*, 2001). The elastic modulus ε ranges from from 0 to 30 MPa for higher plant tissues (Dainty & Preston, 1963;

Dale & Sutcliffe, 1986), allowing a realistic estimation of ε_0 based on D_{out} and Ψ_p^{st} values. For the initial value of Ψ_p^{st}, $\Psi_p^{st(in)}$, a value of 0.7 was applied.

From the derived Ψ_Π^{st} and V_{st}, a measure for the total amount of osmotic active compounds N_{eq} (mol) in the storage tissue can be derived from the Van 't Hoff equation (Eq. 1.3):

$$N_{eq} = \frac{\Psi_\Pi}{RT} V_{st} \qquad (7.9)$$

As no distinction is made between the different compounds or their osmotic activity, N_{eq} will be referred to as a number of osmotic equivalents.

The model, consisting of a set of algebraic and differential equations, was implemented, simulated and calibrated using the modelling and simulation software package PhytoSim (Phyto-IT BVBA, Mariakerke, Belgium). Table 7.2 shows the applied parameter values, based on Génard *et al.* (2001) and Steppe *et al.* (2006).

Table 7.2 *Applied model parameters. These parameters were chosen within the ranges mentioned in literature, based on expert knowledge.*

Parameter	Value
L (m MPa^{-1} s^{-1})	2.85×10^{-9}
ϕ (MPa^{-1} s^{-1})	2.34×10^{-7}
ε_0 (m^{-1})	150

7.3 Applicability of the Sapflow+ method in field conditions

7.3.1 Results

Heat velocity

Unlike in Chapter 6, it was not possible to set up a gravimetric validation experiment at the mangrove site. Therefore, the Sapflow+ method was compared to the HR method (Figure 7.5). Although a high correlation was obtained between the Sapflow+ V_h measurements and those of the HR sensors (correlation coefficient 0.83), a pooled regression of all measured data did not lead to a clear linear relation (R^2=0.68) (Figure 7.5a). However, when regressing these measurements for each tree separately, an average R^2 of 0.93±0.05 was obtained. Moreover, when applying Eq. 6.9 to the downstream and upstream temperatures measured by the Sapflow+ sensor, even the pooled data led to a good linear fit (Figure 7.5b).

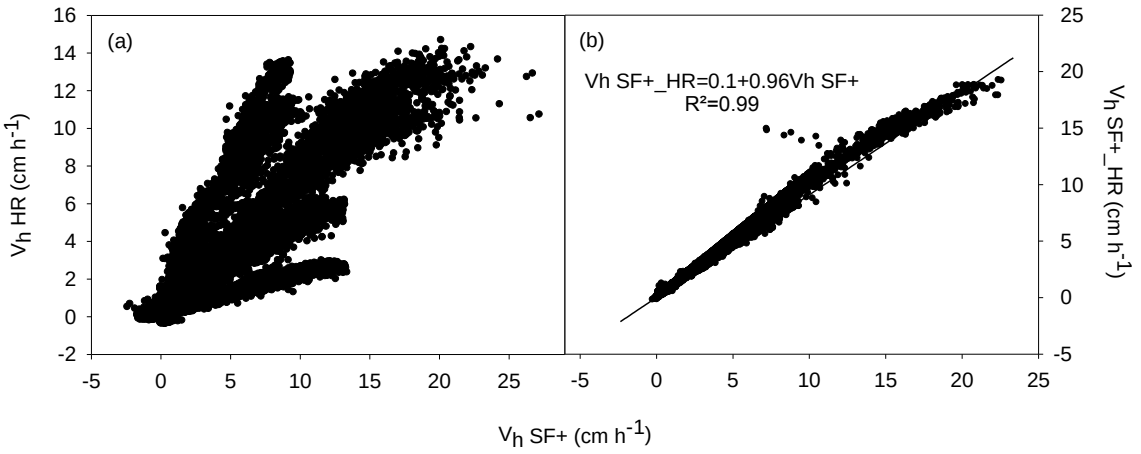

Figure 7.5 *(a) Heat velocity V_h as determined by the HR sensors versus V_h determined by the Sapflow+ (SF+) sensors for all measured trees, both Avicennia and Rhizophora; and (b) V_h as determined applying the HR method to the downstream and upstream temperature measurements of the Sapflow+ sensor (V_h SF+_HR) versus V_h determined by the Sapflow+ sensor, both for Avicennia and Rhizophora. For the application of the HR method to the Sapflow+ temperature measurements, D_{ax} values as obtained by the Sapflow+ method were applied.*

Water content

Figure 7.6a, c indicates that V_h and *MC* patterns are highly correlated (correlation coefficient of 0.90), with *MC* showing a daily pattern similar to the V_h pattern: when daily peaks were registered for V_h, also peaks in *MC* were noted both for *Avicennia* and *Rhizophora* (Figure 7.6a, b), while for those depths for which V_h did not vary, also no daily variation in *MC* was registered for both species (Figure 7.6c, d). However, while V_h measured according to the Sapflow+ method showed no noise throughout the entire measurement period, *MC* data became noisier even though V_h patterns remained accurate (Figure 7.6b, d). While for some installed sensors, this noise only occurred after more than a month, for others it emerged already after a week. Nevertheless, despite this noise the observed *MC* patterns were still somehow visible and remained unaltered throughout the measurement period.

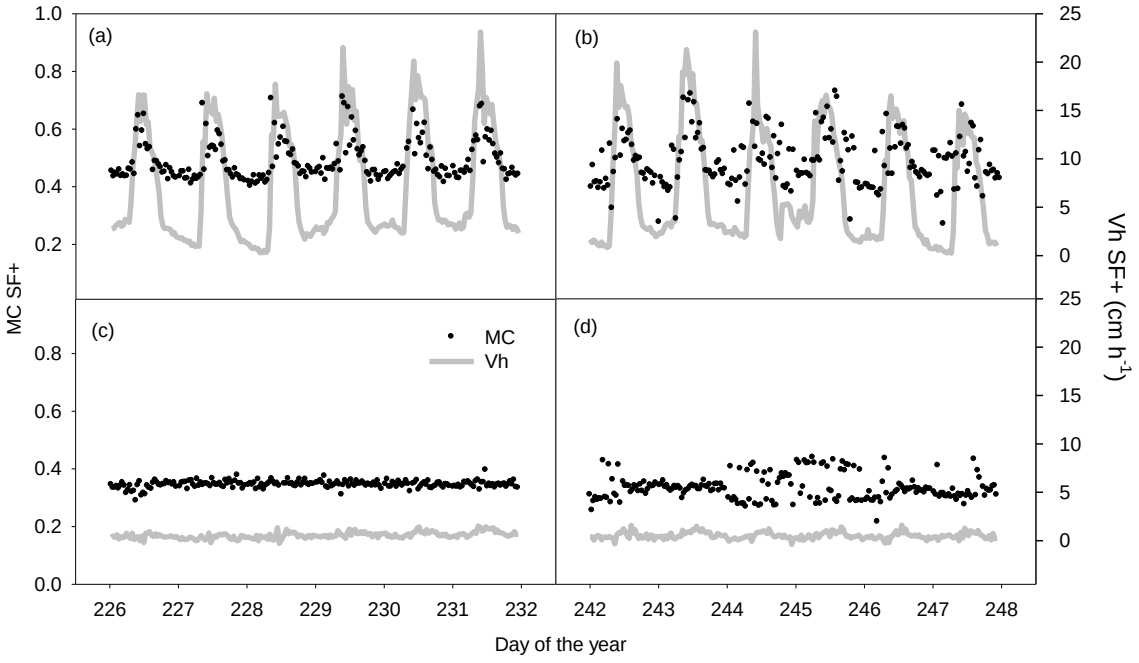

Figure 7.6 *Examples of water content (MC, black dots) and heat velocity (V_h, grey line) measured according to the Sapflow+ method at the beginning of (a, c) and later on during the measurement period (b, d). While a and b show measurements at an outer measurement point where sap flux density showed a clear daily pattern, c and d show measurements at an inner measurement point where there was very little variation in sap flux density. MC values were corrected for flow effects based on the wound corrections mentioned in Figure 6.8 and Figure 6.9.*

As daily measurements of *MC* may be prone to errors, the nightly average of the *MC* values from 19.30 till 5.00 h was determined to investigate the long term changes in stem water content. To this end, data of subsequent days measured with the same sensor were analyzed. Figure 7.7 shows nightly water content for *Avicennia* 3 and *Rhizophora* 3. To assess long-term rise or decline in water content, a weighted linear regression was conducted. This led to significant slopes of 0.1±0.03 % per day for *Avicennia* 1, 0.07±0.02 % per day for *Avicennia* 3 and -0.05±0.01 % per day for *Rhizophora* 3 while for the other trees the slope did not significantly differ from zero.

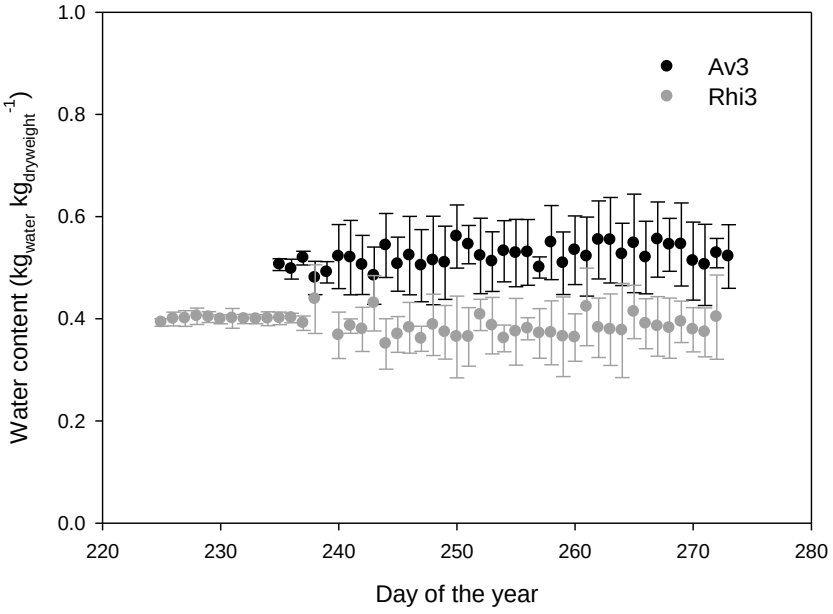

Figure 7.7 *Water content determined as the average of night-time (19.30 - 5.00 h) water content measurements. Av3 and Rhi3 were chosen as for these trees, the longest uninterrupted measurements with the same sensor were obtained.*

7.3.2 Discussion

Heat velocity

As it is known that sap flux density and, hence, heat velocity can greatly vary radially and azimuthally (Ford *et al.*, 2004; Krauss *et al.*, 2007; Saveyn *et al.*, 2008), it was not surprising that the pooled dataset of all Sapflow+ V_h measurements did not lead to a good linear relation with the HR V_h measurements as both sensors measured at different depths and different time intervals (Figure 7.5a). The high correlation coefficient of the pooled dataset and the good linear regressions for

each tree separately, however, indicated that the Sapflow+ sensors were able to capture the same trends in V_h as the HR sensors. This was clearly confirmed when comparing the Sapflow+ data with those obtained by applying the HR method on the temperatures measured upstream and downstream with the Sapflow+ sensor (Figure 7.5b). These results are in agreement with the results from Chapter 6, showing that the Sapflow+ and HR method perform equally for reverse to moderate flows. As the highest measured V_h was 24 cm h^{-1}, possible discrepancies between Sapflow+ and HR measurements at higher flows could not be confirmed.

Unlike the theoretical calculations in Chapter 6, the Sapflow+ results and HR results applying the measurements from the Sapflow+ sensor are not exactly equal as the linear regression led to an offset of 0.1 and a slope of 0.96. This is probably because of small differences between the actual needle distances and those measured and applied in the V_h calculations as it has been shown that small offsets in needle spacing can lead to large differences in V_h determination, both for the Sapflow+ and the HR method (Chapter 6).

For the rest of this chapter, V_h values determined according to the Sapflow+ method will be used. However, because of practical issues, some gaps occurred in the Sapflow+ data. For these periods (approximately 11% of the data), V_h data were interpolated based on the HR results obtained by the HR sensor from the same tree.

Water content

On an hourly time scale, *MC* clearly increased during the day when sap flow rose and decreased again when sap flow declined. This is somewhat counterintuitive as it is known that for most species *MC* should decline during the day and rise during the night because of the lag between transpiration and sap flow (Jameson, 1966; Borghetti *et al.*, 1991). Moreover, the daily fluctuations in *MC* seem very large (up to 20 %). Nevertheless, similar patterns have been shown for gravimetric measurements on twigs of Pinyon species during dry winters, although this pattern was not physiologically explained (Jameson, 1966).

The observed noise is likely due to sensor properties which need further improvement. As such, it was noted that the applied heaters slowly corroded leading to unequal heat pulses and finally heater breakdown. As *MC* is much more sensitive towards heat input than V_h, small changes in heat input can affect *MC* results without affecting V_h. Additionally, *MC* is more closely correlated to thermal

conductivity which in practice may lead to identifiability problems, even though theoretically the model is identifiable (Chapter 6). Optimization of the hardware and a thorough comparison of the model parameters may further improve *MC* measurements.

On the longer term, however, *MC* results were readily interpretable. These results indicated that there was little change in water content throughout the measurement period. Even though these results could not be confirmed by an independent validation, the obtained nightly averages seem realistic and the long-term patterns plausible. As such, these long-term patterns can be coupled to other ecophysiological variables when assessing the water use strategies of the species under investigation.

7.4 Water flow and storage in *Avicennia* and *Rhizophora*

7.4.1 Results

Given the similar patterns in the ecophysiological variables for the three trees of each species, the average of the three trees per species was taken for further analysis. This way, a more general investigation of species water use was conducted, rather than focussing on intra-species variability.

Ecophysiological measurements

Averaged heat velocity showed a good positive correlation with both radiation (correlation coefficients of 0.83 and 0.78 for *Avicennia* and *Rhizophora*, respectively) and *VPD* (correlation coefficients of 0.86 and 0.88 for *Avicennia* and *Rhizophora*, respectively) (Figure 7.8). As soil water potential, at both measured depths, varied very little with an average value of -2.1 MPa and a standard deviation of only 0.1 MPa, heat velocity and soil water potential were not correlated, with correlation coefficients 0.08 and 0.04 for *Avicennia* and *Rhizophora*, respectively (Figure 7.8). While stomatal conductance for *Rhizophora* was very low during the night and increased during daytime, the reverse pattern was measured for *Avicennia*, showing large stomatal conductance at night-time. On average, stomatal conductance values for *Avicennia* were higher than for *Rhizophora* (Figure 7.9).

While average heat velocity patterns were closely correlated for *Avicennia* and *Rhizophora* (correlation coefficient 0.91), their stem diameter changes were

markedly different (Figure 7.8c, d). While *Avicennia* showed the classical pattern where the diameter decreases in the morning and increases at night, diameters for *Rhizophora* increased during the morning and decreased in the late afternoon, remaining more or less stable at night-time. Stem water potentials for both species were again similar, decreasing in the morning and increasing in the afternoon.

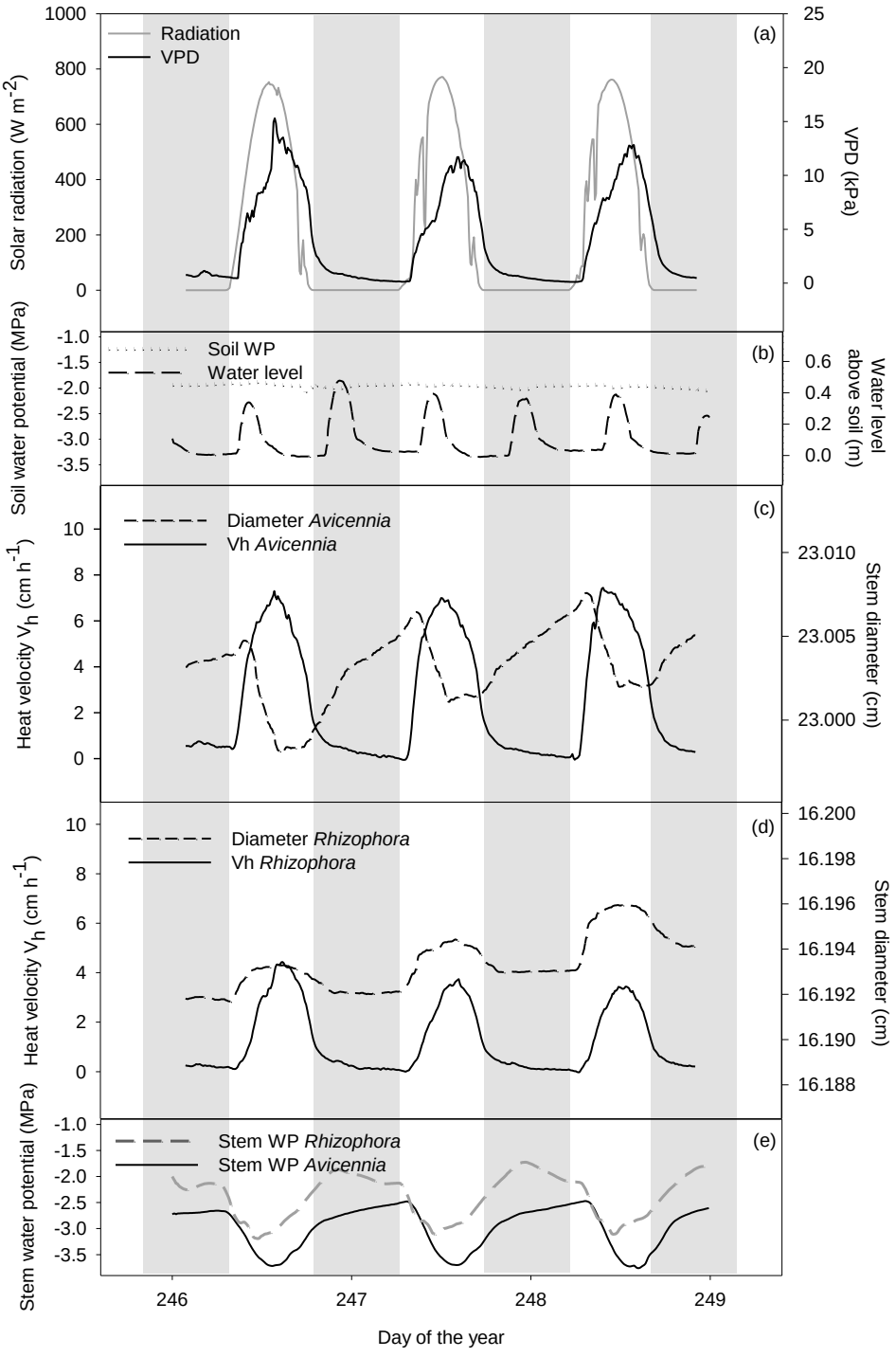

Figure 7.8 *Shortwave solar radiation and vapour pressure deficit (VPD) (a); Soil water potential and water level above the soil (c); heat velocity V_h and diameter change for Avicennia (c) and Rhizophora (d) and stem water potential for Avicennia and Rhizophora (e) during standard days.*

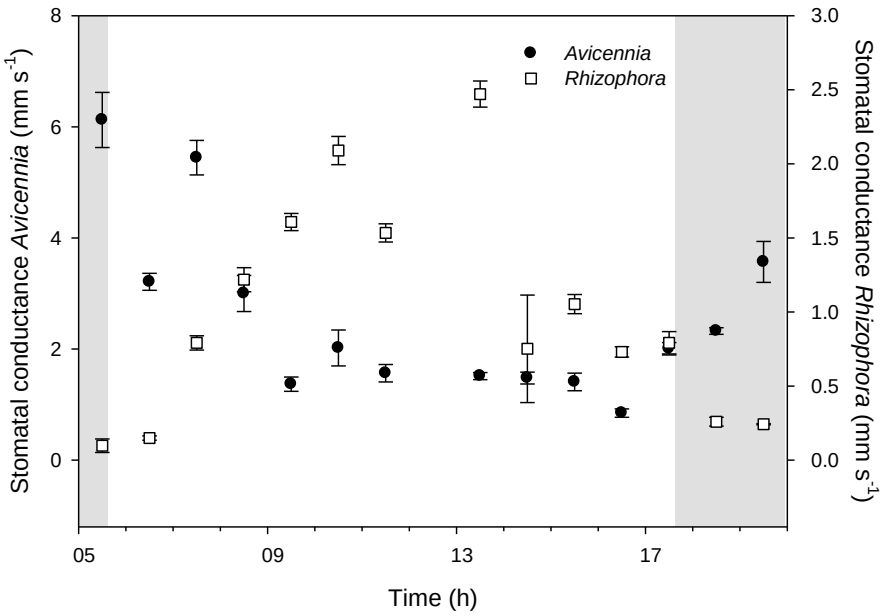

Figure 7.9 *Stomatal conductance for Avicennia and Rhizophora, determined as the average of measurements conducted during 4 standard days (DOY 241, 247, 251 and 254) during the dry period.*

On 5 different days (DOY 231, 238, 245, 252, 258) throughout the dry measurement period (no rain fell from DOY 224, the start of the measurement campaign, till DOY 262), a steep decline in average stem diameter of both *Avicennia* and *Rhizophora* was noted (Figure 7.10 as an example). During these days, the stem diameter of *Rhizophora* hardly increased or even decreased in the morning and further decreased in the afternoon while for *Avicennia*, the decrease in diameter was much larger than on standard days. During these days, it was noted that the *VPD* values were higher during the morning and/or during the afternoon compared to standard days, which was reflected in a steeper decline of stem water potential and corresponding rise of heat velocity in the morning and vice versa in the afternoon.

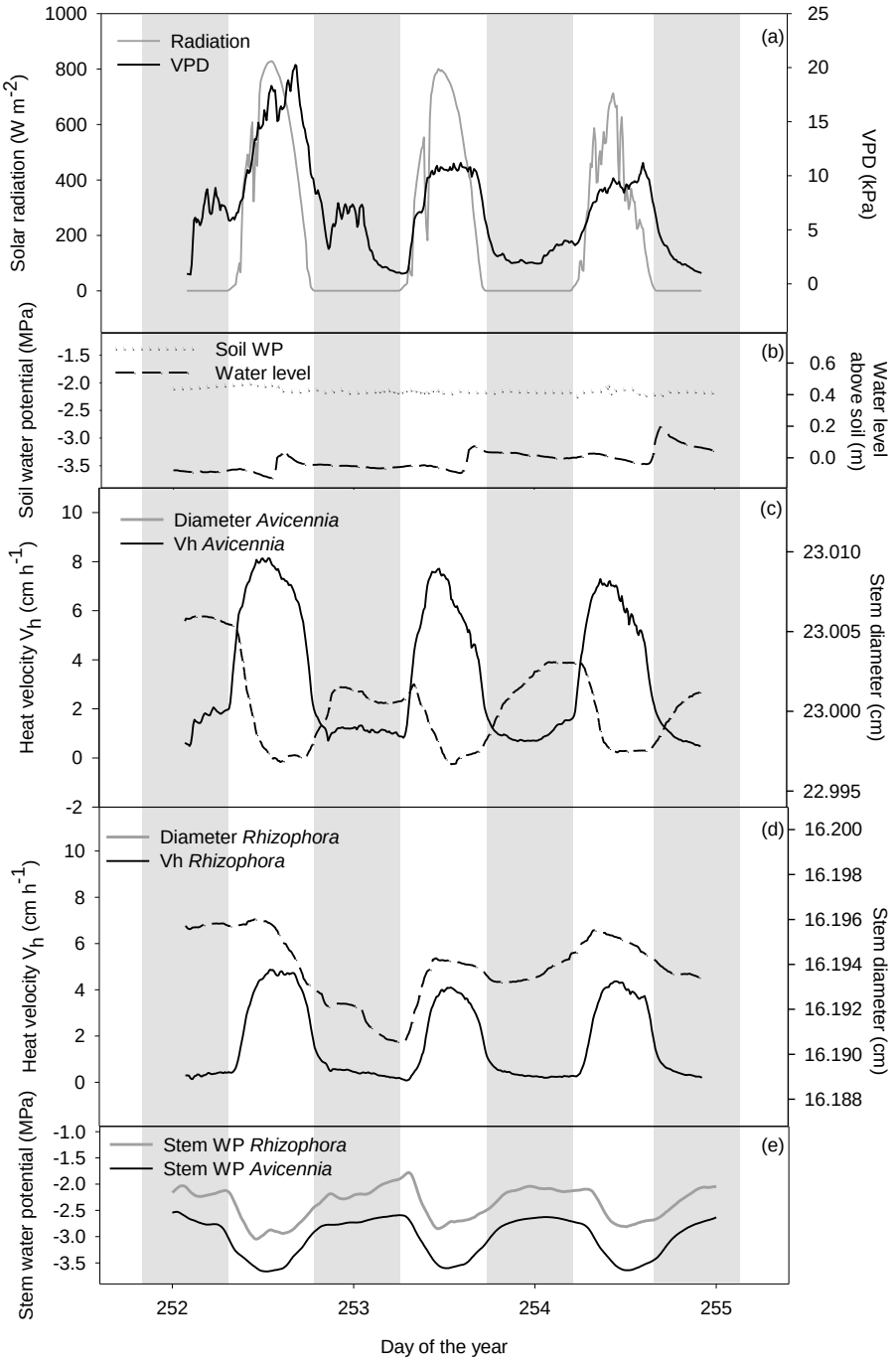

Figure 7.10 *Shortwave solar radiation and vapour pressure deficit (VPD) (a); Soil water potential and water level above the soil (c); heat velocity V_h and diameter change for Avicennia (c) and Rhizophora (d) and stem water potential for Avicennia and Rhizophora (e) during a period with a typical diameter decline.*

Modelled storage water potential patterns

In Figure 7.11 the model results of the standard conditions are shown. While for *Avicennia*, the storage water potential lags behind the xylem water potential, corresponding with a decreasing stem diameter in the morning and an increase of stem diameter in the afternoon, the reverse pattern is visible for *Rhizophora*. This difference in total storage water potential is caused by the time lag in storage osmotic water potential (Figure 7.12a). Although the patterns are very alike, the number of osmotic equivalents increases more rapidly for *Rhizophora* compared to *Avicennia* (Figure 7.12b).

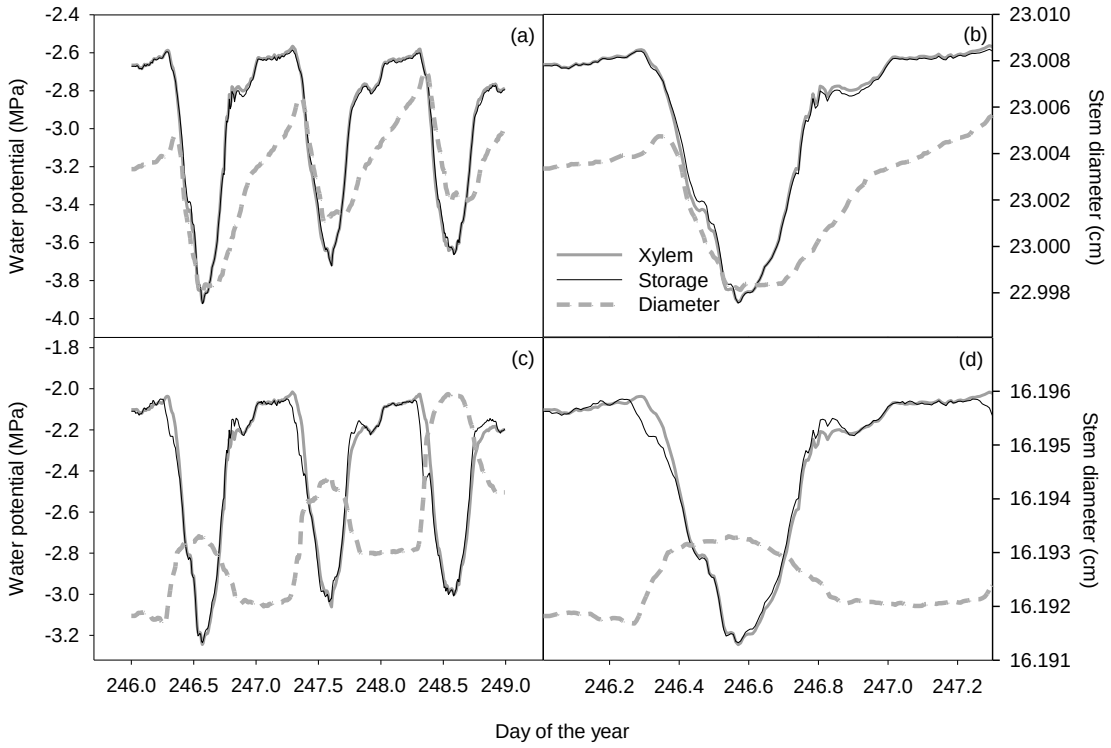

Figure 7.11 *Model results showing the diameter input and xylem and storage water potential output for both Avicennia (a, b) and Rhizophora (c, d) during standard conditions. (b) and (d) are more detailed representations of the model results for a single day.*

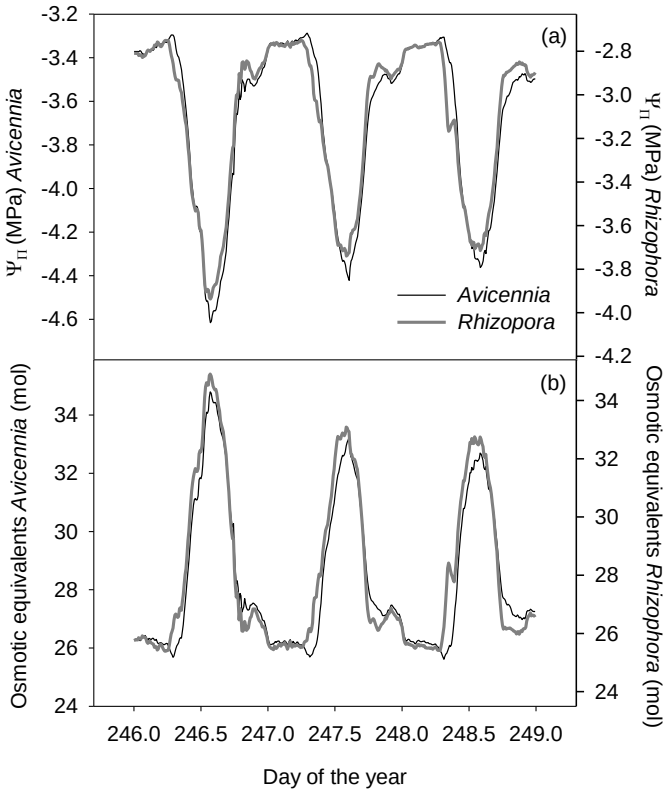

Figure 7.12 *Osmotic potential of the storage tissue (a) and derived osmotic equivalents (b) for Avicennia and Rhizophora during standard conditions.*

For the days where a strong decline in stem diameter was observed, the xylem water potential became more negative, enlarging the difference with storage water potential for *Avicennia* and narrowing this difference for *Rhizophora* in the morning, resulting in a stronger decline and less increase in stem diameter for both species, respectively (Figure 7.13). In the afternoon, the more negative xylem potential led to a larger difference with the storage water potential for *Rhizophora*, magnifying the afternoon shrinkage. While both species show an increase in osmotic equivalents in the stem storage volume (Figure 7.14), the osmotic potential remains insufficiently negative to avoid the diameter decline.

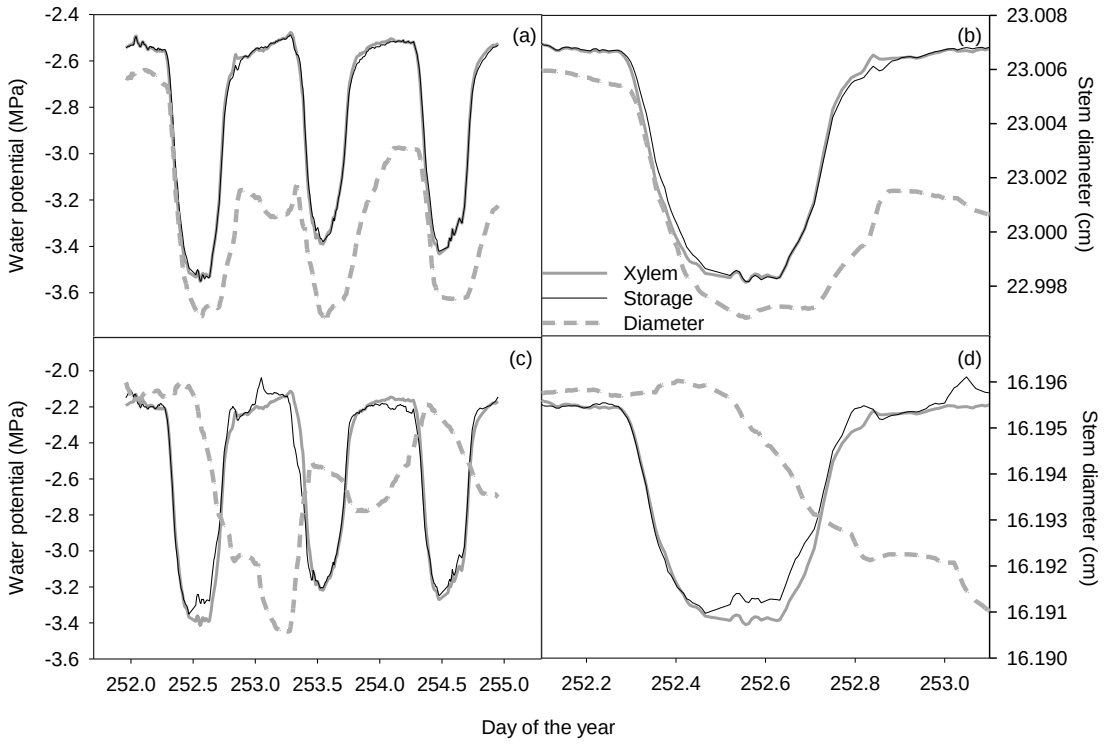

Figure 7.13 *Model results showing the diameter input and xylem and storage water potential output for both Avicennia (a, b) and Rhizophora (c, d) during diameter decline conditions (with a typical diameter decline during DOY 252). (b) and (d) are more detailed representations of the model results for a single day.*

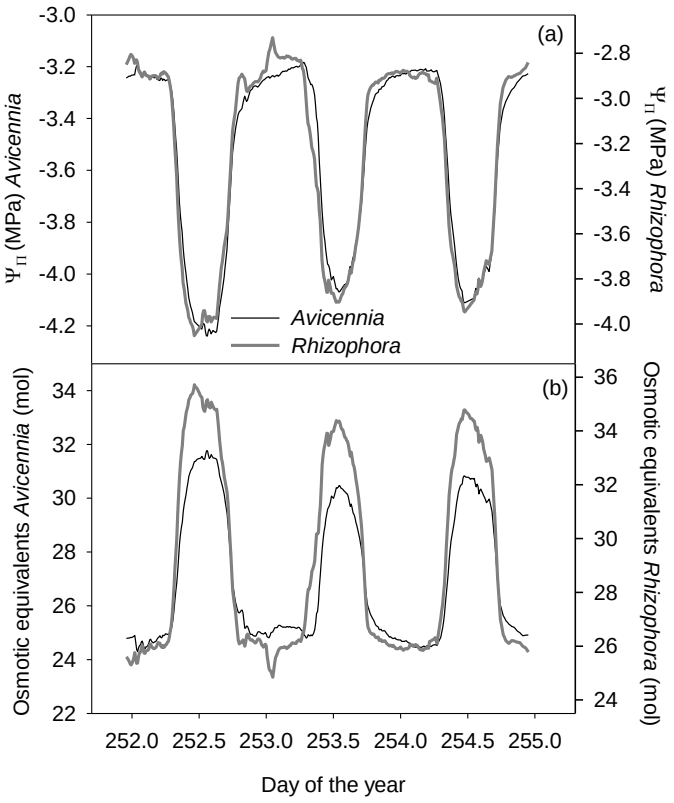

Figure 7.14 *Osmotic potential of the storage tissue (a) and derived osmotic equivalents (b) for Avicennia and Rhizophora during diameter decline conditions (with a typical diameter decline during DOY 252).*

Rain events

Despite their remarkably different growth pattern, stem diameters of both *Avicennia* and *Rhizophora* showed an immediate increase during rain events (Figure 7.15 as an example of the first rain event). During rainfall at daytime, sap flux density fell to zero while xylem water potential and stem diameter for both species increased. However, also during night-time, when sap flux density was already zero (or close to zero during high night-time *VPD* for *Avicennia*), the stem diameter of both species rose rapidly. These rain events were crucial as each time, an increase in diameter of more than double the standard difference in daily maximum and minimum was obtained, muting the gradually decline in stem diameter for *Avicennia* and even leading to stabilization for *Rhizophora* (Figure 7.16).

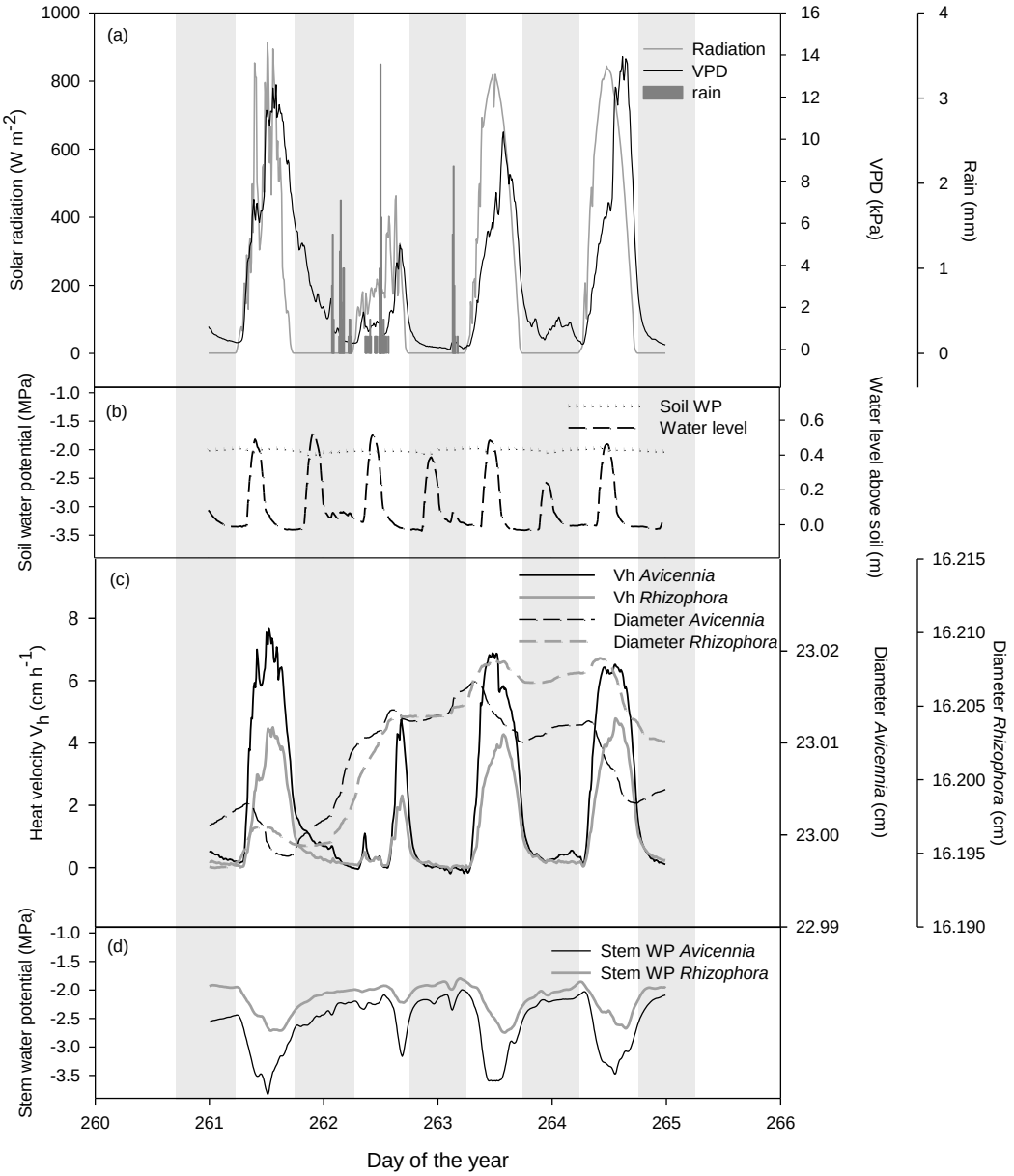

Figure 7.15 *Shortwave solar radiation, vapour pressure deficit (VPD) and rain (a); Soil water potential and water level above the soil (b); heat velocity V_h and diameter change for Avicennia and Rhizophora (c) and stem water potential for Avicennia and Rhizophora (d) during a period with rainfall.*

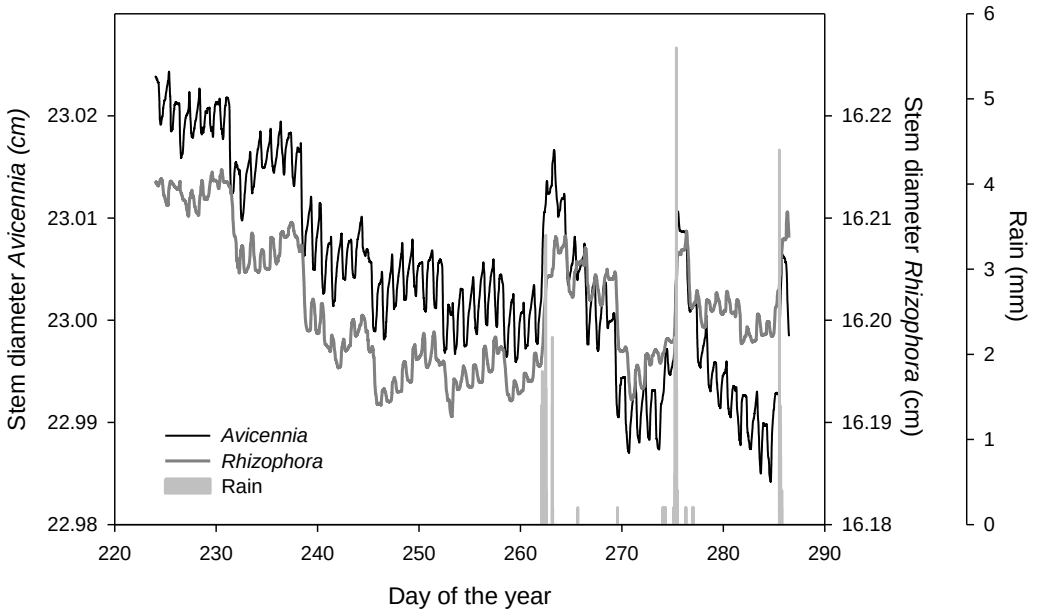

Figure 7.16 *Stem diameter of Avicennia and Rhizophora during the measurement period.*

7.4.2 Discussion

Low flows: an indication of drought stress rather than proof against the cohesion-tension theory

Similarly as suggested or measured in previous studies and reviews on mangroves (Ball, 1988; Zimmermann *et al.*, 1994; Krauss *et al.*, 2007), measured heat velocities and, hence, sap flux densities in our study were very low (maximal recorded heat velocity of 24 cm h^{-1}) (Figure 7.5, Figure 7.8, Figure 7.10, Figure 7.15). Zimmerman *et al.* (1994; 2002) attributed these low flows to the presence of viscous, polymeric substances in the xylem sap and hypothesized that these substances caused the upward water flow by reducing the chemical activity of water. This hypothesis, together with their pressure probe measurements which showed much less negative xylem pressures than those obtained by the pressure bomb (Zimmermann *et al.*, 2004), led these authors to discard the widely accepted cohesion-tension theory (see also Section 1.1.2). Becker *et al.* (1997), however, measured sap flux densities in mangrove species which were very similar to those measured in a tropical heath forest with a similar climate and concluded that sap flow rates of mangrove trees are not necessarily unusually low. Although their experimental plot had freshwater entering from streams and a sewer, it was not known if the trees relied on these freshwater sources. As proven by isotope analysis, mangrove trees often do have

access to freshwater lenses, enhancing water uptake (Lambs *et al.*, 2008). It is, hence, more plausible that the low sap flow rates noted in many mangrove studies can be attributed to the high salinity of the available water, lowering the water potential and thwarting water uptake. Given the very negative soil water potentials (Figure 7.8, Figure 7.10) and the overall decline in stem diameter of both species (Figure 7.16), the measured trees clearly suffered from drought stress. Hence, it is not unexpected that these stressed trees want to reduce their water loss as much as possible, resulting in low flows and rather low stomatal conductances during the day (Figure 7.9). Moreover, the measured stem water potentials in this study show that mangrove trees do establish highly negative stem water potentials, conform the cohesion-tension theory.

Stem diameter variations: time lag and/or osmotic regulation?

When interpreting the plant water status, the radial transport between the xylem and surrounding storage tissues is of crucial importance as it allows turgor to build up which ultimately leads to plastic growth if a threshold pressure is overcome (Lockhart, 1965). Moreover, water in the storage tissue buffers discrepancies between water demand and supply. As such, it has been commonly accepted that a clear time lag exists between the transpiration at leaf level and the water uptake at root level, caused by the hydraulic resistance between the two (Zweifel *et al.*, 2000; e.g. Peramaki *et al.*, 2001; Sevanto *et al.*, 2002; Steppe *et al.*, 2006) (see also Section 1.3.1 and Figure 1.11). This time lag causes a decrease in stem diameter in the morning as then the water supply from the roots lags behind the transpiration at leaf level, necessitating water flow from the storage compartments (Hinckley & Bruckerhoff, 1975). In the afternoon, when xylem water potential rises because of a decreased atmospheric water demand, water again flows back to the storage tissues, resulting in a diameter increase (Molz & Klepper, 1973).

Despite this commonly accepted morning shrinking and afternoon swelling pattern of trees, reverse diameter patterns as shown for *Rhizophora* (Figure 7.8d, Figure 7.10d) have been mentioned before for crasulacean acid metabolism (CAM) plants (Gouws *et al.*, 2005; Matimati *et al.*, 2012). These CAM plants are characterised by night-time acquisition of CO_2 through open stomata, which is then stored as foliar organic acids. During daytime, decarboxylation of these acids allows for photosynthesis behind closed stomata (Osmond *et al.*, 2008). However, the

measurements of low night-time and higher daytime stomatal conductance coupled with a daily sap flux density pattern clearly indicate that *Rhizophora stylosa* Griff. cannot be considered a CAM plant (Figure 7.8d, Figure 7.9, Figure 7.10d).

For many, mostly herbaceous, species, daytime stem diameter increase can be noted during conditions of very low to zero *VPD* and sufficient soil water availability. This phenomenon is caused by the active loading of solutes into the xylem and subsequent osmotic uptake of water and is termed root pressure (Kramer & Boyer, 1995). During conditions of low transpiration, the solutes retained in the endodermis and transported to the xylem allow root pressure to build up, causing an upward water flow which can then be radially transported to the storage tissues (Steudle & Peterson, 1998). Even though for *Avicennia* early morning growth peaks could be seen when *VPD* was zero and root pressure may have been present for both species during these conditions, it cannot explain the daily growth pattern of *Rhizophora* as diameter increase continued when *VPD* increased and xylem water potential decreased (Figure 7.8, Figure 7.10). To our knowledge, a similar combination of morning diameter increase and afternoon decrease together with a classical sap flux density and stem water potential pattern has not been presented in literature so far.

By which mechanism then, if not CAM or root pressure, do these differences in growth pattern for both species, influenced by the same environmental conditions, occur? The results of the mechanistic model based on the cohesion-tension theory, show that the different growth patterns can be explained by a difference in time lag between xylem and storage water potential (Figure 7.11, Figure 7.13) and suggest that both species show a daily pattern of osmoregulation in the storage tissue (Figure 7.12, Figure 7.14). A slightly earlier increase of osmotic active compounds in the storage tissue, allows the storage compartments of *Rhizophora* to draw water from the xylem during the morning, whereas for *Avicennia*, the slightly delayed increase in osmotic compounds causes the storage water potential to be less negative than the xylem water potential, resulting in diameter decrease (Figure 7.12). If, however, *VPD* is high during the morning, xylem water potential decreases relatively more than the storage water potential. Apparently, the osmotic regulation of the storage tissue is not capable of compensating this drop in xylem water potential, resulting in a stronger diameter decline for *Avicennia* and reduced

diameter increase or even decrease for *Rhizophora* (Figure 7.10, Figure 7.13, Figure 7.14).

Rain as important growth factor

Despite the reversed daily diameter variation patterns of *Avicennia* and *Rhizophora*, both species immediately showed a large diameter increase at the onset of rainfall (Figure 7.15, Figure 7.16). While rainfall is known to induce stem diameter increase as it leads to a sudden drop in xylem water potential, similarly as during stomatal closure in the afternoon, here the growth peaks occurred both during daytime and night-time rain events, implying another mechanism. As the diameter responses were immediate, whether at high or low tide, and sap flux density was zero during these growth peaks, also rain water uptake from the soil can be excluded. This leaves direct canopy uptake of the rainwater as the most plausible mechanism resulting in the observed diameter increases.

Foliar water uptake has been described for many species, especially in drought stress conditions, improving photosynthetic performance and growth and is now considered to be a widespread phenomenon (Dawson, 1998; Burgess & Dawson, 2004; e.g. Breshears *et al.*, 2008; Limm *et al.*, 2009; Simonin *et al.*, 2009; Goldsmith *et al.*, 2012). While the pathways for foliar uptake are not entirely unravelled, the cuticle (Yates & Hutley, 1995; Limm & Dawson, 2010), trichomes (Franke, 1967) and hydathodes (Martin & von Willert, 2000) have been identified as gateways for water uptake, while stomatal pores used to be expected not to allow penetration of water films (Schönherr & Bukovac, 1972). Recently, however, Burkhardt *et al.* (2012) showed that stomatal penetration of water is possible, especially in the presence of salts. Hence, given their trichomes and salt exclusion glands, mangrove species seem well fit to allow foliar absorption. Unlike in several other foliar water uptake studies, no reverse sap flow was noted during rain events. It is, however, possible that the rainwater was directly transported to the storage compartments or only occurred in specific parts of the xylem. The latter would be in agreement with the patchy growth pattern that has been noticed for *Avicennia* (Schmitz *et al.*, 2008).

Independent of the mechanism of rainwater uptake, it is clear that the rain events are crucial for the survival of both *Rhizophora* and *Avicennia* as without rain, both species clearly suffered from the stress conditions caused by the saline environment, resulting in highly negative soil water potentials (Figure 7.16). Despite

periods of slight diameter increase, days characterised by high morning or evening *VPD* caused diameters for both species to decline on average during periods without rain, indicating that at this location, both species are functioning close to their hydraulic limits. In these circumstances, only rain seems to allow for sufficient hydraulic recovery.

Endogenous regulation versus environmental dynamics

From the above, it seems that stem diameter variations and coupled growth are the result of both endogenous control and environmental dynamics. This has previously been suggested for growth patterns of leaves and roots (Walter & Schurr, 2005). This implies that, to allow correct predictions of plant behaviour based on mechanistic modelling, the latter must also include these endogenous adaptations, especially as our results show that very small differences in osmotic active compound regulation can have drastic influences on important plant physiological variables such as the stem diameter. Next to these endogenous influences, also alternative hydraulic pathways such as canopy water uptake will need to be included in cohesion-tension based models.

To this end, further research is needed to unravel the complex interactions between environmental and endogenous control of growth, whether on molecular or entire plant level. This will include the determination of storage osmotic water potentials and identification of osmotic active compounds, assessing the variability in xylem and storage hydraulic resistances and further elucidating alternative hydraulic pathways. A more thorough knowledge on how these features influence stem diameter variations will result in more insight into why species differ in growth patterns and, hence, which growth strategies are more beneficial, depending on environmental conditions. Moreover, it will allow assessing the relative importance of endogenous regulation and environmental dynamics to long-term growth.

7.5 Conclusions

Although the time lag between transpiration and root water uptake has proven to greatly influence stem diameter variations, endogenous regulation of growth patterns must not be neglected. We demonstrated that, despite their occurrence in the same environment, *Avicennia marina* (Forssk.) Vierh. and *Rhizophora stylosa* Griff. showed markedly different stem diameter variation patterns. Based on a

mechanistic stem diameter and flow model, these differences were attributed to small shifts in osmotic compound loading in the stem storage compartments. In spite of these daily differences, both species showed an average decline in stem diameter with characteristic short-term declines when *VPD* was high, pointing to drought stress. Similarly, stem diameter of both species immediately increased during rain events. Hence, while daily differences were based on endogenous regulation, the average growth was mainly determined by environmental dynamics.

8

General conclusions and perspectives

The main focus of this PhD study was to improve and critically comment on measurements of sap flux density, based on sound thermodynamic principles. In this concluding chapter, the main findings of this research are briefly summarized. Afterwards, the remaining unanswered questions are discussed and suggestions for future research are put forward.

8.1 Research outcome and scientific contributions

Existing continuous sap flux density methods should be considered empirical and necessitate calibration

Measurements of sap flow are indispensable in plant physiological research and applications as they link hydraulic processes throughout the entire Soil Plant

Atmosphere Continuum (**Chapter** 1). These measurements can be focussed on total sap flow through the stem or a stem section or on changes in sap flux density, allowing to assess spatial differences in sap flow (**Chapter** 2). Within the latter, a distinction can be made between methods applying continuous heating and those based on the application of heat pulses. As mentioned in **Chapter** 2, the continuous Thermal Dissipation method is not derived from the basic heat conduction-convection equation, unlike the heat pulse methods. For these heat pulse methods, actual conditions do not differ too much from the assumptions of an ideal heater in an infinite medium as heat pulses are rapidly dissipated in the medium. For continuous methods, however, this is not the case, as in real life applications, finite boundaries will limit the continuous heat dissipation. This makes theoretical derivations from the heat conduction-convection equation as basis for continuous heat methods difficult. This was confirmed in **Chapter 3**, where it was shown that also the continuous Heat Field Deformation method should be considered empirical, linking an empirically derived temperature ratio to sap flux density. Given their empirical nature, these continuous methods necessitate a species-, or even tree-specific calibration. Even though these methods have their benefits as they allow continuous measurements, are easily applicable because of low costs and simple methodology (TD method) or because of their high sensitivity towards a large sap flux density range (HFD method), they should be used with caution. Moreover, these continuous methods are more susceptible to Natural Temperature Gradients than the heat pulse methods and require more power, making them less suited in remote field locations. Also, wound effects are harder to take into account as it is difficult to assess whether deviations from reference or modelled sap flux densities are due to the empirically determined coefficients or due to actual wounding. Because of these reasons, heat pulse methods seem more adequate to accurately determine sap flux density.

The anisotropy of sapwood needs to be accounted for in sap flow method development and modelling

Although acknowledged by Marshall (1958), the anisotropy of sapwood has often been overlooked during heat pulse sap flow method development and modelling as the existing methods and many of the models are based on the isotropic heat conduction-convection equation for an ideal heater in an infinite medium. Fortunately, **Chapter** 4 shows that, as the Compensation Heat Pulse, Tmax and Heat

Ratio heat pulse methods are derivations from this isotropic equation, these methods remain applicable for anisotropic sapwood. For several model applications and recently developed adaptations of sap flux density approaches, this is, however, not the case. Therefore, it is advised to consequently refer to the anisotropic heat conduction-convection equation instead of the isotropic equation and to clearly distinguish between axial, tangential and radial sapwood properties, as was done during the development of the Sapflow+ method in **Chapter** 6. This will, hopefully, avoid further confusion and future errors in modelling and method development and interpretation.

A distinction must be made between bound and unbound water to determine thermal wood properties based on the method of mixtures.

In **Chapter** 2, it was described how the Heat Ratio method was developed as a method enabling low and reverse flows, which is of crucial importance in studying hydraulic redistribution processes (**Chapter** 1). The developers of this method preferred not to determine axial thermal diffusivity based on the heat pulse itself as was proposed for the Tmax method (**Chapter** 2) as this method necessitates zero flows and is susceptible to errors. Unlike for the Tmax method, a deviation in thermal diffusivity will lead to a percentually equal deviation in heat velocity for the HR method. Therefore, thermal diffusivity determination was based on a method of mixtures for a single cell model, taking into account volumetric heat capacity and thermal conductivity of wood, air and water. This way, axial thermal diffusivity can be derived based on a single wood core from which dry wood density and water content are determined. However, in this method of mixtures, no distinction was made between bound and unbound water, inducing an error which is dependent on dry wood density and water content (**Chapter** 5). Therefore, a new equation was proposed, taking into account the amount of bound water based on the fibre saturation point of the sapwood. Although more accurate, this correction necessitates a good estimate of the fibre saturation point, a parameter which can not readily be measured and must be derived based on an empirical relation with dry wood density.

Directly fitting measured temperature changes on axial and tangential positions from the heater to the anisotropic heat conduction-convection equations allows for independent estimation of heat velocity and thermal wood properties.

In response to the limited measurement range of the Compensaion Heat Pulse, Tmax and Heat Ratio method and the difficulties to accurately determine axial thermal diffusivity, needed to calculate heat velocity for both the Tmax and Heat Ratio method, an improved method, the Sapflow+ method, was proposed (**Chapter** 6). This method directly fits the anisotropic heat conduction-convection equation for an ideal heater in an infinite medium to the temperature profiles measured both axially and tangentially from the heater. The combination of these axial and tangential measurements is necessary for the method to be sensitive towards the entire naturally occurring sap flux density range, a feature that is not present in previously developed heat pulse methods, even though it is applied in the continuous Heat Field Deformation method. The Sapflow+ method has the advantage that heat pulse velocity is determined independently from thermal wood properties. Moreover, these properties are simultaneously estimated during the curve fitting procedure, allowing for water content determination. This method was validated both in laboratory conditions on cut stem segments (**Chapter 6**) and in mangrove field conditions (**Chapter** 7). During the field experiment, the Sapflow+ method performed well in determining heat velocity and allowed the assessment of long-term water content variation. Further validation experiments, in which a better hardware design is coupled to independent water content estimates, should be conducted to investigate the cause of the short-term water content variation and the observed noise.

Small shifts in osmotic loading of the storage tissue can result in markedly different stem diameter variation patterns.

Stem diameter variations are functionally explained by the time lag between the transpiration at leaf level and the water uptake at root level, caused by the hydraulic resistance between the two (**Chapter** 1). Because of this time lag, stem diameters typically decline in the morning and increase again in the late afternoon. This same time lag explains the reverse pattern for CAM plants, as these plants open their stomata at night and close them during the day. In **Chapter** 7, however, we showed that another mechanism must be involved in stem diameter changes as for *Rhizophora*, the stem diameter increased in the morning and decreased in the afternoon, even though stomata were closed during night-time. We hypothesize that this remarkable pattern is caused by endogenous osmotic regulation of the storage water potential which allows refilling of the storage tissues. From our modelling

results, small shifts in osmotic loading can lead to markedly different stem diameter variations patterns. This conclusion has significant implications for hydraulic plant modelling as, besides environmental dynamics, this endogenous control needs to be taken into account to accurately predict plant growth.

8.2 Future perspectives

Increasing the accuracy of sap flow measurements is crucial to assess plant water use, investigate hydraulic pathways and validate hydrodynamic plant models. This PhD study attempted to improve sap flow methodology by pointing to some flaws in existing methods, proposing corrections and presenting an improved approach to determine sap flux density and thermal sapwood properties. Nevertheless, still many questions related to sap flow measurement methodology remain unanswered. These questions together with suggestions for future research are listed below.

Unravelling the mechanisms of short and long term wounding

As indicated in **Chapter 2** and **Chapter** 6, heat velocity measurements are influenced by wound effects, comprising both short and long-term effects. When inserting measurement and heater needles in the plant xylem, flow is locally obstructed which has a direct influence on heat velocity measurements, both for the continuous and the heat pulse methods, as has been shown based on Finite Element Modelling (Swanson & Whitfield, 1981; e.g. Burgess *et al.*, 2001a; Green *et al.*, 2003; Wullschleger *et al.*, 2011). Even though the influence of flow obstruction has been assessed in various models by implementing obstruction zones as regions of zero flow with a width proportional to the installed needle diameter, further research needs to be conducted to determine the actual shape and variability of the xylem zone influenced by needle insertion. It is likely that not only width, but also length of the obstructed zone will be dependent on needle diameter. Moreover, both width and length will depend on thermal wood properties as well. Together with this flow obstruction pattern, also local alteration of sapwood properties such as wood density, fibre direction and water content due to drilling and needle installation need to be further investigated (Barrett *et al.*, 1995). Research on these small-scale phenomena poses, however, several challenges. By varying the width and length of flow obstruction zones in Finite Element Models, combined with varying wood properties, a more profound insight on the effects of wounding on sap flux density

measurements will be obtained. Nevertheless, more advanced methods will be needed to assess wound effects in actual plants. In this respect, a combination of Magnetic Resonance Imaging and wood anatomical studies seems most suited to investigate short-term wound effects for different tree species.

Next to these short-term effects, needle installation also has consequences on the longer term as the defence mechanisms of trees will react to the intrusion of this foreign material. Production of resin and formation of wound tissue will alter wood properties and, hence, heat dissipation in the sapwood in the longer term (Moore *et al.*, 2009). As these influences can be avoided by regularly reinstalling the sensors, little attention has thus far been paid to long-term wounding. Nevertheless, for long measurement periods, attention must be paid not to falsely interpret changes in sap flux density caused by this long-term effect. It would be interesting to set-up an experiment during which sap flux density of several species is measured, applying both stationary sensors and sensors that are frequently relocated on the same tree. This way, an easy assessment of the effect of long-term wounding could be obtained. Additionally, pinning experiments may provide further inside in the anatomical development of wound tissue.

Accounting for differences in wood anatomy in heat based sap flow methods

In **Chapter** 2 it was mentioned that Clearwater *et al.* (1999) proposed a correction factor for the Thermal Dissipation method for those cases where part of the probe was in contact with nonconducting xylem or bark, as heat will also be dissipated in these tissues while they do not contribute to the sap flow. Similarly, it can be expected that additional corrections are needed when measuring in sapwood characterized by a non-uniform distribution of sap conducting elements and/or other functional tissues. While such correction factors can be derived empirically for the measured species (Swanson, 1994), a more mechanistic approach, in which different vessel sizes and tissue characteristics are implemented in sap flow method models, will increase our knowledge as to how these factors influence sap flux density measurements. Similarly, it might be interesting to model and assess the impact of radial and tangential flows as sap flux density methods only take axial flow into account, although for most species axial and tangential flows will only have a marginal contribution to total stem flow.

Further optimization of water content measurements with the Sapflow+ method

The Sapflow+ method (**Chapter** 6) was developed to allow heat velocity measurements across the entire naturally occurring sap flux density range, independent of thermal sapwood properties. Moreover, as the latter were simultaneously obtained from the curve fitting procedure, the Sapflow+ method also enables water content determination. However, the method was only tested in lab conditions on a single species. Further lab validation on other species is necessary to confirm its applicability.

Even though during a field experiment the Sapflow+ method allowed heat-velocity determination and revealed long-term water content patterns (**Chapter** 7), short-term water content profiles were susceptible to noise. The cause of this scattering in field conditions needs to be further investigated, based on validation experiments in which an independent measure of sapwood water content can be obtained. To this end, water contents can be determined based on wood core sampling or Magnetic Resonance Imaging. These methods, however, are not evident. Water content determination based on wood core sampling requires careful core drilling and handling as water content may be influenced by evaporation or water absorption. Magnetic Resonance Imaging, on the other hand, remains difficult to apply in field conditions and needs highly specified parameter tuning. Nevertheless, both methods would be interesting to compare with the Sapflow+ method. Recently, Frequency Domain Reflectometry has been put forward as an accurate method to determine sapwood water content. Combining this method with the Sapflow+ method may allow pinpointing the advantages and disadvantages of both methods, both in laboratory and field conditions.

Integration of stem water content as variable in plant physiological research and modelling

So far, stem water content has often been neglected as an important plant physiological variable because of its impractical determination. Nevertheless, the Sapflow+ method holds the promise of enabling stem water content measurements, enabling the applicability of stem water content as an indicator for drought stress or vulnerability to insect or fungus colonisation. Moreover, it can be related to water capacitance, stem diameter variations and cavitation events. As such, stem water content could be an interesting variable to integrate in hydrodynamic plant models.

Unravelling the importance of endogenous control of stem diameter changes and coupled growth

In **Chapter** 7 it was shown that two species influenced by the same environmental dynamics can show entirely different patterns in stem diameter variation, pointing to endogenous control of stem diameter changes and growth. The mechanisms behind this endogenous regulation, however, still need to be clarified in further studies. Given the complexity of growth regulation, studies will have to focus on the molecular, tissue as well as the entire plant level. Within these studies, plant water and carbon relations need to be coupled, assessing how carbohydrate metabolism influences osmotic storage potential and is linked to diel growth dynamics. By sampling the bark and xylem tissue, diel patterns of osmolite concentrations can be obtained to confirm the modelling results. Based on chemical analysis, it can then be derived which of the osmotic compounds has the greatest influence on storage water potential and could reveal possible species specific metabolism pathways. By varying the salinity and nutrient concentration of the soil water in combination with varying microclimatic conditions in a controlled environment, their influence on the daily stem diameter variations can be assessed, further elucidating the cause of the observed shrinkage events and the difference in pattern between the two species. Additionally, labelled isotope experiments could be applied to confirm the canopy water uptake hypothesis and provide insights into the water uptake pathway.

References

Adl-Zarrabi B, Bostrom L, Wickstrom U. 2006. Using the TPS method for determining the thermal properties of concrete and wood at elevated temperature. *Fire and Materials* **30**(5): 359-369.

Alongi DM. 2011. Early growth responses of mangroves to different rates of nitrogen and phosphorus supply. *Journal of Experimental Marine Biology and Ecology* **397**(2): 85-93.

Ambrose AR, Sillett SC, Dawson TE. 2009. Effects of tree height on branch hydraulics, leaf structure and gas exchange in California redwoods. *Plant Cell and Environment* **32**(7): 743-757.

Ambrose AR, Sillett SC, Koch GW, Van Pelt R, Antoine ME, Dawson TE. 2010. Effects of height on treetop transpiration and stomatal conductance in coast redwood (*Sequoia sempervirens*). *Tree Physiology* **30**(10): 1260-1272.

Angeles G, Bond B, Boyer JS, Brodribb T, Brooks JR, Burns MJ, Cavender-Bares J, Clearwater M, Cochard H, Comstock J, Davis SD, Domec JC, Donovan L, Ewers F, Gartner B, Hacke U, Hinckley T, Holbrook NM, Jones HG, Kavanagh K, Law B, Lopez-Portillo J, Lovisolo C, Martin T, Martinez-Vilalta J, Mayr S, Meinzer FC, Melcher P, Mencuccini M, Mulkey S, Nardini A, Neufeld HS, Passioura J, Pockman WT, Pratt RB, Rambal S, Richter H, Sack L, Salleo S, Schubert A, Schulte P, Sparks JP, Sperry J, Teskey R, Tyree M. 2004. The Cohesion-Tension theory. *New Phytologist* **163**(3): 451-452.

Ayutthaya SIN, Do FC, Pannengpetch K, Junjittakarn J, Maeght J-L, Rocheteau A, Cochard H. 2010. Transient thermal dissipation method of xylem sap flow measurement: multi-species calibration and field evaluation. *Tree Physiology* **30**(1): 139-148.

Baker JM, Van Bavel CHM. 1987. Measurement of mass-flow of water in the stems of herbaceous plants. *Plant Cell and Environment* **10**(9): 777-782.

Balek J, Pavlik O. 1977. Sap stream velocity as an indicator of the transpirational process. *Journal of Hydrology* **34**: 193-200.

Ball MC. 1988. Ecophysiology of mangroves. *Trees-Structure and Function* **2**(3): 129-142.

Barrett-Lennard EG. 2003. The interaction between waterlogging and salinity in higher plants: causes, consequences and implications. *Plant and Soil* **253**(1): 35-54.

Barrett DJ, Hatton TJ, Ash JE, Ball MC. 1995. Evaluation of the heat pulse velocity technique for measurement of sap flow in rain-forest and eucalypt forest species of South-Eastern Australia. *Plant Cell and Environment* **18**(4): 463-469.

Becker P. 1998. Limitations of a compensation heat pulse velocity system at low sap flow: implications for measurements at night and in shaded trees. *Tree Physiology* **18**(3): 177-184.

Becker P, Asmat A, Mohamad J, Moksin M, Tyree MT. 1997. Sap flow rates of mangrove trees are not unusually low. *Trees-Structure and Function* **11**(7): 432-435.

Bieker D, Rust S. 2012. Electric resistivity tomography shows radial variation of electrolytes in Quercus robur. *Canadian Journal of Forest Research* **40**(6): 1189-1193.

Bleby TM, Burgess SSO, Adams MA. 2004. A validation, comparison and error analysis of two heat-pulse methods for measuring sap flow in *Eucalyptus marginata* saplings. *Functional Plant Biology* **31**(6): 645-658.

Bleby TM, McElrone AJ, Burgess SSO 2008. Limitations of the HRM: great at low flow rates, but not yet up to speed?In. *7th Sap Flow Workshop*. Seville.

Bleby TM, McElrone AJ, Jackson RB. 2010. Water uptake and hydraulic redistribution across large woody root systems to 20 m depth. *Plant Cell and Environment* **33**(12): 2132-2148.

Borghetti M, Cinnirella S, Magnani F, Saracino A. 1998. Impact of long-term drought on xylem embolism and growth in *Pinus halepensis* Mill. *Trees-Structure and Function* **12**(4): 187-195.

Borghetti M, Edwards WRN, Grace J, Jarvis PG, Raschi A. 1991. The refilling of embolized xylem in *Pinus sylvestris* L. *Plant Cell and Environment* **14**(4): 357-369.

Bouguerra A. 2001. Measurement of thermal conductivity, thermal diffusivity and heat capacity of highly porous building materials using transient plane source technique. *International Communications in Heat Mass Transfer* **28**(8): 1065-1078.

Bovard BD, Curtis PS, Vogel CS, Su HB, Schmid HP. 2005. Environmental controls on sap flow in a northern hardwood forest. *Tree Physiology* **25**(1): 31-38.

Braun P, Schmid J. 1999. Sap flow measurements in grapevines (Vitis vinifera L.) - 2. Granier measurements. *Plant and Soil* **215**(1): 47-55.

Brazee NJ, Marra RE, Göcke L, Van Wassenaer P. 2011. Non-destructive assessment of internal decay in three hardwood species of northeastern North America using sonic and electrical impedance tomography. *Forestry* **84**(1): 33-39.

Breshears DD, McDowell NG, Goddard KL, Dayem KE, Martens SN, Meyer CW, Brown KM. 2008. Foliar absorption of intercepted rainfall improves woody plant water status most during drought. *Ecology* **89**(1): 41-47.

Brooks JR, Meinzer FC, Coulombe R, Gregg J. 2002. Hydraulic redistribution of soil water during summer drought in two contrasting Pacific Northwest coniferous forests. *Tree Physiology* **22**(15-16): 1107-1117.

Brooks JR, Meinzer FC, Warren JM, Domec JC, Coulombe R. 2006. Hydraulic redistribution in a Douglas-fir forest: lessons from system manipulations. *Plant Cell and Environment* **29**(1): 138-150.

Brun R, Kühni M, Siegrist H, Gujer W, Reichert P. 2002. Practical identifiability of ASM2d parameters: systematic selection and tuning of parameter subsets. *Water Research* **36**(16): 4113-4127.

Bucci SJ, Scholz FG, Goldstein G, Meinzer FC, Hinojosa JA, Hoffmann WA, Franco AC. 2004. Processes preventing nocturnal equilibration between leaf and soil water potential in tropical savanna woody species. *Tree Physiology* **24**(10): 1119-1127.

Buck AL. 1981. New Equations for Computing Vapor Pressure and Enhancement Factor. *Journal of Applied Meteorology* **20**: 1527-1532.

Burgess SSO, Adams M, Turner NC, Beverly CR, Ong CK, Khan AAH, Bleby TM. 2001a. An improved heat pulse method to measure low and reverse rates of sap flow in woody plants *Tree Physiology* **21**(15): 589-598.

Burgess SSO, Adams MA, Turner NC, Ong CK. 1998. The redistribution of soil water by tree root systems. *Oecologia* **115**(3): 306-311.

Burgess SSO, Adams MA, Turner NC, White DA, Ong CK. 2001b. Tree roots: conduits for deep recharge of soil water. *Oecologia* **126**(2): 158-165.

Burgess SSO, Bleby TM. 2006. Redistribution of soil water by lateral roots mediated by stem tissues. *Journal of Experimental Botany* **57**(12): 3283-3291.

Burgess SSO, Dawson TE. 2004. The contribution of fog to the water relations of *Sequoia sempervirens* (D. Don): foliar uptake and prevention of dehydration. *Plant Cell and Environment* **27**(8): 1023-1034.

Burgess SSO, Dawson TE. 2008. Using branch and basal trunk sap flow measurements to estimate whole-plant water capacitance: a caution. *Plant and Soil* **305**(1-2): 5-13.

Burkhardt J, Basi S, Pariyar S, Hunsche M. 2012. Stomatal penetration by aqueous solutions – an update involving leaf surface particles. *New Phytologist* **196**(3): 774-787.

Bush SE, Hultine KR, Sperry JS, Ehleringer JR. 2010. Calibration of thermal dissipation sap flow probes for ring- and diffuse-porous trees. *Tree Physiology* **30**(12): 1545-1554.

Butterfield GB, Meylan BA, eds. 1980. *Three-dimensional structure of wood: an ultrastructural approach*. New York: Chapman and Hall.

Cahoon DR, Hensel P, Rybczyk J, McKee KL, Proffitt CE, Perez BC. 2003. Mass tree mortality leads to mangrove peat collapse at Bay Islands, Honduras after Hurricane Mitch. *Journal of Ecology* **91**(6): 1093-1105.

Campbell GS. 1988. Soil-water potential measurement - an overview. *Irrigation Science* **9**(4): 265-273.

Campbell GS, Calissendorff C, Williams JH. 1991. Probe for measuring soil specific-heat using a heat-pulse method. *Soil Science Society of America Journal* **55**(1): 291-293.

Campbell NA, Williamson B, Heyden RJ, ed.^eds. 2004. *Biology: exploring life* Needham, MA: Pearson Education.

Canny MJ. 1995. A New Theory for the Ascent of Sap - Cohesion Supported by Tissue Pressure. *Annals of Botany* **75**(4): 343-357.

Carlquist S. 2007. Successive cambia revisited: ontogeny, histology, diversity, and functional significance. *Journal of the Torrey Botanical Society* **134**(2): 301-332.

Carslaw HS, Jaeger JC, eds. 1947. *Conduction of Heat in Solids*. London: Clarendon Press, Oxford.

Cermak J, Deml M, Penka M. 1973. New method of sap flow-rate determination in trees. *Biologia Plantarum* **15**(3): 171-178.

Cermak J, Kucera J. 1981. The compensation of natural temperature-gradient at the measuring point during the sap flow-rate determination in trees. *Biologia Plantarum* **23**(6): 469-471.

Chen X, Miller GR, Rubin Y, Baldocchi DD. 2012. A statistical method for estimating wood thermal diffusivity and probe geometry using in situ heat response curves from sap flow measurements. *Tree Physiology* **32**(12): 1458-1470.

Chiesi M, Maselli F, Bindi M, Fibbi L, Bonora L, Raschi A, Tognetti R, Cermak J, Nadezhdina N. 2002. Calibration and application of FOREST-BGC in a Mediterranean area by the use of conventional and remote sensing data. *Ecological Modelling* **154**(3): 251-262.

Choat B, Ball M, Luly J, Holtum J. 2003. Pit membrane porosity and water stress-induced cavitation in four co-existing dry rainforest tree species. *Plant Physiology* **131**(1): 41-48.

Choat B, Jansen S, Brodribb TJ, Cochard H, Delzon S, Bhaskar R, Bucci SJ, Feild TS, Gleason SM, Hacke UG, Jacobsen AL, Lens F, Maherali H, Martinez-Vilalta J, Mayr S, Mencuccini M, Mitchell PJ, Nardini A, Pittermann J, Pratt RB, Sperry JS, Westoby M, Wright IJ, Zanne AE. 2012. Global convergence in the vulnerability of forests to drought. *Nature* **491**: 752-755.

Clearwater MJ, Blattmann P, Luo Z, Lowe RG. 2007. Control of scion vigour by kiwifruit rootstocks is correlated with spring root pressure phenology. *Journal of Experimental Botany* **58**(7): 1741-1751.

Clearwater MJ, Luo ZW, Mazzeo M, Dichio B. 2009. An external heat pulse method for measurement of sap flow through fruit pedicels, leaf petioles and other small-diameter stems. *Plant Cell and Environment* **32**(12): 1652-1663.

Clearwater MJ, Meinzer FC, Andrade JL, Goldstein G, Holbrook NM. 1999. Potential errors in measurement of nonuniform sap flow using heat dissipation probes. *Tree Physiology* **19**(10): 681-687.

Cohen Y. 1991. Determination of orchard water requirement by a combined trunk sap flow and meteorological approach. *Irrigation Science* **12**(2): 93-98.

Cohen Y, Cohen S, Cantuarias-Aviles T, Schiller G. 2008. Variations in the radial gradient of sap velocity in trunks of forest and fruit trees. *Plant and Soil* **305**(1-2): 49-59.

Cohen Y, Fuchs M, Green GC. 1981. Improvement of the Heat Pulse Method for determining Sap Flow in Trees. *Plant Cell and Environment* **4**(5): 391-397.

Cohen Y, Takeuchi S, Nozaka J, Yano T. 1993. Accuracy of sap flow measurement using heat-balance and heat pulse methods. *Agronomy Journal* **85**(5): 1080-1086.

Colmer TD, Flowers TJ. 2008. Flooding tolerance in halophytes. *New Phytologist* **179**(4): 964-974.

Dainty J, Preston RD 1963. Water Relations of Plant Cells. In: eds. *Advances in Botanical Research*. Academic Press, 279-326.

Dale JE, Sutcliffe JF 1986. Water relations of plant cells. In: Steward FC eds. *Plant Physiology, Water and Solutes in Plants*. Orlando: Academic Press, 1-48.

Daum CR. 1967. A method for determining water transport in trees. *Ecology* **48**(3): 425-431.

David TS, David JS, Pinto CA, Cermak J, Nadezhdin V, Nadezhdina N. 2012. Hydraulic connectivity from roots to branches depicted through sap flow: analysis on a *Quercus suber* tree. *Functional Plant Biology* **39**(2): 103-115.

Dawson TE. 1998. Fog in the California redwood forest: ecosystem inputs and use by plants. *Oecologia* **117**(4): 476-485.

de Oliveira Reis F, Campostrini E, Fernandes de Sousa E, Gabetto e Silva M. 2006. Sap flow in papaya plants: Laboratory calibrations and relationships with gas exchanges under field conditions. *Scientia Horticulturae* **110**(3): 254-259.

De Pauw DJW, Steppe K, De Baets B. 2008. Identifiability analysis and improvement of a tree water flow and storage model. *Mathematical Biosciences* **211**(2): 314-332.

De Schepper V, Steppe K. 2010. Development and verification of a water and sugar transport model using measured stem diameter variations. *Journal of Experimental Botany* **61**(8): 2083-2099.

Dixon HH. 1914. *Transpiration and the ascent of sap in plants. By Henry H. Dixon*. London: Macmillan and co., limited.

Dixon HH. 1936. The convection of heat and materials in the stem of a tree. *Scientific Proceedings of the Royal Dublin Society* **21**: 477-488.

Dixon HH, Joly J. 1894. On the ascent of sap. *Philosophical Transactions of the Royal Society London B* **186**: 563-576.

Dixon MA, Tyree MT. 1984. A new stem hygrometer, corrected for temperature-gradients and calibrated against the pressure bomb. *Plant Cell and Environment* **7**(9): 693-697.

Do F, Rocheteau A. 2002a. Influence of natural temperature gradients on measurements of xylem sap flow with thermal dissipation probes. 1. Field observations and possible remedies. *Tree Physiology* **22**(9): 641-648.

Do F, Rocheteau A. 2002b. Influence of natural temperature gradients on measurements of xylem sap flow with thermal dissipation probes. 2. Advantages and calibration of a noncontinuous heating system. *Tree Physiology* **22**(9): 649-654.

Do FC, Ayutthaya SIN, Rocheteau A. 2011. Transient thermal dissipation method for xylem sap flow measurement: implementation with a single probe. *Tree Physiology* **31**(4): 369-380.

Domec J-C, King JS, Noormets A, Treasure E, Gavazzi MJ, Sun G, McNulty SG. 2010. Hydraulic redistribution of soil water by roots affects whole-stand evapotranspiration and net ecosystem carbon exchange. *New Phytologist* **187**(1): 171-183.

Domec JC, Warren JM, Meinzer FC, Brooks JR, Coulombe R. 2004. Native root xylem embolism and stomatal closure in stands of Douglas-fir and ponderosa pine: mitigation by hydraulic redistribution. *Oecologia* **141**(1): 7-16.

Downton W. 1982. Growth and Osmotic Relations of the Mangrove *Avicennia marina*, as Influenced by Salinity. *Functional Plant Biology* **9**(5): 519-528.

Drennan P, Pammenter NW. 1982. Physiology of salt excretion in the mangrove *Avicennia marina* (Forsk) Vierh. *New Phytologist* **91**(4): 597-606.

Duke NC, Meynecke JO, Dittmann S, Ellison AM, Anger K, Berger U, Cannicci S, Diele K, Ewel KC, Field CD, Koedam N, Lee SY, Marchand C, Nordhaus I, Dahdouh-Guebas F. 2007. A world without mangroves? *Science* **317**(5834): 41-42.

Edwards WRN, Warwick NWM. 1984. Transpiration from a kiwifruit vine as estimated by the heat pulse technique and the Penman-Monteith equation. *New Zealand Journal of Agricultural Research* **27**(4): 537-543.

Er-Raki S, Chehbouni A, Boulet G, Williams DG. 2010. Using the dual approach of FAO-56 for partitioning ET into soil and plant components for olive orchards in a semi-arid region. *Agricultural Water Management* **97**(11): 1769-1778.

Fisher JB, Baldocchi DD, Misson L, Dawson TE, Goldstein AH. 2007. What the towers don't see at night: nocturnal sap flow in trees and shrubs at two AmeriFlux sites in California. *Tree Physiology* **27**(4): 597-610.

Flowers TJ, Colmer TD. 2008. Salinity tolerance in halophytes. *New Phytologist* **179**(4): 945-963.

Ford CR, Goranson CE, Mitchell RJ, Will RE, Teskey RO. 2004. Diurnal and seasonal variability in the radial distribution of sap flow: predicting total stem flow in Pinus taeda trees. *Tree Physiology* **24**(9): 941-950.

Franke W. 1967. Mechanisms of foliar penetration of solutions. *Annual Review of Plant Physiology* **18**: 281-300.

Génard M, Fishman S, Vercambre G, Huguet JG, Bussi C, Besset J, Habib R. 2001. A biophysical analysis of stem and root diameter variations in woody plants. *Plant Physiology* **126**(1): 188-202.

Gibbs RD 1958. Patterns in the seasonal water content of trees. In: Thimann KV eds. *The physiology of forest trees*. New York: Ronald, 43-69.

Goldsmith GR, Matzke NJ, Dawson TE. 2012. The incidence and implications of clouds for cloud forest plant water relations. *Ecology Letters*: 10.1111/ele.12039.

Gouws LM, Osmond CB, Schurr U, Walter A. 2005. Distinctive diel growth cycles in leaves and cladodes of CAM plants: differences from C(3) plants and putative interactions with substrate availability, turgor and cytoplasmic pH. *Functional Plant Biology* **32**(5): 421-428.

Granier A. 1985. Une nouvelle méthode pour la mesure du flux de sève brute dans le tronc des arbres. *Annales Scientifique forestières* **42**(2): 193-200.

Granier A. 1987. Mesure du flux de sève brute dans le tronc du Douglas par une nouvelle méthode thermique. *Annales Scientifique forestières* **44**(1): 1-14.

Green PB, Cummins WR. 1974. Growht-rate and turgor pressure - Auxin effect studied with an automated apparatus for single coleoptiles. *Plant Physiology* **54**(6): 863-869.

Green PB, Erickson RO, Buggy J. 1971. Metabolic and physical control of cell elongation rate - In-vivo studies in *Nitella*. *Plant Physiology* **47**(3): 423-430.

Green S, Clothier B, Jardine B 2003. Theory and practical application of heat pulse to measure sap flow.In. *Symposium on the Soil Plant Atmosphere Continuum*. Charlotte, North Carolina. 1371-1379.

Green S, Clothier B, Perie E 2009. A Re-Analysis of Heat Pulse Theory across a Wide Range of Sap Flows.In Fernandez JE, Diaz-Espejo A. *7th International Workshop on Sap Flow*. Acta Horicultura. 95-104.

Green SR, Clothier BE. 1988. Water Use of Kiwifruit Vines and Apple Trees by the Heat-Pulse Technique. *Journal of Experimental Botany* **39**(1): 115-123.

Gricar J. 2010. Xylem and phloem formation in sessile oak from Slovenia in 2007. *Wood Research* **55**(4): 15-22.

Hales S. 1727. *Vegetables staticks, or, an accound of some statical experiments on the sap in vegetables*. London, UK: W & J Innys and T Woodward.

Hanson PJ, Amthor JS, Wullschleger SD, Wilson KB, Grant RF, Hartley A, Hui D, Hunt ER, Johnson DW, Kimball JS, King AW, Luo Y, McNulty SG, Sun G, Thornton PE, Wang S, Williams M, Baldocchi DD, Cushman RM. 2004. Oak forest carbon and water simulations: Model intercomparisons and evaluations against independent data. *Ecological Monographs* **74**(3): 443-489.

Hao G-Y, Wheeler JK, Holbrook NM, Goldstein G. 2013. Investigating xylem embolism formation, refilling and water storage in tree trunks using frequency domain reflectometry. *Journal of Experimental Botany*.

Hao GY, Jones TJ, Luton C, Zhang YJ, Manzane E, Scholz FG, Bucci SJ, Cao KF, Goldstein G. 2009. Hydraulic redistribution in dwarf Rhizophora mangle trees driven by interstitial soil water salinity gradients: impacts on hydraulic architecture and gas exchange. *Tree Physiology* **29**(5): 697-705.

Harada T, Hata T, Ishihara S. 1998. Thermal constants of wood during the heating process measured with the laser flash method. *Journal of Wood Science* **44**(6): 425-431.

Hatton TJ, Moore SJ, Reece PH. 1995. Estimating stand transpiration in a *Eucalyptus-Populnea* woodland with the heat pulse method - measurement errors and sampling strategies. *Tree Physiology* **15**(4): 219-227.

Hearmon RFS, Burcham JN. 1955. Specific Heat and Heat of Wetting of Wood. *Nature* **176**: 978.

Henderson LG, Choong ET. 1968. Variation in moisture content of standing sweetgum trees in Louisiana. *Louisiana Stat Univ Sch For* **For Note 81**: 3pp.

Hernandez-Santana V, Asbjornsen H, Sauer T, Isenhart T, Schilling K, Schultz R. 2011. Enhanced transpiration by riparian buffer trees in response to advection in a humid temperate agricultural landscape. *Forest Ecology and Management* **261**(8): 1415-1427.

Hetherington AM, Woodward FI. 2003. The role of stomata in sensing and driving environmental change. *Nature* **424**(6951): 901-908.

Hill AV. 1930. A thermo-electric method of measuring the vapour pressure of an aqueous solution. *Royal Society of London Proc.* **127**: 9-19.

Hinckley TM, Bruckerhoff DN. 1975. The effects of drought on water relations and stem shrinkage of Quercus alba. *Canadian Journal of Botany* **53**(1): 62-72.

Hirose S, Kume A, Takeuchi S, Utsumi Y, Otsuki K, Ogawa S. 2005. Stem water transport of *Lithocarpas edulis*, an evergreen oak with radial-porous wood. *Tree Physiology* **25**(2): 221-228.

Hogarth P. 2007. *The biology of mangroves and seasgrasses*. New York: Oxford University Press.

Holbrook NM, Burns MJ, Field CB. 1995. Negative xylem pressures in plants: A test of the balancing pressure technique. *Science* **270**: 1193-1194.

Howard AR, Van Iersel MW, Richards JH, Donovan LA. 2009. Night-time transpiration can decrease hydraulic redistribution. *Plant Cell and Environment* **32**(8): 1060-1070.

Hsiang SM, Meng KC, Cane MA. 2011. Civil conflicts are associated with the global climate. *Nature* **476**(7361): 438-441.

Hsiao TC, Frensch J, Rojas-Lara BA. 1998. The pressure-jump technique shows maize leaf growth to be enhanced by increases in turgor only when water status is not too high. *Plant Cell and Environment* **21**(1): 33-42.

Hsiao TC, Xu LK. 2000. Sensitivity of growth of roots versus leaves to water stress: biophysical analysis and relation to water transport. *Journal of Experimental Botany* **51**(350): 1595-1616.

Hu J, Moore DJP, Riveros-Iregui DA, Burns SP, Monson RK. 2009. Modeling whole-tree carbon assimilation rate using observed transpiration rates and needle sugar carbon isotope ratios. *New Phytologist* **185**(4): 1000-1015.

Huber B. 1932. Beobachtung und Messung pflanzlicher Saftstrome. *Berichte der Deutschen botanischen Gesellschaft* **50**: 89-109.

Huber B, Schmidt E. 1937. Eine Kompensationsmethode zur thermoelektrischen Messung langsamer Saftstrome. *Berichte der Deutschen botanischen Gesellschaft* **55**: 514-529.

Hultine KR, Cable WL, Burgess SSO, Williams DG. 2003a. Hydraulic redistribution by deep roots of a Chihuahuan Desert phreatophyte. *Tree Physiology* **23**(5): 353-360.

Hultine KR, Nagler PL, Morino K, Bush SE, Burtch KG, Dennison PE, Glenn EP, Ehleringer JR. 2010. Sap flux-scaled transpiration by tamarisk (Tamarix spp.) before, during and after episodic defoliation by the saltcedar leaf beetle (Diorhabda carinulata). *Agricultural and Forest Meteorology* **150**(11): 1467-1475.

Hultine KR, Scott RL, Cable WL, Goodrich DC, Williams DG. 2004. Hydraulic redistribution by a dominant, warm-desert phreatophyte: seasonal patterns and response to precipitation pulses. *Functional Ecology* **18**(4): 530-538.

Hultine KR, Williams DG, Burgess SSO, Keefer TO. 2003b. Contrasting patterns of hydraulic redistribution in three desert phreatophytes. *Oecologia* **135**(2): 167-175.

Huntington TG. 2006. Evidence for intensification of the global water cycle: Review and synthesis. *Journal of Hydrology* **319**(1-4): 83-95.

Iida Si, Tanaka T. 2010. Effect of the span length of Granier-type thermal dissipation probes on sap flux density measurements. *Annals of Forest Science* **67**(408): 1-10.

Iki T, Tamura A, Iizuka K. 2009. The non-destructive evaluation of green moisture content in Todomatsu (*Abies sachalinensis*) using a lateral impact vibration method. *Mokuzai Gakkaishi* **56**(1): 33-40.

Ittner E. 1968. Der Tageshang der Geschwindigkeit des Transpirationsstromes im Stamm einer 75-jahrigen Fichte. *Oecologia Plantarum* **3**: 177-183.

James WO, Baker H. 1933. Sap pressure and the movements of sap. *New Phytologist* **32**(5): 317-355.

Jameson DA. 1966. Diurnal and Seasonal Fluctuations in Moisture Content of Pinyon and Juniper. *US Department of Agriculture, Forest Service Research Note* **67**: 1-7.

Jimenez MS, Nadezhdina N, Cermak J, Morales D. 2000. Radial variation in sap flow in five laurel forest tree species in Tenerife, Canary Islands. *Tree Physiology* **20**(17): 1149-1156.

Jones HG, eds. 1992. *Plants and microclimate, a quantitative approach to environmental plant physiology*. Cambridge, UK: University Press.

Jones HG, Hamer PJC, Higgs KH. 1988. Evaluation of various heat-pulse methods for estimation of sap flow in orchard trees: comparison with micrometeorological estimates of evaporation. *Trees-Structure and Function* **2**(4): 250-260.

Jones JK, Webb BW, Jimenez D, Reardon J, Butler B. 2004. Development of an advanced one-dimensional stem heating model for application in surface fires. *Canadian Journal of Forest Research-Revue Canadienne De Recherche Forestiere* **34**(1): 20-30.

Jones M, Aptaker PS, Cox J, Gardiner BA, McDonald PJ. 2012. A transportable magnetic resonance imaging system for in-situ measurements of living trees: The Tree Hugger. *Journal of Magnetic Resonance* **218**: 133-140.

Kaniewski D, Van Campo E, Weiss H. 2012. Drought is a recurring challenge in the Middle East. *Proceedings of the National Academy of Sciences of the United States of America* **109**(10): 3862-3867.

Kelsey KE, Clarke LN. 1956. The heat of sorption of water by wood. *Australian Journal of Applied Science* **7**: 160-175.

Kluitenberg GJ, Bristow KL, Das BS. 1995. Error analysis of heat pulse method for measuring soil heat-capacity, diffusivity and conductivity. *Soil Science Society of America Journal* **59**(3): 719-726.

Kluitenberg GJ, Ham JM. 2004. Improved theory for calculating sap flow with the heat pulse method. *Agricultural and Forest Meteorology* **126**(1-2): 169-173.

Knoblauch M, Peters WS. 2010. Munch, morphology, microfluidics - our structural problem with the phloem. *Plant Cell and Environment* **33**(9): 1439-1452.

Kollmann FFP, Côté WA, eds. 1968. *Principles of Wood Science and Technology 1, Solid Wood*. New York: Springer.

Köstner B, Granier A, Cermak J. 1998. Sapflow measurements in forest stands: methods and uncertainties. *Annales Scientifique forestières* **55**: 13-27.

Kottek M, Grieser J, Beck C, Rudolf B, Rubel F. 2006. World map of the Koppen-Geiger climate classification updated. *Meteorologische Zeitschrift* **15**(3): 259-263.

Kramer PJ. 1940. Sap Pressure and Exudation. *American Journal of Botany* **27**(10): 929-931.

Kramer PJ, Boyer JS. 1995. *Water relations of plants and soils.* New York: Academic Press.

Krauss KW, Lovelock CE, McKee KL, Lopez-Hoffman L, Ewe SML, Sousa WP. 2008. Environmental drivers in mangrove establishment and early development: A review. *Aquatic Botany* **89**(2): 105-127.

Krauss KW, Young PJ, Chambers JL, Doyle TW, Twilley RR. 2007. Sap flow characteristics of neotropical mangroves in flooded and drained soils. *Tree Physiology* **27**(5): 775-783.

Kucera J, Cermak J, Penka M. 1977. Improved thermal method of continual recording the transpiration flow rate dynamics. *Biologia Plantarum* **19**(6): 413-420.

Kurpius MR, Goldstein AH. 2003. Gas-phase chemistry dominates O-3 loss to a forest, implying a source of aerosols and hydroxyl radicals to the atmosphere. *Geophysical Research Letters* **30**(7).

Kurpius MR, Panek JA, Nikolov NT, McKay M, Goldstein AH. 2003. Partitioning of water flux in a Sierra Nevada ponderosa pine plantation. *Agricultural and Forest Meteorology* **117**(3-4): 173-192.

Lambs L, Muller E, Fromard F. 2008. Mangrove trees growing in a very saline condition but not using seawater. *Rapid Communications in Mass Spectrometry* **22**(18): 2835-2843.

Lang A. 1979. Relay mechanism for phloem translocation. *Annals of Botany* **44**(2): 141-145.

Langensiepen M, Burgess S, Lambers H, Mitchell P, Veneklaas E. 2006. A model for simulating transpiration of Eucalyptus salmonophloia trees. *Physiologia Plantarum* **127**(3): 465-477.

Lee JE, Oliveira RS, Dawson TE, Fung I. 2005. Root functioning modifies seasonal climate. *Proceedings of the National Academy of Sciences of the United States of America* **102**(49): 17576-17581.

Leonardo Reyes-Acosta J, Lubczynski MW. 2012. Optimization of dry-season sap flow measurements in an oak semi-arid open woodland in Spain. *Ecohydrology*: n/a-n/a.

Limm EB, Dawson TE. 2010. *Polystichum munitum* (Dryopteridaceae) varies geographically in its capacity to absorb fog water by foliar uptake within the redwood forest ecosystem. *American Journal of Botany* **97**(7): 1121-1128.

Limm EB, Simonin KA, Bothman AG, Dawson TE. 2009. Foliar water uptake: a common water acquisition strategy for plants of the redwood forest. *Oecologia* **161**(3): 449-459.

Liu CW, Du TS, Li FS, Kang SZ, Li SE, Tong L. 2012. Trunk sap flow characteristics during two growth stages of apple tree and its relationships with affecting factors in an arid region of northwest China. *Agricultural Water Management* **104**: 193-202.

Lockhart JA. 1965. An analysis of irreversible plant cell elongation. *Journal of Theoretical Biology* **8**(2): 264-275.

Lu P, Chacko E. 1998. Evaluation of Granier's sap flux sensor in young mango trees. *Agronomie* **18**(7): 461-471.

Lu P, Urban L, Zhao P. 2004. Granier's thermal dissipation probe (TDP) method for measuring sap flow in trees: Theory and practice. *Acta Botanica Sinica* **46**(6): 631-646.

Lundblad M, Lagergren F, Lindroth A. 2001. Evaluation of heat balance and heat dissipation methods for sapflow measurements in pine and spruce. *Annals of Forest Science* **58**(6): 625-638.

Ma J-X, Chen Y-N, Li W-H, Huang X, Zhu C-G, Ma X-D. 2012. Sap flow characteristics of four typical species in desert shelter forest and their responses to environmental factors. *Environmental Earth Sciences* **67**(1): 151-160.

Macfarlane C, Bond C, White DA, Grigg AH, Ogden GN, Silberstein R. 2010. Transpiration and hydraulic traits of old and regrowth eucalypt forest in southwestern Australia. *Forest Ecology and Management* **260**(1): 96-105.

Madurapperuma WS, Bleby TM, Burgess SSO. 2009a. Evaluation of sap flow methods to determine water use by cultivated palms. *Environmental and Experimental Botany* **66**(3): 372-380.

Madurapperuma WS, de Costa W, Sangakkara UR, Jayasekara C. 2009b. Estimation of water use of mature coconut (Cocos nucifera L.) cultivars (CRIC 60 and CRIC 65) grown in the low country intermediate zone using the compensation heat pulse method (CHPM). *Journal of the National Science Foundation of Sri Lanka* **37**(3): 175-186.

Maku T 1954. Studies on the heat conduction in wood.In. *Wood Res. Bull.* Kyoto, Japan: Wood Res. Inst., Kyto University. 80.

Marshall DC. 1958. Measurement of sap flow in conifers by heat transport. *Plant Physiology* **33**(6): 385-396.

Martin CE, von Willert DJ. 2000. Leaf epidermal hydathodes and the ecophysiological consequences of foliar water uptake in species of Crassula from the Namib Desert in southern Africa. *Plant Biology* **2**(2): 229-242.

Martin LH, Lang KC. 1933. The thermal conductivity of water. *Proceedings of the Physical Society* **45**: 523-529.

Matimati I, Musil CF, Raitt L, February EC. 2012. Diurnal stem diameter variations show CAM and C-3 photosynthetic modes and CAM-C-3 switches in arid South African succulent shrubs. *Agricultural and Forest Meteorology* **161**: 72-79.

McCarthy EL. 1934. Marriotte's Bottle. *Science* **80**: 100.

McCulloh KA, Winter K, Meinzer FC, Garcia M, Aranda J, Lachenbruch B. 2007. A, comparison of daily water use estimates derived from constant-heat sap-flow probe values and gravimetric measurements in pot-grown saplings. *Tree Physiology* **27**(9): 1355-1360.

McElrone AJ, Bichler J, Pockman WT, Addington RN, Linder CR, Jackson RB. 2007. Aquaporin-mediated changes in hydraulic conductivity of deep tree roots accessed via caves. *Plant Cell and Environment* **30**(11): 1411-1421.

McElrone AJ, Grant JA, Kluepfel DA. 2010. The role of tyloses in crown hydraulic failure of mature walnut trees afflicted by apoplexy disorder. *Tree Physiology* **30**(6): 761-772.

McIntyre D. 1980. Basic relationships for salinity evaluation from measurements on soil solution. *Soil Research* **18**(2): 199-206.

Meinzer FC, Brooks JR, Bucci S, Goldstein G, Scholz FG, Warren JM. 2004. Converging patterns of uptake and hydraulic redistribution of soil water in contrasting woody vegetation types. *Tree Physiology* **24**(8): 919-928.

Miller GR, Chen XY, Rubin Y, Ma SY, Baldocchi DD. 2010. Groundwater uptake by woody vegetation in a semiarid oak savanna. *Water Resources Research* **46**: 1-14.

Mitchell PJ, Veneklaas E, Lambers H, Burgess SSO. 2009. Partitioning of evapotranspiration in a semi-arid eucalypt woodland in south-western Australia. *Agricultural and Forest Meteorology* **149**(1): 25-37.

Molz FJ, Klepper B. 1973. On the Mechanism of Water-Stress-Induced Stem Deformation1. *Agronomy Journal* **65**(2): 304-306.

Monteith JL, Owen PC. 1958. A thermocouple method for measuring relative humidity in the range 95-100%. *Journal of Scientific Instruments* **35**: 443-446.

Moore DJP, Hu J, Sacks WJ, Schimel DS, Monson RK. 2008. Estimating transpiration and the sensitivity of carbon uptake to water availability in a subalpine forest using a simple ecosystem process model informed by measured net CO2 and H2O fluxes. *Agricultural and Forest Meteorology* **148**(10): 1467-1477.

Moore GW, Bond BJ, Jones JA, Meinzer FC. 2009. Thermal-dissipation sap flow sensors may not yield consistent sap-flux estimates over multiple years. *Trees-Structure and Function* **24**(1): 165-174.

Morris JD, Collopy JJ. 1999. Water use and salt accumulation by Eucalyptus camaldulensis and Casuarina cunninghamiana on a site with shallow saline groundwater. *Agricultural Water Management* **39**(2-3): 205-227.

Morton WE, Hearle JWS, eds. 1975. *Physical properties of textile fibres*. New York.

Muller E, Lambs L, Fromard F. 2009. Variations in water use by a mature mangrove of Avicennia germinans, French Guiana. *Annals of Forest Science* **66**(803): 2-10.

Münch E, eds. 1930. *Die Stoffbewegungen in der Pflanze*. Jena, Germany: Gustav Fisher.

Nadezhdina N. 1988. *Apple tree water relations and their optimization under conditions of southern Ukraine (in Russian).* PhD thesis, Kiev.

Nadezhdina N. 1999. Sap flow index as an indicator of plant water status. *Tree Physiology* **19**: 885-891.

Nadezhdina N. 2010. Integration of water transport pathways in a maple tree: responses of sap flow to branch severing. *Annals of Forest Science* **67**(107): 1-10.

Nadezhdina N, Cermak J, Ceulemans R. 2002. Radial patterns of sap flow in woody stems of dominant and understory species: scaling errors associated with positioning of sensors. *Tree Physiology* **22**(13): 907-918.

Nadezhdina N, Cermak J, Gasparek J, Nadezhdin V, Prax A. 2006. Vertical and horizontal water redistribution in Norway spruce (*Picea abies*) roots in the Moravian Upland. *Tree Physiology* **26**(10): 1277-1288.

Nadezhdina N, Cermak J, Nadezhdin V 1998. Heat field deformation method for sap flow measurements.In Cermak J, Nadezhdina N. *Proceedings of the 4th International Workshop on Measuring Sap Flow in Intact Plants.*: Publishing House of Mendel University, Czech Republic. 72-92.

Nadezhdina N, David TS, David JS, Ferreira MI, Dohnal M, Tesar M, Gartner K, Leitgeb E, Nadezhdin V, Cermak J, Jimenez MS, Morales D. 2010. Trees never rest: the multiple facets of hydraulic redistribution. *Ecohydrology* **3**: 431-444.

Nadezhdina N, Ferreira MI, Silva R, Pacheco CA. 2008. Seasonal variation of water uptake of a *Quercus suber* tree in Central Portugal. *Plant and Soil* **305**(1-2): 105-119.

Nadezhdina N, Steppe K, De Pauw DJW, Bequet R, Cermak J, Ceulemans R. 2009. Stem-mediated hydraulic redistribution in large roots on opposing

sides of a Douglas-fir tree following localized irrigaton. *New Phytologist* **184**: 932-943.

Nadezhdina N, Vandegehuchte M, Steppe K. 2012. Sap flux density measurements based on the heat field deformation method. *Trees - Structure and Function* **26**(5): 1439-1448.

Nadler A, Raveh E, Yermiyahu U, Green S. 2006. Stress induced water content variations in mango stem by time domain reflectometry. *Soil Science Society of America Journal* **70**(2): 510-520.

Nadler A, Raveh E, Yermiyahu U, Green SR. 2003. Evaluation of TDR use to monitor water content in stem of lemon trees and soil and their response to water stress. *Soil Science Society of America Journal* **67**(2): 437-448.

Nadler A, Tyree MT. 2008. Substituting stem's water content by electrical conductivity for monitoring water status changes. *Soil Science Society of America Journal* **72**(4): 1006-1013.

Nelder JA, Mead R. 1965. A simplex method for function minimization. *Computer Journal* **7**: 308-313.

Nobel PS, eds. 1999. *Physicochemical and environmental plant physiology*. San Diego: Academic press.

O'Grady AP, Cook PG, Eamus D, Duguid A, Wischusen JDH, Fass T, Worldege D. 2009. Convergence of tree water use within an arid-zone woodland. *Oecologia* **160**(4): 643-655.

Oliveira RS, Dawson TE, Burgess SSO, Nepstad DC. 2005. Hydraulic redistribution in three Amazonian trees. *Oecologia* **145**(3): 354-363.

Oltchev A, Cermak J, Nadezhdina N, Tatarinov F, Tishenko A, Ibrom A, Gravenhorst G. 2002. Transpiration of a mixed forest stand: field measurements and simulation using SVAT models. *Boreal Environment Research* **7**(4): 389-397.

Orians CM, van Vuuren MMI, Harris NL, Babst BA, Ellmore GS. 2004. Differential sectoriality in long-distance transport in temperate tree species: evidence from dye flow, N-15 transport, and vessel element pitting. *Trees-Structure and Function* **18**(5): 501-509.

Osmond B, Neales T, Stange G. 2008. Curiosity and context revisited: crassulacean acid metabolism in the Anthropocene. *Journal of Experimental Botany* **59**(7): 1489-1502.

Page TJ, Marshall JC, Hughes JM. 2012. The world in a grain of sand: evolutionarily relevant, small-scale freshwater bioregions on subtropical dune islands. *Freshwater Biology* **57**(3): 612-627.

Peck EC. 1953. The sap or moisture in wood. *US Forest Service Report FPL-768*: 5.

Peramaki M, Nikinmaa E, Sevanto S, Ilvesniemi H, Siivola E, Hari P, Vesala T. 2001. Tree stem diameter variations and transpiration in Scots pine: an analysis using a dynamic sap flow model. *Tree Physiology* **21**(12-13): 889-897.

Pesonen E, Mielikainen K, Makinen H. 2004. A new girth band for measuring stem diameter changes. *Forestry* **77**(5): 431-439.

Pfautsch S, Bleby TM, Rennenberg H, Adams MA. 2010. Sap flow measurements reveal influence of temperature and stand structure on water use of Eucalyptus regnans forests. *Forest Ecology and Management* **259**(6): 1190-1199.

Pfautsch S, Gessler A, Adams MA, Rennenberg H. 2009. Using amino-nitrogen pools and fluxes to identify contributions of understory Acacia spp. to overstory Eucalyptus regnans and stand nitrogen uptake in temperate Australia. *New Phytologist* **183**(4): 1097-1113.

Phillips NG, Lewis JD, Logan BA, Tissue DT. 2010. Inter- and intra-specific variation in nocturnal water transport in Eucalyptus. *Tree Physiology* **30**(5): 586-596.

Pickard WF. 2003. The riddle of root pressure. I. Putting Maxwell's demon to rest. *Functional Plant Biology* **30**(2): 121-134.

Pittermann J. 2010. The evolution of water transport in plants: an integrated approach. *Geobiology* **8**(2): 112-139.

Prieto I, Armas C, Pugnaire FI. 2011. Water release through plant roots: new insights into its consequences at the plant and ecosystem level. *New Phytologist* **193**(4): 830-841.

Purnobasuki H, Suzuki M. 2005. Aerenchyma tissue development and gas-pathway structure in root of Avicennia marina (Forsk.) Vierh. *Journal of Plant Research* **118**(4): 285-294.

Quisthoudt K, Schmitz N, Dahdouh-Guebas F, Robert EMR, Koedam N. 2012. Temperature patterns at mangrove latitudinal range limits. The genera *Avicennia* and *Rhizophora. Trees - Structure and Function* **26**: 1919-1931.

Raven PH, Evert RF, Eichhorn SE, eds. 1992. *Biology of plants*. New York: Worth Publishers.

Ren T, Ochsner TE, Horton R, Ju Z. 2003. Heat-Pulse Method for Soil Water Content Measurement. *Soil Science Society of America Journal* **67**(6): 1631-1634.

Reyes-Acosta JL, Vandegehuchte MW, Steppe K, Lubczynski MW. 2012. Novel, cyclic thermal dissipation (CHD) method for the correction of natural temperature gradients in sap flow measurements. Part 2. Laboratory validation. *Tree Physiology* **32**(7): 913-929.

Ridge I, eds. 2002. *Plants*. Oxford: Oxford University Press.

Robert EMR, Schmitz N, Boeren I, Driessens T, Herremans K, De Mey J, Van de Casteele E, Beeckman H, Koedam N. 2011a. Successive Cambia: A Developmental Oddity or an Adaptive Structure? *PLoS ONE* **6**(1): e16558.

Robert EMR, Schmitz N, Okello JA, Boeren I, Beeckman H, Koedam N. 2011b. Mangrove growth rings: fact or fiction? *Trees-Structure and Function* **25**(1): 49-58.

Roderick ML, Berry SL. 2001. Linking wood density with tree growth and environment: a theoretical analysis based on the motion of water. *New Phytologist* **149**(3): 473-485.

Rogers R, Westman W. 1977. Seasonal Nutrient Dynamics of Litter in a Subtropical Eucalypt Forest, North Stradbroke Island. *Australian Journal of Botany* **25**(1): 47-58.

Saddler HDW, Pitman MG. 1970. An apparatus for the measurement of sap flow in unexcised leafy shoots. *Journal of Experimental Botany* **21**(69): 1048-1059.

Sakuratani T. 1981. A heat balance method for measuring water flux in the stem of intact plants. *Journal of Agricultural Meteorology* **37**(1): 9-17.

Sakuratani T. 1984. Improvement of the probe for measuring water flow rate in intact plants with the stem heat balance method. *Journal of Agricultural Meteorology* **40**(3): 273-277.

Saveyn A, Steppe K, Lemeur R. 2008. Spatial variability of xylem sap flow in mature beech (*Fagus sylvatica*) and its diurnal dynamics in relation to microclimate. *Botany* **86**(12): 1440-1448.

Schiller G, Cohen Y. 1998. Water balance of Pinus halepensis Mill. afforestation in an arid region. *Forest Ecology and Management* **105**(1-3): 121-128.

Schmitz N, Robert EMR, Verheyden A, Kairo JG, Beeckman H, Koedam N. 2008. A patchy growth via successive and simultaneous cambia: Key to success of the most widespread mangrove species Avicennia marina? *Annals of Botany* **101**(1): 49-58.

Scholander PF, Bradstreet ED, Hemmingsen EA, Hammel HT. 1965. Sap Pressure in Vascular Plants: Negative hydrostatic pressure can be measured in plants. *Science (New York, N.Y.)* **148**(3668): 339-346.

Scholz FG, Bucci SJ, Goldstein G, Meinzer FC, Franco AC. 2002. Hydraulic redistribution of soil water by neotropical savanna trees. *Tree Physiology* **22**(9): 603-612.

Scholz FG, Bucci SJ, Goldstein G, Meinzer FC, Franco AC, Miralles-Wilhelm F. 2007. Removal of nutrient limitations by long-term fertilization decreases nocturnal water loss in savanna trees. *Tree Physiology* **27**(4): 551-559.

Schönherr J, Bukovac MJ. 1972. Penetration of stomata by liquids - dependence on surface-tension, wettability, and stomatal morphology. *Plant Physiology* **49**(5): 813-819.

Scott RL, Cable WL, Hultine KR. 2008. The ecohydrologic significance of hydraulic redistribution in a semiarid savanna. *Water Resources Research* **44**(2): 1-12.

Sevanto S, Vesala T, Peramaki M, Nikinmaa E. 2002. Time lags for xylem and stem diameter variations in a Scots pine tree. *Plant Cell and Environment* **25**(8): 1071-1077.

Siau JF, eds. 1971. *Flow in Wood*. Syracuse Wood Science Series. New York: Syracuse University Press.

Siau JF. 1984. *Transport processes in wood*. New York: Springer-Verlag.

Silva RM, Paco TA, Ferreira MI, Oliveira M 2008. Transpiration of a kiwifruit orchard estimated using the granier sap flow method calibrated under field

conditions. In: Goodwin IOMG eds. *Proceedings of the Fifth International Symposium on Irrigation of Horticultural Crops*. 593-600.

Simonin KA, Santiago LS, Dawson TE. 2009. Fog interception by Sequoia sempervirens (D. Don) crowns decouples physiology from soil water deficit. *Plant Cell and Environment* **32**(7): 882-892.

Simpson W, TenWolde A 1999. Wood handbook - Wood as an engineering material.In. *Forest Products Laboratory. General Technical Report FPL_GTR-113*. Madison: U.S. Department of Agriculture, Forest Service, Forest Products Laboratory. 463 p.

Siqueira M, Katul G, Porporato A. 2009. Soil Moisture Feedbacks on Convection Triggers: The Role of Soil-Plant Hydrodynamics. *Journal of Hydrometeorology* **10**(1): 96-112.

Skaar C. 1972. *Water in Wood*. New York: Syracuse University Press.

Skaar C, eds. 1988. *Wood-water relations*. Springer series in Wood Science. New York, Berlin, Heidelberg.

Slatyer RO, eds. 1967. *Plant - water relations*. London/New York: Academic Press.

Smith DM, Allen SJ. 1996. Measurement of sap flow in plant stems. *Journal of Experimental Botany* **47**(305): 1833-1844.

Snyder KA, Richards JH, Donovan LA. 2003. Night-time conductance in C-3 and C-4 species: do plants lose water at night? *Journal of Experimental Botany* **54**(383): 861-865.

Sormail M, Vachaud G. 1969. Non-saturated soil moisture potential measurement by conventional and osmosis tensiometer. *La Houille Blanche* **24**(8): 849-860860.

Spanner DC. 1951a. The peltier effect and its use in the measurement of suction pressure. *Journal of Experimental Botany* **2**: 145-168.

Spanner DC. 1951b. The Peltier effect and tis use in the measurement of suction pressure. *Journal of Experimental Botany* **2**: 145-168.

Stamm AJ, eds. 1964. *Wood and cellulose science*. New York: The Ronald Press Company.

Stamm AJ, Loughborough WK. 1935. Thermodynamics of the Swelling of Wood. *Journal of Physical Chemistry* **39**(1): 121-132.

Staudt K, Serafimovich A, Siebicke L, Pyles RD, Falge E. 2011. Vertical structure of evapotranspiration at a forest site (a case study). *Agricultural and Forest Meteorology* **151**(6): 709-729.

Steinberg S, Vanbavel CHM, McFarland MJ. 1989. A gauge to measure mass-flow rate of sap in stems and trunks of woody-plants. *Journal of the American Society for Horticultural Science* **114**(3): 466-472.

Steinhagen P. 1977. Thermal conductive properties of wood, green or dry, from -40˚ to +100˚C: a literature review. *Forest Product Laboratory, Forest Service US Department of Agriculture*.

Steppe K, De Pauw DJW, Doody TM, Teskey RO. 2010. A comparison of sap flux density using thermal dissipation, heat pulse velocity and heat field deformation methods. *Agricultural and Forest Meteorology* **150**: 1046-1056.

Steppe K, De Pauw DJW, Lemeur R. 2008. A step towards new irrigation scheduling strategies using plant-based measurements and mathematical modelling. *Irrigation Science* **26**(6): 505-517.

Steppe K, De Pauw DJW, Lemeur R, Vanrolleghem PA. 2006. A mathematical model linking tree sap flow dynamics to daily stem diameter fluctuations and radial stem growth. *Tree Physiology* **26**(3): 257-273.

Steppe K, De Pauw DJW, Saveyn A, Tahon P, Nadezhdina N, Cermak J, Lemeur R. 2009. Radial sap flux profiles and beyond: an easy software analysis tool. *Acta Horticulturae* **846**: 85-92.

Steudle E, Peterson CA. 1998. How does water get through roots? *Journal of Experimental Botany* **49**(322): 775-788.

Stiller V, Sperry JS. 1999. Canny's compensating pressure theory fails a test. *American Journal of Botany* **86**(8): 1082-1086.

Stone R. 2006. Ecology: A rescue effort for tsunami-ravaged Mangrove forests. *Science* **314**(5798): 404-404.

Studhalter R, Glock W, Agerter S. 1963. Tree growth. *The Botanical Review* **29**(3): 245-365.

Suleiman BM, Larfeldt J, Leckner B, Gustavsson M. 1999. Thermal conductivity and diffusivity of wood. *Wood Science and Technology* **33**(6): 465-473.

Swanson RH. 1972. Water transpired by trees is indicated by heat pulse velocity. *Agricultural Meteorology* **10**(4-5): 277-281.

Swanson RH. 1983. *Numerical and experimental analyses of implanted-probe heat pulse velocity theory.* Ph.D. thesis, University of Alberta Edmonton, Canada.

Swanson RH. 1994. Significant historical developments in thermal methods for measuring sap flow in trees. *Agricultural and Forest Meteorology* **72**(1-2): 113-132.

Swanson RH, Whitfield DWA. 1981. A numerical analysis of heat pulse velocity theory and practice. *Journal of Experimental Botany* **32**(126): 221-239.

Taiz E, Zeiger L, eds. 2006. *Plant Physiology*. Sunderland, MA: Sinauer Associates, Inc.

Taneda H, Sperry JS. 2008. A case-study of water transport in co-occurring ring- versus diffuse-porous trees: contrasts in water-status, conducting capacity, cavitation and vessel refilling. *Tree Physiology* **28**(11): 1641-1651.

Tatarinov FA, Kucera J, Cienciala E. 2005. The analysis of physical background of tree sap flow measurement based on thermal methods. *Measurement Science & Technology* **16**(5): 1157-1169.

Testi L, Villalobos FJ. 2009. New approach for measuring low sap velocities in trees. *Agricultural and Forest Meteorology* **149**(3-4): 730-734.

Turnipseed AA, Burns SP, Moore DJP, Hu J, Guenther AB, Monson RK. 2009. Controls over ozone deposition to a high elevation subalpine forest. *Agricultural and Forest Meteorology* **149**(9): 1447-1459.

Turrell FM, Austin SW, McNee D, Park WJ. 1967. Thermal Conductivity of Functional Citrus Tree Wood. *Plant Physiology* **42**(8): 1025-1034.

Tyerman SD, Niemietz CM, Bramley H. 2002. Plant aquaporins: multifunctional water and solute channels with expanding roles. *Plant Cell and Environment* **25**(2): 173-194.

Tyree M, Zimmerman M 2002. Xylem structure and the ascent of sap.In. *Springer-Verlag*. New York. 283.

Tyree MT. 1997. The Cohesion-Tension theory of sap ascent: current controversies. *Journal of Experimental Botany* **48**(10): 1753-1765.

Tyree MT, Ewers FW. 1991. The hydraulic architecture of trees and other woody-plants. *New Phytologist* **119**(3): 345-360.

Uddling J, Teclaw RM, Pregitzer KS, Ellsworth DS. 2009. Leaf and canopy conductance in aspen and aspen-birch forests under free-air enrichment of carbon dioxide and ozone. *Tree Physiology* **29**(11): 1367-1380.

Valiela I, Bowen JL, York JK. 2001. Mangrove forests: One of the world's threatened major tropical environments. *Bioscience* **51**(10): 807-815.

Van As H, Scheenen T, Vergeldt FJ. 2009. MRI of intact plants. *Photosynthesis Research* **102**(2-3): 213-222.

Van der Zande D, Mereu S, Nadezhdina N, Cermak J, Muys B, Coppin P, Manes F. 2009. 3D upscaling of transpiration from leaf to tree using ground-based LiDAR: Application on a Mediterranean Holm oak (*Quercus ilex* L.) tree. *Agricultural and Forest Meteorology* **149**(10): 1573-1583.

Vandegehuchte MW, Steppe K. 2012a. Improving sap flux density measurements by correctly determining thermal diffusivity, differentiating between bound and unbound water. *Tree Physiology* **32**(7): 930-942.

Vandegehuchte MW, Steppe K. 2012b. Interpreting the Heat Field Deformation method: Erroneous use of thermal diffusivity and improved correlation between temperature ratio and sap flux density. *Agricultural and Forest Meteorology* **162-163**(0): 91-97.

Vandegehuchte MW, Steppe K. 2012c. Use of the correct heat conduction-convection equation as basis for heat-pulse sap flow methods in anisotropic wood. *Journal of Experimental Botany* **63**(8): 2833-2839.

Verbeeck H, Steppe K, Nadezhdina N, Op de Beeck M, Deckmyn G, Meiresonne L, Lemeur R, Cermak J, Ceulemans R, Janssens IA. 2007. Stored water use and transpiration in Scots pine: a modeling analysis with ANAFORE. *Tree Physiology* **27**(12): 1671-1685.

Vertessy RA, Hatton TJ, Reece P, Osullivan SK, Benyon RG. 1997. Estimating stand water use of large mountain ash trees and validation of the sap flow measurement technique. *Tree Physiology* **17**(12): 747-756.

Vieweg GH, Ziegler AD. 1960. Thermoelektrische Registrierung der Geschwindigkeit des Transpirationsstromes. *Berichte der Deutschen botanischen Gesellschaft* **73**: 221-226.

Walter A, Schurr U. 2005. Dynamics of leaf and root growth: Endogenous control versus environmental impact. *Annals of Botany* **95**(6): 891-900.

Wanek W, Hofmann J, Feller IC. 2007. Canopy interactions of rainfall in an off-shore mangrove ecosystem dominated by Rhizophora mangle (Belize). *Journal of Hydrology* **345**(1-2): 70-79.

Warren CR, Bleby T, Adams MA. 2007. Changes in gas exchange versus leaf solutes as a means to cope with summer drought in Eucalyptus marginata. *Oecologia* **154**(1): 1-10.

West AG, Hultine KR, Jackson TL, Ehleringer JR. 2007. Differential summer water use by *Pinus edulis* and *Juniperus osteosperma* reflects contrasting hydraulic characteristics. *Tree Physiology* **27**(12): 1711-1720.

Williams DG, Cable W, Hultine K, Hoedjes JCB, Yepez EA, Simonneaux V, Er-Raki S, Boulet G, de Bruin HAR, Chehbouni A, Hartogensis OK, Timouk F. 2004. Evapotranspiration components determined by stable isotope, sap flow and eddy covariance techniques. *Agricultural and Forest Meteorology* **125**(3-4): 241-258.

Windt CW, Vergeldt FJ, De Jager PA, Van As H. 2006. MRI of long-distance water transport: a comparison of the phloem and xylem flow characteristics and dynamics in poplar, castor bean, tomato and tobacco. *Plant Cell and Environment* **29**(9): 1715-1729.

Winters AJ, Adams MA, Bleby TM, Rennenberg H, Steigner D, Steinbrecher R, Kreuzwieser J. 2009. Emissions of isoprene, monoterpene and short-chained carbonyl compounds from Eucalyptus spp. in southern Australia. *Atmospheric Environment* **43**(19): 3035-3043.

Wullschleger SD, Childs KW, King AW, Hanson PJ. 2011. A model of heat transfer in sapwood and implications for sap flux density measurements using thermal dissipation probes. *Tree Physiology* **31**(6): 669-679.

Wullschleger SD, Hanson PJ, Dawson TE. 1996a. Measuring stem water content in four deciduous hardwoods with a time-domain reflectometer. *Tree Physiology* **16**(10): 809-815.

Wullschleger SD, Hanson PJ, Todd DE. 1996b. Measuring stem water content in four deciduous hardwoods with a time-domain reflectometer. *Tree Physiology* **16**(10): 809-815.

Yates DJ, Hutley LB. 1995. Foliar uptake of water by wet leaves of *Sloanea-Woollssii*, an Australian subtropical rain-forest tree. *Australian Journal of Botany* **43**(2): 157-167.

Yepez EA, Williams DG, Scott RL, Lin GH. 2003. Partitioning overstory and understory evapotranspiration in a semiarid savanna woodland from the isotopic composition of water vapor. *Agricultural and Forest Meteorology* **119**(1-2): 53-68.

Zeppel M, Macinnis-Ng C, Palmer A, Taylor D, Whitley R, Fuentes S, Yunusa I, Williams M, Eamus D. 2009. An analysis of the sensitivity of sap flux to soil

and plant variables assessed for an Australian woodland using a soil-plant-atmosphere model (vol 35, pg 509, 2008). *Functional Plant Biology* **36**(12): 1120.

Zeppel M, Tissue D, Taylor D, Macinnis-Ng C, Eamus D. 2010. Rates of nocturnal transpiration in two evergreen temperate woodland species with differing water-use strategies. *Tree Physiology* **30**(8): 988-1000.

Zimmermann U, Schneider H, Wegner LH, Haase A. 2004. Water ascent in tall trees: does evolution of land plants rely on a highly metastable state? *New Phytologist* **162**(3): 575-615.

Zimmermann U, Wagner HJ, Heidecker M, Mimietz S, Schneider H, Szimtenings M, Haase A, Mitlohner R, Kruck W, Hoffmann R, Konig W. 2002. Implications of mucilage on pressure bomb measurements and water lifting in trees rooting in high-salinity water. *Trees-Structure and Function* **16**(2-3): 100-111.

Zimmermann U, Zhu JJ, Meinzer FC, Goldstein G, Schneider H, Zimmermann G, Benkert R, Thurmer F, Melcher P, Webb D, Haase A. 1994. High-molecular-weight organis-compounds in the xylem sap of mangroves - Implications for long-distance water transport. *Botanica Acta* **107**(4): 218-229.

Zweifel R, Item H, Hasler R. 2000. Stem radius changes and their relation to stored water in stems of young Norway spruce trees. *Trees-Structure and Function* **15**(1): 50-57.

Zweifel R, Item H, Hasler R. 2001. Link between diurnal stem radius changes and tree water relations. *Tree Physiology* **21**(12-13): 869-877.

Summary

Just as carbon, water is indispensable for plants to develop and grow. A lack of water causes turgor loss in plant cells which prevents further expansion of these cells and the coupled incorporation of carbon sources in the cell wall. This inhibits growth and, if this water scarcity continues, plant dimensions such as the stem diameter will start to decrease. Finally the plant will lose its vital functions and die.

Worldwide, sap flow methods are applied to monitor plant water status and validate vegetation models. These methods determine flow direction as well as relative and absolute flow, forming the link between plant water uptake, release and storage. Hence, whether to assess the correct irrigation dose, to monitor forest vitality or to obtain trustworthy modelling results, reliable sap flow measurements are indispensable.

The most commonly applied sap flow methods are based on heat dissipation in the sapwood. Within this group, a distinction can be made between those methods determining the total flow per time inside a stem or stem section and those assessing sap flux density, the flow per surface per time. While the former are widely applied in irrigation and other applications necessitating an estimation of total plant water use, the latter are applied to investigate specific hydraulic pathways and processes as they allow to distinguish spatial patterns in sap flow, both axially, radially and azimuthally.

In this PhD study, the accuracy and applicability of the most important sap flux density methods were investigated. To this end, the underlying thermodynamic theory was studied, Finite Element Modelling (FEM) conducted and lab experiments

on cut tree stem segments were undertaken, complemented with a field study on *Avicennia marina* (Forssk.) Vierh. and *Rhizophora stylosa* Griff.

By investigating the thermodynamic interpretation of the thermal diffusivity as sapwood property, it became clear that the link between the Heat Field Deformation (HFD) temperature ratio and sap flux density, based on this thermal diffusivity, was incorrect. It was concluded that therefore, the continuous HFD method should be considered merely empirical, similar to the Thermal Dissipation method. Moreover, based on FEM, an improved empirical correlation between the HFD temperature ratio and sap flux density was proposed.

Also for the methods based on the application of heat pulses, a flaw in the basic theory was noted. These methods are based on the isotropic heat conduction-convection equation for an ideal heater in an infinite medium. Sapwood, however, is known to be anisotropic. Fortunately, the Compensation Heat Pulse, Tmax as well as the Heat Ratio method are based on derivations of this basic equation in a way that is independent of the assumption of isotropy. Hence, for these methods the results are still theoretically correct. Nevertheless, attention should be paid to apply the correct anisotropic equation in modelling and method development, as recent examples show that by neglecting anisotropy, errors can be induced.

Within the heat pulse sap flux density methods, the Heat Ratio method enables measurements of low and reverse flow, unlike the Compensation Heat Pulse and Tmax method. This method, however, is dependent on accurate estimations of axial thermal sapwood diffusivity. In this PhD, it was shown that in the currently applied method of mixtures to determine this diffusivity, no distinction was made between bound and unbound water, resulting in over- or underestimations of axial thermal diffusivity dependent on the dry sapwood density and sapwood water content. A correction to this method was proposed, differentiating between bound and unbound water based on the fibre saturation point. This correction has the disadvantage that fibre saturation point is a sapwood characteristic that is not measurable in-situ and, hence, has to be estimated based on dry sapwood density.

In response to the difficulties encountered when studying the different sap flux density methods, a new method was developed: the Sapflow+ method. This method is based on a curve fitting procedure during which the anisotropic heat conduction-convection equation is directly fitted to measured temperature profiles located both

axially and tangentially from the heater. As was shown by the conducted identifiability analysis and the lab experiments on stem segments of *Fagus sylvatica* L., the Sapflow+ method enables simultaneous measurements of heat velocity, across the entire naturally occurring range, and thermal sapwood properties, from which sap flux density and sapwood water content can be derived. The applicability of the method to determine heat velocity was confirmed in a field experiment on *Avicennia marina* (Forssk.) Vierh. and *Rhizophora stylosa* Griff. For the determination of sapwood water content, further validation experiments and possible optimization of the method are needed.

Next to providing an opportunity to test the Sapflow+ method in harsh field conditions, the experiments conducted on *Avicennia* and *Rhizophora* led to the remarkable finding that both species show a completely different pattern in stem diameter variation, despite being influenced by the same environmental conditions. This led to the hypothesis that endogenous control of stem diameter fluctuations and growth might be much more crucial than previously assumed and could play an important role in plant growth strategies.

In conclusion, the presented PhD study has exposed some limitations of and inaccuracies in existing sap flux density methods and has provided an alternative based on correct theoretical principles. This Sapflow+ method is sensitive towards the entire naturally occurring sap flow range and holds the promise of accurately determining sapwood water content.

.

Samenvatting

Net zoals koolstof is water onontbeerlijk voor de ontwikkeling en groei van planten. Een gebrek aan water zorg voor turgorverlies in de plantcellen. Dit verhindert expansie van deze cellen en de gekoppelde inbouw van koolstofbronnen in de celwand waardoor verdere groei onmogelijk wordt. Als deze waterschaarste aanhoudt, nemen plantdimensies zoals stam diameter af en verliest de plant finaal zijn vitale functies waardoor ze afsterft.

Wereldwijd worden sapstroommethoden gebruikt om de plantwaterstatus op te volgen en vegetatiemodellen te valideren. Deze methoden bepalen zowel de stroomrichting als de relatieve en absolute hoeveelheid sapstroom, waardoor het verband kan gelegd worden tussen de wateropname, -vrijstelling en -opslag van de plant. Bij deze meetmethoden is accuraatheid van de sapstroombepaling onontbeerlijk, of het nu gaat om de bepaling van de correctie irrigatiedosis, het opvolgen van bosvitaliteit of om betrouwbare modelresultaten te bekomen.

De meest gebruikte sapstroommethoden zijn gebaseerd op de verspreiding van warmte in het spinthout. Binnen deze groep kan verder onderscheid gemaakt worden tussen de methoden die de totale hoeveelheid sapstroom per tijd in een stam of stamsectie bepalen en deze die de sapstroomdichtheid bepalen, de hoeveelheid sapstroom doorheen een gegeven oppervlakte per tijd. Waar de eerstgenoemde vooral ingezet worden voor irrigatietoepassingen en andere applicaties waarbij een inschatting van het totale waterverbruik van de plant beoogd wordt, worden de laatstgenoemde vooral aangewend om specifieke hydraulische routes en processen in de plant te onderzoeken, aangezien deze methodes toelaten om ruimtelijke verschillen, zowel axiaal, radiaal als azimuthaal, in de sapstroomdichtheid te bepalen.

In dit doctoraatonderzoek werden de accuraatheid en toepasbaarheid van de belangrijkste sapstroomdichtheidmethoden onderzocht. Hiertoe werd de onderliggende thermodynamische theorie bestudeerd, werden Finite Element Modellen (FEM) toegepast en werden labo experimenten uitgevoerd op afgezaagde stamsegmenten, aangevuld met een veldstudie waarbij op *Avicennia marina* (Forssk.) Vierh. en *Rhizophora stylosa* Griff. werd gemeten.

Door de thermodynamische betekenis van de thermische diffusiviteit als spinthouteigenschap onder de loep te nemen, werd duidelijk dat de op deze parameter gebaseerde link tussen the Heat Field Deformation (HFD) temperatuurratio en sapstroomdichtheid, incorrect was. Op basis daarvan werd besloten dat de continue HFD methode, net zoals de Thermal Dissipation methode, als empirisch moet beschouwd worden. Bovendien werd op basis van FEM een verbeterde empirische correlatie tussen de HFD temperatuurratio en sapstroomdichtheid voorgesteld.

Ook voor de methoden gebaseerd op de applicatie van een warmtepuls werd een gebrek in de toegepaste theorie bemerkt. Deze methoden zijn namelijk gebaseerd op de isotrope warmteconductie-convectievergelijking, ontwikkeld voor een ideale verwarmingsnaald in een oneindig groot medium. Het is echter bekend dat spinthout anisotrope karakteristieken heeft. Gelukkig zijn zowel de Compensation Heat Pulse, Tmax als Heat Ratio methode gebaseerd op afleidingen van deze isotrope vergelijking waarbij de resultaten onafhankelijk zijn van de assumptie van isotropie en geldig blijven voor anisotrope media. De metingen bekomen via deze methoden zijn theoretisch dus nog steeds correct. Toch moet er op gelet worden dat de correcte anisotrope vergelijkingen worden toegepast in modelleerstudies en bij het ontwikkelen van nieuwe warmte gebaseerde methoden aangezien recente voorbeelden aantonen dat het verwaarlozen van het anisotroop karakter van spinthout tot fouten kan leiden.

Binnen de bestaande warmtepulsmethoden, laat de Heat Ratio methode, in tegenstelling tot de Compensation Heat Pulse en Tmax methode, toe om lage en omgekeerde sapstroom te meten. Deze methode is echter afhankelijk van een nauwkeurige bepaling van de axiale thermische diffusiviteit. In dit doctoraatonderzoek werd aangetoond dat in de huidig toegepaste combinatiemethode geen onderscheid wordt gemaakt tussen gebonden en

ongebonden water. Dit kan tot over- of onderschattingen van de axiale thermische diffusiviteit leiden, afhankelijk van de droge dichtheid en het vochtgehalte van het spinthout. Een correctie werd voorgesteld waarbij het onderscheid tussen gebonden en ongebonden water gemaakt wordt op basis van het vezelverzadigingspunt van het spinthout. Deze correctie heeft als nadeel dat het vezelverzadigingspunt een spinthouteigenschap is die moeilijk in situ kan bepaald worden, en dus geschat moet worden op basis van de droge densiteit van het spinthout.

Als antwoord op de beperkingen waarop gebotst werd tijdens het bestuderen van de bestaande sapstroomdichtheidmethoden, werd een nieuwe methode ontwikkeld: de Sapflow+ methode. Deze methode is gebaseerd op een curve fitting procedure waarbij de anisotrope warmteconductie-convectievergelijking rechtstreeks gefit wordt aan opgemeten temperatuurprofielen op specifieke afstanden axiaal en tangentieel van de warmtenaald. Zoals aangetoond via een identificeerbaarheidsanalyse en labo experimenten op stamsegmenten van *Fagus sylvatica* L., laat de Sapflow+ methode toe om gelijktijdig warmtesnelheden, over het volledig natuurlijk voorkomende bereik, en thermische eigenschappen van het spinthout op te meten. Hieruit kan dan sapstroomdichtheid en spinthoutvochtgehalte bepaald worden. De toepasbaarheid van de Sapflow+ methode voor het bepalen van warmtesnelheden werd bevestigd tijdens een veldexperiment via metingen op *Avicennia marina* (Forssk.) Vierh. en *Rhizophora stylosa* Griff. Voor de bepaling van het spinthoutvochtgehalte zijn additionele validatie-experimenten en mogelijks verdere optimalisatie van de methode nodig

Naast de mogelijkheid om de Sapflow+ methode te testen in moeilijke veldomstandigheden, hebben de uitgevoerde experimenten op *Avicennia* en *Rhizophora* tot de merkwaardige vaststelling geleid dat beide soorten een volledig verschillend stamdiametervariatiepatroon vertonen, ondanks dat ze door dezelfde omgevingsomstandigheden beïnvloed worden. Dit leidde tot de hypothese dat endogene controle van de stamdiameterfluctuaties en groei belangrijker kan zijn dan aanvankelijk werd gedacht en bovendien een beduidende rol kan spelen in plantgroeistrategieën.

Samenvattend heeft dit doctoraatonderzoek een aantal beperkingen en onnauwkeurigheden van bestaande sapstroomdichtheidmethoden blootgelegd en biedt het een alternatief aan, gebaseerd op correcte thermodynamische principes.

Dit alternatief, de Sapflow+ methode, is gevoelig tegenover het volledig natuurlijk voorkomend sapstroombereik en houdt de belofte in accurate vochtgehaltes van spinthout te kunnen bepalen.

.

Curriculum vitae

Personal information

Name:	Maurits Willem Vandegehuchte
Date of birth:	20 February 1987
Place of birth:	Oostende (Belgium)
Nationality:	Belgian
Address:	Lisbloemstraat 45, 9000 Gent
Tel:	+32 473 32 22 54
E-mail:	Maurits.Vandegehuchte@UGent.be

Education

2007-2009 M.Sc. in Bioscience Engineering (Environmental Technology), Faculty of Bioscience Engineering, Ghent University, Ghent (Summa Cum Laude)

Master thesis:

Performed at the Laboratory of Plant Ecology, Ghent University, Gent in collaboration with the 'Institut d'Olivier', Sousse, Tunisia.

Title: "Evaluation of several irrigation techniques and sap flow variation for olive tree *Olea europaea* L. 'Meski'".

Promoter: prof. dr. ir. Kathy Steppe

2004-2007	B.Sc. in Bioscience Engineering, Faculty of Bioscience Engineering, Ghent University, Ghent (Magna Cum Laude)
1998-2004	Secondary school, Science-Mathematics, Onze-Lieve-Vrouwecollege, Oostende

Additional education

2009-2013	Doctoral training programme in Bioscience Engineering, Faculty of Bioscience Engineering, Ghent University *Courses followed in the framework of this programme:* Wood technology: material characteristics (2009-2010) Multivariate data analysis (2009-2010) Advanced academic English: writing skills (2010-2011) Effective Scientific Communication (2010-2011) Quality Research Skills (2010-2011) Personal Effectiveness (2010-2011) Leading, Following and Collaborating (2010-2011) Applied isotope studies (2011-2012) Career management: applying for a postdoctoral job (2013)
April 2012	Certificate of succeeding a four day Tree Climbing PRO course organized by The Tree Climbing Company
November 2009	Certificate of instructor at youth work recognized by the Agency of Social-Cultural Work of the Flemish Government
September 2009	Certificate of succeeding the course on international cooperation and development issues (North-South relations) organized by the Belgian Technical Cooperaton (BTC)

Professional experience

2009-2013	Research fellow of the Research Foundation – Flanders (FWO, Flanders, Belgium). The research as preparation for this doctoral thesis was conducted at the Department of

Applied Ecology and Environmental Biology (Laboratory of Plant Ecology) of the Ghent University, Gent.

Other scientific activities

June 2013	Member of the scientific committee of the 9th International Workshop on Sap Flow, Ghent, Belgium, 4-7 June 2013
July-October 2012	Research stay at Moreton Bay Research Station, Queensland University, North Stradbroke Island, Australia in collaboration with the Groundwater Research Centre, Civil Engineering, Queensland University, Bribane, Australia. Mangrove water relations research in the framework of the PhD.
April-May 2012	Research stay at Wageningen NMR Centre, Wageningen University, the Netherlands to be instructed in NMR wood water content research.
October 2010	Research stay at the Institute of Forest Ecology, Mendel University of Agriculture and Forestry, Brno, Czech Republic to discuss sap flow measurement methods with prof. Nadezhdina and prof. Cermak.
2009-2013	Review tasks for Tree Physiology, Plant and Soil, International Journal of Thermal Sciences, Trees - Structure and Function, Hydrological Processes and Australian Journal of Multi-disciplinary Engineering.

Grants and prizes

July 2012	Grant from the Research Foundation – Flanders (FWO – Vlaanderen) for the research visit at the University of Queensland, Australia.
October 2010	Scholarships from the Department of Education and Training (Flemish Government) and the Czech Republic Ministry of Education, Youth and Sport for the research visit at the Mendel University, Brno, Czech Republic.

October 2009	PhD fellowship from the Research Foundation – Flanders (FWO – Vlaanderen) for the PhD research at Ghent University, Belgium
September 2009	Bayer Plant Science award from Bayer Plant and Bayer Crop Science for the master thesis 'Evaluation of several irrigation techniques and sap flow variation for olive tree *Olea europaea* L. 'Meski''.

Educational activities

2009-2013	Guidance of practical courses and technical lectures for the courses "Ecophysiology", "Plant-Water Relations" and "Ecology".
2012-2013	Tutor of the M.Sc. thesis of Mieke Van Houtte (Electrical Resistivity Tomography (ERT) to establish wood water content patterns in living trees), Stefanie de Groote (Canopy water uptake in the mangrove species *Avicennia marina)*, Michiel Hubeau (Water transport and growth patterns in mangrove species *Rhizophora*) and Niels De Baerdemaker (Assessing the water use strategies of *Banksia aemula*).
2011-2012	Tutor of the M.Sc. thesis of Caroline Van der Heyden (Seizoenale relatieve verandering in sapstroomdichtheid en vochtgehalte van het spinthout van beuk (*Fagus sylvatica* L.)) and Dries Vermassen (Validatie van de Sapflow+ sensor: hoe nauwkeurig wordt sapstroomdichtheid en vochtgehalte van het spinthout door deze methode bepaald?)
2010-2011	Tutor of the M.Sc. thesis of Lidewei Vergeynst (Changes in temperature and stem water content evoke erroneous sap flux density estimates with. Thermal Dissipation Probes) and Bart Van de Wal (Ecophysiology of mangrove in Australia: hydraulic functioning).

Publications

International publications with peer review

Vandegehuchte, M. W., Braham, M., Lemeur, R. & Steppe, K. (2012). The importance of sap flow measurements to estimate actual water use of Meski olive trees under different irrigation regimes in Tunisia. *Irrigation and Drainage*, 61: 645-656..

Vandegehuchte, M.W. & Steppe, K. (2012) Comment on "Sap flow measurements by a single thermal dissipation probe: exploring the transient regime" — Ann. For. Sci. 66 (2009) by Mahjoub et al. and "Sap flow measurement by a single thermal dissipation probe in transient regime: implementation of the method and test under field conditions" — Ann. For. Sci. 1-9 (2012) by Masmoudi et al. *Annals of Forest Science*, 69: 769-771.

Vandegehuchte, M.W. & Steppe, K. (2012). Use of the correct heat conduction-convection equation as basis for heat pulse sap flow methods in anisotropic wood. *Journal of Experimental Botany*, 63: 2833-2839.

Vandegehuchte, M.W. & Steppe, K. (2012). Interpreting the Heat Field Deformation method: Erroneous use of thermal diffusivity and improved correlation between temperature ratio and sap flux density. *Agricultural and Forest Meteorology*, 162-163: 91-97.

Vandegehuchte, M.W. & Steppe, K. (2012). Improving sap flux density measurements by correctly determining thermal diffusivity, differentiating between bound and unbound water. *Tree Physiology*, 32: 930-942.

Vandegehuchte, M. W. & Steppe, K. (2012). A triple-probe heat pulse method for measurement of thermal diffusivity in trees. *Agricultural and Forest Meteorology*. 160: 90-99.

Vandegehuchte, M.W. & Steppe, K. (2012). Sapflow+: a four-needle heat pulse sap flow sensor enabling nonempirical sap flux density and water content measurements. *New Phytologist*, 196: 306-317.

Vandegehuchte, M.W. & Steppe, K. (2012). Sap flux density measurement methods: working principles and applicability. *Functional Plant Biology* (accepted).

Reyes-Acosta, J. L., Vandegehuchte, M. W., Steppe, K. & Lubczynski, M. W(2012). Novel, cyclic thermal dissipation (CHD) method for the correction of natural temperature gradients in sap flow measurements. Part 2. Laboratory validation. *Tree Physiology*, 32: 930-42

Nadezhdina, N., Vandegehuchte, M.W. & Steppe, K. (2012). Sap flux density measurements based on the heat field deformation method. *Trees - Structure and Function*, 26: 1439-1448.

Proceedings

Vandegehuchte, M.W. & Steppe, K. (2012). Finite Element Analysis as Aid in Understanding Heat Based Sap Flow Methods with Linear Heating. *8th International Symposium on Sap Flow*, 951: 63-70.

Oral presentations

Vandegehuchte, M.W., Nadezhdina, N. & Steppe, K. (2011) Improved thermodynamic approach for Heat Field Deformation sap flow measurements. *8th International Sap Flow Workshop*, Volterra, Italy, 8-12 May 2011.

Reyes-Acosta, L.J., Vandegehuchte, M.W., Steppe, K. & Lubcsynski, M.W. (2011) Natural thermal gradient (NTG) bias on sap flow measurements when using Thermal Dissipation Probes and Heat Field Deformation sensors: errors and corrections by

applying an alternated power methodology.*8th International Sap Flow Workshop*, Volterra, Italy, 8-12 May 2011

Steppe K., Vandegehuchte M.W., Van de Wal B.A.E., Hoste P., Guyot A., Lovelock C.E., Lockington D. (2013) Reverse sap flow in mangroves: do these trees drink rainwater through their canopy? *International Symposium on Wood Structure in Plant Biology and Ecology (WSE)*, Naples, Italy, 17-20 April 2013.

Vandegehuchte, M.W., Guyot, A., Lockington, D.A. & Steppe, K. (2013) Stem diameter variation: endogenous regulation versus environmental dynamics and its implication for functional modelling. *7th International Conference on Functional-Structural Plant Models*, Saariselkä, Finland, 9-14 June 2013 (accepted)

Vandegehuchte, M.W. & Steppe, K. (2013) Eliminating the heat input as parameter in the Sapflow+ method. *9th International Sap Flow Workshop*, Ghent, Belgium, 4-7 June 2013 (accepted)

de Sousa, E.F., Santolin, M.A., Vandegehuchte, M.W., Compostrini, E. & de Jesus Soares, K. (2013). Development of a mathematical model and its numerical solution to estimate sap flow applying a transient heating system. *9th International Sap Flow Workshop*, Ghent, Belgium, 4-7 June 2013 (accepted)

Poster presentations

Vergeynst, L.L., Vandegehuchte, M.W., McGuire, M.A., Teskey, R.O. & Steppe, K. (2011) Changes in temperature and stem water content evoke erroneous sap flux density estimates with Thermal Dissipation Probes. *8th International Sap Flow Workshop*, Volterra, Italy, 8-12 May 2011

Guyot, A., White, A., Vandegehuchte, M.W., Steppe, K. & Lockington, D.A. (2013) Atmosphere-Vegetation-Groundwater interactions: a case study in the context of the subtropical coastal sandy mass aquifers from Eastern Australia. *Geophysical Research Abstracts*, 15, *EGU*, Vienna, Austria, 7-12 April 2013

Vandegehuchte, M.W., Burgess, S.S.O., Downey, A & Steppe, K. (2013) Stem temperature influence on heat pulse sap flux density measurements. *9th International Sap Flow Workshop*, Ghent, Belgium, 4-7 June 2013 (accepted)

Lubczynski, M.W., Reyes-Acosta, L.J., Chavarro-Rincon, D., Vandegehuchte, M.W., Roy, J., & Steppe, K. (2013) Cyclic heat dissipation (CHD) method for the correction

of natural temperature gradients in sap flow measurements. *9th International Sap Flow Workshop*, Ghent, Belgium, 4-7 June 2013 (accepted)